A TRANSLATIONAL APPROACH TO UNDERSTANDING AND TREATING

AUTONOMIC DYSFUNCTION AFTER SPINAL CORD INJURY

by

Jordan Squair

M.Sc., The University of British Columbia, 2014

A THESIS SUBMITTED IN PARTIAL FULFILLMENT OF

THE REQUIREMENTS FOR THE DEGREE OF

DOCTOR OF PHILOSOPHY

in

THE FACULTY OF GRADUATE AND POSTDOCTORAL STUDIES

(Medicine)

THE UNIVERSITY OF BRITISH COLUMBIA

(Vancouver)

September 2018

The following individuals certify that they have read, and recommend to the Faculty of Graduate and Postdoctoral Studies for acceptance, the dissertation entitled:

A translational approach to understanding and treating autonomic dysfunction after spinal cord injury

submitted by   Jordan W. Squair   in partial fulfillment of the requirements for

the degree of   Doctor of Philosophy

in   Medicine

Examining Committee:

Dr. Andrei Krassioukov
Co-supervisor

Dr. Christopher West
Co-supervisor

Dr. Liam Brunham
Supervisory Committee Member

Dr. Cheryl Wellington

University Examiner

Dr. Timothy O'Connor
University Examiner

Additional Supervisory Committee Members:

Dr. Wolfram Tetzlaff
Supervisory Committee Member

Dr. David Granville
Supervisory Committee Member

Abstract

Spinal cord injury leads to immediate and permanent motor, sensory, and autonomic dysfunction. It is becoming increasingly recognized that autonomic dysfunctions are a top priority for individuals with spinal cord injury, lead to accelerated chronic health conditions, and impair quality of life. Fundamentally, autonomic dysfunctions after spinal cord injury, and cardiovascular dysfunction in particular, are caused by disconnection of descending sympatho-excitatory axons originating in the rostral ventro-lateral medulla and projecting to sympathetic pre-ganglionic neurons in the spinal cord. In this thesis, we develop a clinically relevant rodent model to study autonomic dysfunction after spinal cord injury, investigate the impact of neuroprotective pharmacology on autonomic function, and deploy a framework built around systems genetics to better understand how to target conserved molecular responses. Additionally, we use data from a multi-centre clinical trial to test whether optimization of cardiovascular parameters can be used as an immediately implementable 'neuroprotective' strategy to improve neurologic outcomes. We show that autonomic dysfunction including autonomic dysreflexia and cardiac dysfunction can be modelled in the rodent, and follow a severity-dependent pattern that is directly associated with the number of descending sympatho-excitatory axons. To help preserve these axons after injury, we show that one of the most promising neuroprotective drugs (minocycline) administered one hour after injury can improve autonomic function compared to saline controls. Next, we identify an evolutionarily conserved gene subnetwork that can be leveraged to identify novel treatments and biomarkers. Finally, we show that optimizing cardiovascular parameters leads to improved neurologic outcomes in humans with acute SCI. Overall, the work presented in this thesis provides key mechanistic and translational data that 1)

increases our understanding of autonomic dysfunction after spinal cord injury and 2) provides

tools to discover and translate novel therapies to the clinic.

Lay Summary

Damage to the nervous system, as occurs after spinal cord injury, alters the function of the heart and blood vessels. Consequently, people with spinal cord injury typically have impaired heart function as well as episodes of extremely high uncontrolled blood pressure, a condition referred to as autonomic dysreflexia. In this thesis, we explore how these 'autonomic problems' affect humans with spinal cord injury. We then develop an animal model to test new potential therapies to improve how the blood vessels and heart function after spinal cord injury. Lastly, we use genetic approaches to better understand how to determine how severe spinal cord injury is, and what treatments may work best on the spinal cord. We show that rodent models of spinal cord injury can replicate common clinical problems that cause damage to the heart and blood vessels, and that a promising treatment for spinal cord injury can improve the function of the heart and blood vessels. We provide a genetic framework to test novel biomarkers and which clinically approved drugs are most likely to reverse or prevent damage caused by spinal cord injury and thereby prevent damage to the heart and blood vessels. Finally, we found that a high percentage of individuals experience severely low blood pressure immediately after spinal cord injury, and that optimization of blood pressure is critical to improve neurological recovery.

Preface

All chapters in this thesis have been published or are in review. The work is therefore presented in its published form, and some repetition of key introductory comments is expected.

A version of chapter 1 has been published. **Squair, J.W.**, West, C.R. and Krassioukov, A.V. (2015). Neuroprotection, plasticity manipulation, and regenerative strategies to improve cardiovascular function following spinal cord injury. Journal of Neurotrauma, 32, 1-13. I performed this literature review and drafted the manuscript.

A version of chapter 3 has been published. **Squair, J.W.**, Phillips, A.A., Harmon, M., Krassioukov A.V. (2016). Emergency Management of Autonomic Dysreflexia with Neurological Complications. CMAJ. 88(15): 1100-1103. I discussed the clinical care and diagnosis with the clinical team and drafted the manuscript.

A version of chapter 4 has been published. **Squair, J.W.**, West, C.R. Popok, D., Assinck, P., Liu J., Tetzlaff, W., Krassioukov, A.V. (2016). High thoracic contusion model for the investigation of cardiovascular function post spinal cord injury. Journal of Neurotrauma.34(3), 671-684. I performed all animal care, histological analyses, data analysis, statistics, and drafted the manuscript.

A version of chapter 5 has been published. **Squair, J.W.**, DeVeau, K.M., Harman, K.A., Poormasjedi-Meibod, M.S., Hayes, B., Liu J., Magnusun, D.S.K., Krassioukov, A.V., West, C.R. (2018). Spinal cord injury induced sympathetic decentralization causes cardiac atrophy and

systolic dysfunction. Journal of Neurotrauma. 35(3):424-434. I performed all animal care, histological analyses, data analysis, statistics, and drafted the manuscript.

A version of chapter 6 has been published. **Squair, J.W.,** Liu, J., Tetzlaff, W., Krassioukov, A.V., West, C.R. (2017). Spinal cord injury induced cardiomyocyte atrophy and impaired cardiac function are severity dependent. Experimental Physiology. 103(2):179-189. I performed all animal care, histological analyses, data analysis, statistics, and drafted the manuscript.

A version of chapter 7 has been published. **Squair, J.W.,** Ruiz, I., Phillips, A.A., Zheng, M.M.Z., Sarafis, Z.K., Sachdeva, R., Gopaul, R., Lie, J., Tetzlaff, W., West, C.R., Krassioukov, A.V. Minocycline reduces the severity of autonomic dysreflexia after experimental spinal cord injury. Journal of Neurotrauma. I performed all animal care, animal surgeries, histological analyses, data analysis, statistics, and drafted the manuscript.

A version of chapter 8 has been submitted. **Squair, J.W.,** Kwon, B.K., Krassioukov, A.V., West, C.R., Foster, L.J., Skinnider, M.A. Integrated systems analysis reveals conserved gene networks underlying response to spinal cord injury. I completed all bioinformatics and statistical analyses and drafted the manuscript.

A version of chapter 9 has been published. **Squair, J.W**., Bélanger, L.M., Tsang, A., Ritchie, L., Mac-Thiong, J.M., Parent, S., Christie, S., Bailey, C., Dhall, S., Street, J., Ailon, T., Paquette, S., Dea, B., Fisher, C.G., Dvorak, M.F., West, C.R., Kwon, B.K. (2017). Spinal cord perfusion pressure as measured by lumbar intrathecal catheterization predicts neurological recovery in

acute spinal cord injury: a prospective observational study. Neurology. 89(16), 1660-1667. I performed all statistical analyses and drafted the manuscript.

Table of Contents

List of Tables

List of Figures

List of Abbreviations

AD: autonomic dysreflexia

ANS: autonomic nervous system

AIS: American spinal injury association impairment scale

AR: adrenergic receptors

ASIA: American spinal injury association

CGP: chemical and genetic perturbagens

CGRP: calcitonin gene-related peptide

CN: cranial nerve

CNS: central nervous system

CO: cardiac output

CON: control

CRD: colorectal distension

CSF: cerebrospinal fluid

CSFP: cerebrospinal fluid pressure

CT: computerized tomography

CX: connexin-43

CVD: cardiovascular disease

CVLM: caudal ventrolateral medulla

DBH: dopamine beta-hydroyxlase

DMNX: dorsal vagel motor nerge

DNA: deoxyribonucleic acid

DWI: diffusion-weighted imaging

Ees: end-systolic elastance

EDPVR: end-diastolic pressure-volume relationship

EDV: end-diastolic volume

ESPVR: end-systolic pressure-volume relationship

ESV: end-systolic volume

FLAIR: fluid-attenuated inversion recovery

FG: fluorogold

GCS: Glasgow Coma Scale

GFAP: glial fibrillary acidic protein

GO: gene ontology

GTEx: genotype-tissue expression project

GWAS: genome-wide association study

HR: heart rate

IQR: interquartile range

ISNCSCI: international standards for neurological classification of spinal cord injury

LC: literature curated

LCC: largest connected component

LEMS: lower extremity motor score

LFQ: label free quantification

LV: left ventricle

LVIDd: left ventricular internal diameter during diastole

LVIDs: left ventricular internal diameter during systole

mAb: monoclonal antibody

MAP: mean arterial pressure

MBP: myelin basic protein

MRI: magnetic resonance imaging

MRSA: methicillin-resistant staphylococcus aureus

MS: mass spectrometry

MS/MS: tandem mass spectrometry

MSA: medical services commission

NA: nucleus ambiguus

NGF: neural growth factor

NTS: nucleus of the solitary tract

NT3: neurotrophin 3

OH: orthostatic hypotension

PAGE: polyacrylamide gel electrophoresis

PBS: phosphate-buffered solution

PEG: polyethelene glycol

PRES: posterior reversible encephalopathy syndrome

PRSW: preload recruitable stroke work

PPI: protein-protein interaction

PV: pressure-volume

RNA: ribonucleic acid

RPKM: reads per kilobase million

RVLM: rostral ventrolateral medulla

SBP: systolic blood pressure

SCI: spinal cord injury

SCPP: spinal cord perfusion pressure

SDS: sodium dodecyl sulfate

SPN: sympathetic pre-ganglionic neuron

SV: stroke volume

TMS: total motor score

TFT: transcription factor targets

TH: tyrosine hydroxylase

TOM: topological overlap matrix

UEMS: upper extremity motor score

WGCNA: weighted gene coexpression network analysis

Acknowledgements

I offer my sincerest thanks to my fellow lab members in the Krassioukov and West laboratories, to Laura McCracken for her support and patience, to members of the Tetzlaff lab who provided continual support, and to the Ramer lab who were always encouraging and immensely helpful.

I thank Dr. Wolfram Tetzlaff, Dr. David Granville, and Dr. Liam Brunham for their constant support throughout this journey.

To Dr. Lynn Raymond, Dr. Torsten Nielsen, and Ms. Jane Lee, I sincerely appreciate the opportunity to be a part of the MD/PhD program and have thoroughly enjoyed my journey through this program. I look forward to continuing towards a career as a clinician scientist.

I thank Dr. Christopher West, without whose support I would not be where I am today. His willingness to train me in all aspects of science has never waivered, and his mentorship has pushed me to learn and deeply appreciate the field I work in.

I sincerely thank Dr. Andrei Krassioukov. It has been during my time under his supervision that I have grown to love and appreciate both science and medicine. He has encouraged me to focus not only in science but in all aspects of life and it is for this mentorship that I am forever thankful.

Special thanks are owed to my parents, who have supported me throughout this ten-year process and continually encourage me to pursue my goals. I would never have made it here without you.

Dedication

To my family.

Chapter 1: Literature Review / Background[1]

1.1   Introduction

For years the irreversibility of neural damage caused by spinal cord injury (SCI) has been reluctantly accepted.[1] In recent decades, however, clinicians and scientists alike have begun to delve deep into the mechanisms underlying neural regeneration and protection.[2] Advances in our scientific understanding of the neurobiology underlying SCI have given credence to the notion that one day we might develop therapies to cure this condition. Although not yet realized in full, neural regeneration and protection strategies offer extraordinary promise in the field of SCI research and for those living with an SCI. These strategies are crucial to reverse the loss of supraspinal control following SCI, which usually results in a variety of motor, sensory, and autonomic impairments. While paralysis resulting from SCI is most commonly associated with an impairment or abolishment in voluntary motor and sensory function, an SCI also induces significant autonomic abnormalities.[3] In contrast to our vast understanding of motor and sensory dysfunction following SCI, autonomic dysfunction has received relatively little attention.[4] Autonomic dysfunction contributes to conditions such as autonomic dysreflexia (AD), orthostatic hypotension (OH), bladder and bowel dysfunction, sexual dysfunction, respiratory difficulties, and temperature and sweating abnormalities.[3] Due to the intricacy of these impairments and their complex relation to autonomic neuroanatomy it was not until recently that assessment of these dysfunctions was standardized and included in clinical practice.[3] AD and OH are extremely common in persons with SCI, affecting up to 90%[5-8] and 74%[9] of individuals with cervical or high-thoracic SCI, respectively. AD and OH result in drastic increases (AD) or decreases (OH) in blood pressure, which previous authors have speculated may contribute to

vascular injury and consequently increase cardiovascular disease (CVD) risk.[10] In addition,

people with SCI maintain similar, yet often amplified, CVD risk factors as able-bodied

individuals such as lack of physical exercise, dyslipidemia, smoking status, and abdominal

obesity.[11-14] Indeed, when matched for demographics and CVD risk factors, people with SCI

demonstrate a marked three-fold increase in CVD risk and an early onset of development

compared to controls.[11] Despite this fact, no treatment to date has been able to ameliorate these

cardiovascular anomalies associated with SCI. Thus, people with SCI continue to be afflicted

with dysfunctional cardiovascular control and are subsequently at increased risk for ischemic and

hemorrhagic stroke[15] as well as coronary artery calcification,[12] necessitating the urgent need for

further research in this area.

The preservation of autonomic nervous system fibers extending from the brainstem to the

thoracolumbar spinal cord and the extent of neuronal plasticity will, in part, determine the

severity of cardiovascular dysfunction and accordingly may provide targets for improving

cardiovascular control in people with SCI.[16] Preservation of autonomic neurons and

manipulation of spinal plasticity in the acute stages of SCI through neural regenerative and/or

protective pharmacology is an emerging and exciting field that holds abundant potential for

improving cardiovascular function and reducing CVD in persons with SCI. Therefore, in this

review we will 1) comprehensively characterize the relationship between autonomic

neuroanatomy and cardiovascular dysfunction following SCI 2) review and evaluate the current

knowledge on neural regenerative and protective treatments for improving cardiovascular

outcomes in SCI (See **Table 1.1** for summary) and 3) discuss the need for combinational and

translational approaches to improve autonomic control of cardiovascular outcomes.

1.2   Neural control of cardiovascular function

The heart and peripheral vasculature are the main components of the cardiovascular system.

Tonic neurogenic activity, reflexic autonomic control through baro- and chemoreceptor activity,

and the intricate balance between sympathetic and parasympathetic arms of the ANS are crucial

to regulate cardiovascular parameters under various physiological conditions.[17] The

neuroanatomical organization and specific innervation from both the sympathetic and

parasympathetic divisions of the autonomic nervous system to the cardiovascular system has

been reviewed previously[18] but has important implications for both cardiovascular dysfunction

following SCI and pharmacological treatment strategies and thus is discussed briefly **(Figure**

1.1).

      The degree of cardiovascular impairment is often related to both the injury level and

severity of injury.[19] However, the clinical classification of SCI severity, according to the

International Standards for Neurological Classification of Spinal Cord Injuries,[20] may not

correlate with the degree of cardiovascular impairment.[4] The breadth of cardiovascular

impairments following SCI have been discussed previously;[21] however, for the purposes of this

review, we will briefly outline how these major impairments in both the acute and chronic phases

are related to neuroanatomical changes.

1.3   Cardiovascular dysfunction following spinal cord injury

1.3.1   Acute cardiovascular dysfunction following spinal cord injury

In the acute phase after SCI individuals with cervical or high-thoracic SCI exhibit severe

cardiovascular dysfunction characterized by marked hypotension and bradycardia, termed

3

'neurogenic shock'.[22] These consequences are not surprising given that there is a substantial loss of descending excitatory sympathetic input onto sympathetic pre-ganglionic neurons (SPNs).[23, 24] In addition, parasympathetic innervation to the heart is always preserved following any level of SCI resulting in a consequent parasympathetic domination and ensuing bradycardia in individuals with high lesion SCI.[21] Although neurogenic shock subsides over time and heart rate and blood pressure will stabilize,[21] decreased resting values for blood pressure and heart rate often persist in the chronic phase, are significantly lower than matched able-bodied controls,[21] and are accompanied by abnormal cardiovascular reflexes.[25]

1.3.2   Autonomic dysreflexia

AD is the major cardiovascular reflex dysfunction following SCI, is characterized by dramatic increases in blood pressure ($\geq$20-40mmHg systolic) caused by a noxious or non-noxious stimulus below the level of injury (i.e., bladder distension, bowel impaction), and is often coupled with bradycardia (or rare tachycardia). AD is typically associated with headache, sweating, and piloerection;[6] however, the rise in blood pressure may not always be accompanied by overt symptoms, clinically termed "silent AD".[26, 27] Left untreated, AD may have significant, life-threatening consequences including intracranial hemorrhage, retinal detachments, seizures, and death.[28-30] The prevalence of AD has been well documented and the need to screen people with SCI for this and other autonomic impairments has now been recognized.[4, 31] It should be noted that while AD is most common in the chronic setting, it may also be present in a small percentage of people in the acute setting.[32] The development of clinically viable animal models of SCI has revealed at least two major mechanisms responsible for AD.

First, the integrity of descending supraspinal vasomotor input onto the SPNs (T1-L2) is crucial for the proper regulation of cardiovascular parameters and will influence the severity of AD. For example, the severity of AD is strongly correlated to the density of excitatory serotonergic labelled descending axons within the intermediolateral column, which synapse directly on SPNs.[33] We know that in an intact spinal cord these serotonergic axons are crucial to keep cardiovascular reflexes such as AD fleeting and small in amplitude.[34] In support of this finding, Krassioukov and Fehlings[24] determined, using various severities of injury and retrograde descending sympathetic axon tracing, that the severity of SCI is directly related to the amount of preserved connections with SPNs extending through the injury site from the rostro-ventro-lateral medulla (RVLM), the major cardiovascular regulatory center. Finally, post-mortem evidence from human SCI demonstrates that the extent of descending vasomotor pathways preserved below the injury site is directly related to the degree of cardiovascular dysfunction.[23] Thus, the loss of descending fibers from the RVLM is responsible for resting hypotension and likely prevents descending control from modulating incoming nociceptive information and may allow an environment permissive to abnormal cardiovascular reflexes such as AD.[23, 24, 33] In addition to the loss of descending excitatory pathways, it is also important to note that SCI results in a loss of descending supraspinal *inhibitory* pathways,[35] leaving spinal circuits hyperexcitable, including autonomic reflexes, which may also contribute to exaggerated sympathetic activity and subsequent AD.[36] Thus the basic and clinical evidence suggest AD is a multifactorial condition that results, in part, from a loss of both excitatory and inhibitory descending supraspinal pathways, and the subsequent imbalance in autonomic control.

The second mechanism of AD development has received a relatively large amount of attention in recent years. Namely, the degree of dorsal root intrusion and activation of calcitonin

gene-related peptide expressing (CGRP+) afferent fibers.[37] CGRP is a 37-amino acid peptide and is typically expressed by approximately 50% of both unmyelinated C fibers as well as thinly myelinated Aδ fibers within the dorsal root ganglia,[38] which primarily carry nociceptive information from the periphery and viscera to the spinal cord and terminate in Laminae I-II.[37] Following SCI, the number of CGRP+ containing fibers within Laminae III-V significantly increases.[37] Prior studies investigating the mechanisms of this neural growth suggest CGRP+ afferent neurons (primarily C, Aδ fibers) sprout and extend their axons from their proper location (Laminae I-II) into improper locations (Laminae III-V).[37] The improper location and increased number of CGRP+ axon terminals is thought to result in an inappropriately large amount of nociceptive information being carried into the dorsal horn, where it may influence sympathetic activity through interneuron connections. Previous theories have suggested the interneurons receiving information from the newly sprouted CGRP+ afferents could directly replace the vacated dendrite terminals on the SPNs to induce exaggerated sympathetic activity through spatial summation.[39] However, due to the significant loss of dendritic terminals found on SPNs following SCI,[40] it appears to be more likely the increased amount of incoming afferent information activates interneuronal networks across more spinal levels, influencing a larger number of SPNs without increasing the level of synaptic activity on each SPN.[36] Thus, the incoming nociceptive information plausibly travels rostral in the spinal cord via interneuronal and propriospinal circuits, ultimately exciting the SPNs and resulting in systemic vasoconstriction and a pressor response that defines AD.[41] The increased sprouting and movement of CGRP+ afferents, and subsequent activation of new intraspinal circuits[36] has been proposed as a mechanism for AD due to its time-course[37, 42, 43] and direct correlation to AD severity.[41, 44]

While we acknowledge there may be other mechanisms contributing to the development and severity of AD, such as peripheral plasticity in the dorsal root ganglia[45] as well as hyperexcitability of peripheral and visceral vasculature,[46-48] currently there are no published investigations of therapies targeting these mechanisms. Thus, we have briefly discussed two major mechanisms of AD development, decentralized descending sympathetic control and inappropriate CGRP+ afferent sprouting, which have currently been targeted by various therapies. In addition to the contribution of inflammatory and cell-signaling processes, which may influence these processes, these two mechanisms of AD development provide obvious targets for neural regenerative and protective therapies, which are discussed below.

1.3.3   Orthostatic hypotension

While AD typically results from a combination of impaired inhibitory supraspinal control and the presence of a stimulus (i.e., bladder distension, bowel impaction), persons with high level complete SCI may concomitantly endure other blood pressure abnormalities in the absence of such stimuli due to the parallel loss of descending excitatory vasomotor input onto the sympathetic nervous system,[24] such as OH. OH is defined as a significant drop in blood pressure upon sitting up from a supine position (decrease by ≥20 mmHg in systolic or ≥10mmHg diastolic).[49] OH appears to be more prevalent in persons with SCI above T5 and most prevalent in persons with complete cervical injuries compared to other injury levels and severities.[9] Since the sympathetic innervation to the splanchnic vascular bed occurs via SPNs predominately localized below T6 spinal segment, the cardiovascular impairment's dependence on injury level is not surprising. It has been suggested that persistent OH results from a variety of factors, including impaired excitatory supraspinal input, altered baroreceptor sensitivity, lack of skeletal

7

muscle pump, cardiovascular deconditioning, and altered salt and water balance.[50] Unfortunately, due to a lack of a reliable animal model, there have been few studies examining the exact neural mechanisms underlying OH and, to the authors knowledge, no neural regenerative or protective strategies to curb its development in pre-clinical studies. Therefore, the remainder of this review will focus on the effect of neural regeneration and protective strategies to improve AD.

1.3.4 A role for neural regeneration and protection strategies

Following traumatic injury, a host of biochemical processes occur that result in both positive and negative effects on the neurons in the spinal cord. For example, the influx of macrophages, neutrophils, and microglia approximately 4 days post injury will result in both the clearing of damaged myelin and the degradation of partially preserved neurons.[51-53] In addition, signaling molecules such as nerve growth factor (NGF) serve to enhance neural sprouting at the sympathetic ganglion as well as the dorsal root ganglion.[37] While researchers originally aimed to promote neuronal sprouting following SCI, we now know that inappropriate and unguided sprouting may promote the development of disorders such as AD.[37, 41, 44] Thus, it is evident that to improve cardiovascular control following SCI neural regenerative and protective treatments must take into consideration 1) the extent of inappropriate afferent sprouting in the dorsal root, 2) neuronal and biochemical signaling occurring at the injury site, and 3) preservation of descending sympathetic fibers from the RVLM, through the injury site.

1.4 Neural regeneration and protection for cardiovascular control

In contrast to the plethora of pharmacologic neural regenerative and protective treatments investigated to improve motor and sensory function,[54, 55] there have been relatively few studies

investigating the role of these treatments on cardiovascular function following SCI. Broadly, these studies have investigated three mechanisms to improve cardiovascular control and reduce AD. First, several studies in this area have focused on investigating mechanisms to inhibit the inappropriate sprouting of CGRP+ afferent fibers in the dorsal horn. Second, studies have examined the use of pharmacological drugs in reducing spinal cord inflammation following injury. Third, a small number of studies have investigated descending sympathetic axon regeneration strategies.
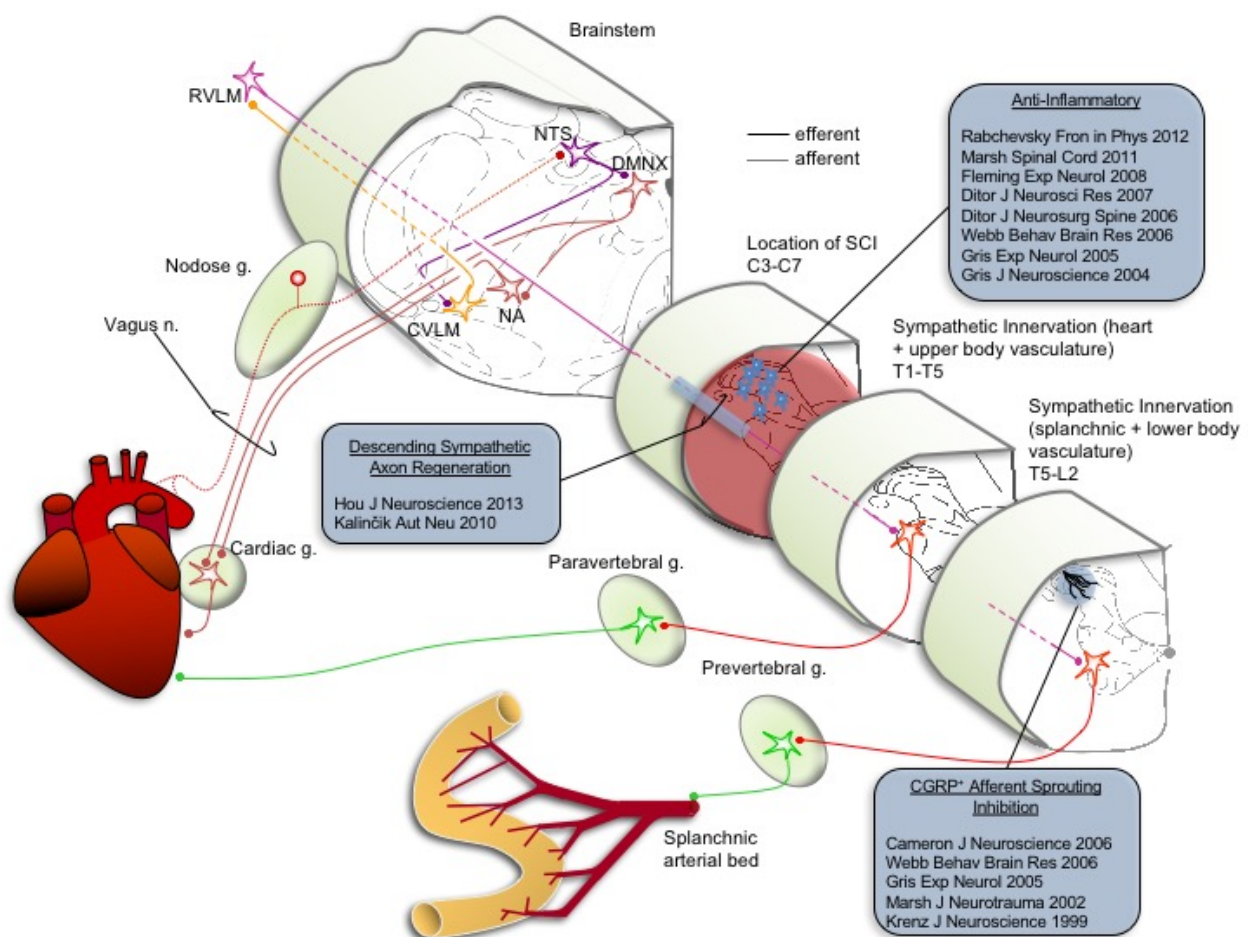
Figure 1.1: Autonomic organization and innervation of the cardiovascular system.

The autonomic nervous system is commonly separated into two divisions: the sympathetic and parasympathetic.[18] Each component is comprised of both pre-ganglionic and post-ganglionic

neurons. [18] Sympathetic pre-ganglionic neurons (SPNs) are located within the lateral horn, intermediolateral nucleus, and near the central canal within the spinal cord and are primarily influenced by descending sympathetic neurons, which mainly originate in the RVLM. [18] In the thoracic segments (T1-T10) and upper lumbar segment's (L1-L2) SPNs exit the spinal cord through the intervertebral foramen, enter the paravertebral or prevertebral sympathetic ganglion, and synapse onto post-ganglionic neurons in the sympathetic chain ganglia.[18] From this point, the post-ganglionic neurons either exit the ganglion, extend into other ganglia within the sympathetic chain, or extend their axons to exert effects on cardiovascular end organs.[18] Post-ganglionic sympathetic neurons exiting from paravertebral ganglia in the T1-T5 segments will exert their influence on both the heart and on the peripheral vasculature in the upper body.[21] These fibers will serve to increase heart rate, contractility, and conduction velocity and to regulate upper limb peripheral vascular diameter.[21] Likewise, post-ganglionic sympathetic neurons exiting from preverterbral ganglia in the T6-T10 region are responsible for the regulation of abdominal and lower limb peripheral vasculature.[21] One crucial note is that within the abdomen and innervated at the T6 level is the splanchnic vasculature bed. This vasculature bed is highly innervated, highly compliant and, at any given time, houses approximately one-fourth of the blood volume in a human.[17] Therefore, autonomic control over this vasculature bed is crucial to maintain cardiovascular haemodynamics. Within the parasympathetic system, often referred to as the "rest and restore" system, pre-ganglionic neurons originate from four cranial nerves (CN III, VII, IX, X) and in sacral spinal cord levels (S2-S4).[18] Parasympathetic pre-ganglionic neurons responsible for cardiovascular regulation (CN X) originate in the rostral medulla and exit the skull through the jugular foramen.[18] The pre-ganglionic neuron then extends well outside the CNS and synapses onto a post-ganglionic neuron within a parasympathetic

ganglion, often near the effector organ.[18] Parasympathetic activity has the opposite effect on physiological parameters compared to the sympathetic division. Post-ganglionic parasympathetic fibers then exert their influence on the sino-atrial node and purkinje fibers, ultimately reducing heart rate, contractility, and conduction velocity.[18] In contrast to the sympathetic division, the parasympathetic system exercises little effect on the peripheral vasculature.[17] Thus, unlike the cardiac structure, where it is the balance between sympathetic and parasympathetic activity that governs its function, it is the removal of sympathetic activity and not the influx of parasympathetic activity that serves to control the contractile state of the peripheral vasculature. Proposed pharmacological mechanisms of action are schematically represented in blue with relevant studies listed (**see Table 1.1**). Abbreviations: AR: adrenergic receptors; CVLM: caudal ventrolateral medulla; DMNX: dorsal vagal motor nerve; g: ganglion; NA: nucleus ambiguous; n: nerve; NTS: nucleus of the solitary tract; RVLM: rostral ventrolateral medulla; (+) denotes excitatory synapses; (-) denotes inhibitory synapses.

1.4.1   Reducing inappropriate afferent sprouting

The investigation of inappropriate afferent sprouting below the level of injury has been one of the most studied mechanisms of AD development following SCI.[37, 41, 44, 56-58] It has been well established that the intrusion of CGRP+ afferents into Laminae III-V is directly related to the development and severity of AD.[37] Subsequently, several neuroprotective agents have been tested to improve cardiovascular control following SCI through this mechanism. Since the original description of this sprouting phenomenon and its relation to AD[37] there have been five studies investigating treatments to reduce the development and size of the CGRP+ dendritic arbor.[41, 44, 56-58] The first, by Krenz and colleagues, targeted NGF to reduce the severity of

11

sprouting. Using an anti-NGF polyclonal neutralizing antibody Krenz and colleagues aimed to reduce the concentration of NGF in the spinal cord following a T4 complete transection and subsequently inhibit CGRP+ sprouting into Laminae III-V of the thoracolumbar cord. Intriguingly, they were successful in reducing intraspinal NGF and were able to significantly reduce the severity of AD resulting from colorectal distension (CRD) by 43% and completely abolished aberrant CGRP+ sprouting.[44] Furthermore, a significant correlation was observed between the severity of AD (increase in mean arterial pressure (MAP)) and the extent of afferent sprouting *(r = 0.8)*.[44] Thus, NGF appeared to be a strong target to reduce CGRP+ sprouting and consequently the severity of AD. Along these lines of enquiry, another study used a soluble receptor trkA-IgG fusion protein to sequester NGF concentration in the spinal cord following a severe clip compression injury.[57] The authors postulated that this was an improvement upon previous work[44] as the trkA-IgG fusion protein was a more selective inhibitor of NGF and that the clip compression model was more clinically relevant.[57] Encouraging evidence was provided in this clinically relevant model, as a significant decrease in AD severity was observed *(35% reduction)*. Unfortunately, the authors did not include an immunocytochemistry analysis of CGRP+ afferent sprouting.[57] Thus, while this work provides convincing evidence for the role of NGF in the development and severity of AD, further studies are needed to conclusively demonstrate the effect of the trkA-IgG fusion protein on aberrant CGRP+ afferent sprouting. Interestingly, the findings from these two studies are supported by a more recent study investigating the effect of transcriptional manipulation of NGF-related genes.[41] Using a T4 complete transection model, NGF promoting (*NGF-Adts*) or NGF inhibiting (*Sema3a Adts*) adenoviruses were injected into various thoracolumbar levels following the injury. Similar to the work by Krenz and colleagues, overexpression of NGF through *NGF-Adts* resulted in a

significant increase in CGRP+ sprouting and subsequent exacerbation of AD severity.

Conversely, inhibition of NGF production by *Sema3a Adts* overexpression resulted in decreased

intraspinal NGF concentration, decreased dendritic arbor cross-sectional area, and a decrease in

AD severity.[41] Lastly, the authors were also able to demonstrate a significant correlation between

the severity of AD (increase in CRD evoked MAP) and the percent CGRP+ areal coverage

(r=0.587, p < 0.0001).[41] In conjunction with the correlation found by Krenz et al[44] *(r=0.8)*, as

well as the time-course relationship to AD development, these results converge to allow the

interpretation that the degree of CGRP+ afferent arborization within the dorsal root is directly

related to and responsible for the development and severity of AD. Further, it appears a reduction

in CGRP+ areal coverage to ~10% of the defined dorsal grey area may likely reduce AD severity

to such an extent that the pressor response would not classify as AD according to clinical

guidelines.[41] While the correlation found by Cameron et al[41] is weaker than that found by Krenz

et al,[44] their results provide convincing evidence for the role of NGF in promoting AD and for

the role of CGRP+ afferents. In fact, the comparison between the two studies may be limited by

varying blood pressure recording techniques as well as the inherent variability of CRD (i.e.

animal position, catheter, inflation volume), despite the author's efforts to standardize the

assessment.

      Two other studies have examined the level of CGRP+ sprouting and, despite showing

improvements in AD, did not show a similar reduction in dendritic arbor cross-sectional area.[56,
58] While the studies were primarily interested in the anti-inflammatory effects of 17β-estradiol[58]

and the anti-CD11d monoclonal antibody (mAb),[56] their findings on CGRP+ afferent arbor area

are worth noting. The effect of 17β-estradiol on reducing AD severity is similar to previous work

(~60% reduction); however, the authors were not able to statistically demonstrate a reduction in

CGRP+ sprouting at the T7-8 *(p = 0.23)*, T11-12 *(p = 0.14)*, or L2-L3 *(p = 0.26)* level.[58] While

comparisons to the above studies[41, 44, 57] are difficult due to the use of a mouse transection model

(Table 1.1), previous studies using mice models had found a correlation between CGRP+ arbor

area and the severity of AD.[59] Thus, the mechanism by which 17β-estradiol reduces AD severity

is still unclear. This finding is paralleled by one other study showing not only no change in

CGRP+ sprouting but, in fact, an increase.[56] Following the treatment of either

methylprednisolone, anti-CD11d mAb, or a combination treatment, Gris and colleagues

demonstrated a *50% decrease* in AD severity (MAP increase following CRD) after each

treatment, with no differences between treatments. However, at a 6-week follow up it was found

that only the anti-CD11d mAb treatment effect persisted. These findings were accompanied by

an *increase* in the CGRP+ dendritic arbor area.[56] The authors note that their findings are not in

contrast to previous work[41, 44] but rather provide evidence that AD severity can be reduced

through different mechanisms.

Overall, there is strong evidence that inappropriate CGRP+ dendritic sprouting plays a

role in the development and severity of AD.[37] In addition, the role of NGF appears to be crucial

in the development of the dendritic arbor and thus provides a mechanism to inhibit this aberrant

activity.[41, 44, 57] Unfortunately, these studies used a variety of animal and injury models and

various methods to influence CGRP+ sprouting, it is difficult to compare across studies. In

addition, a lack of dose-response data and consistent methodology limit the current translational

potential of this therapy and highlight a need to further investigate this mechanism in relation to

cardiovascular control.

As some of the noted studies demonstrate improvements in AD without an accompanied

decrease in CGRP+ sprouting,[56, 58] it is likely other mechanisms such as anti-inflammatory

14

properties or the integrity of descending sympathetic axons also play a role in reducing the severity of AD. In fact, Gris and colleagues suggest that the observed increase in CGRP+ sprouting found following methylprednisolone or anti-CD11d mAb treatment may reflect a consequence of the anti-inflammatory properties of their treatment. Specifically, the reduction of inflammation and further secondary injury processes may have created a more permissive environment for dendritic sprouting to occur,[56] Therefore, an examination of the existing evidence of anti-inflammatory pharmacology effects on reducing AD severity is warranted.

1.4.2 Anti-inflammatory strategies

Following the initial trauma of an SCI (primary injury) there are a host of biochemical processes that subsequently result, termed the 'secondary injury'. The secondary injury process is initially triggered by ischemia, often caused by trauma to the spinal column resulting in disruption to the blood-brain barrier, vasospasm, and intraparenchymal hemorrhage.[51] The ischemia then triggers a series of inflammatory processes including the influx of macrophages, neutrophils, microglia, a variety of cytokines, and matrix metalloproteinases.[52, 53, 60-62] The influx of these cells and the subsequent degradation of neuronal tissue propagate the secondary damage and lead to free radial generation and lipid peroxidation, resulting in the destruction of cellular membranes.[63, 64] The vast destruction of cellular tissue results in a dramatic release of glutamate and subsequent excitotoxicity. These processes ultimately lead to destruction of neural and glial cells through necrosis and signaled apoptosis. Despite the superfluous damage caused by both the primary and secondary injuries it is well known that few SCIs result in complete destruction of all ascending and descending fibers.[65] Thus, therapies targeted at preventing secondary damage and thus preserving maximal amounts of neural tissue are crucial. Anti-inflammatory therapies have been

extensively studied to improve motor and sensory function following SCI;[55] however, their effect on cardiovascular control is less well described.

To date there have been eight studies investigating anti-inflammatory therapies for the treatment of cardiovascular abnormalities following SCI.[56, 58, 66-71] Of these studies, four used similar conceptual models[56, 66, 67, 69] and will be discussed first. Upon central nervous system injury, damaged endothelial cells produce a variety of cytokines and chemokines that trigger the expression of the vascular adhesion molecule-1 *(VCAM-1)* on the surface of endothelial cells.[56] Likewise, the cytokines and chemokines also trigger the expression of the α4β1 and β2 integrins on the surface of leukocytes.[72] The interaction between *VCAM-1* and α4β1/β2 allows the adhesion of leukocytes to endothelial cells, bringing them across the blood-brain barrier into the central nervous system.[72] Thus, it is the function of these two molecules that the first four studies have attempted to inhibit.[56, 66, 67, 69] The first used intravenous treatment of rats with a mAb to the CD11d/CD18 subunit of the β2 integrin and was effective in inhibiting the initial influx of macrophages and neutrophils.[67] Importantly, this transient adhesion block subsided to allow the delayed inflammation response to occur, a crucial aspect of wound healing and subsequent functional recovery.[73] The treatment led to an increase in properly orientated, myelinated axons and approximately a *50% decrease* in AD severity following CRD.[67] A subsequent study investigated the effect of the CD11d/CD18 mAb in comparison with a well-known anti-inflammatory drug, methylprednisolone.[56] Only the CD11d mAb treatment led to a significant reduction in macrophages within the injury site and, thus, a decrease in injury area.[56] This was accompanied by a *50% reduction* in AD severity at both 2 and 6 weeks post injury. In contrast, methylprednisolone did not result in a significant reduction of macrophages and only reduced the severity of AD at the 2 week but not the 6 week time point.[56] It is likely methylprednisolone was

less effective due to its more widespread effect on both the early and late inflammatory responses. Conversely, the specific CD11d/CD18 mAb treatment acted only on the intial influx of neutrophils and macrophages and thus had a more beneficial effect.[56] Ditor and colleagues followed up on this work and sought to determine the therapeutic time window for the anti-CD11d mAb treatment in order to bring more clinical relevance and increase its translational potential.[69] It appears the time window is limited to approximately 6 hours as this was the maximum time post-injury the anti-CD11 mAb was given and still significantly reduced the severity of AD.[69] Additionally, the authors provided a host of mechanistic evidence, demonstrating reduced leukocyte and macrophage influx, reduced DNA oxidation and iNOS concentration, as well as a reduction in reactive oxygen species, COX-2 expression, lipid peroxidation, and protein oxidation.[69] While these three studies laid the groundwork for reducing inflammatory processes to improve AD, one further study has built upon this body of knowledge.[66] Fleming and colleagues exposed a more robust integrin target expressed by leukocytes, the $\alpha 4\beta 1$ integrin, and delivered an intravenously delivered mAb of this integrin at 2 and 24 hours post SCI. The $\alpha 4\beta 1$ mAb significantly reduced the initial influx of neutrophils and macrophages, in line with previous studies.[56, 67] In addition, a significant reduction in various oxidative enzymes, free radical formation, and lipid peroxidation as well as increased preservation of serotonergic axons were also observed.[66] The decrease in inflammation, reduced oxidative damage, and improved neural preservation were also accompanied by an *~50% reduction* in AD severity following CRD.[66] Although the inclusion of oxidative damage and further characterization of neural preservation was conducted, there does not appear to be any significant improvement with the $\alpha 4\beta 1$ mAb treatment versus the CD11d mAb treatment, as reflected by similar AD improvements.[56, 66, 67, 69] While the authors suggest the $\alpha 4\beta 1$ mAb is

17

likely more robust and should have more diverse actions[66] further data is needed to support this contention and improve future treatments that target this specific adhesion mechanism.

Four further studies have examined anti-inflammatory effects on AD; however, they have not based their hypotheses on endothelial-leukocyte adhesion.[58, 68, 70, 71] Intravenous delivery of Reparixin, an allosteric non-competitive inhibitor of G-protein-coupled GXCR2 and CXCR2 receptors significantly reduced AD by 40-50%.[68] Reparixin acts by blocking the signaling cascade for neutrophil recruitment and thus acts as an anti-inflammatory. In addition, Reparixin was also shown to decrease macrophage concentration as well as Fas and p75 levels in the spinal cord following injury, markers of SCI-induced apoptosis[74] and increased neural preservation.[68] In another study, Webb and colleagues demonstrated reduced severity of AD without a concominant reduction in microglia or macrophage intrusion following 17β-estradiol treatment.[58] Unfortunately the authors were not able to determine the exact mechanism by which 17β-estradiol improves AD, as they showed no reduction in CGRP+ sprouting or inflammatory reaction. However, further examination into a broader scope of inflammatory cells and investigation into other classes of primary afferents may elucidate 17β-estradiol's mechanisms. Only one study has investigated the use of magnesium sulfate and polyethelene glycol (PEG) on reducing AD.[70] Neither of these individual agents nor a combination treatment reduced AD severity; however, magnesium sulfate or PEG, given alone, improved basal MAP compared to control, although not significantly.[70] This was accompanied by an increase in myelin preservation and a decrease in lesion volume.[70] Lastly, Rabchevsky and colleagues provided evidence that gabapentin may be able to reduce the severity of AD following acute treatment.[71] However, daily treatment with gabapentin provided no significant improvements in basal MAP or HR and had no effect on AD severity.[71] Thus, while the authors propose gabapentin may exert

its beneficial effect by reducing glutamate release (a crucial inflammatory cascade step), it does not appear gabapentin mainly acts through neuroprotective effects but rather acts as an acute, transient therapy.

While anti-inflammatory therapies will likely be a crucial aspect in future treatments, they appear to be limited to a *reduction* in AD severity, with no studies demonstrating complete amelioration. The homogeneity in animal (Wistar) and injury (T4 clip compression) models in addition to consistent dosage of the CD11d mAb (1mg/kg @ 2, 24, and 48hrs) are encouraging and place this therapy at the forefront of reducing inflammation and improving cardiovascular outcomes.[56, 67, 69] In addition, the move towards a more robust integrin target ($\alpha 4\beta 1$) is an important next step in this mechanism and is likely to yield further encouraging results. However, while anti-inflammatory agents and possibly combined therapy including a suppressor of CGRP+ afferent sprouting may improve cardiovascular outcomes, these neuroprotective treatments will always be limited to the functionality of often minimal surviving axons. Thus, a third line of research is necessary to investigate the use of various cell lines in order to promote the regeneration of descending sympathetic axons within the spinal cord, re-establish supraspinal control, and improve cardiovascular outcomes.

1.4.3   Increasing preservation of descending supraspinal input

The loss of tonic activity from supraspinal sympathetic neurons to the spinal cord is, as discussed, a major cause of cardiovascular dysfunction following SCI. Therefore, treatment approaches that serve to regenerate these neural circuits may prove fruitful in the amelioration of cardiovascular dysfunctions such as AD following SCI. Despite a wealth of research

investigating the effects of regenerative approaches on motor and sensory function[75] only two studies have examined the effect of introducing stem cells on cardiovascular function.[16, 76]

The first of these studies implanted olfactory ensheathing cells, harvested from within each animal, to improve AD following SCI.[76] Although no improvements in basal MAP or HR were observed, the olfactory cell transplantation significantly reduced the duration of AD episodes by 25%.[76] In addition, the authors also observed a decrease in sympathetic pre-ganglionic soma size compared to control animals at 9 weeks post T4 transection. In a follow up study the authors investigated a host of variables to explain the underlying mechanisms behind the improvement.[77] Unfortunately, the authors observed no neural regeneration, decrease in CGRP+ sprouting, or decrease in injury size and thus attributed the improvements in AD following cell treatment to the cells' release of beneficial trophic factors such as brain-derived neurotrophic factor and glial cell-derived neurotrophic factor, known to promote neuron survival.[77] While this study was a strong attempt at inducing axonal regeneration, the olfactory ensheathing cells appear to act more as a neuroprotective strategy than a regeneration strategy.

More recently, Hou and colleagues investigated the effects of brain-stem derived and spinal cord-derived neural stem cell injection into the spinal cord on cardiovascular function.[16] Following the implantation of brain-stem derived neural stem cells a marked reduction *(~50%)* in AD severity following CRD was observed.[16] In addition, a remarkable recovery of basal MAP and HR was also observed. This finding is particularly unique when considering that none of the previously discussed treatments were able to restore basal cardiovascular parameters to pre-injury baseline.[41, 44, 56-58, 66-71, 76] The re-establishment of basal cardiovascular parameters highlights a major mechanistic difference in neural regeneration versus protection therapies. It appears the restoration of basal MAP and HR may be contingent upon tonic supraspinal input

from regenerated catecholaminergic and serotonergic neurons.[16] Thus, it is likely neuroprotection alone may not be sufficient to improve basal cardiovascular parameters, especially in severe injuries. In fact, the authors reject the notion that the observed restoration of basal haemodynamics and reduction in AD severity are a result of growth factor-mediated neuroprotective influences and that, instead, they are a result of regenerated descending input through stem-cell grafts. This notion is supported by a strong control group that was implanted with spinal cord-derived neural stem cells (with the same growth factor solution), which showed significantly less cardiovascular improvements. Additionally, re-transection of the spinal cord below the level of transplantation abolished any observed functional recovery, suggesting a crucial role for descending sympathetic input. Although the authors observed a remarkable restoration of basal MAP and HR, the reduction in AD severity was similar to that found in previous studies *(~50%)* targeting CGRP+ sprouting or inflammatory processes. Therefore, while stem cell therapy holds great promise in improving basal cardiovascular parameters, it is likely a combination approach is needed to attend to the various other mechanisms responsible for the development of AD.

Table 1.1 Neural regenerative and protective effects on cardiovascular outcomes

Paper	Animal Model & Injury Model	Intervention & Timing	Experimental Groups	Reported Outcomes:
Hou *J Neuroscience* 2013	*Model:* Adult Female Fischer Rats, 150-200g *Injury:* T4 Complete Transection	**E14 BS-NSC Transplantation:** • 10μl @ 2 wks PI **SC-NSC Transplantation:** • 10μl @ 2 wks PI	SCI + **BS-NSC (n = 16)** **SC-NSC (n = 9)** Control (n = 11)	*Cardiovascular:* BS-NSC restores baseline MAP and HR values. BS-NSC reduces severity of AD @ 8 wks post-implantation (10wks PI). *Histologic / Biochemical:* BC-NSC and SC-NSC transplantation reduced glial scar, showed excellent innervation. BC-NSC axons extended into IML and created catecholaminergic synapses.
Rabchevsky *Frontiers in Physiology* 2012	*Model:* Adult Female Wistar Rats, 225g *Injury:* T4 Complete Transection	**Gabapentin IP:** • 50mg/kg @ 1d PI	SCI+ **Gabapentin (n = 5)** Saline (n = 6)	*Cardiovascular:* Gabapentin showed no significant treatment effect on MAP or HR following SCI. Acute, not chronic, administration of gabapentin reduced AD severity compared to saline. Bradycardia was also improved but not significantly. *Histologic / Biochemical:* Not reported.
Marsh *Spinal Cord* 2011	*Model:* Adult Female Wistar Rats, 225g *Injury:* T4 Clip Compression (60s @ 35g)	**Reparixin IV:** • 11.5mg/ml, 300μl then 15mg/kg @ 12 hr PI • 11.5mg/ml, 300μl then 15mg/kg @ 72 hr PI • 11.5mg/ml, 300μl then 7.5mg/kg @ 72 hr PI	SCI+ (n = 6 for all) **Reparixin 15 @ 12hr** **Reparixin 15 @ 72hr** **Reparixin 7.5 @ 72hr**	*Cardiovascular:* Low and high dose Reparixin improved AD following CRD and cutaneous stimulation @ 28 days PI. Average and peak MAP was diminished but no effect on HR during CRD or cutaneous stimulation. *Histologic / Biochemical:* Low and high dose Reparixin reduced TNF-α, CINC-1, and macrophage content @ 72hr PI. High dose Reparixin reduced Fas and p75 levels compared to control. Reparixin reduced the lesion area and increased grey matter neuron counts compared to controls.
Kalinčík, *Aut Neu* 2010	*Model:* 11-14 Week Male Australian Albino Wistar Rats, 350-400g *Injury:* T4 Complete Transection	**OEC Transplantation:** • 2 μl Gelfoam sponge soak (500,000 cells/μl)	SCI+ **OEC-Treated (n = 6)** Culture Medium (n = 7) *remainder of animals used for cell survival study (n = 18)	*Cardiovascular:* OEC treatment had no effect on resting MAP or HR values. Conversely, OEC treatment reduced AD severity (decrease in MAP change, not HR) and duration starting at 21 days PI. *Histologic / Biochemical:* Sympathetic preganglionic neurons rostral to the injury site treated with OECs showed greater dendritic process length. OEC treatment decreased soma size in neurons caudal to the injury compared to controls.
Fleming *Exp Neurol* 2008	*Model:* Adult Female Wistar Rats *Injury:* T4 Clip Compression (60s @ 35g)	**Anti-α4β1 mAb IV:** • 2.5 mg/kg @ 2h or at 2hr and 24hr PI **Control mAb IV:** • 2.5 mg/kg @ 2hr or at 2hr and 24hr PI	SCI+ **Anti-α4β1 mAb (n = 6)** **Control mAb (n = 6)** Saline (NR)	*Cardiovascular:* Anti-α4β1 mAb did not improve resting MAP or HR but reduced the severity of AD (decreased MAP following CRD (2-4wks PI)). *Histologic / Biochemical:* Anti-α4β1 mAb decreases neutrophil and monocyte/macrophage influx into injured spinal cord, reduces oxidative damage (reduced oxidative enzymes, free radicals), and improves serotonergic axon integrity.

(continued)

22

Paper	Animal Model & Injury Model	Intervention & Timing	Experimental Groups	Reported Outcomes:
Ditor *J Neurosci Res* 2007	*Model:* Adult Male Wistar Rats, 200-250g *Injury:* T4 Clip Compression (60s @ 50g)	**PEG IV:** • 1g/kg @ 15min and 6hr PI **MgSO₄ IV:** • 300mg/kg @ 15min and 6hr PI	SCI+ **PEG (n = 10)** **MgSO₄ (n = 5)** **MgSO₄ in PEG (n = 6)** Vehicle (n = 10)	*Cardiovascular:* Neither PEG, MgSO₄, or combined treatment improved the severity of AD following CRD @ 40 days PI. However, both PEG and MgSO₄ improved basal MAP. Combined treatment had no significant effect on basal MAP. *Histologic / Biochemical:* MgSO₄ and combined treatment significantly increased myelin sparing dorsal to the lesion epicenter. In addition, combined treatment significantly reduced the lesion volume. At the lesion epicenter, treatment with MgSO₄ significantly improved myelin sparing.
Ditor *J Neurosurg Spine* 2006	*Model:* Adult Female Wistar Rats, 250-300g *Injury:* T4 Clip Compression (60s @ 50g)	**Anti-CD11d 217L mAb IV:** • 1mg/kg @ 2, 24, and 48hr PI or @ 6, 24, and 48hr PI or @ 12, 24, and 48hr PI or @ 24 and 48hr PI **IB7 control mAb IV:** • 1mg/kg @ 2, 24, and 48h PI or @ 6, 24, and 48hr PI or @ 12, 24, and 48hr PI or @ 24 and 48hr PI	SCI+ **Anti-CD11d mAb (n = 43)** IB7 (n = 44) No SCI (n = 10)	*Cardiovascular:* Anti-CD11d mAb treatment significantly reduced the severity of AD following CRD at 5wks PI. This effect persisted when animals were delayed treatment until 6h PI. No change in basal MAP was observed. *Histologic / Biochemical:* Anti-CD11d mAb treatment starting at 2hr or 6hr reduced MPO (leukocyte), ED-1 (macrophage) activity, DNA oxidation, and iNOS @ 72hrs PI but not when treatment started at 12hr. Reactive oxygen species, COX-2 expression, lipid peroxidation, and protein oxidation @ 72hr PI were reduced with treatment starting @ 2hr, 6hr, and 12hr but not at 24hr. Protein nitration was reduced @ 72hr only if treatment started at 2hr.
Cameron *J Neuroscience* 2006	*Model:* Adult Female Wistar Rats, 250g *Injury:* T4 Complete Transection	**NGF Adts PI:** • 500nl of 5x10⁶ pfu/μl @ 0 days **GFP Adts (control) PI:** • 500nl of 5x10⁶ pfu/μl @ 0 days **Sema3a Adts PI:** • 500nl of 5x10⁶ pfu/μl @ 0 days	SCI+ **NGF Adts T5/6 (n = 5)** **GFP Adts T13/L1 (n = 5)** **NGF Adts T13/L1 (n = 9)** **GFP Adts L6/S1 (n = 9)** **NGF Adts L6/S1 (n = 8)** **Sema3a Adts L6/S1 (n = 14)** Sham (n = 9) Uninjured control (n = 3)	*Cardiovascular:* Overexpression of NGF in the lumbar segments significantly increased AD in response to CRD at 14 days PI. Conversely, overexpression of Sema3a significantly reduced AD compared to GFP Adts controls. Decrease in AD was characterized by a decrease in MAP following CRD but no change in HR. *Histologic / Biochemical:* Overexpression of NGF led to increased CGRP+ afferent sprouting into Laminae III-V. Overexpression of Sema3a led to the opposite effect and the CGRP+ fiber area in Laminae III-V was correlated with severity of AD.
Webb *Behavioural Brain Research* 2006	*Model:* 3-4 Month Old Male B6; 129-UCP2^tmlLowl and B6; 129 Mice *Injury:* T2 Complete Transection	**17β-estradiol SC:** • 0.5mg pellet @ -1wk (3 wk constant rate release)	SCI+ **17β-estradiol (n = 7)** Placebo (n = 7) *remainder of animals used for serum concentration evaluation (n = 32)	*Cardiovascular:* 17β-estradiol treatment reduced AD in response to CRD but not cutaneous stimulation (decrease in MAP response) in both WT and KO mice at 14 days PI *Histologic / Biochemical:* CGRP+ arbor size was not decreased following treatment with 17β-estradiol. 17β-estradiol also had no effect on microglia or macrophage intrusion into the injury site.

(continued)

23

Paper	Animal Model & Injury Model	Intervention & Timing	Experimental Groups	Reported Outcomes:
Gris *Exp Neurol* 2005	*Model:* Adult Female Wistar Rats, 230g *Injury:* T4 Clip Compression (60s @ 50g)	**Methylprednisolone IV:** • 30mg/kg @ 2hr then 15mg/kg at 24 and 48hr **Anti-CD11d mAb IV:** • 1mg/kg @ 2hr then 1mg/kg at 24 and 48hr **Methylprednisolone + Anti-CD11d 217L mAb IV:** • 30mg/kg @ 2hr then 15mg/kg at 24 and 48hr • 1mg/kg @ 2hr then 1mg/kg at 24 and 48hr	SCI+ (@ 2wks) **Methylprednisolone (n = 7)** **Anti-CD11d mAb: (n = 10)** **Methylprednisolone + Anti-CD11d mAb (n = 7)** **Control mAb/Saline (n = 14)** SCI+ (@ 6wks) **Methylprednisolone (n = 6)** **Anti-CD11d mAb: (n = 7)** **Control mAb (n = 7)**	*Cardiovascular:* Methylprednisolone and anti-CD11d mAb reduced AD and improved MAP @ 2wks. Only anti-CD11d improved AD @ 6wks but not resting MAP. Combined treatment did not show additive effects. *Histologic / Biochemical:* Methylprednisolone and anti-CD11d mAb treatment increased CGRP+ arbor near the injury site. Both treatments also reduced macrophage infiltration into the injury site.
Gris *J Neuroscience* 2004	*Model:* Adult Female Wistar Rats *Injury:* T4 Clip Compression (60s @ 50g)	**Anti-CD11d 217L mAb IV:** • 1mg/kg @ 2hr then 1mg/kg at 24 and 48hr	SCI+ **Anti-CD11d mAb: (n = 10)** **Control mAb (n = 14)**	*Cardiovascular:* anti-CD11d mAb treatment significantly reduced AD following CRD @ 2 and 6 wks but had no effect on resting MAP or HR. *Histologic / Biochemical:* anti-CD11d mAb treatment improved myelin sparing following SCI and increased neurofilament volume, reflecting sparing of both grey and white matter rostral and caudal to the injury site.
Marsh *J Neurotrauma* 2002	*Model:* Adult Female Wistar Rats, 250-370g *Injury:* T4 Clip Compression (60s @ 50g)	**trkA-IgG IT:** • 4μg/day @ 0 days **human IgG IT:** • 4μg/day @ 0 days	SCI+ **trkA-IgG (n = 6)** **human IgG (n = 6)**	*Cardiovascular:* trkA-IgG reduced AD following CRD and cutaneous stimulation at 14 days PI but had no effect on HR responses during CRD or cutaneous stimulation. *Histologic / Biochemical:* trkA-IgG significantly reduced presence of NGF in spinal cord.

Krenz *J Neuroscience* 1999	**Model:** Adult Male Wistar Rats, 300-400g **Injury:** T4 Complete Transection	**Anti-NGF Ab IT:** • 0.2mg/ml @ 5.4 µl/hr (entire cord) • 0.08mg/ml @ 5.4 µl/hr (lumbar cord only) **Nonimmune IgG IT:** • 0.2mg/ml @ 5.4 µl/hr (entire cord) **Anti-NGF Ab SC:** • 0.4mg/ml @ 5.4 µl/hr	SCI+ (n = 6 for all) **Anti-NGF Ab IT (entire cord)** **Anti-NGF Ab IT (lumbar cord only)** **Nonimmune IgG IT (entire cord)** Sterile CSF (lumbar cord only) **Anti-NGF Ab SC** Saline SC	*Cardiovascular:* Anti-NGF Ab (entire cord) significantly reduced AD following CRD at 14 days PI. MAP response to CRD was reduced but no effect on HR was demonstrated. MAP responses to CRD were strongly correlated with afferent arbor area. *Histologic / Biochemical:* Anti-NGF Ab (entire cord) significantly reduced CGRP+ fiber sprouting into Laminae III-V. Anti-NGF effect was localized, evidenced by reduced sprouting in lumbar only group (within subject control) and was not a result of reduction in peripheral NGF (SC group).

Ab: antibody; AD: autonomic dysreflexia; Adts: temperature-sensitive adenoviruses; BS-NSC: brain-stem derived neural stem cells; CGRP-IR+: calcitonin gene-related peptide immunoreactive; CINC-1: cytokine-induced neutrophil chemoattractant-1; COX-2: cyclooxygenase-2;CRD: colorectal distension; CSF: cerebrospinal fluid.d: day, days; DNA: deoxyribonucleic acid; g: grams; E14: embryonic day 14; GFP: green fluorescent protein; HR: heart rate; hr: hour, hours; IgG: immunoglobulin G; IML: intermediolateral fasciculus; iNOS: inducible nitric oxide synthase; IB7: isotype matched irrelevant antibody; IP: intraperitoneal; IT: intrathecal; IV: intravenous; kg: kilograms; KO: knock-out; L1: lumbar vertebra 1; L6: lumbar vertebra 6; mAb: monoclonal antibody; MAP: mean arterial pressure; mg: milligrams; MGSO$_4$: magnesium sulfate; min: minute, minutes; ml: milliliters; MPO: myeloperoxidase; NGF: nerve growth factor; nl: nanoliter; NR: not reported; OEC: olfactory ensheathing cells; PEG: polyethylene glycol; PI: post injury; pfu: plaque forming unit; s: second, seconds; S1: sacral vertebra 1; SC: subcutaneous; SCI: spinal cord injury; SC-NSC: spinal cord-derived neural stem cells; Sema3a: semaphorin-3A; T2: thoracic vertebra 2; T4: thoracic vertebra 4; T5: thoracic vertebra 5; T6: thoracic vertebra 6; T13: thoracic vertebra 13; TNF-α: tumor necrosis factor-alpha; trkA: tyrosine kinase receptor type 1; UCP2: uncoupling protein 2; wks: week, weeks; WT: wild-type; α4β1: alpha-4-beta-1 integrin; µl: microliter

1.4.4   Necessity for translational approaches

While most pre-clinical and clinical investigations currently seek to improve motor function, it is clear from the neuroanatomy and pre-clinical data that stem-cell therapy may improve cardiovascular control and, possibly, other autonomic functions. This provides clinicians and researchers a clear rationale to include clinically relevant measures of cardiovascular control such as blood pressure, heart rate, as well as incidence of OH and AD. In fact, international standards to document these functions are already in use.[3] In summary, a multi-disciplinary approach must be used to investigate pre-clinical approaches while also expediting the translational process by including cardiovascular outcome measures.

1.5   Conclusions

There are currently 13 studies investigating neural regenerative and protective pharmacological approaches to improve cardiovascular function following SCI (**Table 1.1).** These studies have investigated a variety of targets to reduce the severity of AD including aberrant CGRP+ afferent sprouting, anti-inflammatory cascade mechanisms, and neuron regeneration therapies. While most studies observed a reduction in the severity of AD, none were able to completely ameliorate it and only one study was able to restore basal MAP and HR following SCI.[16] Given that CVD is the leading cause of death in this population, we hope that further studies exposing molecular, neuronal, and behavioural aspects of cardiovascular dysfunction, while addressing novel pharmacological and non-pharamacological treatments and acute effects, will facilitate the translational process for people with SCI and other traumatic or neurodegenerative diseases, while improving our mechanistic understanding of autonomic cardiovascular control.

Chapter 2: Overall thesis goals and hypotheses

This thesis will seek to address four main goals with a central theme of understanding autonomic dysfunction after SCI across the translational spectrum. Specifically, the included work will:

1) **Develop a clinically relevant rodent model to examine the chronic consequences of autonomic dysfunction after SCI.** This will be accomplished by first highlighting a clinical case describing the real-world consequences of chronic autonomic dysfunction after SCI **(Chapter 3)**. Next, a rodent model will be developed to replicate key clinical features (e.g., autonomic dysreflexia, cardiac dysfunction), and to link these with their neuroanatomical underpinning **(Chapters 4-6)**. It is hypothesized that animals with a severe contusion would exhibit the most severe autonomic dysfunction (i.e., autonomic dysreflexia, cardiac dysfunction), compared to more moderate injuries, and that the degree of dysfunction would be related to the preservation of sympatho-excitatory axons.

2) **Examine the impact of minocycline on autonomic function**. This will be accomplished by leveraging our rodent model of autonomic dysfunction to examine one of the most promising neuroprotective drugs, and to determine its effect of both autonomic and motor function **(Chapter 7)**. It is hypothesized that the delivery of a neuroprotective drug in the acute phase after injury would lead to more spared sympatho-excitatory axons and reduce the severity of autonomic dysfunction (i.e., autonomic dysreflexia and cardiac dysfunction).

3) **Deploy a framework built around systems genetics to better understand how to rationally repurpose neuroprotective drugs and identify biomarkers of injury severity.** This will be accomplished by applying a fully integrated bioinformatics approach to identify key gene subnetworks that underlie the response to SCI **(Chapter 8)**.

4) **Lastly, given the significant and immediate impact SCI has on autonomic control, an immediately implementable neuroprotective strategy for humans with acute SCI is examined.** This will be accomplished by leveraging a novel statistical approach to develop management guidelines for individuals with acute SCI based on key hemodynamic criteria **(Chapter 9).** It is hypothesized that optimal hemodynamic ranges could be identified by leveraging relative risk analyses to identify individuals at risk of poor recovery.

The goal to understand and develop novel solutions for autonomic dysfunction after SCI is driven by an aspiration to reduce the morbidity and mortality of individuals with SCI suffering from these conditions. In the next chapter, I highlight a potentially life-threatening consequence of autonomic dysreflexia **(Chapter 3).** Following this, I begin the development of a clinically-relevant rodent model to study these same dysfunctions **(Chapters 4-6)**.

Chapter 3: Autonomic dysfunction after spinal cord injury: a clinical example[1]

3.1   Case report

A 59-year-old man with a T4 complete (American Spinal Injury Association Impairment Scale A) spinal cord injury (SCI) secondary to a motor vehicle accident 42 years prior and no documented previous history of seizures, stroke, traumatic brain injury, or diabetes mellitus presented to the emergency department with dramatic hypertension (219/113 mmHg; heart rate 56 beats/minute), an altered level of consciousness (Glasgow Coma Scale (GCS) score 10/15), and 12 hour history of headaches, vision loss, and nausea. Upon arrival to the emergency department the patient suffered a generalized tonic-clonic seizure, which was witnessed by the spouse and immediately responded to. Immediate physical exam revealed 3 mm unreactive pupils and 3/15 on the GCS. No relevant alcohol consumption or use of recreational drugs was noted; however, a previous history of severe and recurrent urinary tract infections with concomitant autonomic dysreflexia (AD) was recorded. The patient was immediately given hydralazine, phenytoin, sedated with propofol, and admitted to the intensive care unit. Following the administration of hydralazine and propofol the patient's blood pressure promptly decreased to 100/50 mmHg and remained in safe limits at 120/80 mmHg twelve hours later. Axial and

---

[1] A version of chapter 3 has been published. **Squair, J.W.**, Phillips, A.A., Harmon, M., Krassioukov A.V. (2016). Emergency Management of Autonomic Dysreflexia with Neurological Complications. CMAJ. 88(15): 1100-1103.

sagittal magnetic resonance imaging (MRI) of the head revealed subcortical T2 and fluid-attenuated inversion recovery (FLAIR) signal abnormalities in the posterior parietal and occipital lobes bilaterally, slightly more predominant on the left **(Figure 3.1).** This presentation was deemed consistent with posterior reversible encephalopathy syndrome (PRES), secondary to an episode of AD due to a suspected urinary tract infection. This led to the administration of antimicrobials and a computerized tomography (CT) scan of the pelvis. Urinary cultures later confirmed the presence of methicillin-resistant staphylococcus aureus (MRSA), at which time appropriate antibiotics were initiated. While admitted, electrolytes, blood glucose levels, serum lactate, and other laboratory tests were unremarkable. On the third day of intensive care unit admission the patient was extubated and titrated off propofol. Within six days the patient's PRES symptoms had resolved and no recurrent seizures or other neurological sequelae were documented. The patient was then discharged on an oral dose of phenytoin. Two weeks later he was seen in a follow up appointment. He was free from seizures and phenytoin was discontinued. Ethical approval from the institutional research ethics board was obtained to review this chart and the patient provided written consent.
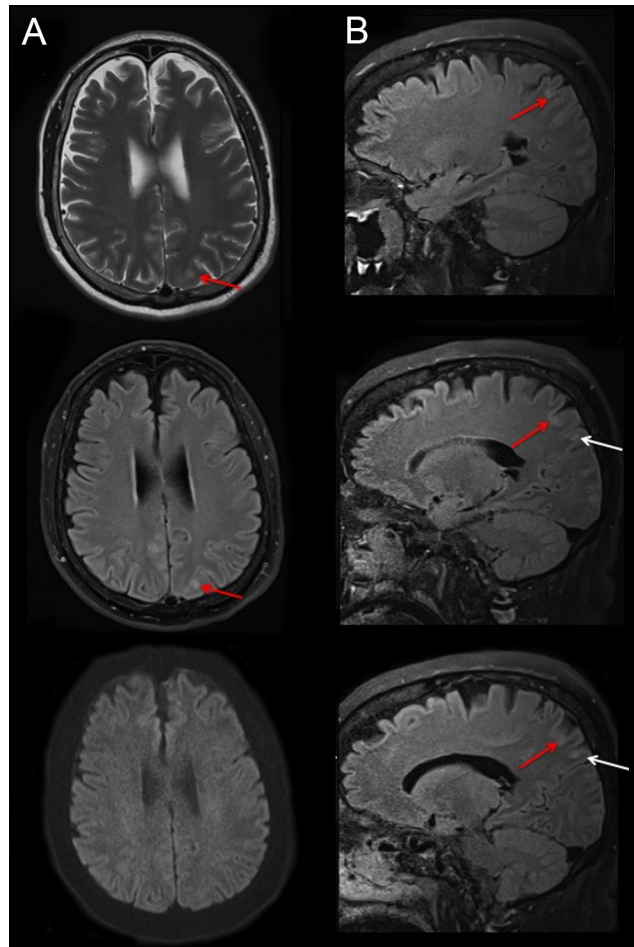
Figure 3.1: Axial and sagittal MRI images of the brain**.**

Axial T2 (A, top), FLAIR (A, middle) and diffusion-weighted imaging (DWI) (A, bottom) images demonstrate cortical edema in the left parietal lobe (red arrows). A lack of abnormality on DWI (A, bottom) suggests vasogenic rather than cytotoxic edema. Contiguous sagittal FLAIR images confirmed vasogenic edema (B) in cortical (red arrows) and subcortical (white arrows) areas. Further areas of cortical and subcortical edema presented throughout the parietal and occipital lobes bilaterally (not shown). Considering the patient's acute severe hypertension,

imaging findings of cortical and subcortical vasogenic edema in the parietal and occipital lobes were consistent with mild but evolving PRES.

3.2   Discussion

Individuals with high thoracic or cervical complete spinal cord injury (SCI) commonly suffer from dramatic hypertensive episodes known as autonomic dysreflexia (AD),[79] which likely contribute to their 300-400% increased risk of stroke.[11] In fact, AD is reported in 90% of individuals with high-thoracic/cervical SCI and may be experienced up to 40 times per day.[79] Further, primary care providers should be aware that the majority of AD is a direct result of urogenital complications (e.g. urinary tract infection, bladder distension, catheter blockage).[79] Here, we present a severe case of AD that resulted in profound clinical complications (i.e. blurred vision, headache, tonic-clonic seizures,) and subtle posterior T2 and FLAIR abnormalities consistent with posterior reversible encephalopathy syndrome (PRES). In addition, we outline the critical steps in the clinical management of this complex and rare presentation of AD.

3.2.1   Autonomic dysreflexia (AD)

AD is defined as an episodic and uncontrolled increase in systolic blood pressure of more than 20 mmHg, which may or may not be accompanied by bradycardia.[79] AD typically develops following complete high-thoracic (i.e. above T6) or cervical SCI as this level of injury disrupts supraspinal control to the majority of sympathetic pre-ganglionic neurons responsible for blood pressure control (i.e. splanchnic circulation). Without descending supraspinal control, these sympathetic pre-ganglionic neurons become susceptible to bouts of hyperactivity resulting from

stimuli below the level of injury, ultimately constricting the corresponding vasculature and dangerously elevating blood pressure **(Figure 3.2; see Chapter 1).**[79] Although AD is life-threatening, some individuals with SCI may self-elicit AD in an effort to combat low resting blood pressure (i.e. boosting);[79] a practice that is not clinically recommended.

3.2.2   Posterior reversible encephalopathy syndrome (PRES)

PRES is a condition characterized by transient and sudden onset of headaches, seizures, and vision loss in conjunction with abnormal T2 and FLAIR imaging primarily in posterior regions,[80] and is commonly associated with severe hypertensive episodes such as pre-eclampsia.[80] Two conflicting theories exist to explain PRES. First, excessive sympathetically driven cerebrovascular constriction resulting from hypertension was thought to underlie the resulting vasogenic edema due to observations of a watershed distribution and imaging-evident focal vasospasms.[81] Alternatively, a more recent hypothesis suggests that the dramatic hypertension exceeds the autoregulatory range, which has been supported by pre-clinical evidence demonstrating breakthrough of the blood-brain-barrier and subsequent edema during hypertensive crises.[81] Given that there is evidence supporting both hypotheses, it is likely PRES represents a complex condition associated with both vasospasm and blood-brain-barrier leakage. However, our patient's case, linked to complete SCI at the T4 level, may support the latter contention (i.e., exceeding the autoregulation range). People with high-thoracic SCI may be at increased risk of surpassing the upper-limit of cerebral autoregulation due to sympathetic hyperstimulation during AD. Pre-ganglionic neurons extending to the superior cervical ganglia, which transmit post-ganglionic sympathetic signals to the cerebral vasculature, emerge from the spinal cord at the T1-T3 spinal segments. As a result, people with a T4 SCI have partially

preserved central autonomic control to the cerebral vasculature. During episodes of AD

secondary to aberrant increases in sympathetic activity caudal to the T4 injury, a

counterproductive decrease in sympathetically-mediated cerebrovascular tone rostral to the

injury would have occurred due to baroreflex loading. Relaxation of the cerebral vasculature

during hypertension in our patient may have reduced the upper-limit of autoregulation and

exacerbated the distending forces on the blood-brain barrier worsening the severity of PRES

(Figure 3.2). These issues demonstrate the importance of injury level when managing AD in

patients with SCI.
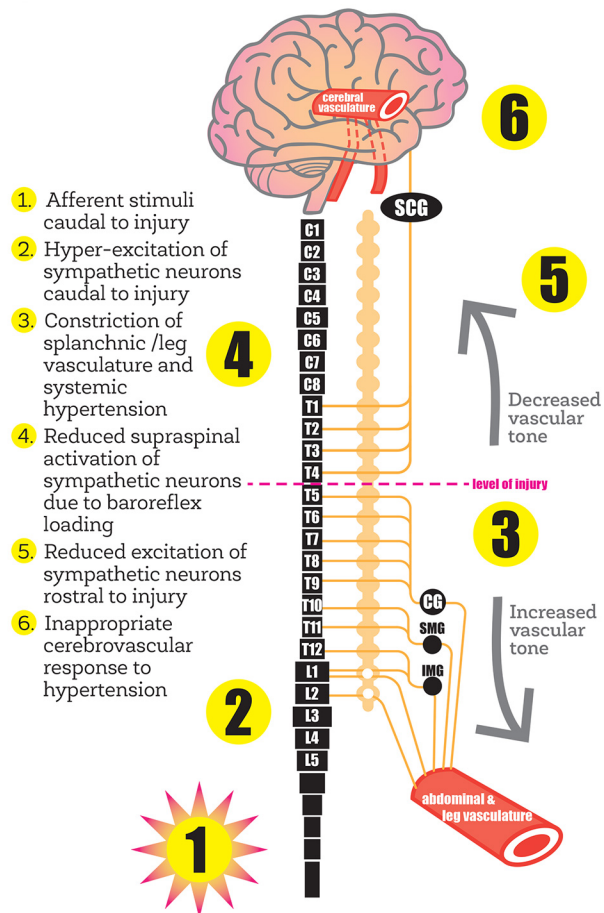
Figure 3.2: Theoretical framework underlying AD-induced cerebrovascular events.

The level of the patient's injury may have played a role in the development of the AD induced-PRES. Specifically, hyper-excitation of sympathetic pre-ganglionic neurons below the injury level and subsequent increase in blood pressure would result in dilation of the cerebral blood vessels due to intact supraspinal regulation of the superior cervical ganglion. A paradoxical baroreflex-mediated relaxation of the cerebral arteries would impair autoregulation of increasing blood pressure and expose delicate cerebral microvasculature to insulting elevations in cerebral blood flow, and potentially compromise blood-brain-barrier integrity.

3.2.3   Management of autonomic dysreflexia

According to current AD management guidelines, a combination of non-pharmacological and pharmacological measures are critical to avoid secondary complications.[82] The first step typically involves moving the patient to an upright position in order to elicit an orthostatic reduction in blood pressure, which can be quite dramatic in individuals with SCI due to disrupted supraspinal regulation of blood vessel tone.[79] This is followed by identification and elimination of possible triggers for the elevated blood pressure (i.e. bladder distension, kinked Foley catheter, urinary tract infection, bowel impaction, etc.), with a specific emphasis on the bladder and bowel. If, following these steps, systolic blood pressure still does not drop below 150 mmHg, oral anti-hypertensive medications with a short onset of action (i.e. nifedipine, captopril) are recommended to reverse the hypertensive episode.

Our case provides a useful illustration highlighting the management of PRES linked to AD.[83-85] Clinical evidence suggests that episodes of AD exceeding 180 mmHg systolic can lead to cerebral vascular insult and death.[79] Further, PRES is associated with cerebral hemorrhage in

15-65%[81.86] of cases (and has previously been reported in an individual with SCI[6]). Therefore, our patient, presenting with an AD-related decreased level of consciousness as well as seizures, was at high risk of progressing to a life-threatening outcome. We used hydralazine to rapidly reduce vascular tone, while we used propofol to control seizures, aid in sedation, inhibit central sympathetic tone[87] and to further decrease the excitability of various sensory afferents, all of which play a major role in propagating AD. The recent follow up in the present case revealed no lasting neurological deficits and no seizure recurrence, emphasizing the critical importance of proper recognition and prompt management of complicated episode of AD.

3.3   Conclusions

Autonomic dysfunction after SCI can lead to life-threatening cardiovascular events. However, there are currently no treatments to prevent the development of conditions such as autonomic dysreflexia **(see Chapter 1)**. As such, my next goal is to use a neuroanatomical framework to understand how the severity of SCI scales with key autonomic dysfunctions such as autonomic dysreflexia, and to develop potential solutions to combat these aberrant conditions. An immediate limitation in the existing literature surrounding autonomic dysfunction after SCI **(Chapter 1),** however, is the lack of a standardized, widely implementable rodent model that can be used during the investigation of novel neuroprotective strategies. In the next chapter **(Chapter 4)** I will address this limitation and develop a rodent model of autonomic dysfunction after SCI using equipment and methodology that are widely used in the field. I will then build on these results by implementing state-of-the-art *in-vivo* and *ex-vivo* assessments of cardiac function to 1) establish for the first time how SCI impacts cardiac mechanics and cardiomyocyte

structure, and 2) to expand our capacity to examine the impact potential treatments have on

autonomic dysfunction after SCI **(Chapters 5 and 6)**.

Chapter 4: High thoracic contusion model for the investigation of cardiovascular function post spinal cord injury[2]

4.1 Introduction

Spinal cord injury (SCI) is a debilitating condition that causes not only motor/sensory dysfunction but also impairments in autonomic function (i.e., cardiovascular, bowel, bladder, sex, respiratory).[79] In particular, disordered cardiovascular control following SCI results in a myriad of conditions including resting hypotension, orthostatic hypotension (frequently associated with a variety of symptoms common for low blood pressure including pre-syncopal episodes) and episodic hypertension (a condition known as autonomic dysreflexia [AD]). Episodes of AD are typically unpredictable, difficult to control, potentially life-threatening, and occur in response to a sub-lesional sensory stimulus.[79,88] The dramatic lability in blood pressure and disruption of descending sympathetic modulation are thought to impair vascular function and ultimately increase this population's cardiovascular disease risk (CVD).[10,11,89,90] In fact, CVD is the leading cause of death in the SCI population, where there is a 300% and 400% increased risk

---

[2] A version of chapter 4 has been published. **Squair, J.W.**, West, C.R. Popok, D., Assinck, P., Liu J., Tetzlaff, W., Krassioukov, A.V. (2016). High thoracic contusion model for the investigation of cardiovascular function post spinal cord injury. Journal of Neurotrauma.34(3), 671-684.

for heart disease and stroke, respectively, neither of which are explained by traditional risk factors (i.e., smoking, obesity, inactivity).[11]

The major mechanisms purported to underlie cardiovascular dysfunction after SCI broadly relate to changes within the medullary cardiovascular control center (i.e. rostral ventrolateral medulla (RVLM)) and the extent of neural damage at the site of injury. The disconnection of descending sympatho-excitatory neurons from the RVLM to sympathetic pre-ganglionic neurons is associated with loss of descending sympathetic control,[23] a series of plastic changes including the transient atrophy of pre-ganglionic cell bodies,[91] as well as the development of intraspinal plasticity.[36,37,92] Therefore, therapies aimed at restoring or preserving maximal amounts of descending sympathetic axons through the lesion site may prove fruitful in maintaining cardiovascular control after SCI. This may be achieved by enhancing supraspinal control and preventing aberrant plasticity in the lumbosacral spinal cord, ultimately decreasing this population's dramatic abnormalities in cardiovascular control **(see Chapter 1)**.[93]

Driven by the advancement in pre-clinical models, the re-establishment of functional behavior following experimental SCI has seen significant advancement in recent years.[54,55,93] Due to the high proportion of blunt injuries in the human population,[94] most investigations into restorative treatment following experimental SCI have utilized contusion models.[55,95,96] The development of these models in rodents and higher mammals has aided the translational process and allowed for testing of potential treatments through pre-clinical studies. Despite these advances, the implementation of promising therapies still has significant barriers, as there is often conflicting evidence, insufficient mechanistic insight surrounding therapeutic agents, or little success upon clinical translation.[55,97,98] Therefore, the development of models that achieve wide-spread functional impairments (i.e. motor/sensory/autonomic) and are aligned with the

common clinical pattern (i.e. high-thoracic/cervical) are critical to synthesize findings across laboratories. Further to this, the functional behavioral outcomes typically studied (i.e. motor/sensory behavior) represent the most complex and evolutionarily mammalian functions. Conversely, autonomic function is an evolutionarily old system, governed by a few medullary and pontine centres, and requires an exponentially lower number of descending projections necessary for normal control opposed to the motor/sensory system.[23,99,100] This raises the possibility that the cardio-therapeutic benefit of neuroprotective or regenerative therapies previously studied in the SCI population may have been missed as a result of only examining motor/sensory function.

Given that recovery of autonomic function is rated among the highest health priorities for individuals with SCI,[101] there continues to be a paucity of research investigating therapies to improve these functions **(see Chapter 1)**.[93] This is in large part due to a lack of a standardized model across laboratories to study autonomic dysfunction after SCI. Previous experiments investigating the mechanisms underlying autonomic dysfunction following SCI have typically used high-thoracic complete transections,[16,36,41,42,47,89,90,102] clip-compression,[33,103-106] or contusion models.[107] Moreover, while much of the pre-clinical SCI field is moving towards cervical contusions, these models spare a significant amount of white matter either due to being unilateral[108–113] or because of their inherent severity,[114–118] which is difficult to increase without causing dramatic mortality. Therefore, these models are either unlikely to result in autonomic impairment or are ethically problematic. While transection models have been critical to provide numerous insights into the development of AD, cardiac impairments, cerebrovascular abnormalities, and other autonomic complications, they are limited in their applicability for neuroprotective strategies, as they do not provide a mechanism of injury congruent with such

strategies. Further, clip-compression models are difficult to apply across a wide array of laboratories due to specialized equipment. Lastly, while a previous T3 contusion model examined hemodynamics, no data were included to characterize the AD response to this injury,[107] which is important as AD is likely one of the most life-threatening autonomic dysfunctions that occur and thus is often the autonomic clinical target. Therefore, we sought to develop a clinically relevant high-thoracic contusion model to study cardiovascular dysfunction after SCI, including AD, using the Infinite-Horizons (IH) impactor in order to provide a model that can be easily accessed by numerous laboratories.

Herein, we describe the attributes of a consistent model of high-thoracic contusion SCI that results in cardiovascular (i.e. impaired resting hemodynamics, AD) and hind-limb dysfunction. Further, we describe a subset of histological changes that may contribute to the observed cardiovascular abnormalities. Specifically, we describe (1) the lesion volume, white matter sparing, and locomotor functional outcomes, (2) the severity-dependent difference in sympatho-excitatory medullary neurons, and (3) the extent of aberrant afferent plasticity within the lumbosacral spinal cord that has previously been linked to the development of AD.

4.2   Methods

4.2.1   Ethical approval

All procedures were conducted in accordance with the Canadian Council for Animal Care. Ethical approval was obtained from the University of British Columbia.

4.2.2 Experimental design

27 male adult Wistar rats (age = 9 weeks, mass = 300-450g; Harlan Laboratories, Indianapolis, IN, USA) were used in this study, as we and others have described the reliable development of autonomic dysreflexia in this species, in contrast to Sprague-Dawley rats.[89,119–121] Rats were randomly assigned to one of three groups: sham-injured control (SHAM; n = 5), moderate SCI (MODERATE; n = 5), or severe SCI (SEVERE; n = 5) (details given below). Following SCI surgery, animals underwent behavioral assessment according to the Basso, Beattie, and Bresnahan (BBB) method at day 7 and day 30. On day 31 animals were implanted with a telemetric blood pressure monitor in the carotid artery. Basal hemodynamics and the severity of AD in response to colorectal distension (CRD) were assessed. All animals were then immediately perfused and used for spinal cord lesion characterization, colonic afferent sprouting quantification, and to determine the number of remaining adrenergic-positive cell bodies within the RVLM.

In order to confirm the immunohistochemistry findings in the RVLM, an additional 12 animals were used to perform retrograde axonal tracing to the RVLM (SHAM, n = 2; MODERATE, n = 5; SEVERE, n = 5). At day 31, these animals underwent a spinal cord re-transection at the TVII vertebral level in order to place FluoroGold for retrograde sympatho-excitatory neuron tracing and subsequent cell-body quantification in the RVLM (see details below). No other behavioural or histological analyses were conducted on these animals.

4.2.3 Spinal cord surgery and animal care

Surgery and animal care procedures were conducted according to our laboratory's standard operating procedures.[47,122] Three days prior to surgery animals were provided a prophylactic

dose of enrofloxacin (Baytril; 10 mg kg^{-1}, s.c., Associated Veterinary Purchasing (AVP),

Langley, Canada). On the day of spinal cord contusion animals were anesthetized (initial

chamber induction at 4% isoflurane with 2l min^{-1} oxygen, followed by maintenance on a Bain's

system at 1.5-2% isoflurane with 1.5-2l min^{-1} oxygen) and pre-operatively administered

enrofloxacin (Baytril; 10 mg kg^{-1}, s.c, Associated Veterinary Purchasing, Langley, Canada.),

buprenorphine (Temgesic; 0.02 mg kg^{-1}, s.c., McGill University), and warmed lactated Ringer's

solution (5 ml, s.c.) while the surgical site was prepared. A dorsal midline incision was made in

the superficial muscle overlying the C8-T3 vertebrae. A T3 laminectomy was performed to

expose the T3 spinal segment. The spinal column was then stabilized by clamping the TII and

TIV spinous bodies with modified Allis forceps. Each forceps was secured in place by locking

universal joints, which were mounted on a secure metal stage that the animal was placed upon.

The animal was then placed such that the impactor tip (2.5mm) of an Infinite Horizon (IH)

Impactor (Precision Systems and Instrumentation, LLC, Fairfax Station, VA[123]) was directly

over the exposed T3 dura. Care was taken to ensure the tension and alignment of the vertebral

column was consistent. Further, the alignment of the impactor tip in relation to the T3 segment

was confirmed as midline by two separate experimenters according to the surface anatomy. In

addition, a surgical microscope was positioned from the side such that both experimenters could

more easily visualize the position of the impactor tip. Once properly aligned, the impactor tip

was lowered until contact with the dura was made and then retracted 2mm above the dura. It was

at this point SHAM animals were removed from the surgical stage and subsequently sutured. For

spinal cord-injured animals, injuries were induced by driving the impactor tip downward with

either 200 kilodynes (kdyn; MODERATE) or 400 kdyn (SEVERE) of pre-defined force. The IH

impactor was set to dwell on the injury site for 5s prior to retracting to enhance injury severity.

The wound was subsequently irrigated with saline and the muscle and skin were closed with 4-0 Monocryl (Ethicon, USA) and 4-0 Prolene sutures (Ethicon, USA), respectively. Animals recovered in a temperature-controlled environment (Animal Intensive Care Unit, Los Angeles, CA, USA). Animals were then administered enrofloxacin (10 mg kg-1, s.c.), buprenorphine (0.02 mg kg-1, s.c.) and ketoprofen (5 mg kg-1, s.c.) every 12 hours for 3 days post-operatively. Bladders were manually expressed three times per day until spontaneous bladder voiding was restored (approximately 1 week post-injury in SEVERE animals).

4.2.4   Determination of injury parameters (Pilot work)

Based on previous work,[103] we know that autonomic dysfunction is often accompanied by low BBB scores (i.e. < 4). Thus, in order to establish the impact severity necessary to elicit autonomic dysfunction we sought an injury severity that would result in little hind limb motor recovery (i.e. no weight supported stepping). At 300 kdyn we observed near immediate recovery of paw placement after injury. Based on previous incomplete models of autonomic dysfunction it was expected that this level of function was likely to result in little to no autonomic dysfunction.[103] As such, we increased the severity of injury by adding 5s of dwell time in order to obviate further increases in force. Despite this, we still observed hind limb recovery and paw placement within 2 days post injury. Lastly, we increased the level of force to 400 kdyn and included the 5s of dwell time (SEVERE). At one week post injury we observed only un-coordinated slight hind limb movements (i.e. BBB score < 4). We thus opted to move forward with this injury severity and included an equivalent injury, with half the force (i.e. 200 kdyn) as our MODERATE injury.

4.2.5   BBB functional behavior assessment

Hindlimb locomotor function was assessed using an open field test according to the BBB method.[124] Briefly, rats were acclimatized to the testing area for three sessions of 4 minutes one week prior to baseline testing. Rats had their bladders expressed prior to the session and were then placed in a 1.5m x 1.5m box[124] for 4-minutes while two experienced, blinded experimenters scored hind limb locomotor function. Animals were tested 1 day prior to contusion, and then 7 days and 31 days post contusion (prior to telemetry implantation), always at the same time of day. Scores and subscores were averaged across the left and right hindlimbs.

4.2.6   Implantation of telemetry device

At day 31 animals were acutely implanted with a telemetric monitoring device. Prior to surgery, the telemetry devices were prepared for implantation, according to the manufacturer's guidelines (Telemetry Research, USA). Animals were anesthetized using isoflurane (initial chamber induction at 4% isoflurane with 2l min^{-1} oxygen, followed by maintenance on a Bain's system at 1.5-2% isoflurane with 1.5-2l min^{-1} oxygen), the hair on the neck was shaved, and the surgical site was cleaned with alcohol and iodine.[89] The left common carotid artery was exposed and isolated from the internal jugular vein using blunt dissection. The carotid artery was then permanently occluded rostrally and temporarily occluded caudal to the implantation site using 4-0 silk sutures. A small incision was made in the artery wall using a bent tip 20 gauge needle and the telemetry device was guided into the lumen and advanced caudally to approximately 5-6mm rostral to the aortic arch. The catheter was secured with a small amount of tissue adhesive and two 4-0 silk sutures, and the body of the transducer was placed between the scapulae. The muscle and skin were closed using 4-0 Monocryl (Ethicon, USA) and 4-0 Prolene (Ethicon,

USA) sutures, respectively. Animals were then transferred to a temperature-controlled environment (Animal Intensive Care Unit, Los Angeles, CA, USA) for 90 minutes in order for the effects of isoflurane to dissipate. Surgeries were completed at approximately the same time of day for all animals.

4.2.7   Resting hemodynamics and autonomic dysreflexia

Ninety minutes following telemetry implantation on day 31, and at a similar time of day for all animals, animals were transferred to a SmartPad (TR181; Millar Telemetry Research, TX, USA) where resting beat-by-beat arterial pressure and heart rate (HR) were recorded for 10 minutes, analog-to-digital converted (PowerLab; AD Instruments, CO, USA), and sampled at 1000Hz (LabChart; AD Instruments, CO, USA). Ninety minutes was used in order to allow sufficient time (half-life = approximately 5 minutes) for isoflurane to be metabolized out of the circulation due to its known effects on blood pressure.[107,126] Prior to baseline recordings, bladders were expressed to avoid any confounding effects of distension. Systolic, diastolic, and mean arterial pressure were then derived on a beat-by-beat basis over 10 minutes to establish resting hemodynamics. Following resting hemodynamic recordings, an experienced researcher who was blinded to injury severity initiated colorectal distension (CRD) (i.e., induction of AD) according to previously described methods.[43] Briefly, a latex 2mm balloon-tipped catheter (AA6110-COLOPLAST Folysil "Foley" Pediatric 2-way indwelling catheter, straight, 10 French, 3mL, 35cm, Latex Free) was inserted 2cm into the rectum and secured to the tail with tape. This procedure was done without restraint, even for animals with some hind-limb function. Animals were covered with a towel in order to reduce any unneeded stimulation and to reduce any large movements, which can affect the blood pressure recording. Following a baseline recording (10

minutes), the balloon was slowly inflated with 2mL of air over 10 seconds, and maintained for 60 seconds. Following 60 seconds of distension, the air was released and the animal rested for 5 minutes. This procedure was repeated a second time. Hemodynamic parameters were recorded before (baseline; 10 minutes), during (distension; 60 seconds), and after (recovery; 60 seconds) balloon inflation. For each animal, the difference in systolic blood pressure (SBP), mean arterial pressure (MAP), diastolic blood pressure (DBP), and HR from baseline and the peak value during distension was subsequently calculated for each trial and averaged across the two trials. Data were averaged every 1s using a rolling average and the peak was calculated as the highest value during the distension phase.[89] Finally, trials were time-locked according to the beginning of distension and averaged across animals in order to produce a representative trace. However, this trace was not used to calculate any peak or delta values due to potential underestimation of such indices arising from between-animal differences in the temporal AD response.

4.2.8   FluoroGold placement

Animals (SHAM, n = 2; MODERATE, n = 5; SEVERE, n = 5) underwent a transection of the spinal cord at T7 at day 31 post-injury.[24] Pre- and post-operative care was identical to that provided for the original contusion injury (see above). A TVII laminectomy was performed following a dorsal midline incision and blunt dissection of superficial musculature. The T8/9 segment of the spinal cord was completely transected using microscissors and completeness was confirmed by two separate experimenters. Following haemostasis, Gelfoam soaked in 10µl of 4% FluoroGold (FG, Fluorochromes Inc., CO, USA) in sterile saline was placed against the rostral stump of the transected spinal cord. The muscle and skin were closed using 4-0 Monocryl

and 4-0 Prolene sutures, respectively. Animals were euthanized and perfused 8 days following

FluoroGold injection to allow sufficient time for retrograde transport to the RVLM.

4.2.9   Tissue processing, histology, and immunohistochemistry

4.2.10   Image analysis and histological quantifications

Immediately following resting hemodynamic and autonomic dysreflexia assessments, or on day

8 post Fluorogold injection, animals were overdosed with chloral hydrate and perfused

transcardially with 500 ml of 0.1 $_M$ PBS, followed by 500 ml of 4% formaldehyde in PBS.

Brains, lesion sites (±4mm of epicenter), and lumbar enlargements were immediately dissected

and post-fixed for 24hr and then transferred to 20% sucrose for cryoprotection.[89,55] A segment of

medulla oblongata was dissected from the brain beginning 1mm caudal to the obex and spanning

rostral 5mm in order to isolate the RVLM.[24] Each tissue was embedded in cryomatrix, frozen in

liquid nitrogen, and stored in -80°C for histological and immunohistochemical investigation.

Medulla oblongatae were cross-sectioned at 30 µm in the cryostat, with sections mounted on

alternating slides (Fisherbrand Superfrost; 6 sections/slide) in order to create paired slide sets

(total of 15 sets per medulla). Thus, the inter-section distance was 60 µm, preventing the

possibility of double-counted RVLM cell-bodies, which span only ~30 µm.[54] Injury site sections

were cross-sectioned at 20 µm and mounted on sets of 10 slides, with 8 sections per slide (total 8

sets of slides) and an inter-section distance of 200 µm.[125] L6/S1 (i.e. innervation to the rectum)

was identified using the appropriate spinal ganglia prior to dissection and sections were serially

cut at 20 µm.[89]

All sections were prepared for immunohistochemistry according to the following

methods.[125] Sections were thawed at room temperature for 1 hour, at which time a hydrophobic

barrier was drawn. Section were then re-hydrated in 0.1M PBS for 10 minutes then incubated

with 10% normal donkey serum for 30 minutes, followed by incubation with primary antibodies

overnight at room temperature. The following morning, sections were washed with 0.1M PBS

three times (10 minutes each), incubated with secondary antibodies for two hours, then washed

in 0.1M PBS three times (10 minutes each). Lastly, sections were cover slipped using

Immunomount and stored at 4°C. The following primary antibodies were used: chicken anti-

myelin basic protein (MBP, 1:200, Aves, MBP), goat anti-glial fibrillary acidic protein (GFAP,

1:1000, Dako), guinea pig anti-neuronal nuclei (NeuN, 1:500, Millipore, ABN90P), mouse anti-

dopamine β-hydroxylase (DBH, 1:500, Millipore, MAB308), and goat anti-CGRP (CGRP,

1:200, Abcam, ab36001). Secondary antibodies included: Alexa Fluor 647 Donkey Anti Goat

(1:200; Jackson ImmunoResearch; 705-606-147), Alexa Fluor 488 Donkey Anti Mouse (1:200;

Jackson ImmunoResearch; 715-546-151), Alexa Fluor 647 Donkey Anti Guinea Pig (1:200;

Jackson ImmunoResearch; 706-606-148), Alexa Fluor 488 Donkey Anti Chicken (1:200;

Jackson ImmunoResearch; 703-546-155), and Alexa Fluor 488 Donkey Anti Goat (1:200,

Invitrogen, A11055).

Immunofluorescence was imaged digitally using an Axioplan 2 microscope (Zeiss) using

ZEN 2 Blue software (Zeiss). Images were digitally processed using Photoshop (Photoshop CC)

or ImageJ (ImageJ NIH) software.

4.2.10.1   Lesion site analysis

Images were taken in quadrants at 5X and prepared for analyses using Photoshop CC. Cord size

and lesion area were quantified (GFAP channel) every 400µm from 4.0mm rostral to 4.0mm

caudal to the injury epicenter. The injury epicenter section was identified by a blinded rater

based on the section with the least intact GFAP signal. Lesion area was manually outlined based on the following definition: GFAP-negative or GFAP-positive area with disrupted or abnormal cytoarchitecture.[128] Care was taken to avoid inclusion of any artifacts. Myelin preservation (i.e. white matter sparing) was estimated by manually outlining based on MBP-positive area with normal or near-normal cytoarchitecture. The total number of pixels within each section was measured using Photoshop CC. Lesion volume was then calculated according to the following formula volume = $\sum$ [area x section thickness x number of sections between samples].[125,128] Neuronal preservation and astrogliosis were qualitatively evaluated using the NeuN and GFAP signals, respectively. All individuals conducting analyses were blinded to grouping details.

4.2.10.2 RVLM localization and neuronal counts

The general location of the RVLM was first determined using a cresyl violet stain. Briefly, sections were immersed in cresyl violet for 20 minutes and dehydrated through successive alcohol washes before being placed in xylene and cover-slipped. The nucleus ambiguous and hypoglossal nucleus were then identified and used as landmarks for the identification of the RVLM **(Figure 4.3)**. Paired slides of the identified sections were then prepared for immunohistochemistry according to established methodology.[24] Immunofluorescent images were imaged at 5x over the ventrolateral column where the RVLM is localized. Neurons labeled with DBH were counted manually for the entirety of the RVLM (15 sections) for each animal. For Fluorogold animals, an identical procedure was completed for the DBH analyses; however, Fluorogold-labelled neurons were also individually counted. Further, co-labelled neurons (DBH, Fluorogold) were identified by examining both channels and counted on ZEN 2 Blue software (Zeiss) in order to estimate the number of descending sympatho-excitatory neurons crossing the

injury site. For all neuronal counts, the total number of counted neurons on both the left and right side were tabulated.

4.2.10.3   CGRP+ axon density quantifications

Five images were taken per animal on five individual sections with randomization of left and right side of the cord and 20µm inter-section distance. Images were taken at 20x over Laminae III-V (identified beginning at the deep border of lamina II and stopping at the central canal) at the L6/S1 spinal level and analyzed using ImageJ. Images were converted to 8-bit and a threshold (Default Dark) was set. Particle analyses was then used to determine the percent area labelled as CGRP+.[89] The average across all images per animal was then used.

4.2.11   Statistical analyses

All statistical analyses were conducted using SPSS 19/20 (IBM, Armonk, NY, USA) and all graphical representations of data were made using Prism 6 (GraphPad, La Jolla, CA, USA) in combination with Photoshop CC 2014 release (Adobe, San Jose, CA, USA). All behavioral and cardiovascular data were statistically analyzed using independent-samples t tests, one-way analysis of variance (ANOVA) or repeated-measures ANOVA, as appropriate and are presented in text as mean ± standard deviation and visualized using mean ± standard error. Significant main or interaction ANOVA effects, as appropriate, were further probed using Tukey's HSD *post-hoc* testing. Between-group differences in the severity of autonomic dysreflexia were analyzed using an independent samples t-test (MODERATE/SEVERE). Correlational analyses were conducted using parametric statistics (Pearson's correlation coefficient [r]). The significance level for all statistical tests was set at $P < 0.05$.

4.3 Results

4.3.1 Infinite-horizons impactor produces consistent biomechanical output in T3 spinal cord contusion

We report that a spinal cord contusion can be performed at the T3 spinal segment using the IH impactor. The biomechanical outputs from the IH were consistent across all metrics (i.e. force, displacement, velocity) for both the SEVERE and MODERATE groups. As expected, the SEVERE injury parameters were more extreme compared to the MODERATE injury in terms of force (400 ± 14 *vs.* 210 ± 2.5; p < 0.001) and displacement (1692 ± 69 *vs.* 1120 ± 59; p < 0.001); however, the velocity of impact was similar (121 ± 2.2 *vs.* 120 ± 1.4; p = 0.469).

4.3.2 T3 spinal cord contusion impairs resting hemodynamics

SBP was significantly reduced at rest compared to SHAM animals (**Figure 4.1a; Table 4.1**) in both MODERATE (p = 0.015 *vs.* SHAM) and SEVERE (p = 0.040 *vs.* SHAM) injured animals. Mean arterial pressure (MAP) was also significantly lower after MODERATE SCI (p = 0.016 *vs.* SHAM) and SEVERE SCI (p = 0.046 *vs.* SHAM), consistent with previous reports using transection models.[16,78,89] In addition, we observed a concomitant increase in heart rate (HR) compared to SHAM following MODERATE SCI (p = 0.017) and SEVERE SCI (p = 0.005). In contrast, we did not observe any significant reductions in resting diastolic blood pressure (DBP) after either MODERATE SCI (p = 0.095 *vs.* SHAM) or SEVERE SCI (p = 0.111 *vs.* SHAM). No significant differences between MODERATE and SEVERE SCI were observed for any basal hemodynamic measures (all p > 0.05).

Table 4.1: Baseline Hemodynamics and Autonomic Dysreflexia Responses

Outcome	SHAM			MODERATE			SEVERE		
Baseline									
SBP	134	±	3.7	115	±	13.0[†]	118	±	7.6[*]
DBP	87	±	3.2	75.8	±	12.5	76.3	±	4.2
MAP	103	±	2.4	87.6	±	11.1[†]	90.3	±	5.4[*]
HR	377	±	44	457	±	42.3[†]	473	±	25.9[*]
Autonomic Dysreflexia									
Delta SBP				23.0	±	13.7	57.0	±	16.7[‡]
Delta DBP				24.5	±	13.0	50.7	±	11.3[‡]
Delta MAP				25.6	±	13.1	52.6	±	12.6[‡]
Delta HR				-21.4	±	52.1	-105	±	45.0[‡]

Abbreviations: SBP: systolic blood pressure; DBP: diastolic blood pressure; MAP: mean arterial pressure; HR: heart rate. Delta, reflects change form baseline Data are presented as mean ± standard deviation. * = $p < 0.05$ SHAM vs. SEVERE; † = $p < 0.05$ SHAM vs. MODERATE; ‡ = $p < 0.05$ MODERATE vs. SEVERE
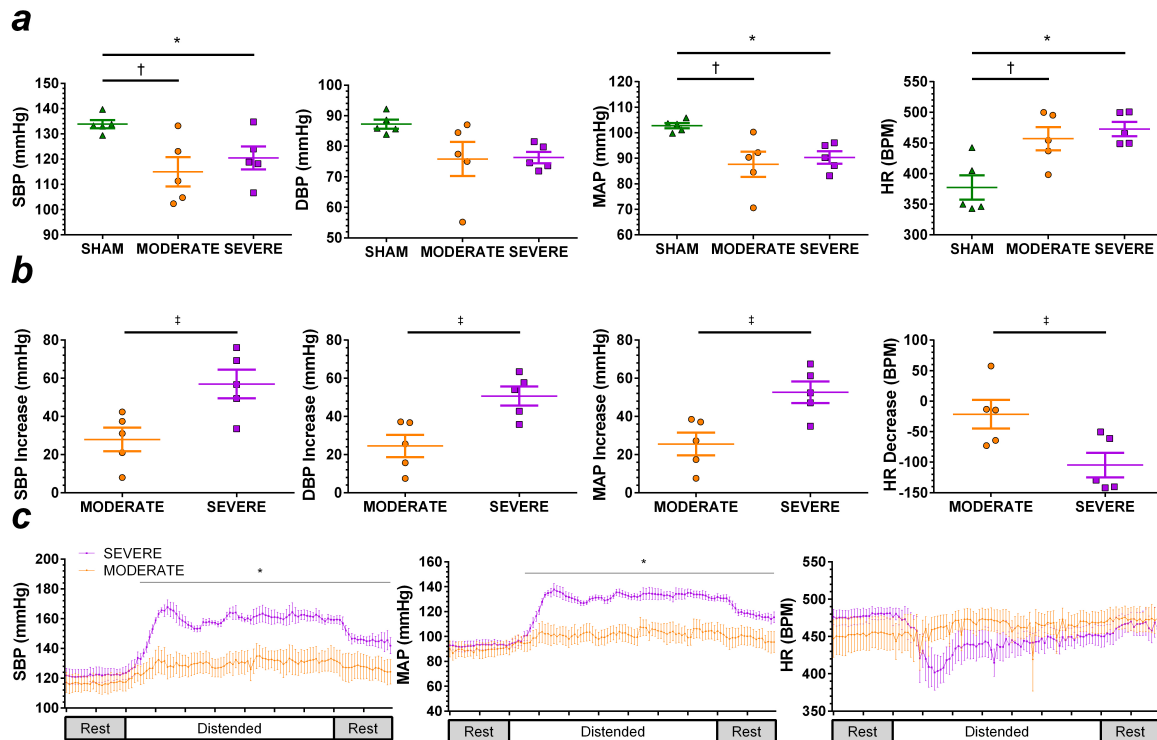
Figure 4.1: Resting hemodynamic and autonomic dysreflexia responses.

(a) At 5 weeks post-injury animals underwent a carotid artery catheter implantation to assess resting hemodynamics. Both MODERATE (n = 5) and SEVERE (n = 5) SCI induced significant reductions in SBP, MAP as well as an increase in resting HR compared to SHAM (n=5). **(b)** We observed marked autonomic dysreflexia, induced by colorectal distension. The maximum change in SBP, DBP, and MAP was significantly greater following SEVERE SCI compared to MODERATE. Further, HR reduced significantly more in the SEVERE group. **(c)** Time-locked group average data revealed a significant interaction effect highlighting the dramatic increase in SBP and MAP immediately following distension of the rectum; however, no interaction effect was observed for HR. Data are displayed as mean ± SEM. Tick marks on **(c)** represent 10 seconds. * = $p < 0.05$ SHAM vs. SEVERE; † = $p < 0.05$ SHAM vs. MODERATE; ‡ = $p < 0.05$ MODERATE vs. SEVERE. Abbreviations: SBP: systolic blood pressure; DBP: diastolic blood pressure; MAP: mean arterial pressure; BPM: beats per minute.

4.3.3   T3 spinal cord contusion induces autonomic dysreflexia

In all cases SEVERE SCI induced a greater hypertensive and bradycardic response to CRD than MODERATE **(Figure 4.1b; Table 4.1)**. SBP maximally increased from baseline in the SEVERE SCI animals and was significantly greater than the response in MODERATE SCI animals ($p = 0.017$). This finding was similar for MAP ($p = 0.011$) and DBP ($p = 0.009$). Further, SEVERE SCI animals demonstrated a larger decrease in HR compared to MODERATE SCI ($p = 0.027$). Time-locked group average SBP data revealed a significant interaction effect ($p = < 0.001$) whereby SEVERE injured animals' SBP rose significantly above MODERATE injured animals immediately after distension (all $p < 0.01$; **Figure 4.1c**). We observed similar results for MAP ($p < 0.01$ following distension) but not for HR (ANOVA $p < 0.001$; Tukey HSD $P > 0.05$).

4.3.4 Lesion size, myelin preservation, neuronal preservation, and astrogliosis are severity dependent

MODERATE and SEVERE T3 contusion induced marked damage at the spinal cord lesion epicenter, which extended in both rostral and caudal directions (**Figure 4.2b, 4.2c**). Qualitative analyses of both GFAP and NeuN immunoreactivity suggest that SEVERE SCI resulted in enhanced astrogliosis extending both rostrally and caudally. Further, few neuron cell bodies were observed near the epicenter. Conversely, MODERATE animals revealed increased GFAP density at the epicentre (**Figure 4.2a**) and neuronal cell bodies appeared as closer to the lesion epicenter. We observed significant decreases in spinal cord area compared to SHAM animals at 5 weeks following both MODERATE and SEVERE SCI (ANOVA $p < 0.001$), with MODERATE animals showing recovered cord area approximately 3.5mm from the lesion epicenter (**Figure 4.2b**). Lesion area was quantified every 400μm and a significant main effect was observed between MODERATE and SEVERE SCI, whereby SEVERE animals demonstrated significantly more lesion area (ANOVA $p < 0.001$). Lesion volume was then quantified and was significantly greater following SEVERE compared to MODERATE SCI (16.0 ± 2.6 *vs.* 8.6 ± 0.97; $p < 0.001$; **Figure 4.2d**). SEVERE animals demonstrated significantly less white matter sparing (ANOVA $p = 0.022$; **Figure 4.2e**). Individual animal lesion volumes were significantly correlated with impact force ($R^2 = 0.804$; $p < 0.001$; **Figure 4.2g**), displacement ($R^2 = 0.667$; $p = 0.007$; **Figure 4.2j**), In addition, AD severity was correlated to white matter sparing ($R^2 = 0.567$; $p = 0.012$; **Figure 4.2f**; **Table 4.2**), lesion area at the epicenter ($R^2 = 0.411$; $p = 0.046$; **Table 4.2**), but not lesion volume ($R^2 = 0.313$; $p = 0.093$; **Figure 4.2i**; **Table 4.2**).

Table 4.2: Regression analyses for autonomic dysreflexia vs. neuroanatomical measures and BBB

Predictor Variable	R^2, Lesion Area Epicentre	R^2, Lesion Volume	R^2, White Matter Sparing Epicentre	R^2, BBB
Autonomic Dysreflexia				
ΔSBP	0.411*	0.313	0.567*	0.555*
ΔDBP	0.622**	0.459*	0.742**	0.638**
ΔMAP	0.550*	0.410*	0.689**	0.619**
ΔHR	0.366	0.458*	0.621**	0.583*

Abbreviations: BBB: Basso, Beattie, Bresnahan functional scale; SBP: systolic blood pressure; DBP: diastolic blood pressure; MAP: mean arterial pressure; HR: heart rate. * Indicates $P < 0.05$ ** $P < 0.01$
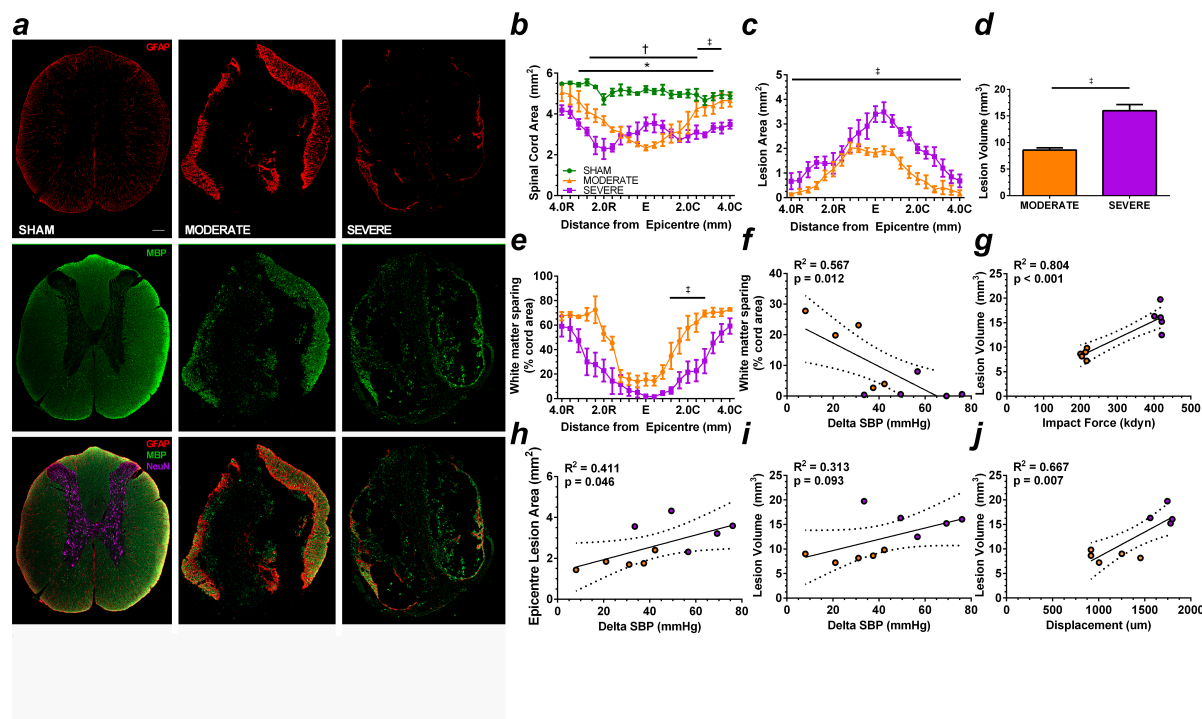
Figure 4.2: Lesion site characterization.

(a) Immunohistochemistry revealed substantial tissue damage in both MODERATE (middle panels; n = 5) and SEVERE (right panels; n = 5) animals compared to SHAM (left panels; n = 5), including increased reactive astrogliosis (top row), ablation of nearly all white matter (middle

56

row), and less neuronal cell bodies (bottom row). Scale bar represents 200μm. Data were quantified every 400μm from the lesion epicenter and reveal significant decreases in spinal cord area **(b)** extensive lesion area **(c)**. Lesion volume was calculated and revealed a significant increase following SEVERE SCI compared to MODERATE **(d)**. Considerable white matter damage was observed and was most concentrated at the lesion epicenter and reduced in severity moving rostral and caudal **(e)**. Further, Autonomic dysreflexia severity (Delta systolic blood pressure (SBP)) was negatively correlated with white matter sparing **(f)**. Spinal cord lesion volume was significantly correlated with impact force **(g)** and displacement (one animal excluded due to improper reading) **(j)**. Autonomic dysreflexia was positively correlated with lesion area at the epicenter **(h)**, but not with lesion volume **(i)**. Data are presented as mean ± SEM. * = $p < 0.05$ SHAM vs. SEVERE; [†] = $p < 0.05$ SHAM vs. MODERATE; [‡] = $p < 0.05$ MODERATE vs. SEVERE.

4.3.5 Sympatho-excitatory neurons projecting from the RVLM are impaired following T3 spinal cord contusion

The RVLM was located immediately anterior and medial to the nucleus ambiguous, caudal to the inferior olivary nucleus, and immediately rostral to the facial nucleus (**Figure 4.3a**). Consistent with previous reports,[24,130–133] the RVLM extended for approximately 1000 μm and thus fifteen 30 μm sections were taken for all analyses to estimate the number of neurons within the RVLM. For non-Fluorogold animals, there was a significantly lower number of DBH-positive neurons in the SEVERE animals compared to SHAM animals (286 ± 32 *vs.* 379 ± 8; $p = 0.011$). In animals with Fluorogold placed below the level of injury, the number of DBH-positive neurons was not different between any groups ($p = 0.149$; **Figure 4.3c$_i$**). In contrast, the number of Fluorogold-

labelled neurons was significantly reduced in the SEVERE animals (5 ± 2.8) compared to both

MODERATE (77 ± 10.7; $p < 0.001$) and SHAM (188 ± 33; $p < 0.001$; **Figure 4.3c$_{ii}$**) animals.

Further, the MODERATE group was also significantly reduced compared to SHAM animals ($p = 0.001$). When examining DBH/Fluorogold co-labelled neurons there was a similar finding, where SEVERE animals (3 ± 2.5) had the fewest co-labelled neurons compared to both

MODERATE (51 ± 14.3; $p < 0.001$) and SHAM (117 ± 9.2; $p < 0.001$; **Figure 4.3c$_{iii}$**) animals.

MODERATE animals also showed a significant reduction compared to SHAM ($p < 0.001$).
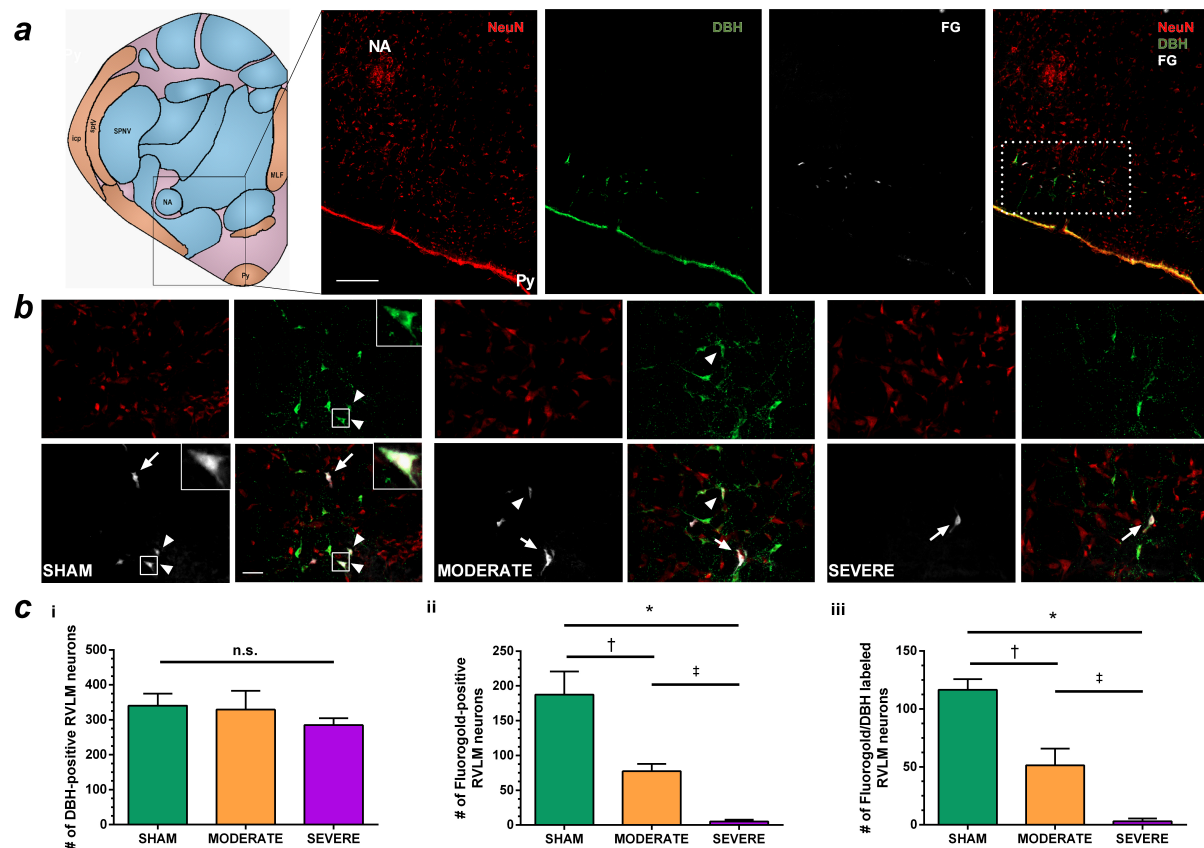
Figure 4.3: Anatomical localization of the rostral ventro-lateral medulla (RVLM) and examination of the severity dependent difference in descending sympatho-excitatory axons of Fluorogold traced animals.

(a) Localization of the RVLM was based on surrounding anatomy.[129] Specifically, it was located anterior to the nucleus ambiguous (NA) and lateral to the Pyramids (Py). The localization can be observed in the schematic and the accompanying immunofluorescent stains observed in a SHAM animal, with the region of interest highlighted the white box. **(b)** The number of both Fluorogold (FG) (arrows) and co-labelled (arrow-heads) was lower with increasing severity of injury and can be observed at high-power. **(c)** The number of dopamine beta hydroxylase (DBH), Fluorogold, and co-labeled was significantly different between severities. **i)** DBH-positive neurons in animals that received a spinal cord transection and Fluorogold injection, **ii)** Fluorogold positive neurons, **iii)** Fluorogold/DBH co-labeled neurons within the RVLM. Data are presented as mean ± SEM. * = $p < 0.05$ SHAM vs. SEVERE; † = $p < 0.05$ SHAM vs. MODERATE; ‡ = $p < 0.05$ MODERATE vs. SEVERE. Scale bars indicate 500μm **(a)** and 50μm **(b)**.

4.3.6 T3 spinal cord contusion induces dorsal horn afferent plasticity

Following SEVERE SCI we observed a significant increase in the positive proportional area of CGRP+ axons within deep laminae (III-V) of the L6/S1 dorsal horns compared to both MODERATE SCI (1.56 ± 0.69 *vs.* 0.70 ± 0.08; $p = 0.043$) and SHAM (1.56 ± 0.69 *vs.* 0.58 ± 0.22; $p = 0.023$). No significant difference was observed between MODERATE SCI and SHAM ($p = 0.913$; **Figure 4.4**).
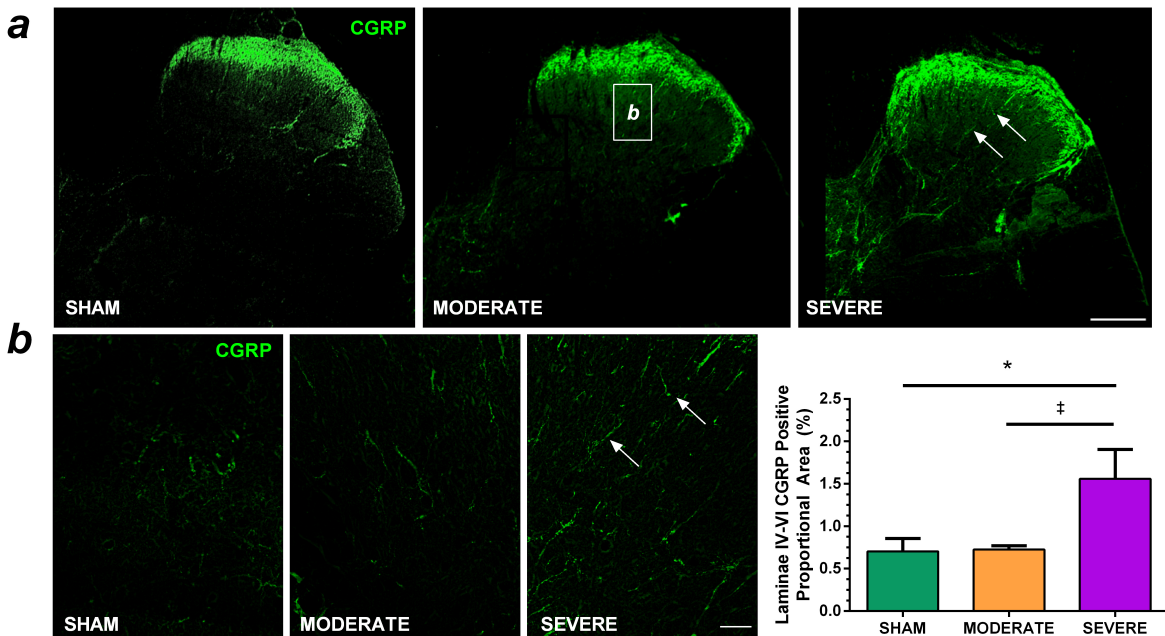
Figure 4.4: Calcitonin gene-related peptide (CGRP) immunohistochemistry in the L6/S1 dorsal horn.

SHAM (n = 5), MODERATE (n = 5), and SEVERE (n =4) SCI. One SEVERE SCI animal was excluded due to damaged tissue. **(a)** Example 5x images taken of the dorsal horn indicate sprouting of axons into deep laminae (III-V; white arrows). **(b)** 20x images were then taken for each section and quantified. Quantification revealed significant differences between SEVERE SCI *vs.* SHAM as well as SEVERE SCI *vs.* MODERATE SCI. Data are presented as mean ± SEM. *p < 0.05 SEVERE *vs.* SHAM. Scale bars indicate 500μm **(a)** and 50μm **(b)**.

4.3.7   T3 spinal cord contusion induces severity-dependent decrease in functional motor behaviour

Locomotor behavior was impaired after MODERATE and SEVERE SCI compared to SHAM.

At 1-week post-injury there were significant differences in total BBB score (maximal score = 21;

Figure 4.5a) between SEVERE SCI and SHAM (1.6 ± 1.1 *vs.* 18.9 ± 3.5; p < 0.001),

MODERATE SCI and SHAM (5.8 ± 1.3 *vs.* SHAM; p < 0.001), as well as SEVERE SCI and

MODERATE SCI (p < 0.001). Similar results were observed at 5 weeks, whereby there were

significant differences in total BBB Score between SEVERE SCI (2.3 ± 1.9), MODERATE SCI

(10.1 ± 1.0), and SHAM (19.3 ± 1.6; all p < 0.001). BBB Subscore indicated that SEVERE SCI

(0 ± 0) did not regain any weight bearing ability on their hindlimbs at either 1-week or 5-weeks

post injury (**Figure 4.5b**). At 1-week post MODERATE SCI displayed no weight bearing ability

(0 ± 0) but did regain small amounts by 5 weeks (1.6 ± 2.3). Both MODERATE and SEVERE

SCI were significantly different from SHAM (11.4 ± 1.5; all p < 0.001). Lastly, there was a

significant correlation between the lesion volume and BBB score for MODERATE and SEVERE

animals at the 5-week time point (R^2 = 0.694; p = 0.003; **Figure 4.5c**), as well as between delta

SBP and BBB score (R^2 = 0.555; p = 0.013; **Figure 4.5d**).
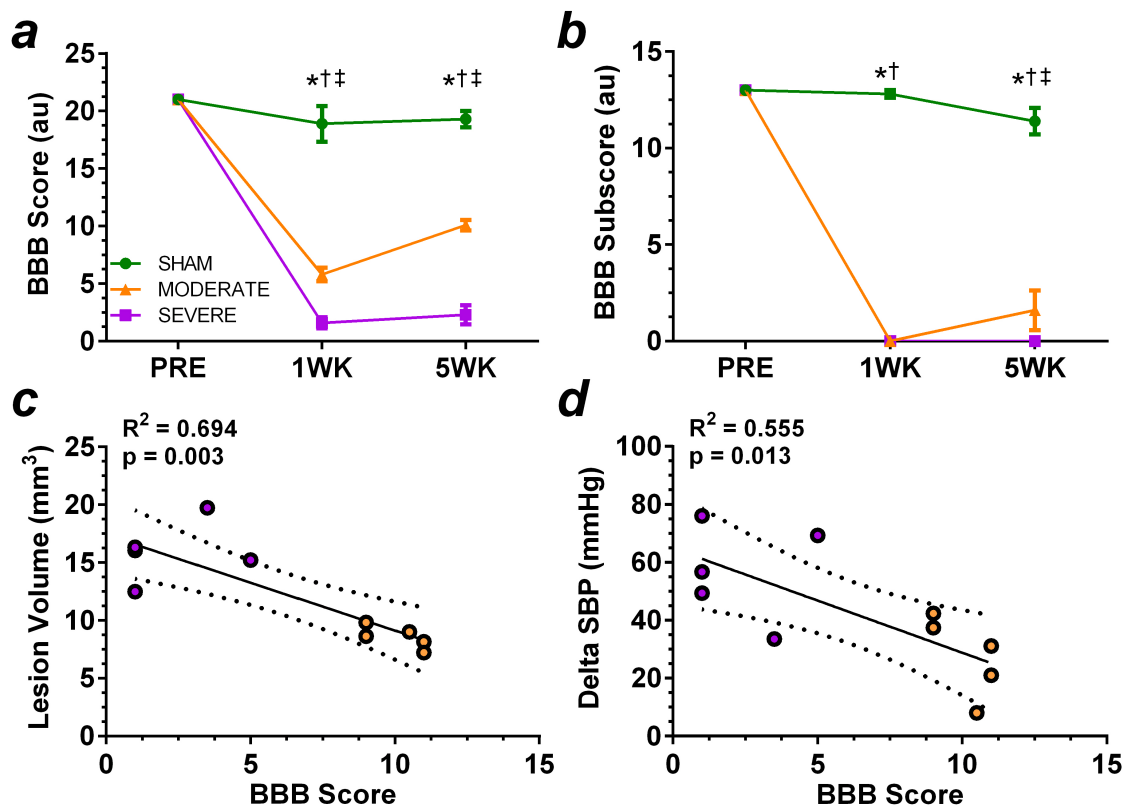
Figure 4.5: Overground locomotion of the animals was scored using the BBB scale (SHAM n=5; MODERATE n=5; SEVERE n=5).

There was a significant decline in locomotor function in both the MODERATE and SEVERE injury groups compared to SHAM, with the SEVERE group demonstrating even greater dysfunction in both the total score (**a**; maximal score=21;) and the subscore (**b**; maximal score=13). Further, there was a significant correlation between BBB score and lesion volume **(c)** and delta systolic blood pressure (SBP; **d**) for MODERATE and SEVERE animals at 5WK. *$p < 0.001$ SEVERE vs. SHAM. † $p < 0.001$ MODERATE vs. SHAM. ‡$p < 0.001$ SEVERE vs. MODERATE. Data are displayed as mean ± SEM.

4.4   Discussion

Here, we present our findings that a T3 severe contusion SCI provided by an IH impactor produces a severity-dependent decline in autonomic and motor function in the rodent. Further, we provide neuroanatomical histological data underlying autonomic dysfunction after T3 contusion and demonstrate novel relationships between injury site metrics and AD. The ability to model higher and more severe SCIs is of high importance within the pre-clinical SCI field. This new model may serve as a research standard to test different potential neuroprotective/neuroregenerative strategies and look at a variety of outcome measures including autonomic, locomotor and sensory changes.

4.4.1   T3 spinal cord contusion impairs resting hemodynamics

A reduction in resting SBP and MAP has been demonstrated in a variety of animal models of SCI,[16,66,89,127,134] in addition to its long established impact in the clinical SCI population.[135,136] Resting hypotension reflects the decentralized state of the sympathetic nervous system after SCI and thus is a critical outcome measure, as it has been linked to cardiac dysfunction,[127] cerebrovascular dysfunction,[90,137,138] and likely contributes to the SCI population's dramatically risk for heart disease and ischemic stroke.[11,15] We demonstrate here that both MODERATE and SEVERE T3 spinal cord contusion induces decreases in both SBP and MAP. While the absolute BP is difficult to compare across studies, here we demonstrate a 15 mmHg reduction in SBP compared to SHAM animals. These decreases are in line with previous work utilizing both T3 transection models and clip compressions.[16,66,89] The mechanism of this decrease has been previously established to result from a decrease in resting sympatho-excitatory influence on sympathetic pre-ganglionic neurons responsible for vasomotor tone (i.e. T6-T12 spinal segments

that provide major sympathetic output to the splanchnic vasculature).[18] This vasculature comprises the major branches of the celiac trunk, superior mesenteric artery, and the inferior mesenteric artery, and is responsible for holding approximately one third of the resting blood volume in both rodents and humans.[18] Thus, a disconnection between sympatho-excitatory neurons in the RVLM and pre-ganglionic sympathetic neurons responsible for controlling the vasomotor tone results in a decreased resting SBP and MAP. This mechanism is further supported by our finding of reduced counts of sympatho-excitatory RVLM neurons (i.e. DBH-positive) with preserved axons extending below the injury (**Figure 4.3**). That we observed a significant decrease in resting hemodynamics in both the MODERATE and SEVERE group suggests that partial loss of descending sympatho-excitatory control over the splanchnic and lower limb vasculature beds may be sufficient to reduce systemic arterial tone. Moreover, the larger variability in the MODERATE SCI group may indicate differential loss of axons within the dorsolateral funiculus leading to variability in descending control, in contrast to the more consistent SEVERE SCI group where there was near complete loss of all white matter. Our data also demonstrate that rodents with a T3 SCI of both MODERATE and SEVERE severity exhibit an increase in resting HR compared to SHAM animals. An increase in resting HR following high thoracic SCI has previously been reported by us and others,[127,139] and has been purported to be a result of increased sympathetic activity to the myocardium,[139] which importantly leaves animals at higher risk for repurfusion-induced arrhythmias.[139]

4.4.2   T3 spinal cord contusion results in autonomic dysreflexia

Clinically, AD is one of the most dangerous secondary complications individuals with SCI experience.[88,135] Further, AD has long been the target of neuroprotective and regenerative

therapies aiming to restore cardiovascular function **(see Chapter 1)**.[93] Therefore, it is critical SCI

models aiming to investigate cardiovascular dysfunction exhibit clear and consistent AD. The

current model demonstrates consistency in the AD response within both the MODERATE and

SEVERE SCI groups, and provides a methodology accessible to many laboratories, which is a

major limitation of previous models.[33,57,67,104-106]

In the current experiment, the SEVERE group demonstrates responses in line with

previous work utilizing transection models[44,89] and represent blood pressure increases well above

physiologically safe limits,[88] a critical determinant for a clinically-relevant model. For example,

clinically, SBP increases above 180 mmHg have been associated with cerebrovascular events

(i.e. hemorrhagic stroke), and SBP values above 200 mmHg are associated with fatal outcomes.[88]

Thus, the AD responses evoked in response to CRD in this model represent a strong starting

point for investigating further mechanisms and therapeutic options.

4.4.3   Lesion size, cavity size, myelin preservation, neuronal preservation, and reactive astrogliosis are severity-dependent

Following SEVERE T3 spinal cord contusion, a lesion was formed and it extended more than 4

mm in both caudal and rostral directions. This was accompanied by near complete abolishment

of any spared white matter at the lesion epicenter, similar to a complete transection but with a

critical difference in mechanism of injury. These findings are in line with previous studies

utilizing severe clip compression models, where they observed similar levels of tissue

destruction and distance in injury site.[24,39] While the white matter sparing was consistent in the

SEVERE SCI group, we did see two outliers in the MODERATE SCI group, which

demonstrated white matter sparing more in line with SEVERE SCI. Further, these two animals

demonstrated significant AD compared to others in the group despite having BBB scores in line with the rest of the MODERATE group (i.e. 9 and 11). Moreover, one of the animals did demonstrate relatively low DBH neuron counts in the RVLM (274), similar to the SEVERE SCI group. However, this ultimately highlights our critical finding that the severity of AD appears to be significantly related to white matter sparing at the injury epicenter (**Figure 4.2f**), which is a crucial piece of evidence when considering potential therapeutic options.

We observed only minimal GFAP-positive expression at the lesion epicentre in the SEVERE group. Conversely, there was relatively large of amounts of GFAP production at the lesion epicenter in the MODERATE injury group. Moving away from the epicenter, SEVERE animals tended to exhibit increased levels of GFAP expression relative to SHAM animals. The overall increase in GFAP is a well-characterized phenomenon after SCI and likely reflects both the dramatic hypertrophy and excess production of intermediate filaments (i.e. GFAP)[140] as well as the influx of neural progenitor cells from the surrounding spinal cord into the injury site, which then proliferate into astrocytes.[141-144] These two mechanisms thus account for what is known as the glial scar. This scar prevents axonal regeneration through the production of substances such as chondroitin sulfate proteoglycans.[140,145] In addition to the current findings surrounding GFAP, NeuN staining revealed that SEVERE injured animals have no sparing of neuronal cell bodies at the lesion epicenter. This lack of neuronal cell bodies extended in both directions, reflecting the extensive damage and glial scar formation. Overall, SEVERE T3 spinal cord contusion resulted in near complete ablation of all MBP and NeuN positive cells. This damage extended both rostral and caudal and the full extent of the lesion volume was intimately related to the force of impact, the displacement of the cord, hind-limb function, as well as the severity of AD.

4.4.4 Sympatho-excitatory neurons projecting from the RVLM are impaired following T3 spinal cord contusion

Our main finding was that T3 spinal cord contusion resulted in a severity-dependent decline in both the number of Fluorogold positive neurons within the RVLM and the number of co-labelled Fluorogold/DBH-positive neurons, similar to our previous report.[24] The RVLM has been extensively characterized for its impact on cardiovascular function and primary composition of C1 adrenaline-synthesizing neurons.[16,24,130-133,146,147] For example, electrical and pharmaceutical stimulation of C1 adrenergic neurons within the RVLM increases blood pressure,[148,149] while pharmaceutical blockade of this area induces sympathetic hypoactivation.[150–153] Adrenergic neurons within the RVLM project their axons to the spinal cord, which travel within the dorsolateral funiculus to stimulate sympathetic pre-ganglionic neurons.[23,130] As such, the maintenance of these axons around the site of injury is of critical importance to maintain appropriate inputs to sympathetic pre-ganglionic neurons and preserve cardiovascular function after injury.

While the raw number of RVLM neurons is difficult to compare across studies due to variance of animal models, the methods of counting of neurons, the number of sections examined, as well as the chosen phenotypic marker, the relative decrease in number of positively traced neurons we report here is consistent with previous findings.[24,147,154-156] For example, following MODERATE SCI, there was a 56% decrease in the number of co-labelled Fluorogold/DBH neurons within the RVLM. Moreover, SEVERE SCI resulted in a 97% decline in the number of co-labelled neurons.[24] As the RVLM axons project down the spinal cord within the dorsolateral funiculus,[7] this dramatic decrease in both groups likely reflects the extensive

destruction of white matter both at the injury epicenter as well as the extension of that injury rostrally and caudally. Accordingly, both MODERATE and SEVERE SCI induces a dramatic reduction in the number of sympatho-excitatory axons maintaining their connection with sympathetic pre-ganglionic neurons.

The number of Fluorogold/DBH-positive neurons was consistently lower than the number of DBH-positive neurons across all groups. At approximately 65%, this proportion of co-labeled neurons most likely reflects the level at which the tracer was inserted. For example, the remaining ~35% of the DBH-positive cell bodies likely project to sympathetic pre-ganglionic neurons above the level of tracer placement and thus would not be co-labelled. This proportion of co-labelled neurons has previous been reported for similar levels of tracer placement.[24,147,154-156]

Our final finding was that the total number of DBH positive neurons was significantly decreased following SEVERE SCI in animals that we did not place tracer. It is possible that the axons extending from the RVLM to the injury site underwent retrograde degeneration (i.e. axonal dieback), which is a well-established consequence of traumatic axotomy.[157–160] This contention is further supported by our observation of less DBH expressing neurons in the SHAM group following spinal cord re-transection for Fluorogold placement, which may be mediated by similar mechanisms. However, while there was some reduction in the number of RVLM DBH-positive neurons, we demonstrate that the vast majority (75%) of these neurons continue to express DBH, and therefore likely remain functional. This suggests that neuroprotective/neuroregenerative therapies may be useful in restoring function of these neurons. In fact, a recent study demonstrated an improvement in both resting hemodynamics as well as the severity of AD following neural stem cell grafting and subsequent regeneration.[16] Moreover,

previous evidence implicating serotonergic fibers in the development of AD[33] suggests that the maintenance of other descending bulbospinal pathways may aid in the resolution of AD.

4.4.5   T3 spinal cord contusion induces dorsal horn afferent plasticity that scales with injury severity

Extensive animal and human research has demonstrated both a severity-dependent relationship as well as a time-course relationship between the extent of CGRP+ immunoreactivity within the dorsal horn and the severity of AD.[37, 39,41,44,161] CGRP is expressed primarily by nociceptive unmyelinated C fibers as well as Aδ fibers within the dorsal root ganglia and superficial laminae.[37] However, following neuronal injury these axons extend deep to Lamniae III-V where they interact with intraspinal networks and activate an inappropriately large number of sympathetic pre-ganglionic neurons, which ultimately results in the exaggerated vasoconstriction response (i.e. AD) to stimuli below the level of injury.[36,37,39,40]

We found that T3 spinal cord contusion results in an increase in the expression of CGRP within the deep laminae. The increased expression of CGRP and influx of axons into the deep laminae following SEVERE T3 contusion is likely a direct result of increased neural growth factor (NGF) influx from the dorsal root ganglia. In fact, the concentration of NGF within the cord is intimately related to the influx of these axons[44] and manipulation of the levels of NGF has been shown to reduce or amplify the severity of AD.[41] Our observed increase in CGRP axons within the dorsal horn may act in concert with other previously established consequences of aberrant plasticity after SCI. Namely, previous electrophysiological and morphological work has highlighted that ascending propriospinal axons undergo aberrant plasticity, which may further aid the rostro-caudal spread of pre-ganglionic neuron stimulation.[36,92] However, as we did not

assess these outcomes in the current study further work would need to substantiate this hypothesis.

While several studies have examined methods to reduce the severity of CGRP+ afferent sprouting, many have utilized a transection model,[41,44] further mechanistic data are needed to determine the utility of these axons. Our data provides similar findings to previous models and provides a clinically relevant model with established mechanisms to further examine this phenomenon.

4.4.6   T3 spinal cord contusion induces severity-dependent decrease in functional motor behavior

T3 spinal cord contusion resulted in a severity-dependent difference in functional hind-limb behavior, as assessed using the BBB open-field locomotion assessment. BBB scores were significantly correlated with lesion volume, indicating our data replicate the well-established relationship between the sparing of descending pathways and hind-limb function.[162] Similar to previous studies, MODERATE animals regained more function by the 5 week time-point, while SEVERE animals regained very little function and were not able to weight-bear.[103,67] However, longer-term studies may be needed to establish if this behavior is sustained over time.

4.5   Conclusion

Here, I present cardiovascular, histological and locomotor data that demonstrate the utility of this new midline T3 contusion model. This T3 contusion model may therefore be used to investigate the mechanisms and the therapeutic potential of various neuroprotective/neuroregenerative agents to improve cardiovascular control after SCI. This model is of critical importance as

cardiovascular dysfunction is the leading cause of death for individuals with SCI and is rated among the top health priorities of these individuals. Further, utilization of the IH contusion apparatus, that is common to numerous SCI labs, will aid this model's widespread use.

Having now developed a rodent model of autonomic dysfunction after SCI, the next chapter **(Chapter 5)** will seek to build on this work by implementing state-of-the-art *in vivo* and *ex vivo* assessments of cardiac function and cardiomyocyte structure to provide a deeper understanding of how severe SCI influences cardiovascular function and end-organ health. These additional outcomes will be important to completely characterize the potential effects of novel treatment strategies.

Chapter 5: Spinal cord injury causes systolic dysfunction and cardiomyocyte atrophy[3]

5.1   Introduction

Clinical and pre-clinical studies investigating cardiac function after spinal cord injury (SCI) report that individuals with SCI demonstrate impaired systolic function,[163,164] left-ventricular (LV) atrophy.[163,165] electrocardiogram abnormalities,[166] increased risk of reperfusion induced arrhythmias,[167,168] and decreased resting heart rates.[136] The major mechanisms purported to cause cardiac abnormalities after SCI are the loss of descending sympatho-excitatory cardiac control from medullary centres,[23,127] as well as significant LV unloading, secondary to sympathetic decentralization of the peripheral vasculature, reduced blood volume,[169] and reduced physical activity.[136]

We have recently shown in an *ex vivo* setting that when the hearts of SCI and uninjured rats are paced at 300bpm, SCI rats exhibit a significant down and rightward shift of the Starling curve and impaired rate (dP/dt_{max}) of LV pressure rise.[127,170] Impaired dP/dt_{max} post-SCI in the face of eurythmic stimulation suggests that changes in LV function are not due to SCI-induced reductions in heart rate. Instead, it is likely that a disruption in either 1) direct descending

---

[3] A version of chapter 5 has been published. **Squair, J.W.**, DeVeau, K.M., Harman, K.A., Poormasjedi-Meibod, M.S., Hayes, B., Liu J., Magnusun, D.S.K., Krassioukov, A.V., West, C.R. (2018). Spinal cord injury induced sympathetic decentralization causes cardiac atrophy and systolic dysfunction. Journal of Neurotrauma. 35(3):424-434.

sympathetic control of the heart, 2) the sympathetic nerves that control venoconstriction (i.e., preload), 3) the sympathetic nerves that control systemic arterial tone and thus vascular resistance (i.e. afterload), or 4) reduced catecholaminergic release contribute independently or in unison to reduce LV contractile function *in vivo*. Decoupling the confounding effects of preload and afterload on the heart is inherently challenging in humans. In rodents, direct catheterization of the LV with a pressure-volume catheter and subsequent manipulation of loading conditions via inferior vena cava occlusions provides a direct *in vivo* assessment of LV contractile function *per se,* independent of afterload and preload.[171] Removing the confounding effects of loading is critical to elucidate true differences in intrinsic LV function, particularly in populations such as SCI where significant reductions in both preload and afterload may mask LV dysfunction (i.e. normal ejection fraction). To date, however, no studies have applied this technique after SCI. Moreover, with the exception of three studies that have either examined changes in the extracellular matrix[167,127] or changes in cardiac metabolism,[172] no studies have investigated how or if there is anatomical cardiomyocyte remodeling following SCI. Our lack of understanding about the basic cardiac phenotype that develops post-SCI hampers effective treatment. Given that people with SCI are living longer than ever before and are reported to develop heart disease more commonly than people without SCI[11] this lack of understanding is a profound limitation.

In the present study, we tracked temporal changes in cardiac parameters post-SCI using echocardiography and also combined the first 'load-independent' assessment of cardiac function with morphological and transcriptional analyses of the LV free wall. We utilized a level of injury (T2) that significantly disrupts descending sympatho-excitatory control of the heart[173] in order to specifically investigate the importance of intact descending cardiac sympathetic control in the regulation of cardiac inotropy after SCI.

5.2   Methods

5.2.1   Ethical approval

All procedures were conducted according to the Canadian Council for Animal Care. Ethical approval was also obtained from the University of British Columbia.

5.2.2   Experimental design

The experiment was conducted on 24 male Wistar rats (age = 9 weeks, mass = 300-350g; Harlan Laboratories, Indianapolis, IN, USA). Animals were randomly assigned to one of two groups: uninjured control (CON; n=13) or T2 SCI (SCI; n=11). *In vivo* echocardiography was used to investigate temporal changes in cardiac structure and function at pre-injury at day 7 and day 30 post-injury. On day 31, a subset of animals (n=5 per group) underwent pressure-volume catheterization *via* a right common carotid artery approach to assess load-independent LV function. Furthermore, these animals were harvested for fresh tissue, which was subsequently used for qPCR analysis. The remaining animals were used for cardiac immunohistochemistry to investigate structural changes at the myocyte and sarcomeric level.

5.2.3   Spinal cord surgery and animal care

Animals were treated prophylactically with enrofloxacin (Baytril; 10 mg kg^{-1}, s.c., Associated Veterinary Purchasing (AVP), Langley, Canada) three days prior to surgery. For spinal injury contusion surgery animals were prepped (surgical site shaved, cleaned, sterilized) and anesthetized with isoflurane (initial chamber induction at 4% isoflurane with 2l min^{-1} oxygen, followed by maintenance on a Bain's system at 1.5-2% isoflurane with 1.5-2l min^{-1} oxygen). A dorsal midline incision was made and the superficial and deep paraspinal musculature dissected.

74

A TII laminectomy was performed. Following this the TI and TIII vertebrae were clamped with modified Allis forceps. Forceps were secured in place with locking universal joints and mounted on a secure metal stage. After proper alignment, the animal was injured at the T2 spinal segment with 400 kdyn of pre-defined force (5s dwell) using the Infinite Horizons Impactor (2.5mm tip), as this severity of injury has been shown to produce a similar reduction in afterload and preload to that observed in the high-thoracic and cervical SCI clinical population **(see Chapter 4)**.[174] Post-operative management included enrofloxacin (10 mg kg-1, s.c.), buprenorphine (0.02 mg kg-1, s.c.) and ketoprofen (5 mg kg-1, s.c.) every 12 hours for 3 days post-operatively. As we have previously described, this injury resulted in a sustained inability to weight bear on the hind-limbs and a near complete loss of all descending sympatho-excitatory neurons; however, animals were able to freely use their forelimbs and showed no other signs of distress (i.e. feeding well, no hunching, socialization with cage mates).[174] Manual bladder expression was continued for approximately one week post-injury, until animals regained spontaneous voiding.[122]

5.2.4 *In vivo* echocardiography

To assess temporal changes in cardiac structure and function, echocardiography was performed as described in detail elsewhere.[127] Briefly, measures of LV structure and function were imaged while animals were under isoflurane anesthesia (initial chamber induction at 4% isoflurane with 2l min-1 oxygen, followed by maintenance on a Bain's system at 1.5-2% isoflurane with 1.5-2l min-1 oxygen). LV structure and systolic function (i.e. stroke volume, ejection fraction) were assessed using M-mode echocardiography and diastolic function was assessed using pulsed-wave Doppler during an apical four-chamber view. Estimated volumes were calculated according to the Teichholz method.[127] Reported results were quantified by a blinded experimenter using

commercially available software (Echopac; GE Healthcare, Horton, Norway) and determined

from the average of 5 cardiac cycles during expiration.

5.2.5 Pressure-volume catheterization

To further determine inherent changes in LV pressure and volume indices as well as conduct a

novel investigation into load-independent cardiac function, LV function was assessed *in vivo*

under isoflurane anesthesia using a pressure-volume (PV) conductance catheter (SPR-869,

Millar, USA) inserted directly into the LV via a closed-chest right common carotid artery

approach according to standard guidelines.[171] The presoaked catheter (for 30 min into

physiological saline solution) was left in the carotid artery for 10 min to allow hemodynamic

stabilization and for the determination of arterial blood pressure, which was subsequently used to

examine the low frequency power spectrum component as a measure of sympathetic influence.[175]

Following this, the catheter was advanced into the LV under pressure guidance until the PV

signal was visualized and subsequently optimized. After stabilization of the LV pressure-volume

signal basal PV data was collected for 10 min after which Dobutamine (Dobutamine, I.V.,

Hospira), a specific beta-1 agonist, was infused in a step-wise manner via catheterization of the

tail vein in order to mimic a sympatho-excitatory response. Following the return of all indices to

pre-Dobutamine, baseline cardiac preload was manipulated via complete inferior vena cava

occlusions for the measurement of load-independent outcomes (i.e., end-systolic elastance (Ees),

end-diastolic pressure-volume relationship (EDPVR), preload recruitable stroke work (PRSW),

dP/dt-EDV). Briefly, a midline laparotomy was performed and the inferior vena cava isolated

immediately caudal to the liver. Occlusions were performed using a cotton-tipped applicator.

Data analysis was conducted in Labchart 8.1 (ADInstruments, USA) using the built in PV loop analyses program.

5.2.6   Fresh tissue and qPCR

Following PV measures, animals were sacrificed (overdose isoflurane and thoracotomy), the heart was excised, the great vessels were removed, and the heart was weighed for the determination of wet heart mass, at which point the harvested hearts were preserved at -80°C. To assess gene transcription changes in the LV between groups, total RNA was extracted from the left ventricle using Trizol reagent with the PureLink RNA Mini Kit (Thermo Fisher Scientific). The purity and concentration of the isolated RNA were checked using NanoDrop 2000 Spectrophotometer (Thermo Scientific, USA). Subsequently, 5 µg of total RNA was reverse transcribed into cDNA using SuperScript® VILO™ cDNA Synthesis Kit (Invitrogen). Real time qPCR was carried out on the Applied Biosystems 7500 Fast Real-Time PCR System, using the SYBR Green PCR Master-Mix kit (Applied Biosystems, Warrington, UK). Group comparisons were drawn using the $2^{-\Delta C_T}$ method according to recommended guidelines.[176] **Table 9.1** contains the list of the primers used in this study. Targets included were: Collagen (Col), matrix metalloproteinase 9 (MMP9), tissue inhibitor of metalloproteinase 1 (TIMP1), alpha smooth muscle actin (α–SMA), transforming growth factor beta (TGF-β), transforming growth factor beta receptor (TGF-βR), connective tissue growth factor (CTGF), angiotensinogen (AGT), angiotensin-converting enzyme (ACE), type 1a angiotensin II receptor (AgtR1a), beta-1 adrenergic receptor (B1R), vascular endothelial growth factor (VEGF), nerve growth factor (NGF), and muscle LIM protein (MLP). β-actin was used as the reference gene.

Target	Primary Sequence	T2/CON		
Table 5.1: qPCR targets, primers, and fold changes				
Target	**Primary Sequence**	**T2/CON**		
ColIA1	Forward 3'- CTGCTGGTCCTAAGGGAGAG -5' Reverse 3'- GACAGCACCATGGTTACCAC -5'	0.60	±	0.12
COLIIIA1	Forward 3'- TGGTGAGCGAGGACGACCA -5' Reverse 3'- AGGTCCAACCTCACCCTTAGCAC -5'	0.60	±	0.22
MMP9	Forward 3'- TCAGCCGGGAACGTATCTGGA -5' Reverse 3'- CTGGTTCACCCGGTTGTGGA -5'	9.30	±	6.02*
TIMP1	Forward 3'- TTCTCATCGCGGGCCGTTTA -5' Reverse 3'- CACCCCACAGCCAGCACTAT -5'	1.58	±	0.43†
α-SMA	Forward 3'- TCCCAGACACCAGGGAGTGA -5' Reverse 3'- GCCACGCGAAGCTCGTTAT -5'	1.48	±	0.41
TGF-β1	Forward 3'- CTGAACCAAGGAGACGGAATACA -5' Reverse 3'- CATGAGGAGCAGGAAGGGTC -5'	0.88	±	0.22
TGF-β2	Forward 3'- TCCGAAACTGTCTGCCCAGTTGTT -5' Reverse 3'- TGTAGAAAGTGGGCGGGATGG -5'	1.01	±	0.23
TGF-βR1	Forward 3'- TCCGAAACTGTCTGCCCAGTTGTT -5' Reverse 3'- TGTAGAAAGTGGGCGGGATGG -5'	1.07	±	0.24
TGF-βR2	Forward 3'- GGGCGAGGAATAAAGGCGCA -5' Reverse 3'- TCGCTGTTAACCGACTTGGGAA -5'	0.83	±	0.23
CTGF	Forward 3'- AACTGTGCACGGAGCGTGAT -5' Reverse 3'- CTTTGGAAGGACTCGCCGCT -5'	0.86	±	0.41
AGT	Forward 3'- TCAGCACGGACAGCACCCTA -5' Reverse 3'- GAAGTTGCCAGTGCCCGAGA -5'	0.91	±	0.46
Renin	Forward 3'- TCCCAGAGGGTGCTAAAGGAGG -5' Reverse 3'- CACAGAGACCCCCTTCATGGTGAT -5'	0.72	±	0.32
ACE	Forward 3'- CTGCCTCCCAACGAGTTAGAA -5' Reverse 3'- CGGGACGTGGCCATTATATT -5'	0.72	±	0.20
AgtR1a	Forward 3'- GGCTTGAGTCCTGTTCCACCC -5' Reverse 3'- CCACTTGACCTGGTGATCACTTTC -5'	0.78	±	0.21
B1R	Forward 3'- ACCCCAAGTGCTGCGATTT -5' Reverse 3'- AACACCCGGAGGTACACGAA -5'	1.23	±	0.14
B2R	Forward 3'- GCAACAGCAACGGTAGGACA -5' Reverse 3'- CAGTGGCGAGTCGTTTGTGT -5'	0.68	±	0.17
VEGF-a	Forward 3'- ACAGGGGTCCTGGCAAAGAGA -5' Reverse 3'- GTCCTGCCCCATTGCTCTGT -5'	3.27	±	0.63
NGF	Forward 3'- CCTGGAGCCGAAGGGGA -5' Reverse 3'- GGACATTACGCTATGCACCTCA -5'	0.92	±	0.24
α2-Actinin	Forward 3'- ATGGGCTATGACTTGGGTGAA -5' Reverse 3'- GTGTCCGTGTCTGCGGTCT -5'	1.03	±	0.14
β-actin	Forward 3'- TATCGGCAATGAGCGGTTCC -5' Reverse 3'- GTGTTGGCATAGAGGTCTTTACG -5'	n.a.		

Col, Collagen; **MMP**, Matrix metalloproteinase; **TIMP**, Tissue inhibitor of metalloproteinase; **α–SMA**, alpha smooth muscle actin; **TGF-β**, Transforming growth factor beta; **TGF-βR**, Transforming growth factor beta receptor; **CTGF**, connective tissue growth factor; **AGT**, angiotensinogen; **ACE**, Angiotensin-converting enzyme; **AgtR1a**, Type 1a Angiotensin II Receptor; **B1R**, Beta-1 adrenergic receptor; **VEGF**, Vascular endothelial growth factor; **NGF**, Nerve growth factor; **MLP**, Muscle LIM protein. n = 5 per group. *$P < 0.05$ †$P<0.1$.

5.2.7 Tissue processing and immunohistochemistry

5.2.7.1 Tissue processing

Animals were overdosed with isoflurane (5% isoflurane with 2l min^{-1} oxygen) and underwent a thoracotomy. Hearts were arrested with ~150mg KCl, and perfused with an aortic approach in order to preserve the LV with 500 ml of 0.1 $_M$ phosphate buffered saline (PBS), and fixed with 500 ml of 4% formaldehyde in PBS. Hearts were immediately dissected[127] and prepared for immunohistological analysis according to our previously described methods **(see Chapter 4)**.[174]

5.2.7.2 Immunohistochemistry

Sections were thawed for 1hr at room temperature and pap-penned, followed by re-hydration in 0.1M PBS for 10 minutes. Sections were then incubated with 10% normal donkey serum for 30 minutes. After removal of normal donkey serum, sections were incubated in primary antibody prepared in 0.1M PBS-Triton overnight at room temperature. The next morning three 10 minute 0.1M PBS washes were done to remove the primary antibodies, after which they were incubated with secondary antibodies for two hours. Sections were then cover slipped using immunomount and stored at 4°C. The following primary antibodies were used: rabbit anti-α actinin (αA, 1:100, Abcam, ab68167) to stain the z-disks of cardiomyocytes, and to measure cell width, and goat anti-connexin 43/GJA1 (CX, 1:250, Cedarlane, NBP1-51938), to identify the end-plates and thus calculate cardiomyocyte length. Secondary antibodies used were: Alexa Fluor 647 Donkey Anti Goat (1:200; Jackson ImmunoResearch; 705-606-147), Alexa Fluor 594 Donkey Anti Rabbit (1:200; Jackson ImmunoResearch; 711-586-152), and Hoechst Reagent (1:1000).

5.2.7.3 Imaging

Immunofluorescence was digitally imaged using an Axioplan 2 microscope (Zeiss) and AxioVision 4.8 ZEN Blue (Zeiss) was used for all digital image capture procedures. Post-processing was completed using ImageJ (ImageJ NIH) software.

5.2.8 Quantification of immunolabelling

5.2.8.1 Myocyte length quantification

All cardiomyocyte measurements were taken from the mid-ventricular level of the LV free wall. Myocyte length was determined by taking the distance between two CX-labelled end-plates and confirmed by the localization of at least one nucleus between these two sites. Five myocytes were measured per 20x image, for a total of 30 measured myocytes per animal, which were subsequently averaged for each animal.

5.2.8.2 Z-disk width quantification

Z-disk width was estimated based on the width of individual αA labels. Ten individual measurements were made per 20x image, for a total of 60 estimations of z-disk width per animal. These 60 estimations were subsequently averaged for each animal. Myocyte length/width ratio was then calculated.

5.2.8.3 Sarcomere length quantification

In order to measure individual sarcomere lengths, the distance between two αA was utilized. Specifically, the measurement was taken from the inner border of one αA and continued to the inner border of the next αA. Ten individual measurements were made per 20x image and

averaged, as above. Based on the average myocyte length and sarcomere length for each animal, the number of sarcomeres per myocyte was then estimated.

5.2.9   Statistical analyses

Statistical analyses and all graphical representations of data were made using GraphPad Prism 6 and all immunohistochemical images were taken using ZEN blue (Zeiss). All basal cardiac and immunohistochemical data were analyzed using independent samples t-test or repeated-measures analysis of variance (ANOVA), as appropriate. Data are presented in text as mean ± standard deviation and visualized using mean ± standard error. Significant main or interaction ANOVA effects were further investigated using Sidak's *post-hoc* testing. Load-independent cardiac data was analyzed using mixed-model regression analyses (STATA v12.1), as recommended in the literature.[177] The significance level for all statistical tests was set at $p < 0.05$.

5.3   Results

We tracked temporal changes in global cardiac function after SCI using time-course echocardiography **(Figure 5.1)**, and found a significant decrease in LV diameter during diastole (LVIDd) following SCI compared to uninjured control (CON). Estimated volumetric indices obtained from echocardiography, including stroke volume (SV) and cardiac output (CO), were significantly lower after SCI compared to CON animals (all *P* < 0.05; **Figure 5.2a-d**). Diastolic function did not differ between groups (**Table 5.1**).
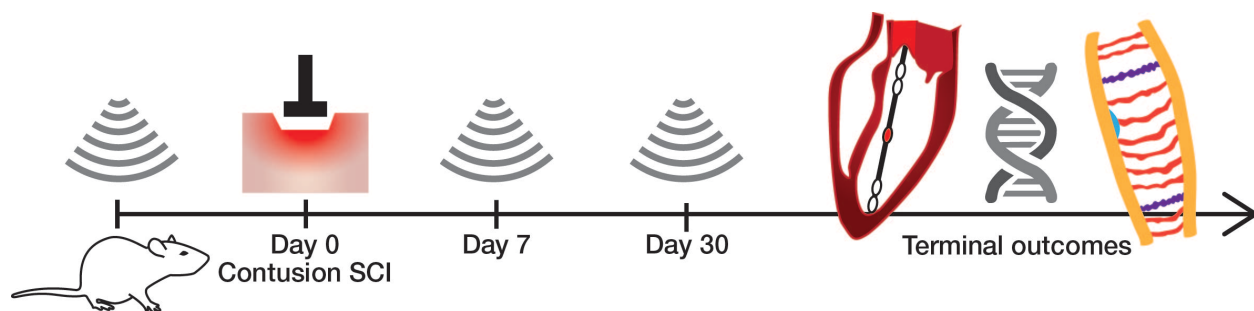
Figure 5.1: Overview of experimental design to determine how spinal cord injury impacts cardiac function.

Adult Wistar rats underwent echocardiography prior to injury in order to establish pre-injury parameters. Next, rats were given a severe spinal cord contusion (day 0). At 7 and 30 days post-SCI, each rat was assessed using echocardiography to determine structural and functional changes to the left ventricle. At 31 days post-injury the left ventricle was cannulated with a pressure-volume conductance catheter via a closed chest approach to assess *in vivo* load-independent cardiac contractile function. Following this, animals were sacrificed and their organs were harvested and processed in preparation for histology and molecular biology.

Basal hemodynamics at study termination demonstrated significant reductions in blood pressure (i.e. systolic, diastolic, and mean blood pressure) after SCI **(Figure 5.2e, 5.2f)**, as well as significantly lower resting heart rate (HR; **Figure 5.2g; Table 5.1**) and low frequency systolic blood pressure power **(Figure 5.2h)**.
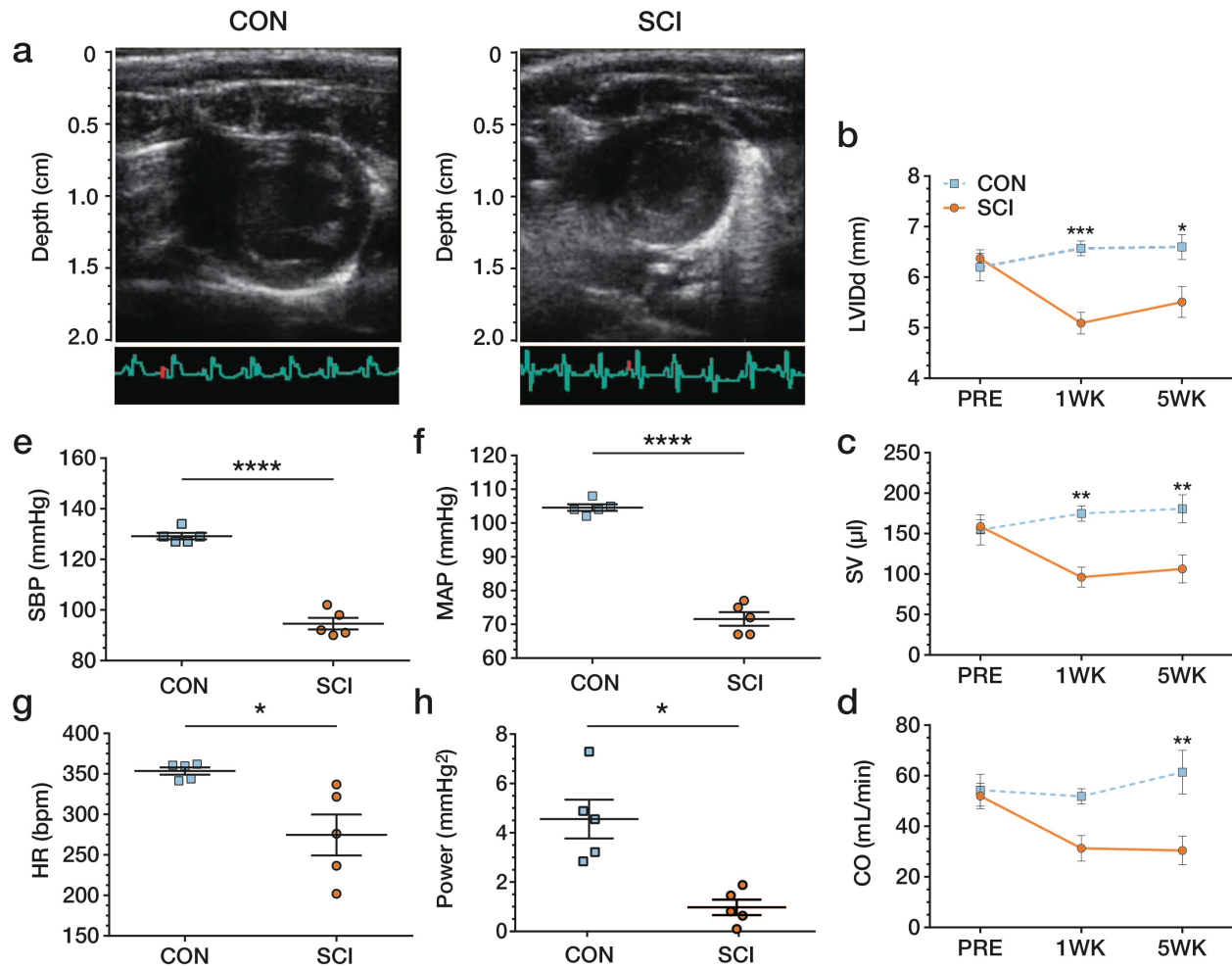
Figure 5.2: Representative echocardiography images of CON and SCI

(panel a). Left ventricular internal diameter during diastole (LVIDd; **panel b**), stroke volume

(SV; **panel c**), and cardiac output (CO; **panel d**) were all significantly reduced following SCI

compared to CON **(p < 0.05; Table 9.1; n=4).** At study termination, the SCI rats exhibited lower

systolic blood pressure (SBP; **panel e; n=5**) and mean arterial pressure (MAP; **panel f**). We

observed a significantly lower resting heart rate (HR; **panel g**) and low frequency SBP power

(panel h) following SCI (p < 0.05). Data are displayed as mean ± standard error. ****p < 0.0001

CON vs. SCI ***p < 0.001 CON vs. SCI **p < 0.01 CON vs. SCI *p < 0.05 CON vs. SCI.

To determine the pressure generating capacity of the heart, we assessed LV function at the study end-point using pressure-volume catheterization. We found significantly lower pressure generating capacity (i.e., dP/dt_{max}) after SCI at rest and confirmed our echocardiographic findings of reduced volumetric indices in SCI **(Table 5.1)**. The critical dependence of the LV on sympathetic input to maintain normal inotropy was clarified when we found that the pressure generating capacity of the LV could be restored in the T2 SCI group by pharmacologically administering the specific beta-1 agonist Dobutamine **(Figure 5.3)**.
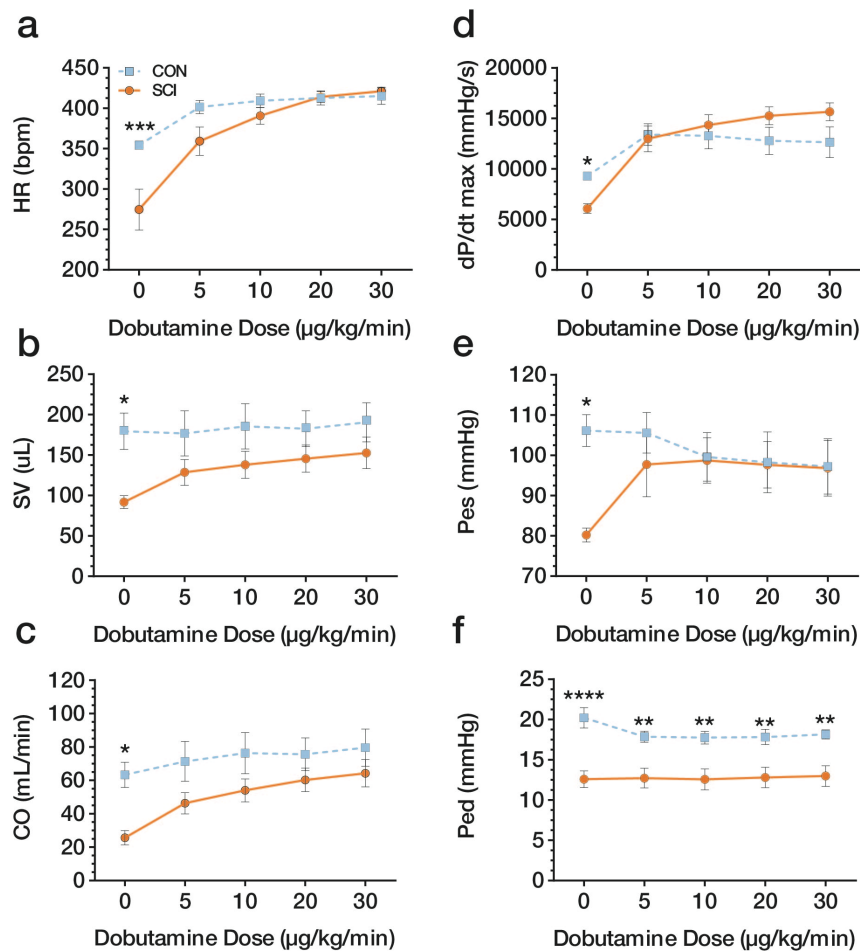
Figure 5.3: Pressure-volume derived indices in response to Dobutamine infusions at increasing concentrations.

Note the progressive increase in heart rate (HR; **panel a**) and dP/dt$_{max}$ **(panel d)**. Of note is the significant increase in dP/dt$_{max}$ **(panel d)** after spinal cord injury (SCI). However, end-diastolic pressure (Ped) was persistently low in SCI despite increasing Dobutamine concentrations **(panel f)**. All outcomes demonstrated a significant interaction effect. n=5. * = ****p < 0.0001 CON vs. SCI ***p < 0.001 CON vs. SCI **p < 0.01 CON vs. SCI *p < 0.05 CON vs. SCI. Abbreviations: SV: stroke volume; CO: cardiac output.

To partition the confounding effects of loading on LV function, we next assessed load-independent LV contractility by manipulating preload *via* inferior vena cava occlusions. We found that SCI exhibited significantly reduced end systolic pressure volume relationship (i.e., Ees), PRSW, as well as dP/dt-EDV relationships **(Figure 5.4)**, suggesting LV contractility is impaired in SCI.

Table 5.2: Anatomical, hemodynamic, echocardiographic, pressure volume, and cardiomyocyte data for CON and T2 rats at 5WK post-SCI

	CON			T2		
Anatomical Data						
Body mass (g)	438	±	12.7	331	±	43.0***
Heart Mass (g)	1.48	±	0.24	0.96	±	0.09**
Hemodynamic Data						
SBP (mmHg)	129	±	2.92	94.6	±	5.18****
DBP (mmHg)	91.6	±	2.79	60.2	±	6.22****
MAP (mmHg)	104	±	2.49	71.6	±	4.56****
HR (BPM)	354	±	10.9	275	±	56.6*
SVR (mmHg·min/μl)	1.61	±	0.29	3.02	±	0.78**
Echocardiographic Data						
Dimensions and volumes						
LVIDd (mm)	6.60	±	0.50	5.51	±	0.61*
LVIDs (mm)	3.26	±	0.50	3.25	±	0.37
LVPWd	2.03	±	0.39	2.29	±	0.57
RWT	0.63	±	0.17	0.85	±	0.30
EDV (μl)	225	±	36.7	150	±	38.5*
ESV (μl)	44.0	±	17.4	43.7	±	11.5
Systolic Function						
SV (μl)	181	±	34.6	106	±	34.7*
EF (%)	80.3	±	6.66	70.1	±	7.56
CO (ml/min)	61.4	±	17.3	30.5	±	11.3*
Diastolic Function						
E (mm/s)	0.80	±	0.08	0.80	±	0.07
Pressure Volume Data						
Systolic Function						
SW (mmHg·mL)	17.5	±	3.34	6.56	±	1.74***
SWI (mmHg·mL/100g)	4567	±	946	1874	±	447***
CO (ml/min)	66.3	±	12.5	25.7	±	9.62***
CI (ml/min·100g)	17.3	±	3.16	7.32	±	2.59***
SV (μl)	188	±	37.4	91.7	±	17.7***
Pes (mmHg)	105	±	7.95	80.2	±	3.83***
EF (%)	70.4	±	8.11	49.0	±	10.5*
dP/dt$_{max}$ (mmHg/s)	9225	±	414	6079	±	1054***
Ea (mmHg/μl)	0.59	±	0.15	0.90	±	0.13**
Ees^ (mmHg/μl)	1.32	±	0.15	0.65	±	0.19**
PRSW^ (mmHg)	112	±	10.0	72.6	±	14.7**
+dP/dt$_{max}$-EDV^ (mmHg/s·μl)	50.0	±	2.09	37.2	±	2.76***
Diastolic Function						
dP/dt$_{min}$ (mmHg/s)	-7006	±	959	-5825	±	815
Ped (mmHg)	19.7	±	1.99	12.6	±	2.31***
τ (ms)	11.2	±	0.76	13.4	±	2.33
EDPVR^ (mmHg/μl)	0.05	±	0.01	0.05	±	0.02
Cardiomyocyte Data						
Myocyte Length (μm)	121	±	5.98	93.9	±	8.54**
Alpha-Actinin Width (μm)	9.82	±	1.80	7.25	±	0.82*
Length/Width Ratio	12.7	±	2.16	13.0	±	1.13
Sarcomere Length (μm)	2.07	±	0.33	1.88	±	0.23
Estimated # Sarcomeres	59.4	±	7.69	50.1	±	3.78

Abbreviations: SBP: systolic blood pressure; DBP: diastolic blood pressure; MAP: mean arterial pressure; HR: heart rate; BPM: beats per minute; SVR: systemic vascular resistance; LVIDd: left ventricular internal diameter during diastole; LVIDs: left ventricular internal diameter during systole; LVPWd: left ventricular posterior wall thickness during diastole; RWT: relative wall thickness; EDV: end-diastolic volume; ESV: end-systolic volume; SV: stroke volume; EF: ejection fraction; CO: cardiac output; E: transmitral filling velocities during early diastole; SW: stroke work; SWI: stroke work index; CI: cardiac index; Pes: end systolic pressure; Ea: arterial elastance; Ees: end systolic pressure volume relationship; PRSW: preload recruitable stroke work; Ped: end diastolic pressure; EDPVR: end diastolic pressure volume relationship. P-values represent significance following independent samples t-test. Data are displayed as mean ± SD. ****$p < 0.0001$ vs. CON ***$p < 0.001$ vs. CON **$p < 0.01$ vs. CON *$p < 0.05$ vs.. ^Values were derived from mixed model linear regression and not from averaged individual animal data per se, error represented as standard error of the mean for these metrics.
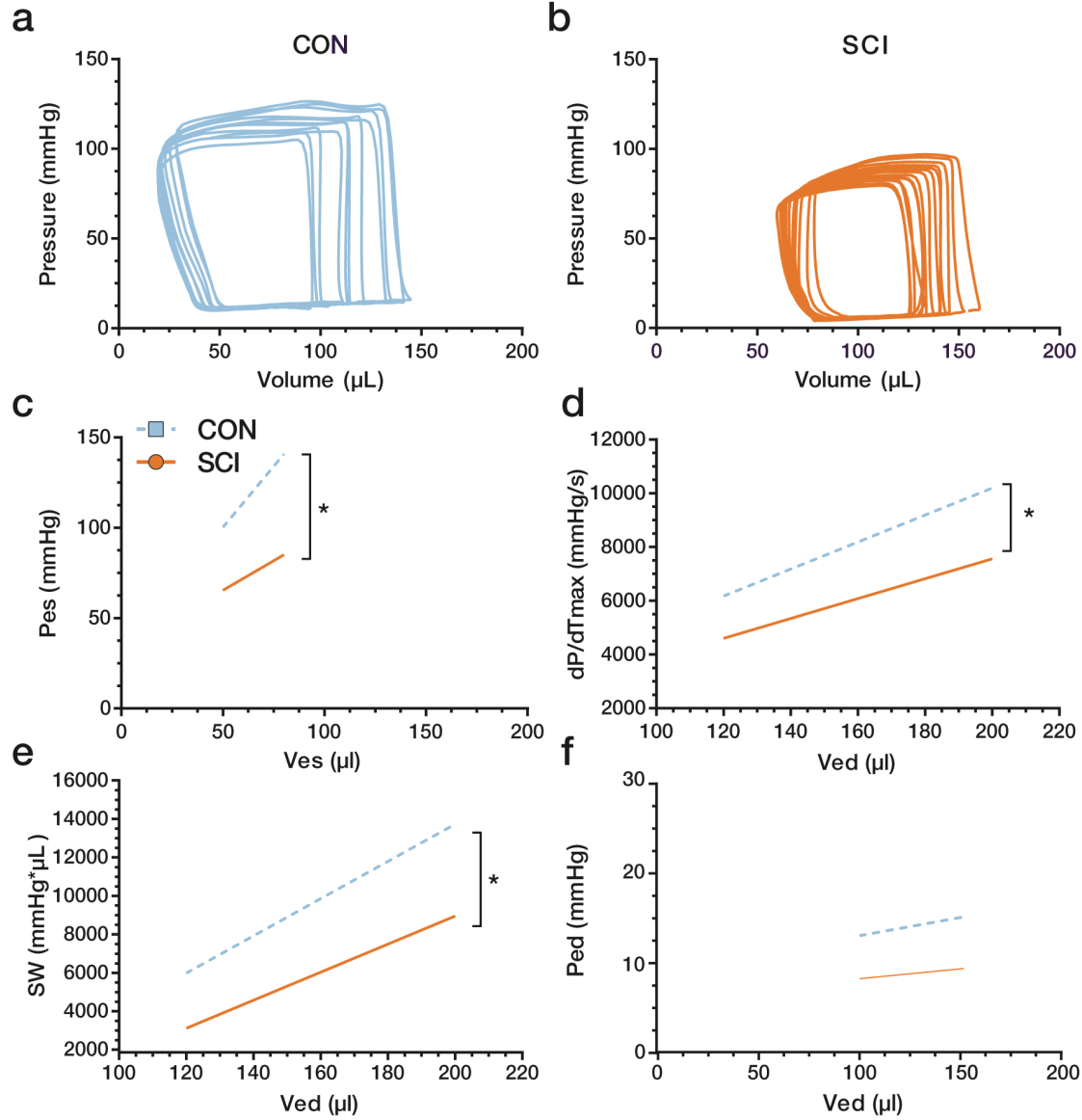
Figure 5.4: Pressure-volume analysis.

Representative pressure-volume loops obtained from 1 animal per group during inferior vena cava occlusions demonstrate the significant decrease in pressure and volume generating capacity after SCI **(panels a,b)**. Mixed model linear regression reveals significant decreases in all three measure of load-independent contractility including the end-systolic pressure (Pes) to volume (Ves) relationship **(panel c)**, dP/dt$_{max}$-end diastolic volume (Ved) relationship **(panel d)**, as well as preload recruitable stroke work **(**SW; **panel e)**. Moreover, we observed a significant decrease

in the end diastolic pressure (Ped) to volume relationship after both SCI **(panel f)**. n=5. * = p < 0.05 CON vs. SCI.

Next, we investigated the morphology of the cardiomyocytes at the mid-ventricular level. SCI resulted in significantly smaller myocyte length and z-disk width **(Figure 5.5)**. We did not, however, observe any changes in the length of individual sarcomeres **(Table 5.1)**. Thus, to explain the decrease in myocyte length, we estimated the number of sarcomeres and found that the average number of sarcomeres tended to be lower (p=0.07) after T2 SCI (**Table 5.1**). Lastly, we investigated the cellular milieu of the LV using qPCR to determine the potential underlying mechanisms leading to cardiomyocyte atrophy. We found that the degrading matrix metalloproteinase (MMP9) and the tissue inhibitor of matrix metalloproteinases (TIMP1) were significantly upregulated in SCI relative to CON **(Table 5.2)**.
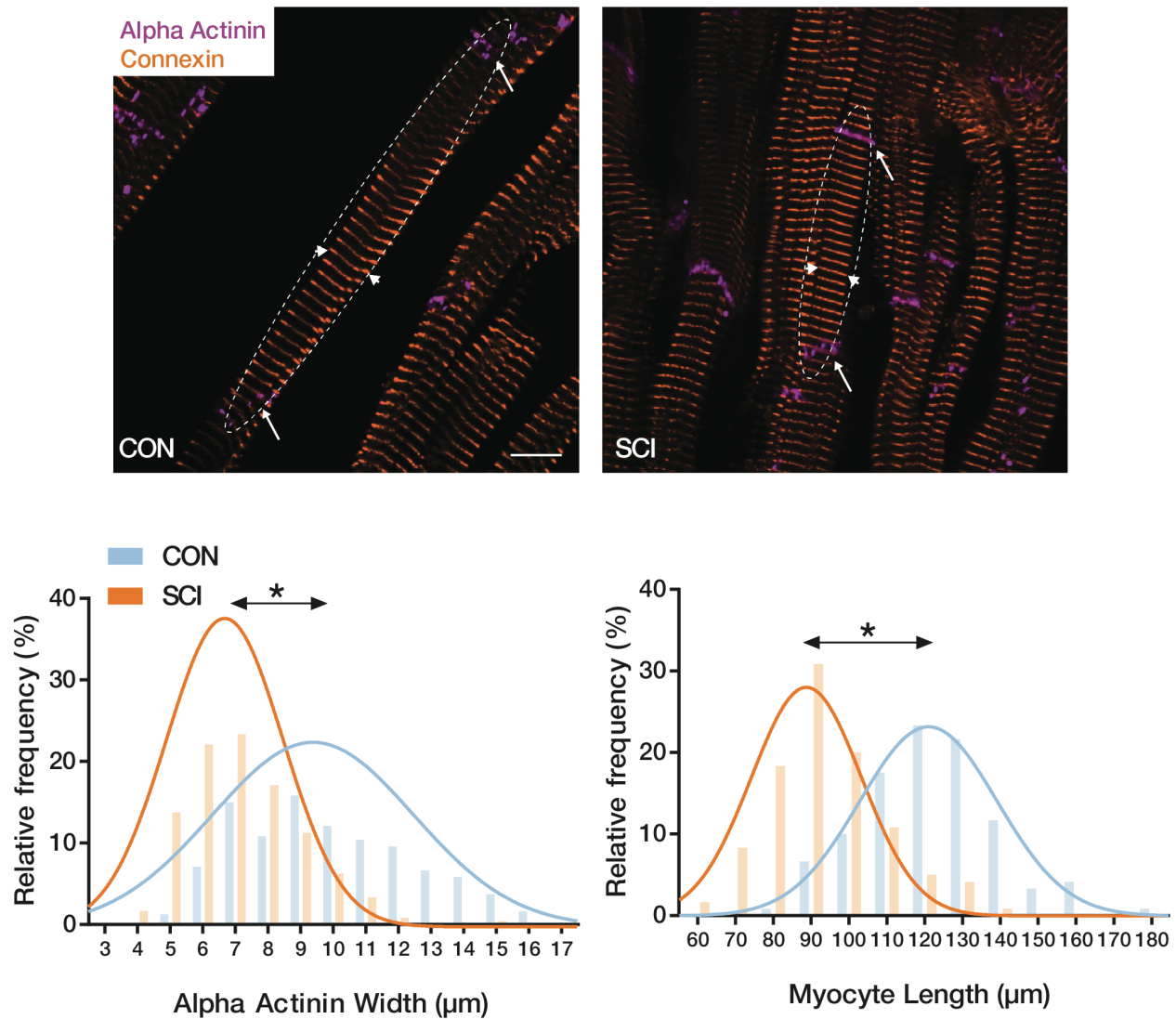
Figure 5.5: Cardiomyocyte immunohistochemistry.

Cardiomyocyte immunohistochemistry reveals a significant decrease in myocyte length, as well as a significant decrease in myocyte width after SCI (n=4) compared to CON (n=4). Histograms represent binned data at either every 1µm (αA width) or every 10µm (myocyte length), overlaid with a Gaussian curve. Scale bar = 10µm. * = $p < 0.05$ CON vs. SCI.

5.4   Discussion

The current results provide novel and mechanistic insight into the impact of SCI and specifically sympathetic control on both LV pressure generating capacity and 'contractility'. We observed a rapid decline in LV cavity size and volumetric indices that were accompanied by expected changes in peripheral hemodynamics. We demonstrate for the first time that SCI reduces LV pressure-generating capacity and impairs load-independent metrics of LV contractility *in vivo*. Importantly, we demonstrate the critical role of sympathetic influence to the LV by completely restoring pressure generating capacity with Dobutamine. Finally, we provide the first immunohistochemical and transcriptional evidence that SCI induces atrophic remodeling of cardiomyocytes and increases in cardiac tissue protease transcription.

Our first finding was that LV cavity size and volumetric cardiac indices were significantly reduced following SCI. This phenomenon has been well characterized by us and others using clinical and pre-clinical experiments. [127,163–165,178] Further, this finding is consistent with both short- and long-term bed rest and simulated microgravity exposure,[179,180] and is likely a response to chronic volume unloading. Our results are consistent with the volume unloading hypothesis, given that our injury model has near complete sympathetic decentralization. We have previously confirmed the lack of descending sympathetic control with retrograde neuronal tracing **(see Chapter 4)**,[174] where almost no descending sympatho-excitatory neurons cross the lesion site.[174] Moreover, we have shown via direct sympathetic nerve recordings that a model similar to ours significantly reduces sympathetic activity below the injury.[134] We currently demonstrate reduced sympathetic activity by reduced HR and low frequency systolic blood pressure power, the latter of which has been shown to indicate reduced sympatho-excitatory

drive from the brainstem.[181] This, in conjunction with a diminished skeletal muscle pump

impairs venous return. On the other side of the heart, SCI induced a significant decrease in mean

arterial pressure **(Figure 5.2e; Figure 5.6; Table 5.1)** as expected given the decentralization of

the peripheral vasculature. Specifically, the rat celiac ganglia, superior mesenteric ganglia, and

inferior mesenteric ganglia, which together are responsible for smooth muscle tone of the

splanchnic vasculature are entirely removed from medullary control with this SCI.[173] While both

reduced preload and afterload are capable of unloading the LV and reducing cavity size, our

previous finding that passive-hind limb exercise completely restores chamber diameter and

improves volumetric indices to a greater extent than peripheral hemodynamics[127] implies

reduced preload is playing a larger role in LV unloading in SCI.

Second, our data reveal a robust and significant impairment in pressure-derived cardiac

indices following SCI. Previous research has shown that dP/dt_{max} is maintained in an *in vivo*

setting following T5 SCI,[168] which preserves direct cardiac sympathetic control. These elegant *in*

vivo physiological studies have been performed in a T5 injury model and it has been repetitively

shown that this model results in sympathetic hyperactivity in rostral sympathetic circuits (i.e., the

ones controlling the heart). [139,167] While this model is ideal to examine the role of sympathetic

hyperactivity on the heart and vasculature, the majority of individuals with SCI who exhibit

cardiac dysfunction have either a high thoracic or cervical SCI,[163,164] and have clinically been

shown to exhibit low sympathetic activity.[182] This contrast between an overactive versus

underactive sympathetic nervous system likely produces very different cardiac and vascular

remodeling/dysfunction. In the high-thoracic (T2/T3) model, we know that sympathetic activity

is low and that the heart exhibits fibrotic remodeling;[127,134,170] however, a thorough investigation

of *in vivo* hemodynamics and cardiac function has never been performed. To confirm the reduction in these pressure-derived indices is dependent on sympathetic input, we show that both indices can be completely restored after SCI with the administration of Dobutamine, a specific beta-1 adrenergic receptor agonist. In contrast to the normalization of pressure indices with Dobutamine, we observed only a small increase in stroke volume **(Figure 5.3)** that was likely due only to an increased strength of contraction (i.e., ejecting a greater volume of blood and reducing end-systolic volume), as opposed to increased pre-load, as we did not observe a change in end-diastolic volume. Although our contusion model potentially spares more autonomic fibers than a typical transection model, the degree of reduction in dP/dt_{max} is similar to that reported with transection models.[127,170] We believe the severity of our contusion injury, which results in only 1% white matter sparing **(see Chapter 4)**,[174] is such that it acts almost similar to a transection model. To this end, we also demonstrate clear evidence of exaggerated responses to adrenergic stimulation which concurs with that reported in the peripheral vasculature at a similar time point in rodents with a complete spinal cord transection at the T3 level.

Third, our data conclusively demonstrate that SCI causes intrinsic inotropic dysfunction as all load-independent metrics of systolic function, including those indexed to heart size,[177] were impaired after SCI. Although the exact mechanism causing impaired contractile function remains to be elucidated, our Dobutamine data provide compelling evidence that loss of descending sympathetic drive is the primary cause of LV dysfunction after SCI. Nevertheless, reduced LV contractility is likely also influenced by the chronic loss of control to the adrenal medulla, which is responsible for providing circulating catecholamines. For example, adrenal release of catecholamines is impaired after high-thoracic or cervical SCI, and that the loss of

circulating catecholamines induces cardiomyocyte atrophy,[182-184] which is critically linked to contractile function.[185-186] We believe the importance of demonstrating load-independent systolic dysfunction extends to clinical practice. Recent work in the setting of heart failure with preserved ejection has shown that PV relationships can aid diagnosis and provide novel mechanistic understanding.[187] Furthermore, the importance of demonstrating load-independent function extends to clinical practice. This latter point may be particularly poignant to the SCI population give ejection fraction is often preserved or even enhanced due to the substantial reduction in end-diastolic volume. As such the increased odds for heart disease often reported in SCI may in fact be a gross underestimation of the true incidence of heart disease in SCI. Put together, our findings that LV contractility is impaired in vivo and independent of loading conditions following SCI provides an important step forward in our understanding of how SCI impacts in the heart and the specific role that the sympathetic nervous system plays in controlling inherent LV contractility.

Although we did not seek to investigate the temporal response of our contractile indices in the present study we have previously reported that the gross changes in size and function of the heart are apparent within 1 week following injury and remain relatively stable thereafter.[127] We have also reported that HR response to Dobutamine is similarly compromised in rodents with T2 contusion SCI at 1 vs. 6 weeks after injury, implying SCI rapidly and persistently induces systolic cardiac dysfunction.[188] Since the systolic dysfunction reported here is likely due to reduction in global sympathetic outflow from the rostral ventrolateral medulla, and such a reduction would occur almost immediately following injury, it is expected load-independent dysfunction would be apparent relatively quickly following SCI.

Compared to the wealth of studies investigating mechanisms of cardiac hypertrophy relatively less is known about the regulation of cardiomyocyte atrophy. In the present study we observed consistent cardiomyocyte atrophy (decrease in myocyte length, z-disc width, and the number of sarcomeres per myocyte) in all SCI animals. These results are broadly in line with previous work in cardiac unloading studies, which identified similar changes in cardiomyocyte morphology.[189] In fact, previous studies have suggested that the direct link between alterations in cardiomyocyte morphology and LV contractile reserve are likely related to changes in cardiomyocyte cytoskeletal architecture (e.g. intracellular coupling of myocytes,[190] availability of titin binding sites[185]), as well as alterations in protein phosphorylation[191] and/or prolonged calcium transients.[192] While investigation of all of these mechanisms is beyond the scope of the current experiments, we did find that both MMP9 and the inhibitor TIMP1, which play a pivotal role in the degradation of the extracellular matrix, were both upregulated after SCI **(Table 5.2)**. Increased activation of MMP9 and TIMP1 has been implicated in numerous pathological conditions including heart failure.[193] Moreover, it has been reported that elevated serum MMP9 and TIMP1 are also associated with an increased risk of all-cause mortality in the general population,[193] and TIMP1 appears inversely related to systolic function in elderly individuals free from heart disease.[194] Thus, we suggest that changes within the LV related to degradation of the extracellular matrix and integrity of myocyte z-disk create an environment conducive for cardiomyocyte atrophy.

An intriguing finding of the present study was that we were able to restore pressure generating capacity of the LV following SCI with the administration of Dobutamine, which implies that the observed cardiomyocyte atrophy may not entirely limit the capacity of the LV to

generate pressure given sufficient stimulation. In comparing the responsiveness of SCI and CON rats to Dobutamine, the SCI rats exhibited a greater increase in contractile indices at 5µg. Therefore, we suggest that either through hyper-responsive beta receptors or through altered recruitment of cardiomyocytes, the LV appears able to adequately generate pressure given sufficient sympathetic stimulation. This notion is supported by our finding that beta receptor transcription is unchanged after SCI (**Table 5.2)** and our previous finding that beta receptor density is also unchanged after SCI.[170] An important distinction to make is that while the normalization of dP/dt_{max} and Pes with Dobutamine implies improved pressure-generating capacity it does not necessarily reflect a normalization of inherent inotropic function, as dP/dt_{max} is known to be load-dependent and may therefore change only because of altered loading conditions.[195,196]
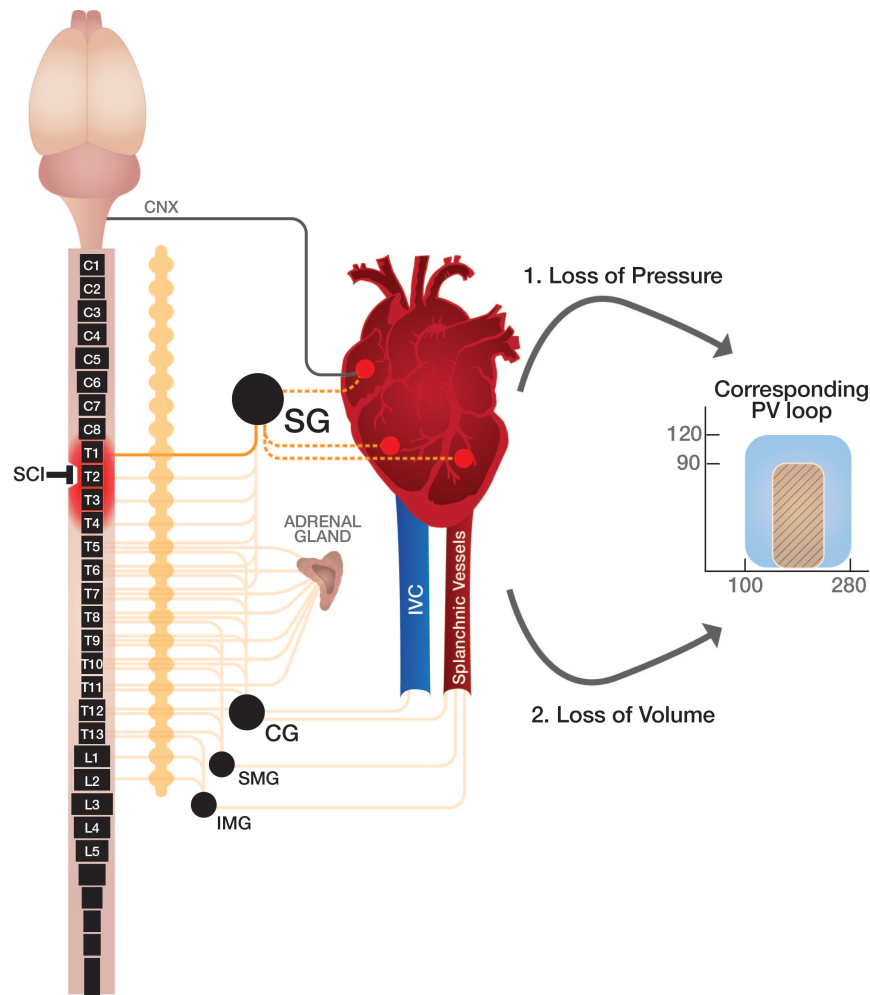
Figure 5.6: Neuroanatomical representation of the sympathetic-mediated pathophysiology leading to cardiac dysfunction after spinal cord injury (SCI).

Under normal physiological conditions pre-ganglionic neurons within the thoracic and lumbar spinal cord are controlled by supraspinal brainstem centres (i.e. rostral ventrolateral medulla). To maintain cardiac function, direct sympathetic control to the heart itself, as well as control over major venous, arterial, and adrenergic systems (i.e. adrenal medulla) is critical. Here, we depict the decentralization of the sympathetic nervous system after T2 contusion SCI that ultimately leads to cardiac dysfunction and maladaptive remodeling. Schematic representations of pressure-

volume loops for SCI (orange) are displayed, overlaid on a representation of a normal physiological response (blue). SCI resulted in significantly decreased pressure generating capacity, which may be attributed to the significant decentralization of the heart itself and/or the adrenal medulla, leading to decreased circulating catecholamines and reduced beta stimulation to the left-ventricle (i.e. "1. Loss of Pressure"). This hypothesis is further supported by the complete restoration of pressure generating capacity with Dobutamine, a beta agonist **(Figure 9.3)**. Furthermore, SCI induced a loss of volume generating capacity (i.e. "2. Loss of Volume"), which can be attributed to loss of control over the inferior vena cava, preventing optimal blood flow return to the right atrium (i.e. pre-load). The extent of injury spread depicted in this schematic is based on previous modelling of this experimental injury.[16] Solid lines indicate intact sympathetic control. Dotted lines indicate partial sympathetic ganglionic control from remaining sympathetic pre-ganglionic neurons. Faded lines indicate decentralization of sympathetic pre-ganglionic neurons and thus improper control of ganglionic neurons. Pressure-volume loops are depicted in the classical volume (x-axis) vs. pressure (y-axis). Abbreviations: SG: stellate ganglion, CG: celiac ganglion, SMG: superior mesenteric ganglion, IMG: inferior mesenteric ganglion; IVC: inferior vena cava; SCI: spinal cord injury; CNX: cranial nerve X (vagus nerve).

5.5   Conclusion

In summary, our data provide novel *in vivo* evidence to demonstrate that severe high-thoracic spinal cord contusion reduces volumetric and pressure derived left-ventricular indices as well as contractile dysfunction. Moreover, we provide observations that changes in the contractile function are accompanied by changes in the structure of the cardiomyocytes, and

provide novel insight into the potential underlying mechanisms related to cardiac dysfunction in this population by identifying transcriptional changes in proteins and promoters of extracellular matrix degradation. Whilst we are unable to conclusively demonstrate the causal relationship with respect to the relative temporal changes in LV contractility and myocyte/matrix remodeling, our data provide clear evidence of LV dysfunction *per se*. Collectively, these results represent an important step forward in our understanding of how the heart functions post-SCI and demonstrate the clear need for future therapies to target preservation of the descending sympathetic pathways to prevent cardiac contractile dysfunction. An important clinical implication of the present work is that it suggests rehabilitation strategies which target only the normalization of ventricular filling (i.e., activation of the lower-limbs with functional electric stimulation, cycling, or rowing) may not be sufficient to normalize all aspects of cardiac dysfunction after SCI and prevent early heart disease.

Given these important findings showing inherent left-ventricular dysfunction after SCI, the next chapter **(Chapter 6)** will build on these results and investigate the relationship between cardiac dysfunction and injury severity using clinically relevant and translatable imaging techniques. Using imaging techniques that are accessible in humans is a necessary step, as left-ventricular catheterization is not an implementable technique in the clinic. Therefore, the next chapter will focus on echocardiography to provide foundational evidence from which further human studies can be designed.

Chapter 6: Spinal cord injury induced cardiomyocyte atrophy and impaired cardiac function are severity dependent[4]

6.1   Introduction

Cardiovascular disease has emerged as the number one cause of both morbidity and mortality for individuals living with spinal cord injury (SCI).[197] Furthermore, recent epidemiological data has indicated that the SCI population is at significantly increased odds of developing heart disease (adjusted odds ratio 2.72, 95% confidence interval 1.94-3.82).[11]

A recent surge in the number of pre-clinical rodent experiments has enhanced our understanding of cardiac dysfunction in this population. When sympathetic pre-ganglionic neurons to the upper-thoracic spinal cord are removed from supraspinal control, our group showed that SCI (T3) induces a reduction in global LV dimensions **(see Chapter 5)**,[127,170,198] LV mechanics[170] and impairs LV contractility **(see Chapter 5)**,[127,198] all of which are perpetuated by chronic exposure to autonomic dysreflexia.[89] Further, we have more recently shown that load-independent LV function is impaired following T3 SCI, and is accompanied by atrophy of cardiomyocytes **(see Chapter 5)**.[198] In contrast, when descending sympatho-excitatory input to the upper thoracic spinal cord is intact, there is an increased density of tyrosine hydroxylase

---

[4] A version of chapter 6 has been published. **Squair, J.W.,** Liu, J., Tetzlaff, W., Krassioukov, A.V., West, C.R. (2017). Spinal cord injury induced cardiomyocyte atrophy and impaired cardiac function are severity dependent. Experimental Physiology. 103(2):179-189.

positive terminals in the heart and enlargement of stellate soma, suggesting increased cardiac sympathetic nerve activity.[167,168] This manifests as electrophysiological changes including altered sinus rhythms, increased risk of arrhythmias,[167,168] and a greater reliance on adrenergic stimulation to maintain contractile function.[168] Importantly, in both of these injury models the lack of descending control to the splanchnic region reduces stroke volume and has been recently shown to cause significantly dysfunctional hemodynamic responses to coronary ischemia.[139,199] Put together, these findings suggest that the global systolic dysfunction observed in experimental SCI is heavily dependent on descending sympatho-excitatory control. However, how global and regional systolic function change with differing severities of SCI (and therefore different amounts of intact sympathetic control) is unclear.

Therefore, the principle aim of the present study was to extend previous research into cardiac function after SCI by examining how the severity of SCI impacts regional cardiac function as well as underlying cardiomyocyte morphology. We have recently shown that the number of intact descending sympatho-excitatory axons responsible for maintaining sympathetic cardiac control is severity dependent (less intact axons with a more severe injury), and can be reliably modelled in the rodent **(see Chapter 4)**.[174] Using this as our guiding framework, we combined speckle tracking echocardiography, a clinically-relevant and angle-of-insonation independent measure of LV mechanics,[200,201] with a robust analysis of cardiac myocyte structure in rodents with differing severities of contusion SCI to examine how injury severity impacts cardiac structure and function.

6.2   Materials and methods

6.2.1   Ethical approval

All procedures were conducted according to the Canadian Council for Animal Care. Ethical approval was also obtained from the University of British Columbia (A14-0152).

6.2.2   Experimental design

Fifteen male Wistar rats (age = 9 weeks, mass = 300-450g; Harlan Laboratories, Indianapolis, IN, USA) were randomly assigned to one of three groups: sham-injured control (SHAM; n = 5), moderate T3 SCI (MODERATE; n = 5), or severe T3 SCI (SEVERE; n = 5). Three SHAM animal hearts were damaged during harvesting and therefore three separate SHAM animals were used to supplement the immunohistochemistry analysis. These animals were not used in any correlation analyses. We used *in vivo* echocardiography and speckle tracking analyses to determine temporal changes in cardiac structure and function. We conducted assessments at pre-injury and at day 14 and day 30 post-injury. At the study endpoint (day 31) all animals were used for cardiac immunohistochemistry **(Figure 6.1a; Figure 6.1b).**

6.2.3   Spinal cord surgery and animal care

Spinal cord contusions were conducted as we have previously described **(see Chapters 4, 5)**.[174,198] Animals were started on a prophylactic dose of enrofloxacin (Baytril; 10 mg kg^{-1}, s.c., Associated Veterinary Purchasing (AVP), Langley, Canada) three days prior to surgery. On the day of spinal cord contusion, animals were anesthetized (initial chamber induction at 4% isoflurane with 2l min^{-1} oxygen, followed by maintenance on a Bain's system at 1.5-2% isoflurane with 1.5-2l min^{-1} oxygen) and administered enrofloxacin (Bayril; 10 mg kg^{-1}, s.c,

Associated Veterinary Purchasing, Langley, Canada.), buprenorphine (Temgesic; 0.02 mg kg^{-1}, s.c., McGill University), and warmed lactated Ringer's solution (5 ml, s.c.). The superficial muscles overlying the C8-T5 vertebrae were opened with a dorsal midline incision. The T2 and T4 spinous bodies were stabilized with custom modified Allis forceps, which were mounted on a secure metal stage. The custom-made impactor tip (2.5mm, Infinite Horizons (IH) Impactor) was placed midline directly over the exposed T3 dura. SHAM animals were removed from the surgical stage at this stage and subsequently sutured. For spinal cord-injured animals, the impactor tip was driven downward with either 200 kilodynes (kdyn; MODERATE) or 400 kdyn (SEVERE) of pre-defined force, with 5s of dwell time for each injury. The wound was then irrigated and closed with 4-0 Monocryl (Ethicon) for muscle and 4-0 Prolene sutures (Ethicon) for skin. Animals were allowed to recovery in a temperature-controlled environment (Animal Intensive Care Unit, Los Angeles, CA, USA) and were administered enrofloxacin (10 mg kg-1, s.c.), buprenorphine (0.02 mg kg-1, s.c.) and ketoprofen (5 mg kg-1, s.c.) every 12 hours for 3 days post-operatively. Bladders were manually expressed three times per day until spontaneous bladder voiding was restored (approximately 1 week post-injury in SEVERE animals).

6.2.4 *In-vivo* echocardiography and speckle tracking analyses

We completed echocardiography using a commercially available imaging system (Vivid 7, GE Health Care, Horton, Norway) and specialized transducer specifically designed for use in rodents (GE Healthcare i13L, 5.6-14.1 MHz; Horton, Norway), as we have previously described **(see Chapter 5)**.[127,170,198] Animals were anesthetized using isoflurane (initial chamber induction at 4% isoflurane with 2l min^{-1} oxygen, followed by maintenance on a Bain's system at 1.5-2% isoflurane with 1.5-2l min^{-1} oxygen) with heart rate maintained between 300-350 beats per

minute. Measures of LV structure and function were imaged using M-mode echocardiography in a parasternal short-axis view. Estimated volumes were calculated according to the Teichholz method.[127] Pulsed-wave Doppler during an apical four-chamber view was used to estimate early diastolic filling velocity. Results were quantified (Echopac; GE Healthcare, Horton, Norway) and determined from the average of 5 cardiac cycles. Speckle tracking analysis (Echopac; GE Healthcare, Horton, Norway) was used to calculate radial strain, an index of LV mechanics, in a parasternal short-axis papillary view. Five cardiac cycles were used and the average for each animal was taken. Each cardiac cycle was taken from the peak of the p-wave to the peak of the next p-wave and standardized to 100% cardiac cycle using customized software in order to obviate expected differences in heart rate across animals.

6.2.5   Tissue processing and immunohistochemistry

6.2.5.1   Tissue processing

Animals were overdosed with chloral hydrate (1g kg^{-1}, I.P.), perfused transcardially with 500 ml of 0.1 M phosphate buffered saline (PBS), and fixed with 500 ml of 4% formaldehyde in PBS. Hearts were dissected and prepared for immunohistological analysis according to our previously described methods **(see Chapter 5)**.[127,174,198] Briefly, hearts were sectioned along the longitudinal axis into thirds. The left mid-ventricular level was placed in a custom mold, covered with cryomatrix, and stored at -80°C. Cross-sections (10µm) were then obtained using a cryostat. The right femur was removed from each animal to provide length-corrected measures for all structural echocardiographic indices at 5-weeks post-injury. Lesion sites (±4mm of epicenter, spinal segments T1-T5) were dissected following perfusion and post-fixed identically to the heart

tissue. Injury site sections were cross-sectioned at 20 µm and mounted on sets of 10 slides (Fisherbrand Superfrost), with 8 sections per slide and an inter-section distance of 200 µm.

6.2.5.2 Immunohistochemistry

LV sections were first thawed for one hour at room temperature and pat-penned, followed by re-hydration in 0.1M PBS for 10 minutes. Next, sections were incubated with 10% normal donkey serum for 30 minutes. After removal of normal donkey serum, sections were incubated in primary antibody prepared in 0.1M PBS-Triton overnight at room temperature. The next morning three 10 minute 0.1M PBS washes were done to remove the primary antibodies, after which they were incubated with secondary antibodies for two hours. Sections were then cover slipped using immunomount and stored at 4°C. The following primary antibodies were used: mouse anti-collagen I (COL1, 1:2000, Abcam, ab90395), rabbit anti-α actinin (αA, 1:100, Abcam, ab68167), goat anti-connexin 43/GJA1 (CX, 1:250, Cedarlane, NBP1-51938). Secondary antibodies used were: Alexa Fluor 647 Donkey Anti Goat (1:200; Jackson ImmunoResearch; 705-606-147), Alexa Fluor 594 Donkey Anti Rabbit (1:200; Jackson ImmunoResearch; 711-586-152), Alexa Fluor 488 Donkey Anti Mouse (1:200; Jackson ImmunoResearch; 715-546-151), and Hoechst Reagent (1:1000).

6.2.5.3 Imaging

Immunofluorescence was digitally imaged using an Axioplan 2 microscope (Zeiss) or a Zeiss AxioObserver Z1 confocal microscope equipped with a CSU-X1 spinning disc (Yokogawa Electric) and AxioVision 4.8 ZEN Blue (Zeiss) was used for all digital image capture procedures. Post-processing was completed using ImageJ (ImageJ NIH) software.

6.2.6   Quantification of immunolabelling

All myocyte measurements were made over the LV free wall by a blinded experimenter.
Myocyte length was measured as the distance between two CX-labelled end-plates and
confirmed by the localization of at least one nucleus between these two sites. Five myocytes
were measured per 20x image, for a total of 40 measured myocytes per animal. Z-disk width was
measured as the width of individual αA labels. Ten individual measurements were made per 20x
image, for a total of 80 estimations of z-disk width per animal. Myocyte length/width ratio was
then calculated. To measure individual sarcomere lengths, the distance between two αA was
utilized, as we have previously described **(see Chapter 5)**.[198] Ten individual measurements were
made per 20x image. For COL1 quantification a standardized particle density quantification was
utilized. Briefly, images were processed using ImageJ, where each image was converted to 8-bit
and a particle threshold (Default Dark) was set. Integrated particle density was then calculated as
number of pixels x area (1,443,520 pixels) of image. Eight images across 4 individual sections
per animal were taken at 20x over the LV myocardium. Lesion site sections were stained with
eriochrome cyanine, according to standard operating procedures. The epicenter of the lesion was
defined as the section with the least amount of white matter sparing. White matter sparing was
defined as normal or near normal myelin-positive staining and was then quantified every 1mm
from the lesion site epicenter in both the rostral and caudal directions.

6.2.7   Statistical analyses

All statistical analyses presented were conducted using SPSS 19/20 software. All graphical
representations of data were made using GraphPad Prism 6 and all immunohistochemical images
were taken using ZEN blue (Zeiss) and processed with Adobe Photoshop CC. All cardiac and

immunohistochemical data were analyzed using independent-samples t tests, one-way analysis of variance (ANOVA) or repeated-measures ANOVA, as appropriate. Data are presented in text and visualized as mean ± standard deviation. Where appropriate, the raw data is presented in order to aid in interpretation. Significant main or interaction ANOVA effects were further investigated using Tukey's HSD *post-hoc* testing with a Dunnett correction. Correlational analyses were conducted using parametric (Pearson's correlation coefficient [r]). The significance level for all statistical tests was set at $P = 0.05$.

6.3   Results

6.3.1   Severe T3 spinal cord contusion impairs cardiac structure and function

Time-course echocardiography revealed a significant decrease in absolute LV diameter during both diastole (LVIDd) and systole (LVIDs) following SEVERE SCI but not MODERATE SCI or SHAM at 5-weeks post-injury vs. pre-injury **(Figure 6.1c; Figure 6.1d)**. After correcting all structural values to femur length following dissection, we observed a near universal decline in all echocardiographic indices after SEVERE SCI but not MODERATE SCI at the 5WK time-point **(Table 6.1)**. Specifically, LVIDd, LVIDs, EDV, ESV, and SV were all reduced following SEVERE SCI compared to both MODERATE SCI and SHAM animals (all $P < 0.01$). Conversely, no differences were noted between MODERATE SCI and SHAM (**Table 6.1**; all $P > 0.05$), or in posterior and septal wall metrics (**Table 6.1**; all $P > 0.05$). No differences in body mass or femur length were noted between groups **(Table 6.1)**.

Table 6.1: Anatomical and echocardiographic data for SHAM, MODERATE, and SEVERE rats at 5WK post-SCI

	SHAM ($n = 5$)	MODERATE ($n = 5$)	SEVERE ($n = 5$)
Anatomical Data			
Body mass (g)	466 ± 15	430 ± 37	420 ± 33
Femur Length (cm)	3.97 ± 0.07	3.89 ± 0.09	3.95 ± 0.15
Echocardiographic data			
Dimensions and volumes			
LVIDd (mm)	7.49 ± 0.49	7.05 ± 0.53	5.83 ± 0.46***††
LVIDs (mm)	4.14 ± 0.34	3.97 ± 0.34	2.94 ± 0.40***††
IVSd (mm)	2.01 ± 0.25	1.87 ± 0.16	1.99 ± 0.09
LVPWd (mm)	2.14 ± 0.29	2.09 ± 0.20	2.01 ± 0.07
IVSs (mm)	3.77 ± 0.52	3.81 ± 0.67	3.68 ± 0.40
LVPWs (mm)	3.50 ± 0.39	3.23 ± 0.43	3.04 ± 0.12
RWT	0.56 ± 0.07	0.57 ± 0.08	0.69 ± 0.07*
EDV (μl)	295 ± 45	261 ± 43	170 ± 30***††
ESV (μl)	76.5 ± 14	69.5 ± 14	34 ± 11***††
Systolic Function			
SV (μl)	219 ± 41	192 ± 38	136 ± 21**
EF (%)	73.9 ± 4.97	73.1 ± 5.13	80.2 ± 3.79
CO (ml/min)	39.0 ± 7.6	38.8 ± 14.8	27.2 ± 5.9
Diastolic Function			
E (mm/s)	86.0 ± 8.2	84.1 ± 6.6	76.7 ± 13.2

Note the near uniform decline in echocardiographic indices following SEVERE SCI. Abbreviations: LVIDd, left ventricular internal diameter during diastole; LVIDs, left ventricular internal diameter during systole; IVSd: interventricular septal wall during diasole; left ventricular posterior wall thickness during diastole; IVSs interventricular wall thickness during systole; LVPWs: left ventricular posterior wall thickness during diastole; RWT: relative wall thickness (IVSd+LVPWd / LVIDd); EDV, end-diastolic volume; ESV, end-systolic volume; SV, stroke volume; EF, ejection fraction; CO, cardiac output; E, transmitral filling velocities during early diastole. All echocardiographic structural values are corrected for femur length. P-values represent *post-hoc* testing following a significant one-way ANOVA. Data are displayed as mean ± SD. ***$P < 0.001$ vs. SHAM **$P < 0.01$ vs. SHAM *$P < 0.05$ vs. SHAM †$P < 0.05$ vs. MODERATE. ††$P < 0.01$ vs. MODERATE.
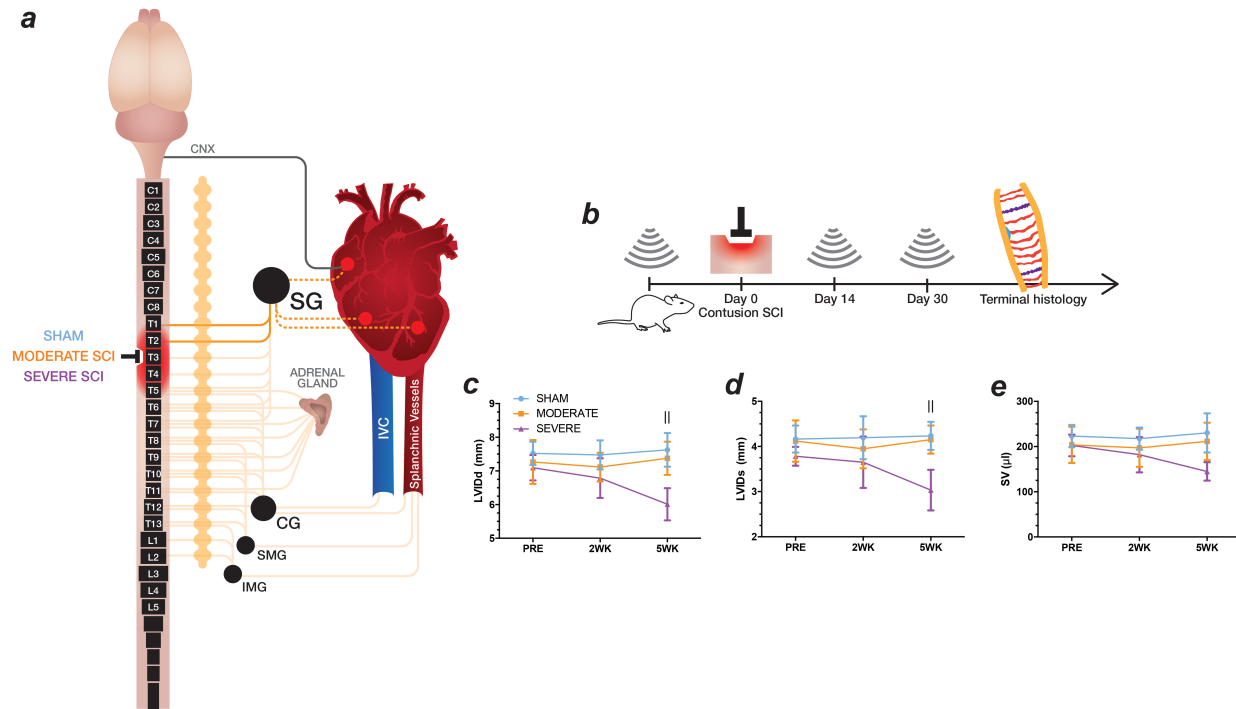
Figure 6.1: Overview of the sympathetic nervous system (adapted from Squair et al., 2017 [Chapter 5]).

The spread of injury spread in this schematic is based on previous modelling of this experimental injury (Squair et al., 2016; **see Chapter 4**). Solid lines indicate intact sympathetic control. Dotted lines indicate partial sympathetic ganglionic control from remaining sympathetic pre-ganglionic neurons. Faded lines indicate decentralization of sympathetic pre-ganglionic neurons. Pressure-volume loops are depicted in the classical volume (x-axis) vs. pressure (y-axis). Abbreviations: SG: stellate ganglion, CG: celiac ganglion, SMG: superior mesenteric ganglion, IMG: inferior mesenteric ganglion; IVC: inferior vena cava; SCI: spinal cord injury; CNX: cranial nerve X (vagus nerve). **(b)** Experimental design to determine how the severity of spinal cord contusion impacts cardiac function. Adult Wistar rats underwent echocardiography prior to injury in order to establish pre-injury parameters. Rats were then given a severe spinal cord contusion (day 0).

At 14 and 30 days post-SCI, each rat was assessed using echocardiography to determine structural and functional changes to the left ventricle. At 31 animals were sacrificed and their heart was harvested and processed in preparation for histological analyses of cardiomyocytes. **(c)** Left ventricular internal diameter during diastole (LVIDd) was significantly reduced at 5WK compared to PRE following SEVERE SCI (6.01mm ± 0.48mm *vs.* 7.09mm ± 0.38mm; *P* = 0.0054). **(d)** Left ventricular internal diameter during systole (LVIDs) was significantly reduced at 5WK (3.03mm ± 0.4498mm) compared to PRE (3.78mm ± 0.209m; *P* = 0.006) and 2WK (3.65mm ± 0.568mm *P* = 0.024) following SEVERE SCI. **(e)** Estimated stroke volume (SV) was not statistically different at 5WK from PRE following SEVERE SCI (ANOVA *P* = 0.264). ||= SEVERE 5WK different from SEVERE PRE (*post-hoc* following ANOVA interaction *P* < 0.05). Data are displayed as mean ± standard deviation.

6.3.2   T3 spinal cord injury globally reduces left-ventricular strain

Global radial strain was significantly reduced following SEVERE SCI at 5WK post-injury **(Figure 6.2b)**. No differences were noted between LV regions **(Figure 6.2b)**. By 5WK post-injury, radial strain throughout the systolic component of the cardiac cycle was significantly impaired in SEVERE SCI compared to both MODERATE SCI and SHAM **(Figure 6.2c)**. This was in contrast to the relatively similar patterns seen at PRE and at 2WK post-injury **(Figure 6.2c)**. When examining the average peak strain, a time-course dependent relationship was observed whereby SEVERE SCI decreased significantly at 5WK compared to PRE **(Figure 6.2d)**. Conversely, no differences between 5WK and PRE were noted for MODERATE SCI or SHAM **(Figure 6.2d)**. Lastly, a significant correlation was noted between peak radial strain and SV as well as CO **(Figure 6 .2d)**.
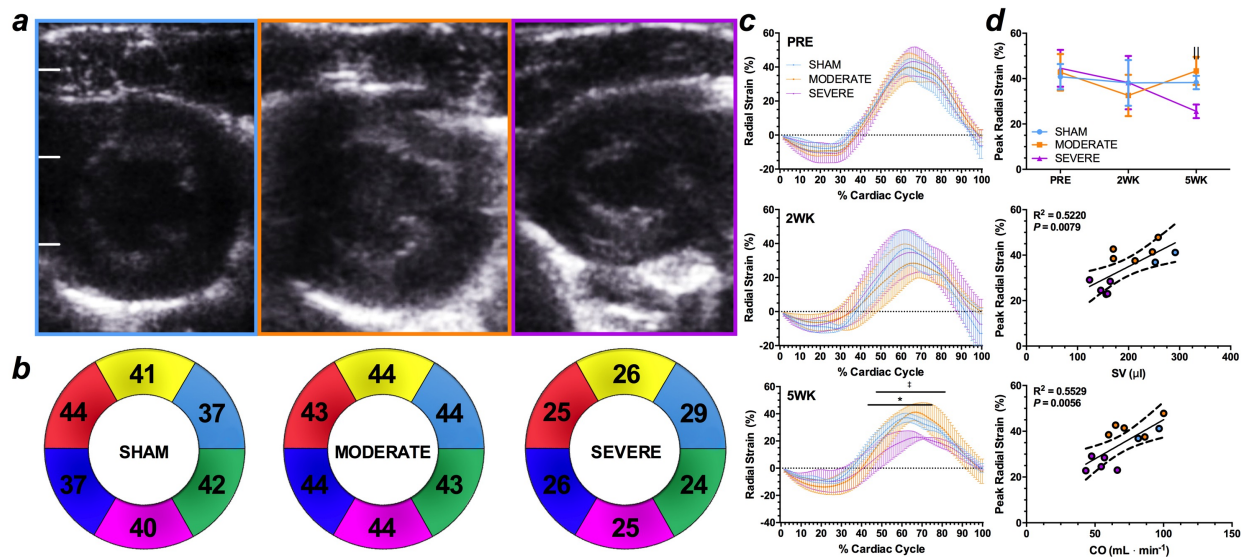
Figure 6.2: Echocardiography results.

(a) Representative parasternal short-axis images demonstrating the dramatic decrease in left-ventricular size following SEVERE SCI (n = 5). White lines indicate 0.5cm. **(b)** Color wheels indicating the mean radial strain for each region of the left ventricle. *Of note is the consistent decrease in all regions following SEVERE SCI.* Further, it is critical to note that no regional differences were observed in any groups (all $P > 0.05$). **(c)** Radial strain standardized to cardiac cycle length for each measurement revealed a significant decrease in radial strain throughout the systolic component of the cardiac cycle. Specifically, a significant difference was observed between SEVERE SCI and MODERATE SCI (n = 5) as well as between SEVERE SCI and SHAM (n = 4; all $P < 0.05$). No differences were noted between any groups at PRE or at 2WK post-injury (ANOVA $P > 0.05$). **(d)** At 5WK post-injury peak radial strain was significantly reduced from PRE for SEVERE SCI (25.6 ± 3.0 vs. 44.5 ± 8.1; $P = 0.0029$) but not for MODERATE SCI or SHAM. Finally, significant relationships were noted between peak radial

strain and stroke volume (SV) as well as cardiac output (CO). Note: one SHAM was removed from the speckle tracking analysis due to poor image quality. *$P < 0.05$ SEVERE *vs.* SHAM ‡ $P < 0.05$ SEVERE *vs.* MODERATE. || $P < 0.01$ SEVERE 5WK *vs.* SEVERE PRE. All data are displayed as mean ± standard deviation.

6.3.3 Spinal cord injury elicits changes in myocyte and sarcomere structure but not myocardial fibrosis

SEVERE SCI resulted in significantly lower myocyte length and z-disk width as well as an increase in the myocyte length/width ratio compared to SHAM and MODERATE **(Figure 6.3a, 6.3b, 6.3c)**. In addition to the group differences, we observed that the myocyte length/width ratio was significantly correlated with SV **(Figure 6.3c).** Despite the decrease in average myocyte length, sarcomere length did not change following SEVERE SCI **(Figure 6.3c)**. Thus, to explain the decrease in myocyte length, we estimated the number of sarcomeres based on the myocyte length and sarcomere length. The average number of sarcomeres tended to be reduced after SEVERE SCI (**Figure 6.3c**; ANOVA $P = 0.0848$). Finally, in contrast to the structural changes after SEVERE SCI, we observed no differences in COL1 deposition between any groups (data not shown).
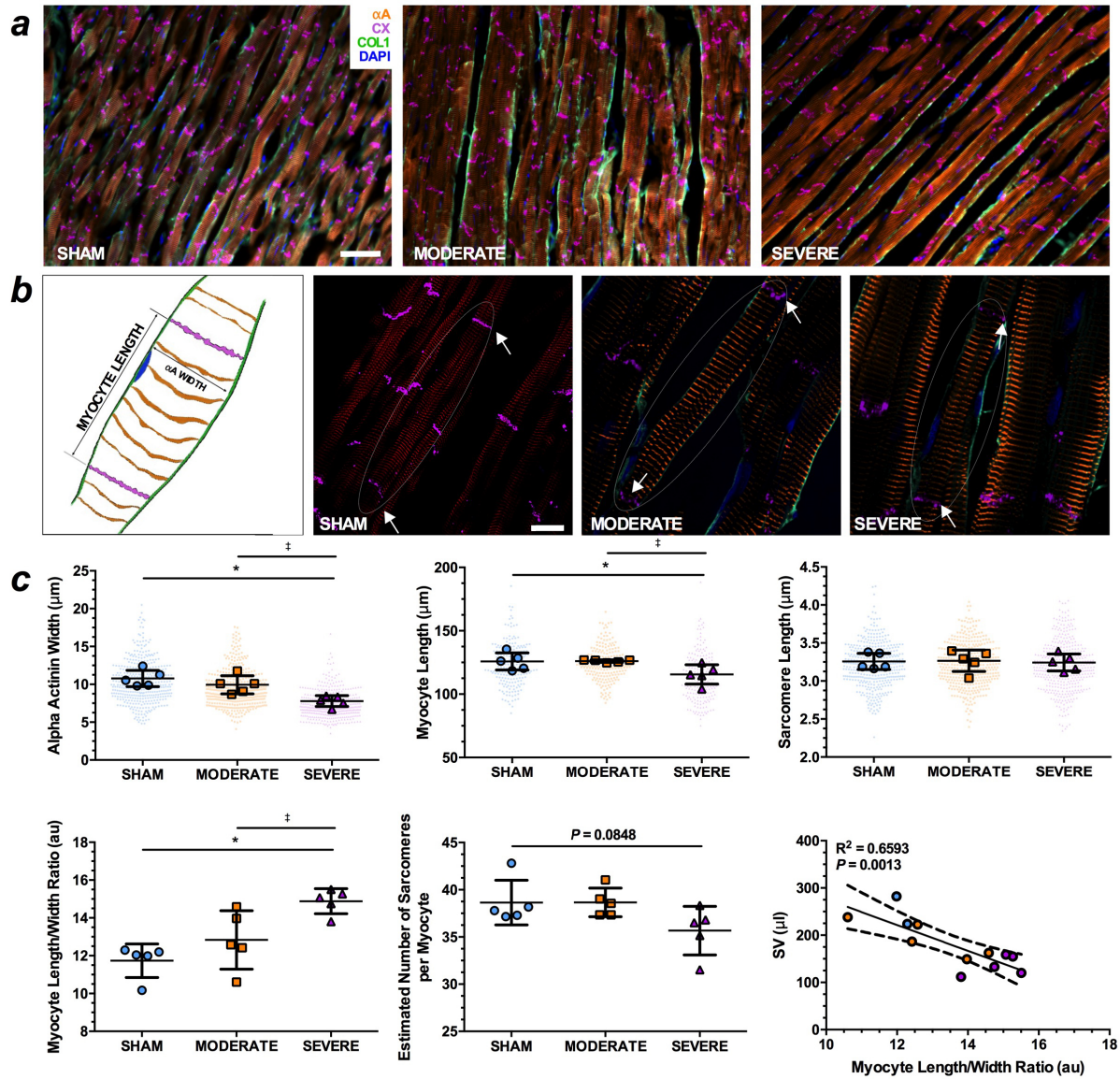
Figure 6.3: Cardiomyocyte immunohistochemistry after SCI.

(a) Representative 20x (Axioplan 2) immunohistochemistry images from SHAM (n = 5), MODERATE SCI (n = 5), and SEVERE SCI (n = 5) demonstrating the characteristic cardiomyocyte structure and organization. **(b)** High magnification (63x) images taken on a confocal microscope (AxioObserver Z1) illustrating the decrease in myocyte length and width after SEVERE SCI. Schematic on the left indicates how each measurement was made. Circles

indicate the approximate area of one myocyte. White arrows indicate the presence of gap junctions, labeled using Connexin-43 (CX). Scale bar indicates 10μm. **(c)** In each of the top row panels the raw data is presented with each biological replicate average overlaid. Bars represent the mean ± standard deviation. Z-disk width (top left panel) was significantly lower following SEVERE SCI (7.78μm ± 0.71), compared to both SHAM (10.78μm ± 1.08 *vs.* SEVERE; *P* = 0.0015) as well as MODERATE SCI (9.94μm ± 1.19 *vs.* SEVERE; *P* = 0.0147). Similarly, myocyte length (top middle panel) was significantly lower at 5WK after SEVERE SCI (115.6μm ± 7.63), compared to both SHAM (125.8μm ± 6.75 *vs.* SEVERE; *P* = 0.0458) as well as MODERATE SCI (126.1μm ± 1.00 *vs.* SEVERE; *P* = 0.0389). Sarcomere length (top right panel), taken as the distance between each αA labeled z-disk, was not different between any group (*P* = 0.9570). Myocyte length/width ratio (bottom left panel) was then derived and was significantly higher after SEVERE SCI (14.88 ± 0.66), compared to both SHAM (11.74 ± 0.89 *vs.* SEVERE; *P* = 0.0018) as well as MODERATE SCI (12.83 ± 1.55 *vs.* SEVERE; *P* = 0.0304). Based on myocyte length and sarcomere length, the average number of sarcomeres per myocyte was estimated and SEVERE SCI (35.7 ± 2.56) tended to demonstrate less sarcomeres than SHAM (38.6 ± 2.37) and MODERATE SCI (38.7 ± 1.52; ANOVA *P* = 0.0848). Lastly, a significant correlation was derived between stroke volume (SV) and the myocyte length/width ratio (R^2 = 0.6593; *P* = 0.0013).

6.3.4   T3 contusion spinal cord injury induces a severity dependent decrease in white matter sparing

MODERATE and SEVERE T3 contusion induced significant damage at the spinal cord lesion epicenter that then extended up to 4mm in the rostral and caudal directions **(Figure 6.4)**. There

was a severity-dependence in white matter sparing at 5 weeks, whereby MODERATE SCI retained significantly more white matter at numerous points along our quantification compared to SEVERE SCI ($P < 0.05$). In fact, in SEVERE SCI, there was a near complete abolishment of all white matter at the lesion site epicenter **(Figure 6.4)**.
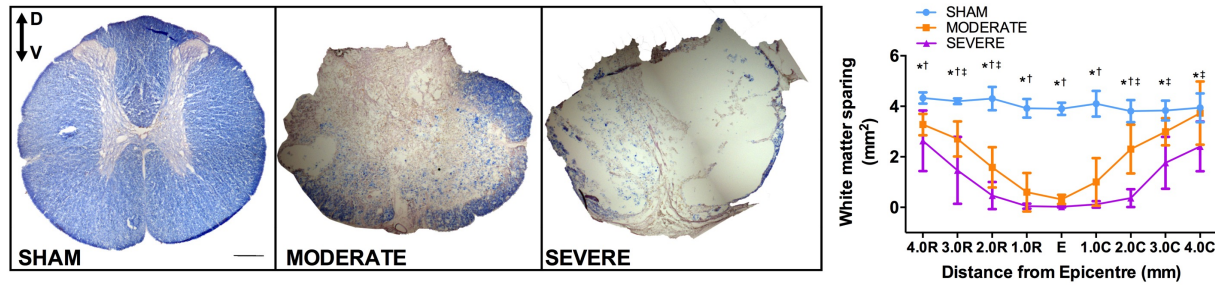
Figure 6.4: Lesion site characterization**.**

Representative histological images at the lesion epicentre for SHAM, MODERATE, and SEVERE animals. White matter sparing was quantified at the lesion epicenter and every 1mm in both rostral (R) and caudal (C) directions. Two-way ANOVA revealed a significant interaction effect, whereby SEVERE SCI exhibited the most profound and extended damage, demonstrated by a significantly smaller amount of normal or near normal myelin-positive cytoarchitecture. Scale bar = 200μm. *$P < 0.05$ SEVERE *vs.* SHAM †$P < 0.05$ MODERATE *vs.* SHAM ‡$P < 0.05$ SEVERE *vs.* MODERATE.

6.3.5   Discussion

Here, we utilized two severities of T3 spinal cord contusions to provide novel insight into the effect of SCI severity on the heart. We found that severe contusion SCI elicited a decrease in myocyte length, width and a subsequent increase in the length-to-width ratio. These decreases were strongly related to a significant reduction in flow generating capacity (i.e. stroke volume).

That we found no appreciable changes in myocyte morphology or cardiac dysfunction following moderate contusive SCI, put in conjunction with our recent findings demonstrating differential sympatho-excitatory axon sparing in these injuries **(see Chapter 4)**,[174] demonstrates the critical importance of preserving spinal sympathetic pathways to prevent cardiac dysfunction after SCI.

The first major finding of this study was that spinal cord contusion was associated with a severity dependent decline in global indices of cardiac structure (i.e. LVIDd, LVIDs), estimates of global systolic dysfunction (i.e. SV), as well as *in vivo* LV strain. The prevailing explanation for the characteristic decline in LV dimensions is reduced venous return resulting from the loss of descending sympatho-excitatory control from the rostral ventrolateral medulla[24,93] as well as reduced muscle pump activity[202,203] and impaired venous compliance.[204] In line with this, we show that white matter within the spinal cord, and thereby any descending sympatho-excitatory axon populations, was nearly abolished after SEVERE SCI and was accompanied by profound cardiac dysfunction. Conversely, we found preserved cardiac function in our MODERATE group with only ~10% white matter sparing at the lesion epicenter, a finding that is potentially explained by the relatively few axons required to regulate cardiovascular function **(see Chapter 4)**.[174] Importantly, we found that *in vivo* LV strain was reduced in the absence of changes in ejection fraction or fractional shortening. This observation highlights the limitations of purely dimensional measurements, as they can be heavily influenced by whole heart motion[205,206] and is in line with the notion that *in vivo* LV strain potentially represents of "impending" cardiac pathology, prior to any overt reductions in classical measures of LV function.[206]

The second major finding of this study was that the morphology of individual cardiomyocytes is impaired following SEVERE, but not MODERATE SCI, and that these changes were significantly correlated with an impairment in LV function (i.e. stroke volume and

117

strain). Following SEVERE SCI, we observed a decrease in myocyte length, decreased myocyte width, and an increase in the length/width ratio. These findings, in addition to the global decrease in LV chamber size found on echocardiography **(Figure 6.1; Figure 6.2)**, are consistent with previous findings in rodents with severe high thoracic SCI[198] **(see Chapter 5)** as well as reports of cardiac atrophy following unloading conditions such as microgravity exposure,[207] acute cardiac unloading,[189] LV assist device,[208] where LV atrophy is associated with decreased myocyte width and cross-sectional area.[189] Importantly, we found that the alterations in cardiomyocyte morphology in response to SEVERE SCI (reduced width, length and a subsequent increase in the myocyte length/width ratio) are strongly correlated with a decrease in SV **(Figure 6.2)**. The specific mechanisms that explain how changes in cardiomyocyte morphology regulate contractile function are beyond the scope of this study. However, we suggest a scenario by which chronic unloading of cardiac myocytes following SEVERE SCI reduces stroke work and ventricular wall stress according to Laplace's law **(see Chapter 5)**.[198] The unloading could be a combination of both reduced pre-load (i.e. end-diastolic volume) as well as reduced afterload, the latter of which is characteristic of the tetraplegic population due to low-arterial blood pressure[136] and reduced catecholaminergic vasomotor projections.[24] We suggest, however, that reduced afterload contributes less to the observed cardiac structural changes as we have previously reported that MODERATE and SEVERE SCI induce a similar decrease in resting arterial blood pressure **(see Chapter 4)**.[174]

Thirdly, we found that the lesion in the SEVERE contusive SCI at the T3 level extends approximately 4.0mm rostral and caudal from the T3 segment **(Figure 6.4)**. Thus, we expect that descending sympathetic control from the rostro-ventrolateral medulla over the sympathetic pre-ganglionic neurons that exit the spinal cord at T2 and below is lost **(see Chapter 4)**.[174] In

contrast, the MODERATE injury histology showed ~10% sparing even at the injury epicenter. This difference is important as the majority of cardiac projecting sympathetic pre-ganglionic neurons exit the spinal cord at T2 and below (84%), with only a few exiting at the T1 level.[173] Furthermore, our SEVERE contusion is also likely to completely impair vasomotor control of the majority of the body's arteriole and venule systems that originate in T6-L1.[209] The loss of both arteriole[127] and central venous tone[204] combined with an inactive sub-lesional muscle pump[202,203] dramatically influences cardiac pre-load in a severity dependent manner. Over time, the reduced pre-load to the left-ventricle and loss of inotropy results in an inward remodeling, whereby the lumen of the ventricle decreases in size (i.e. LVIDd, LVIDs) without any obvious changes in the wall thickness (i.e. eutrophic remodeling, indicated here by an increase in RWT in SEVERE). This finding is consistent with both short- and long-term bed rest and either simulated or real microgravity exposure.[179,180,207] While it has been speculated that a decrease in the absolute size of the left ventricle in isolation could be seen as a potential adaptive feature to reduced loading,[178] our current finding that *in vivo* strain is reduced and our previous findings that the Starling Curve is shifted[127] and maximal pressure generating capacity is impaired points to the potential long-term consequences of reduced venous return. It is likely, therefore, that decreased contractility and/or deformation represents a combined consequence of both decreased sympatho-excitatory control over the cardiac sympathetic pre-ganglionic neurons, as well as the inherent mechanisms related to the pre-load exerted on the ventricle noted above (i.e. Frank-Starling mechanism), both of which are critically dependent on the severity of the SCI, and thus the amount of descending sympatho-excitatory control.

We have previously shown that blood pressure is significantly lower following our MODERATE injury **(see Chapter 4)**,[174] suggesting a loss of descending supraspinal control, yet

we report here that this same injury induces no cardiac dysfunction. Given that we have no reason to believe the cardiac projecting sympathetic pre-ganglionic neurons are more resistive to injury than the splanchnic sympathetic pre-ganglionic neurons, it is plausible that the heart is better able to compensate for reduced descending sympathetic drive than the vasculature. To this end, it has been reported that sympathetic nerve terminal density in the LV is actually higher following a mid-thoracic contusion injury[167] – a finding that appears to be driven by increased peripheral nerve growth factor. It is possible, therefore - perhaps as a compensatory response – that the few remaining descending spinal sympathetic pathways that ultimately provide sympathetic input to the heart (i.e., those that originate from the T1 spinal segment), coupled with an increased arborization of the ganglionic sympathetic fibers in the heart, were able to maintain normal cardiac structure and function.

An alternative explanation for the severity dependent decline in cardiac structure and function is that SEVERE injured animals have of a lower amount of in-cage activity compared to MODERATE injured animals. Although we cannot specifically rule this out we believe it is unlikely to be the principle cause of our between-group differences as we have shown that upper-limb exercise alone (i.e., swim training) exerts no influence on contractile cardiac function.[210] It is important to note, however, that rodents with a MODERATE T3 contusion injury recover some weight bearing stepping **(see Chapter 4)**,[174] and are therefore likely to partially maintain their preload through muscle pump mediated increases in flow back to the heart. Though this likely contributes to the maintenance of stroke volume we do not believe it contributes to the maintenance of radial strain and contractile function in our MODERATE group, as we have previously found that hind-limb exercise can only improve stroke volume but not systolic contractile function.[210] In fact, the only intervention we have found that normalizes contractile

function post-SCI is Dobutamine, a specific beta-1 agonist **(see Chapter 5)**.[198] Taken together, we suggest that the greater preservation of descending sympathetic pathways in MODERATE injury[174] preserves systolic contractile function and, in concert with weight-bearing stepping, maintains pre-load, stroke volume, and radial strain.

6.4 Conclusion

We report that SCI is associated with a severity dependent decrease in cardiomyocyte length and width, as well as an increase in the length-width ratio. Further, we show decreases in left-ventricular structure (i.e. LVIDd, LVIDs) as well as estimated measures of flow-generating capacity (i.e. SV) are impaired. Lastly, we demonstrate that *in vivo* left-ventricular contractility is impaired throughout the entire systolic portion of the cardiac cycle following SEVERE SCI and is significantly correlated with cardiomyocyte morphology changes. These findings provide preliminary mechanistic insight into the role of descending sympatho-excitatory influence in maintaining cardiac function after SCI and suggest that that consideration should be given to interventions that target SCI site pathophysiology as a potential method to preserve cardiac contractile function after SCI.

With an autonomic dysfunction model in hand coupled with extensive hemodynamic and cardiac outcome measures in place, the next chapter **(Chapter 7)** will examine whether one of the most promising neuroprotective drugs, minocycline, can reduce autonomic dysfunction after severe spinal cord contusion in the rodent.

Chapter 7: Minocycline reduces the severity of autonomic dysreflexia after experimental spinal cord injury[5]

7.1   Introduction

Spinal cord injury (SCI) is a devastating neurological condition for which there is no effective treatment to improve functional outcome. The development of neuroprotective treatments for SCI may be hampered by a focus on improving motor function, which is limited in both sensitivity and variability.[211] The insensitivity of these measures necessitates significantly large sample sizes,[211] placing tremendous financial and logistical burdens on investigators willing to embark on a trial.[212] In contrast, autonomic pathways that travel through the spinal cord may require relatively few preserved spinal cord connections as compared to motor function.[93,174] As such, from many perspectives it may be beneficial to both the research and clinical community to re-align the focus of SCI treatment trials to include autonomic function.

Treatments aimed at preserving neuronal function through anti-inflammatory pathways (i.e., neuroprotection) have been a mainstay of pre-clinical SCI research for decades.[53,55,213] Plagued with inconsistencies in animal models, in addition to the significant barriers to

---

[5] A version of chapter 7 has been published. **Squair, J.W.,** Ruiz, I., Phillips, A.A., Zheng, M.M.Z., Sarafis, Z.K., Sachdeva, R., Gopaul, R., Lie, J., Tetzlaff, W., West, C.R., Krassioukov, A.V. Minocycline reduces the severity of autonomic dysreflexia after experimental spinal cord injury. Journal of Neurotrauma.

beginning a clinical trial for acute SCI, few treatments have ever made it through the translational pipeline. To date, only five drugs have progressed through to a large scale clinical trial in humans.[214–217] Minocycline is among the most recent of these, having shown tremendous promise in a variety of pre-clinical models.[218–221] Moreover, minocycline is currently in Phase III clinical trial to improve motor function after acute SCI.[215] Minocycline is a tetracycline antibiotic, which in the spinal cord acts through multiple mechanisms including reducing microglia activation,[221,222] stabilizing mitochondrial membranes,[218] and thereby reducing expansion of the secondary injury. Theoretically, these principles should also preserve descending sympatho-excitatory pathways and preserve cardiovascular control; however, this has yet to be experimentally tested.

Here, we leveraged our recently developed T3 severe contusion model in the rat **(see Chapter 4)**[174] to determine the ability of minocycline to preserve descending sympatho-excitatory axons, and improve cardiovascular control after SCI. We explored the neuroanatomical and functional aspects of this system, as it is the number one cause of death in individuals with SCI,[197] a top health priority,[101] and a potentially more sensitive measure of neurological improvement compared to motor function. We also compared autonomic and motor control to determine the relative capacity of each outcome to detect alterations due to the intervention. Lastly, we examined whether minocycline treatment led to improved cardiac structure and function, as we have previously shown this model leads to significant cardiac impairment.

7.2 Materials and methods

7.2.1 Ethical approval

Ethical approval was obtained by the University of British Columbia Behavioural Research Ethics Board (A14-0152) and all procedures strictly adhere to the guidelines issues by the Canadian Council for Animal Care.

7.2.2 Experimental design and statistical analysis

The described experiments were performed as a vehicle controlled drug trial **(Figure 7.1A)**. All experimenters performing outcome measure assessments were blinded to the grouping status of all animals. Adult male Wistar rats (aged 10-12 weeks) were randomly assigned at the time of spinal cord contusion to either a minocycline (n=18; n = 2 euthanized after contusion) or vehicle (n=21) group. Animals underwent a severe T3 contusion, as we have previously described **(see Chapter 4)**.[174] One hour post-injury animals were given either a minocycline or vehicle intraperitoneal injection.[218] Additionally, a pilot study was conducted (n=14) to optimize drug delivery to avoid abdominal irritation. On a weekly basis, hind-limb locomotor performance was assessed using the Basso-Beattie-Bresnahan (BBB) open field test.[124] At 60 days post-injury, each animal underwent carotid catheterization for the assessment of baseline hemodynamics, and colorectal distension to establish the severity of autonomic dysreflexia.[134,174] Following this, animals were sacrificed and tissues harvested for lesion area analyses[128] and lumbosacral plasticity assessments.[37,174] One week before the study end-point (60 days) a subset (n=4 per group) of animals underwent a re-transection of the spinal cord for FluoroGold tracing (Fluorochromes Inc., CO, USA).[24,174] All statistical analyses were completed using the statistical computing software R (R Core Team, 2012, R version 3.4.0). Infinite-horizons (IH) impactor

(Precision Systems and Instrumentation, LLC, Fairfax Station, VA[123]) parameters, baseline hemodynamics, autonomic dysreflexia severity, lesion area, sympatho-excitatory axon preservation, lumbar afferent plasticity, and neuronal counts in the RVLM were compared between groups using independent samples t-tests (R package `stats`). Autonomic dysreflexia was also examined using two-way repeated measures analysis of variance (ANOVA; R package `car`). To determine between group differences in lesion transection status, a Fisher's exact test was utilized (R package `stats`). Linear discriminant analysis was utilized (R packages `MASS` and `ROCR`) to examine the sensitivity and specificity of lesion area, autonomic dysreflexia and BBB as individual predictors of treatment stratification. To assess the goodness of fit for each outcome, we conducted a "leave-one-out" cross validation on each outcome independently. Receiving operating characteristics curves (ROC) were produced to compare which outcomes were most accurate in predicting treatment group. Alpha was set at 0.05.

7.2.3   Spinal cord surgery and animal care

The present study was completed using our recently established T3 contusion model **(see Chapter 4)**, developed with the specific aim of investigating cardiovascular dysfunction after SCI.[174] Briefly, animals were started on prophylactic enrofloxin (Baytril; 10 mg kg^{-1}, s.c., Associated Veterinary Purchasing (AVP), Langley, Canada) three days prior to surgery. On the day of spinal cord contusion animals were anesthetized using isoflurane (initial induction 5% and maintained on a Bain's system at 2%). After achieving surgical depth of anesthesia, pre-operative buprenorphine (Temgesic; 0.02 mg kg^{-1}, s.c., McGill University), enrofloxin (Baytril; 10 mg kg^{-1}, s.c., Associated Veterinary Purchasing (AVP), Langley, Canada), and Ringers solution were administered subcutaneously. The skin was prepared by shaving the surgical site,

125

followed by three successive chlorohexidine and 70% ethanol washes. A dorsal midline incision was made from CVIII-TV, followed by blunt dissection through the superficial and deep paraspinal musculature. The TII spinous process was identified as the vertebra prominens. A laminectomy was performed on the TIII vertebra to expose the T3 spinal segment. Following this the animal was transferred to the IH impactor stage, where the TII and TIV spinous processes were securely clamped using modified Allis forceps. The animal was stabilized on the platform and the impactor tip (2.5 mm) was properly aligned using a 3-dimensional coordinate system moving platform. The position of the impactor was confirmed as midline by two separate experimenters. The IH system was set to deliver an impact of 400 kdyn of pre-defined force, with a 5 second dwell time. We have previously found through successive experiments that this injury produces the most consistent autonomic dysfunction, and prevents the regaining of meaningful weight bearing in the hind-limbs.[4] Following hemostasis, the deep and superficial paraspinal muscles were sutured using 5-0 Monocryl sutures (Ethicon, USA), followed by 5-0 Prolene (Ethicon, USA) sutures in the skin. Animals were then given 5 mL of Ringers solution subcutaneously and allowed to recover in a temperature controlled environment (Animal Intensive Care Unit, Los Angeles, CA, USA). Post-operatively, animals were given buprenorphine (10 mg kg-1, s.c.) and enrofloxin (0.02 mg kg-1, s.c.) once daily for three days, after which buprenorphine was given on an as needed basis. Bladders were manually expressed for approximately one week, after which time animals regained reflexive voiding.

7.2.4   Minocycline administration

Minocycline was prepared according to the manufacturer's instructions (Sigma). Briefly, minocycline was dissolved in distilled water to a concentration of 30 mg/mL daily. This stock

solution was then used to provide a loading intraperitoneal dose at one hour post-injury 90 mg/kg

and a 45 mg/kg dose to animals every twelve hours.[218] All stock solutions were stored at 4 °C, as

per the manufacturer's instructions, and freshly prepared each day.

7.2.5   BBB functional behavior assessment

Functional hind-limb motor behaviour was assessed using the well-established BBB open-field

test.[124] Two blinded experimenters scored animals placed in a 1.2x1.5 m enclosed box for four

minutes. Each hind-limb was scored independently and the scores were then averaged to provide

a single score for each animal. BBB subscores were excluded from our final analysis as the vast

majority of animals (all but two) did not regain weight bearing on their hind-limbs. However, no

animals were excluded based on their BBB scores. BBB scores were rank-transformed prior to

any parametric statistical analysis (minocycline, n = 18, vehicle, n = 21).[223,224]

7.2.6   FluoroGold placement

Animals (minocycline, n = 4; vehicle, n = 4)[174] underwent a transection of the spinal cord at T8

at day 53 post-injury. Pre- and post-operative care was identical to that provided for the original

contusion injury (see above). A TVII laminectomy was performed following a dorsal midline

incision and blunt dissection of superficial musculature. The T8 segment of the spinal cord was

completely transected using microscissors and completeness was confirmed by two separate

experimenters. Following haemostasis, Gelfoam soaked in 10 μl of 4 % FluoroGold in sterile

saline was placed against the rostral stump of the spinal cord.[24,174] The muscle and skin were

closed using 4-0 Monocryl and 4-0 Prolene sutures, respectively. Animals were euthanized and

perfused 8 days following FluoroGold injection to allow sufficient time for retrograde transport to the rostral ventrolateral medulla (RVLM).[24,174]

7.2.7 Blood pressure cannula placement

At study end-point all animals (excluding those sent for FluoroGold placement) underwent a terminal procedure to measure resting blood pressure and the severity of autonomic dysreflexia. Animals were anesthetized with urethane (1.5mg/kg) in order to prevent inhibition of spinal reflexes and synaptic activity.[225] Blood pressure was recorded invasively while animals were anesthetized in order to ensure consistent and stable signals, as movement can disrupt the signal and, due to our expectation that any observed changes may be minimal, we opted for this more controlled scenario. However, we have extensively described the blood pressure responses in T3 injured animals both awake and anesthetized.[36,120,134,174] As such, we found this to be a prudent method to ensure the most careful assessment of blood pressure was performed. Once in surgical place, a ventral midline incision was performed over the trachea. The superficial muscles were bluntly dissected and retracted. The right common carotid artery was gently isolated from the vagus nerve and surrounding structures. Three silk sutures were passed under the artery and one moved rostral to the carotid bifurcation, where it was ligated, while the caudal suture was moved as caudal as possible towards the sternal notch, where it was left untied. The middle suture was tied loosely in preparation for securing the cannula. The caudal suture was then used to temporarily occlude the blood flow to the right common carotid artery. A small hole was punctured in the artery using a bent 25 gauge needle. The blood pressure cannula (SPR-869, Millar, USA) was then advanced into the artery and secured using the previously mentioned middle suture. The caudal suture was then released and visual inspection was performed to

ensure there was no leaking through the entry hole of the cannula. The cannula was then advanced approximately 1 cm to provide a consistent and reliable blood pressure signal. Data analysis was conducted in Labchart 8.1 (ADInstruments, USA).

7.2.8   Resting blood pressure and autonomic dysreflexia

Resting systolic, diastolic, and mean arterial blood pressure, as well as heart rate, were assessed over a ten-minute period prior to colorectal distension. Following this period, a blinded experimenter inserted a Foley balloon catheter (AA6110-COLOPLAST Folysil "Foley" Pediatric 2-way indwelling catheter, straight, 10 French, 3mL, 35cm, Latex Free) 2 cm into the rectum, according to standard protocols.[134] The balloon was inflated with two milliliters of air. The severity of autonomic dysreflexia was assessed as the maximum change in blood pressure (systolic, diastolic, and mean taken independently) over the one minute period of distension.[134,174] Following one minute the balloon was deflated, and a ten-minute rest period was provided to let hemodynamics stabilize. Two trials were performed for each rat to obtain a reliable estimation of the severity of autonomic dysreflexia.

7.2.9   In-vivo echocardiography and pressure-volume catheterization

To assess whether minocycline administration led to changes in cardiac structure and function, echocardiography was performed at the study endpoint.[198,243] For this comparison an uninjured control group was included (n = 5), and five animals from both the minocycline group and vehicle treated control group were examined.[243] Measures of left ventricular (LV) structure and function were imaged while animals were under isoflurane anesthesia (initial chamber induction at 4% isoflurane with 2l min^{-1} oxygen, followed by maintenance on a Bain's system at 1.5-2%

129

isoflurane with 1.5-2l min^{-1} oxygen). LV structure and systolic function (i.e. stroke volume, ejection fraction) were assessed using M-mode echocardiography and diastolic function was assessed using pulsed-wave Doppler during an apical four-chamber view. Estimated volumes were calculated according to the Teichholz method.[198,243] Reported results were quantified by a blinded experimenter using commercially available software (Echopac; GE Healthcare, Horton, Norway) and determined from the average of 5 cardiac cycles during expiration.

To determine inherent changes in LV pressure and volume indices as well as load-independent cardiac function, LV function was assessed *in vivo* under urethane anesthesia using a pressure-volume (PV) conductance catheter (SPR-869, Millar, USA) inserted directly into the LV via a closed-chest right common carotid artery approach according to standard guidelines.[171] The presoaked catheter (for 30 min into physiological saline solution) was left in the carotid artery for 10 min to allow hemodynamic stabilization and for the determination of arterial blood pressure. Following this, the catheter was advanced into the LV under pressure guidance until the PV signal was visualized and subsequently optimized. After stabilization of the LV pressure-volume signal basal PV data was collected for 10 min. Next, baseline cardiac preload was manipulated via complete inferior vena cava occlusions for the measurement of load-independent outcomes (i.e., end-systolic elastance (Ees), end-diastolic pressure-volume relationship (EDPVR), preload recruitable stroke work (PRSW), dP/dt-EDV). Briefly, a midline laparotomy was performed and the inferior vena cava isolated immediately caudal to the liver. Occlusions were performed using a cotton-tipped applicator. Data analysis was conducted in Labchart 8.1 (ADInstruments, USA) using the built in PV loop analyses program.

7.2.10 Tissue processing, histology, and immunohistochemistry

Animals were overdosed with urethane until cessation of breathing, after which a thoracotomy was performed. Animals were transcardially perfused with 300 mL of PBS followed by 500 mL of 4% paraformaldehyde. The lesion site, lumbar enlargement, and brainstem were harvested for further histological analysis. Lesion sites were measured and blocked in cryomatrix +/- 7mm from the visually identified lesion epicentre. These were then sagitally sectioned at 20 μm with 10 sections per slide in sets of 10 slides.[128,226] Brainstems were blocked from the obex and 7mm rostrally.[174] They were then cross sectioned (i.e. in the transverse plane) at 30 μm on paired slides for the entirety of the blocked section.[24,174] One set of slides was stained with cresyl violet according to standard procedures in order to identify the relevant sections containing the RVLM. This was identified as sections with a present nucleus ambiguus and/or present hypoglossal nucleus, as these nuclei correspond to the location of the RVLM.[24,174] Lastly, the lumbar enlargement was blocked and cross sectioned at 20 μm for the investigation of peptidergic afferent plasticity.[37,41,44,174] Immunohistochemistry was performed according to the following procedures. First, sections were thawed for one hour at room temperature. Next, sections were rehydrated in PBS for 10 minutes. Normal donkey serum was then placed on the slides for 30 minutes. Lastly, primary antibodies (350 μl) were placed on the sections and allowed to incubate overnight. The following primary antibodies were used: rabbit anti-glial fibrillary acidic protein (GFAP, 1:1000, Dako), guinea pig anti-neuronal nuclei (NeuN, 1:500, Millipore, ABN90P), mouse anti-dopamine β-hydroxylase (DBH, 1:500, Millipore, MAB308), sheep anti-tyrosine hydroxylase (TH, 1:200, Millipore, AB1542), and rabbit anti-calcitonin gene related peptide (CGRP, 1:200, Sigma, C8198). Secondary antibodies included: Alexa Fluor 594 Donkey Anti Rabbit (1:200; Jackson ImmunoResearch; 711-586-152), Alexa Fluor 647 Donkey Anti Guinea

Pig (1:200; Jackson ImmunoResearch; 706-606-148), Alexa Fluor 488 Donkey Anti Mouse

(1:200; Jackson ImmunoResearch; 715-546-151), and Alexa Fluor 488 Donkey Anti Sheep

(1:200, Jackson ImmunoResearch; 713-545-147). Immunofluorescence was imaged digitally

using an Axioplan 2 microscope (Zeiss) using ZEN 2 Blue software (Zeiss, Oberkochen,

Germany). Images were digitally processed using ImageJ (ImageJ NIH) software.

7.2.11   Image analysis and histological quantification

7.2.11.1   Lesion site analyses

Images of sagittal sections were taken and automatically tiled to obtain images exceeding the

distance of the injury site at 50x. Lesion area was quantified (GFAP channel) on two images per

animal (minocycline, n=12; vehicle, n=16).[226] Lesion area was manually outlined based on the

following definition: GFAP-negative or GFAP-positive area with disrupted or abnormal

cytoarchitecture.[128,174] Care was taken to avoid inclusion of any artifacts. The total number of

pixels within each section was measured using Image J and converted to square millimeters for

reporting and downstream statistical analyses. All individuals conducting analyses were blinded

to grouping details.

7.2.11.2   Sympatho-excitatory axon preservation analyses

Images were taken and automatically tiled, according to the lesion site protocol. TH+ axons were

identified, as this protein is housed along the axon within vesicles and can therefore be

visualized. Briefly, the number of TH+ axons within healthy tissue rostral to the lesion and

caudal to the lesion were quantified across a single plane. The percent was calculated and

averaged for each animal (minocycline, n=12; vehicle, n=16).

7.2.11.3   RVLM localization and neuronal counts

The RVLM contains C1 adrenaline-synthesizing neurons and is one of the primary regulators of cardiovascular control.[16,24,130-132,146,147] RVLM neurons project their axons down the spinal cord, which synapse and stimulate sympathetic pre-ganglionic neurons.[23,130] We therefore aimed to investigate the integrity of these axons due to their importance in maintaining appropriate cardiovascular control. The general location of the RVLM was first determined using a cresyl violet stain. Briefly, cross sections were immersed in cresyl violet for 20 minutes and dehydrated through successive alcohol washes before being placed in xylene and cover-slipped. The nucleus ambiguus and hypoglossal nucleus were then identified and used as landmarks for the identification of the RVLM.[174] Paired slides of the identified sections were then prepared for immunohistochemistry according to established methodology.[24,174] Immunofluorescent images were imaged at 100x over the ventrolateral column where the RVLM is localized. Neurons labeled with DBH were counted manually for the entirety of the RVLM (15 sections) for each animal, and in the adjacent sections outside the identified RVLM zone. FluoroGold-labelled neurons were also individually counted. Further, co-labelled neurons (DBH, FluoroGold) were identified by examining both channels and counted on ZEN 2 Blue software (Zeiss, Oberkochen, Germany) to estimate the number of descending sympatho-excitatory neurons crossing the injury site. For all neuronal counts, the total number of counted neurons on both the left and right side were averaged prior to statistical comparisons.

7.2.11.4   CGRP+ axon density quantifications

Images were taken at 200x over Rexed Laminae III-V (identified beginning at the deep border of lamina II and stopping at the central canal) at the L6/S1 spinal level, where visceral afferents from the descending colon and rectum project. All images were analyzed using ImageJ.[4] Images were converted to 8-bit and a threshold (Default Dark) was set. Particle analyses was then used to determine the percent area labelled as CGRP positive.[37,89,174] The average across all images (n=15 per animal) was then used for downstream statistical analyses.

7.3   Results

7.3.1   Clinical status of animals

All included animals could freely use their forelimbs and showed no other signs of distress (i.e., feeding well, no hunching, socialization with cage mates). Pre-surgical and end-point animal weights were similar between groups.

7.3.2   Infinite-horizons impactor produces consistent biomechanical output in T3 contusion

To first ensure that the impact parameters were similar between groups, we examined the IH impactor output. The biomechanical output parameters following T3 contusion were consistent across all metrics, and no differences were observed between the minocycline and vehicle group for force, displacement, or velocity (**Figure 7.1B-D**).
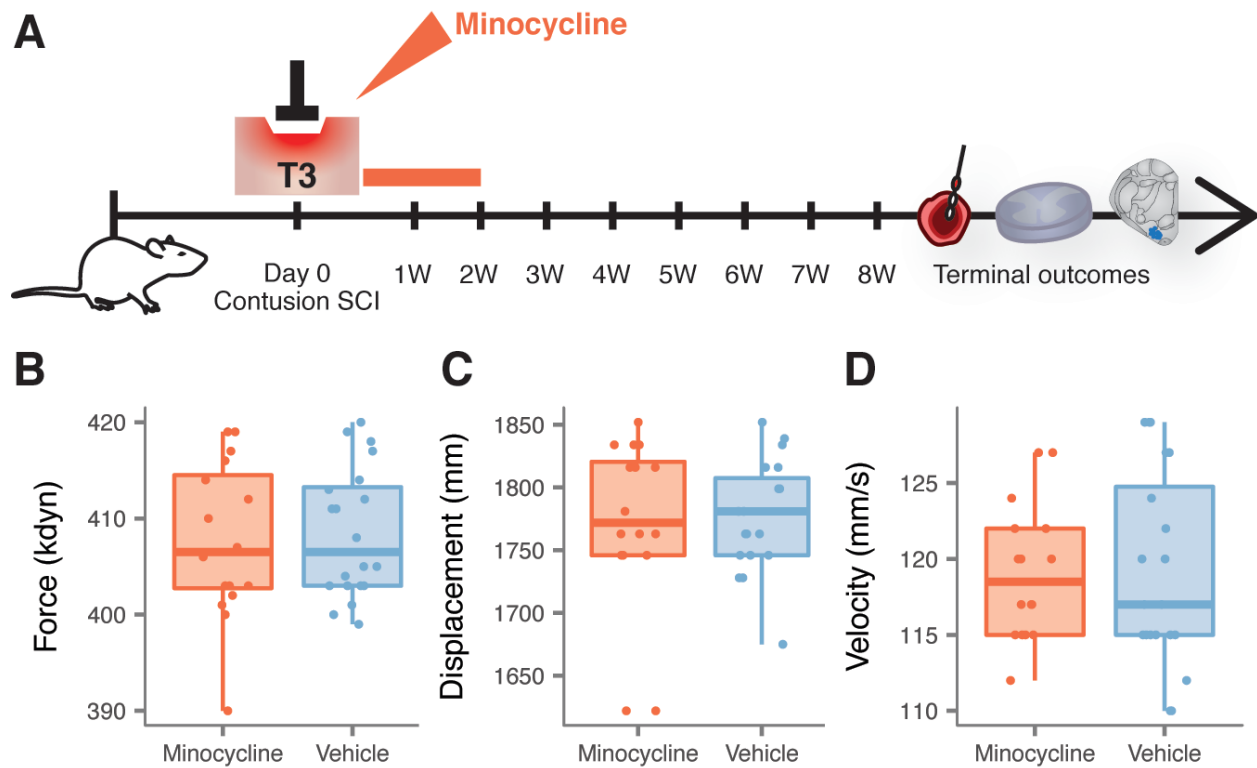
Figure 7.1: Infinite-horizons impactor produces consistent biomechanical output in T3 contusion**.**

[A] Timeline of experimental protocol. [B] Infinite-Horizons impactor force output was not different between minocycline (n=12; 407.08 ± 6.61 kdyn) and vehicle (n=16; 406.94 ± 6.28 kdyn) treated animals (t(27) = 0.059, p = 0.953, independent samples t-test). [C] Impactor displacement output was not different between minocycline (1778 ± 63.4 μm) and vehicle (1660 ± 445 μm) treated animals (t(27) = 1.047, p = 0.311, independent samples t-test). [D] Impactor velocity output was not different between minocycline (119 ± 4.10 cm/s) and vehicle (119 ± 6.57 cm/s) treated animals (t(27) = 0.051, p = 0.959, independent samples t-test). Only animals included in the final lesion analysis are included here.

7.3.3   Acute minocycline administration reduces lesion area

Numerous studies, in both mouse and rat models of experimental SCI have reported that minocycline reduces lesion area.[218,219,221,227-229] However, how minocycline may affect lesion area in our severe model of T3 contusion may be different from previous reports. Therefore, we assessed the efficacy of minocycline to reduce lesion area after a severe spinal cord contusion in our rat model. We found that the GFAP-negative or GFAP-positive area with disrupted or abnormal cytoarchitecture (demarcation by activated astrocytes) was significantly reduced in animals treated with minocycline versus vehicle control animals (**Figure 7.2B).**
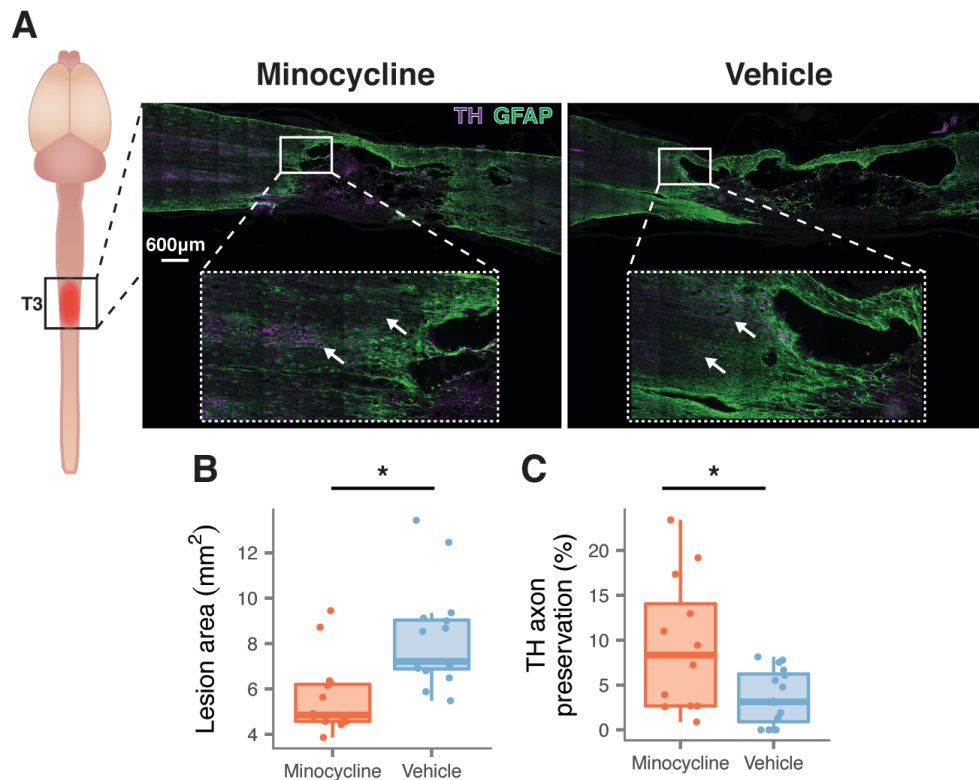
Figure 7.2: Minocycline reduces lesion area and increases sympatho-excitatory axon preservation.

[A] Representative images demonstrating the reduction in lesion area between minocycline treated animals (left) and vehicle treated animals (right) at the third thoracic segment (T3). Glial fibrillary acidic protein (GFAP) is denoted in green, and tyrosine hydroxylase (TH) in purple. Outsets indicate TH+ sympatho-excitatory axons. **[B]** Traced lesion area was significantly smaller in minocycline treated (n=12; 5.67 ± 1.76 mm^2) compared to vehicle treated (n=16; 8.17 ± 2.20 mm^2) rats ($t(27) = 3.34$, $p = 0.0025$, independent samples t-test). **[D]** TH positive axon preservation was significantly higher in minocycline treated (n=12; 9.4 ± 7.5 %) compared to vehicle treated (n=16; 3.6 ± 3.0 %) rats ($t(27) = 2.56$, $p = 0.0229$, independent samples t-test).

7.3.4 Minocycline increases sympatho-excitatory axon preservation

After treatment with minocycline, sympatho-excitatory axon preservation was significantly higher at 60 days after injury compared with vehicle treated animals (**Figure 7.2A, C**). On average, we observed ~10-15% preservation of TH+ axons following minocycline treatment, suggesting minocycline may aid in the protection of descending axons necessary for proper autonomic control.

7.3.5 Minocycline preserves descending sympatho-excitatory axons that cross the injury site

We identified the RVLM initially using a standard cresyl violet stain, and found that it was located immediately anterior and medial to the nucleus ambiguus, caudal to the inferior olivary nucleus, and immediately caudal to the facial nucleus. The RVLM extends for approximately 1000 μm[130-133,174] and thus we used fifteen 30 μm sections for all analyses to estimate the number of neurons within the RVLM. We confirmed our anatomical localization by examining

enrichment for DBH positive neurons within the identified RVLM, compared to the adjacent regions (**Figure 7.3A, C**). One vehicle animal was excluded from the analysis due to tissue quality. Within the RVLM, we did not observe a significant difference between groups for DBH positive neurons (**Figure 7.3D**). Conversely, the Minocycline group had significantly more FluoroGold positive (**Figure 7.3E**) and co-labeled (FluoroGold/DBH) neurons (**Figure 7.3F**), compared to the vehicle control group, indicating greater preservation of descending sympatho-excitatory axons that successfully cross the injury site.
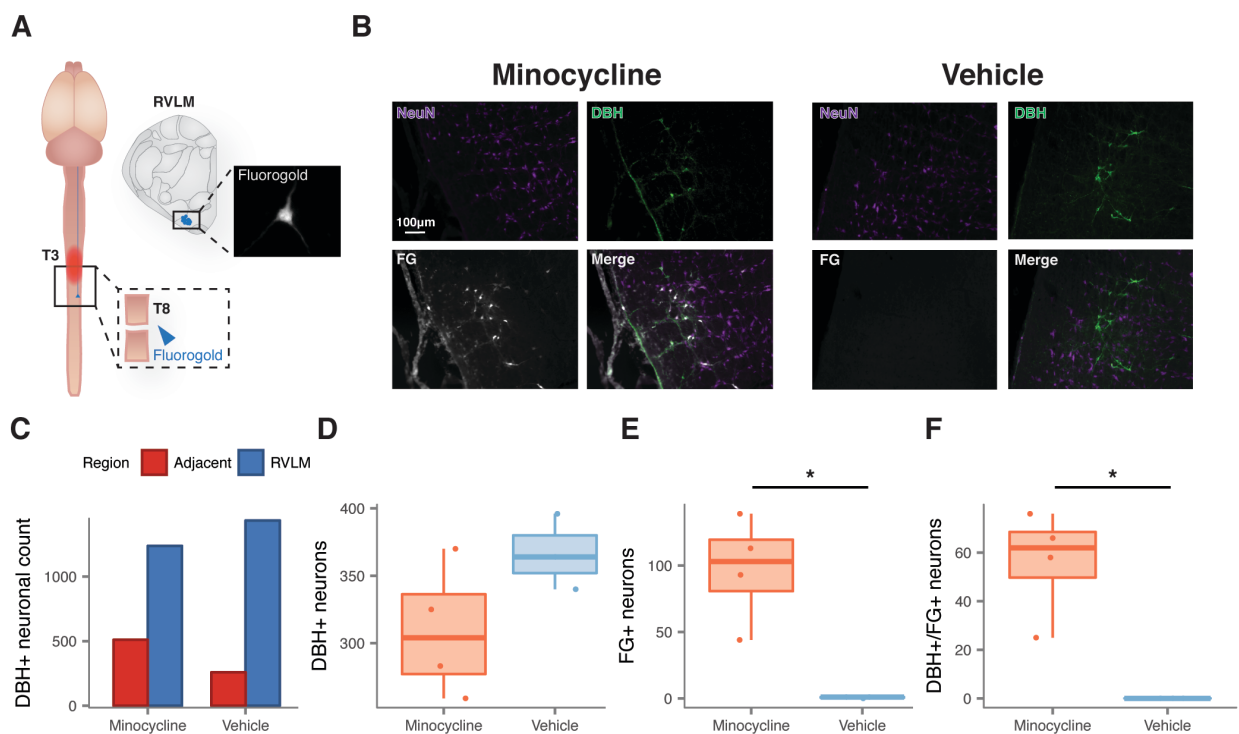
Figure 7.3: Minocycline preserves descending sympatho-excitatory axons that cross the injury site.

[A] FluoroGold injections into the transected spinal cord (T8 level) were followed and cells counted in the rostral ventrolateral medulla (RVLM). **[B]** Example images demonstrate the populous FluoroGold (FG) dopamine beta-hydroxylase (DBH), and NeuN labelled cells

compared to the near absence of FG cells in the vehicle control group. **[C]** Analysis of DBH

neurons revealed significant enrichment within the RVLM, compared to the adjacent areas,

confirming our localization (OR = 2.28, 95% CI = 1.92-2.71, p = 7.49e^{-17}). **[D]** No differences

were observed between minocycline (n=4; 309 ± 49) and vehicle rats (n=3; 367 ± 28) for DBH

neuronal counts within the RVLM (t(6) = -1.95, p = 0.109, independent samples t-test).

However, there were significantly more **[E]** FG labelled cells (t(6) = 4.91, p = 0.017,

independent samples t-test, 97 ± 40 vs. 0.7 ± 0.58), as well as **[F]** co-labeled cells (t(6) = 5.09, p

= 0.015, independent samples t-test, 56 ± 22 vs. 0 ± 0) in the minocycline group compared to the

vehicle control group.

7.3.6   Dorsal horn afferent plasticity is unchanged following minocycline administration

To exclude the possibility that minocycline could also reduce the severity of autonomic

dysreflexia by reducing aberrant lumbosacral plasticity, we examined CGRP positive axon

sprouting in the L6/S1 segment. This area is intimately linked to the development and severity of

autonomic dysreflexia.[37,41,44] We found no difference between animals treated with minocycline

and those treated with vehicle control **(Figure 7.4)**.
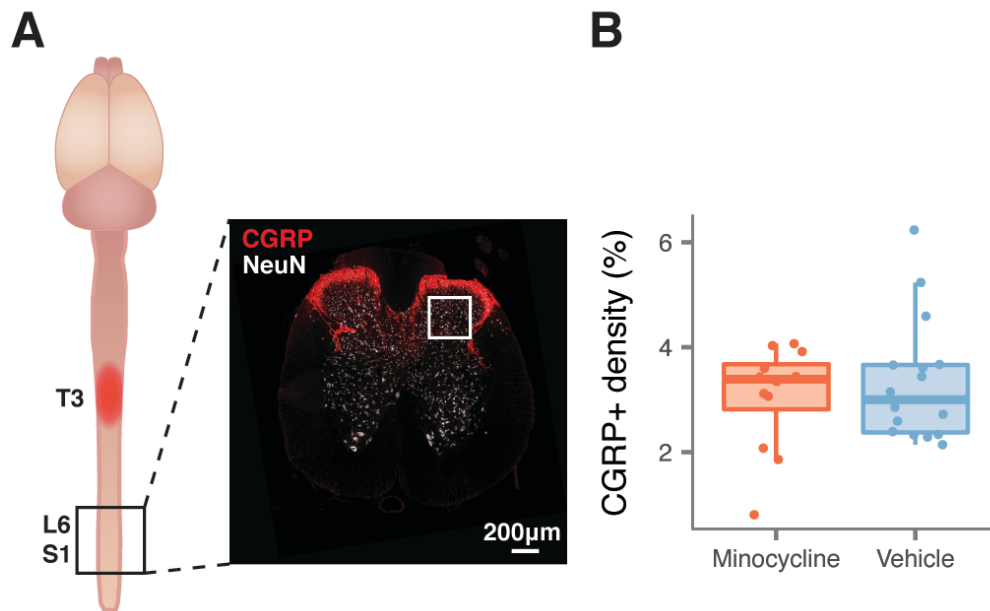
Figure 7.4: Dorsal horn afferent plasticity is unchanged following minocycline administration. **[A]** Calcitonin gene-related peptide (CGRP) positive axons were labelled in the lumbosacral spinal cord (L6/S1) to examine this mechanism of autonomic dysreflexia development. The white box indicates the region of interest. **[B]** Within Rexed III-VI there was no difference in the axonal CGRP positive axonal density between minocycline treated (n=12; 3.06 ± 0.99) and vehicle treated (n=16; 3.33 ± 1.17) rats ($t(27) = 0.647$, $p = 0.523$, independent samples t-test).

7.3.7 Minocycline preserves baseline blood pressure following spinal cord injury

At the end-point of the experiment we aimed to determine if minocycline treatment resulted in better blood pressure control. Of the 18 minocycline animals and 21 vehicle rats included in this series of experiments, 4 minocycline treated rats and 4 vehicle treated rats were excluded from hemodynamic outcome analyses due to transection of the spinal cord and subsequent FluoroGold placement. Of the remaining 14 minocycline animals, 2 were excluded due to excessive bleeding

during the end-point assessment surgery, and 1 vehicle rat was excluded due to unstable blood pressure resulting from poor cannulation. These three animals were thus not included in any histological analyses. We observed significantly higher systolic blood pressure, diastolic blood pressure, and mean arterial pressure, while heart rate was unchanged with minocycline treatment (**Figure 7.5A-D**).
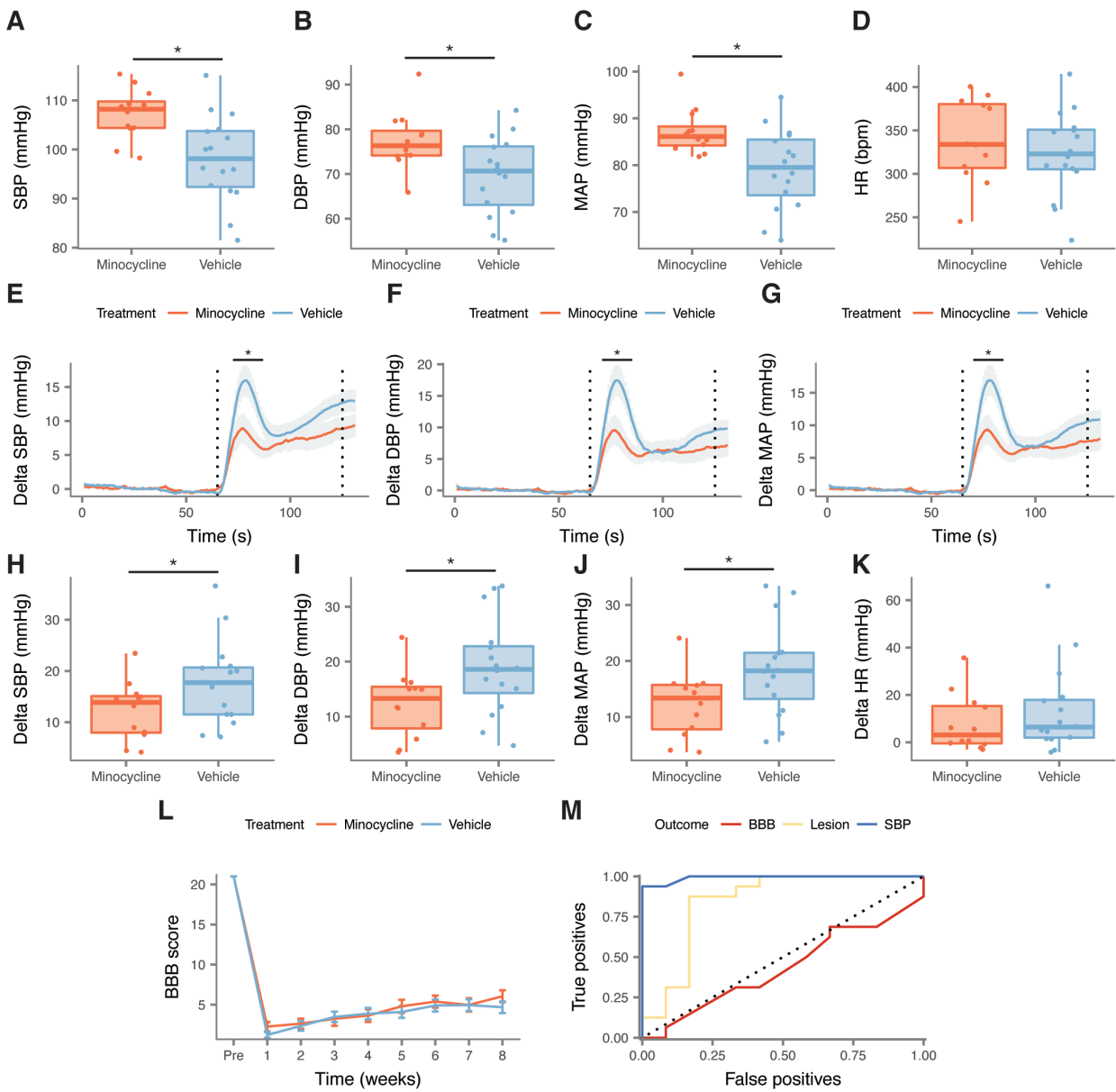
Figure 7.5: Autonomic functions, but not motor behavior, are improved with minocycline treatment and is a superior predictor of treatment stratification.

[A-D] Baseline hemodynamics were improved in animals treated with minocycline (n=12) compared to vehicle controls (n=16). We observed an increase in **[A]** systolic blood pressure (SBP; 107 ± 5 vs. 98 ± 9; $t(27) = 3.42$, $p = 0.002$, independent samples t-test) , **[B]** diastolic blood pressure (DBP; 77 ± 6 vs. 70 ± 9; $t(27) = 2.71$, $p = 0.012$, independent samples t-test), **[C]** mean arterial pressure (MAP; 87 ± 5 vs. 79 ± 9; $t(27) = 3.15$, $p = 0.004$, independent samples t-test), and **[D]** heart rate (HR; 339 ± 48 vs. 323 ± 48; $t(27) = 0.823$, $p = 0.418$, independent samples t-test). **[E-G]** There was a significant interaction effect between group and time when examining autonomic dysreflexia in response to colorectal distention (distension denoted by the black dotted lines) for **[E]** delta SBP ($F(1, 27) = 17.1$, $p = 3.69e^{-05}$, ANOVA), **[F]** delta DBP ($F(1, 27) = 6.67$, $p = 0.009$, ANOVA), and **[G]** delta MAP ($F(1, 27) = 9.93$, $p = 0.002$, ANOVA). **[H-K]** We next examined the peak change during colorectal distension and observed significant differences between groups. There were significant differences for **[H]** delta SBP (12 ± 6 vs. 18 ± 8; $t(27) = -2.13$, $p = 0.043$, independent samples t-test), **[I]** delta DBP (12 ± 6 vs. 19 ± 9; $t(27) = -2.40$, $p = 0.024$, independent samples t-test), **[J]** delta MAP (12 ± 6 vs. 18 ± 8; $t(27) = -2.35$, $p = 0.027$, independent samples t-test), but not for **[K]** delta HR (8 ± 12 vs. 13 ± 18; $t(27) = -0.943$, $p = 0.354$, independent samples t-test). **[L]** No between group differences were observed for motor behavior, as assessed using the Basso-Beattie-Bresnahan open-field locomotor scale ($F(1, 27) = 0.157$, $p = 0.69$, ANOVA). **[M]** Linear discriminant analysis revealed that the severity of autonomic dysreflexia was the most sensitive and specific marker of treatment stratification (AUC $= 0.992$).

7.3.8 Minocycline reduces the severity of autonomic dysreflexia

Next, we investigated the severity of autonomic dysreflexia by examining the development of hypertension throughout colorectal distension, and by quantifying the maximum change in blood pressure. We found that the severity of autonomic dysreflexia was significantly reduced throughout the peak distension response following administration of minocycline (**Figure 7.5E-G**). Moreover, when examining the maximum change in blood pressure from baseline, we found that minocycline reduced the change in systolic blood pressure (**Figure 7.5H**), diastolic blood pressure (**Figure 7.5I**), and mean arterial pressure (**Figure 7.5J**), but not heart rate (**Figure 7.5K**).

7.3.9 Minocycline does not improve functional motor behavior following spinal cord injury

As numerous studies have found differences in motor behaviour following minocycline treatment,[218,219,221,227,228,230,234-239] we examined BBB scores throughout the experiment. While we did find a significant effect of time, we did not observe significant differences between groups (**Figure 7.5L**), indicating that the administration of minocycline has no impact on functional motor recovery, as assessed by the BBB scale, of rodents following severe T3 contusion.

7.3.10   Autonomic dysreflexia is a more sensitive marker of treatment status than motor behavior

To better stratify the utility of different outcome measures we trained a linear discriminant analysis **(Figure 7.5M),** to predict treatment stratification. We found that the severity of autonomic dysreflexia was highly sensitive and specific (AUC = 0.992), while lesion area and motor behaviour were relatively ineffective at predicting treatment group.

7.3.11   Minocycline preserves pressure- but not volume-generating capacity of the left-ventricle after severe SCI contusion

Using echocardiography to examine the structure and function of the left-ventricle, we found a significant decrease in LV diameter during diastole (LVIDd) following SCI compared to uninjured control **(Table 7.1)**. This effect was not mitigated with minocycline treatment **(Table 7.1)**. Additionally, estimated volumetric indices obtained from echocardiography, including stroke volume (SV) and cardiac output (CO), were significantly lower after both vehicle treatment and minocycline treatment compared to uninjured animals **(Table 7.1).**

      To examine the pressure generating capacity of the heart, as well as load-independent function, we assessed LV function using pressure-volume catheterization. We found significantly lower pressure generating capacity (i.e., Pmax, dP/dt_{max}) after SCI, which was mitigated with minocycline treatment **(Table 7.1, Figure 7.6A-D)**. Conversely, volume generating capacity (i.e., SV) was still reduced in animals treated with minocycline, confirming our echocardiographic findings **(Table 7.1)**. We next assessed load-independent LV contractility by manipulating preload *via* inferior vena cava occlusions. We found that vehicle treated animals exhibited significantly reduced end systolic pressure volume relationship (i.e., Ees), PRSW, as

well as dP/dt-EDV relationships **(Table 7.1, Figure 7.6E-G),** whereas this effect was not present

in animals treated with minocycline.

Table 7.1: Anatomical, hemodynamic, echocardiographic, and pressure volume for uninjured, vehicle treated, and minocycline treated rats at 8WK.

	Uninjured			Vehicle			Minocycline		
Echocardiographic Data									
Dimensions and volumes									
LVIDd (mm)	7.20	±	0.30	6.43	±	0.41***	6.36	±	0.27***
LVIDs (mm)	3.13	±	0.47	3.12	±	0.67	3.58	±	0.47
LVPWd	1.83	±	0.21	2.03	±	0.42	1.79	±	0.35
EDV (μl)	273	±	25	212	±	31***	206	±	20***
ESV (μl)	39.89	±	14.57	41.19	±	18.97	54.99	±	17.19
Systolic Function									
SV (μl)	233	±	25	170	±	27***	151	±	17***
EF (%)	90.17	±	3.85	86.08	±	7.05	79.80	±	6.39**
CO (ml/min)	81.24	±	10.20	59.24	±	10.64***	52.91	±	8.96***
Pressure Volume Data									
Systolic Function									
SW (mmHg·mL)	14.7	±	2.1	6.3	±	2.7**	8.3	±	3.9**
SWI (mmHg·mL/100g)	3.8	±	0.4	1.7	±	0.7***	2.2	±	0.9**
CO (ml/min)	54.6	±	9.8	25.3	±	5.6**	33.0	±	15.8*
CI (ml/min·100g)	14.2	±	2.4	6.8	±	1.5***	8.8	±	3.4**
SV (μl)	150.9	±	19.5	97.5	±	33.2*	98.7	±	38.3*
HR (bpm)	359.7	±	25.6	268.1	±	49.9**	327.2	±	38.1
Pes (mmHg)	100.9	±	11.6	80.6	±	15.0*†	109.8	±	12.1
Pdev (mmHg)	117.8	±	6.1	83.9	±	6.1***†	97.0	±	9.0***
EF (%)	78.7	±	8.4	67.1	±	15.1	58.6	±	17.9
dP/dt$_{max}$ (mmHg/s)	12307	±	2756	4663	±	861**†	8405	±	2989*
Ea (mmHg/μl)	0.7	±	0.2	0.9	±	0.2	1.3	±	0.5*
Ees (mmHg/μl)	1.2	±	0.1	0.5	±	0.1***†††	1.2	±	0.1
PRSW (mmHg)	108	±	3.3	49	±	5.5***†††	104	±	6.7
+dP/dt$_{max}$-EDV (mmHg/s· μl)	77.2	±	3.1	32.1	±	5.3***†††	52.4	±	6.4***
Diastolic Function									
dP/dt$_{min}$ (mmHg/s)	-6182	±	579	-4539	±	634**†††	-6938	±	972
Ped (mmHg)	7.4	±	7.1	14.8	±	10.0	26.1	±	4.6**
τ (ms)	9.3	±	2.6	16.5	±	7.9	21.0	±	6.0*
EDPVR (mmHg/μl)	0.04	±	0.00	0.08	±	0.01†††	0.05	±	0.01***

Abbreviations: SBP: systolic blood pressure; DBP: diastolic blood pressure; MAP: mean arterial pressure; HR: heart rate; BPM: beats per minute; SVR: systemic vascular resistance; LVIDd: left ventricular internal diameter during diastole; LVIDs: left ventricular internal diameter during systole; LVPWd: left ventricular posterior wall thickness during diastole; EDV: end-diastolic volume; ESV: end-systolic volume; SV: stroke volume; EF: ejection fraction; CO: cardiac output; E: transmitral filling velocities during early diastole; SW: stroke work; SWI: stroke work index; CI: cardiac index; Pes: end systolic pressure; Ea: arterial elastance; Ees: end systolic pressure volume relationship; PRSW: preload recruitable stroke work; Ped: end diastolic pressure; EDPVR: end diastolic pressure volume relationship. P-values represent significance following independent samples t-test. Data are displayed as mean ± SD. ***$p < 0.001$ vs. Uninjured **$p < 0.01$ vs. Uninjured *$p < 0.05$ vs. Uninjured † $p < 0.05$ vs. Minocycline ††$p < 0.01$ vs. Minocycline †††$p < 0.001$ vs. Minocycline.
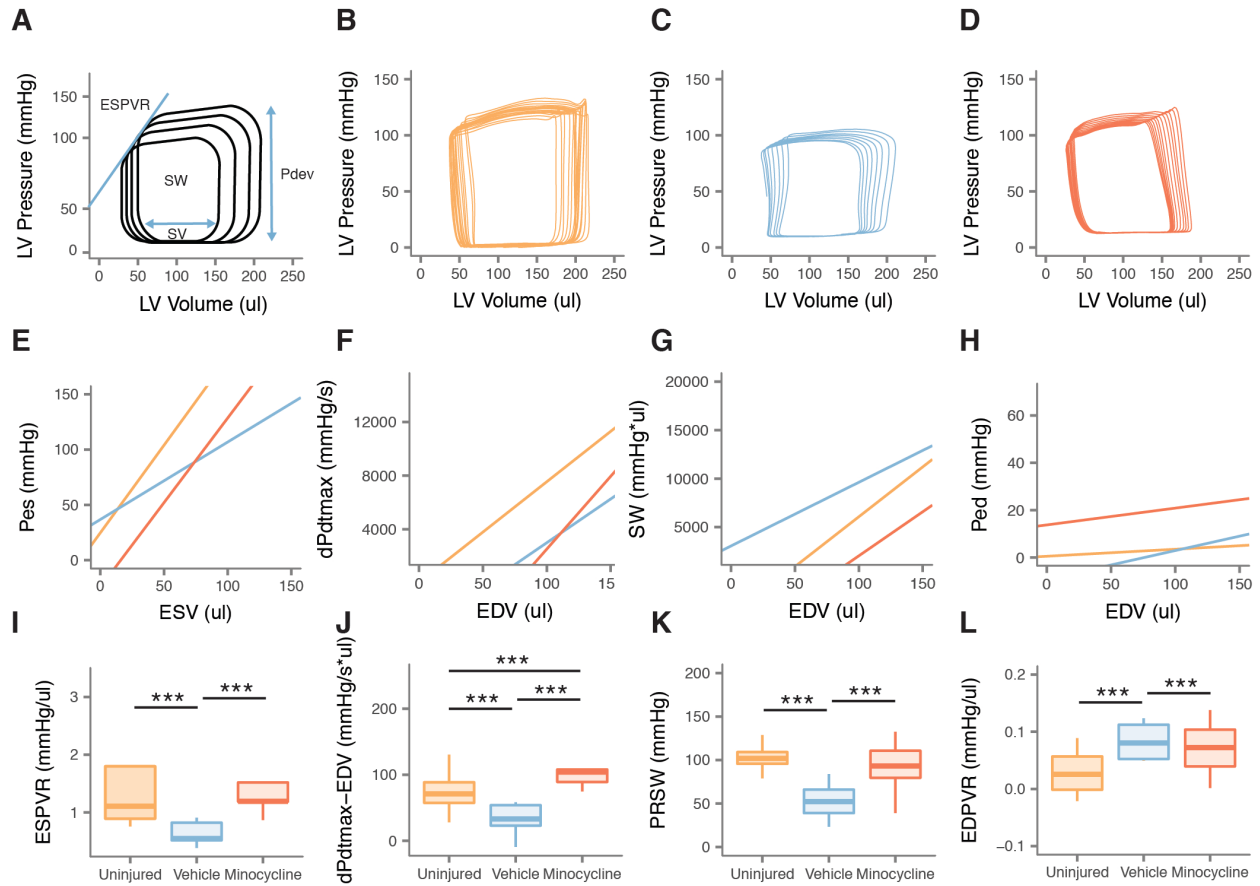
Figure 7.6: Pressure-volume analysis.

Representative pressure-volume loops obtained from 1 animal per group during inferior vena cava occlusions demonstrate the significant decrease in pressure and volume generating capacity with vehicle treatment, and the maintenance of pressure-generating capacity in animals treated with minocycline **(panels A-D)**. Linear regression reveals significant decreases in all three measure of load-independent contractility including the end-systolic pressure (Pes) to volume (Ves) relationship **(panel E)**, dP/dt$_{max}$-end diastolic volume (Ved) relationship **(panel F)**, as well as preload recruitable stroke work **(**SW; **panel G)** in vehicle treated animals. However, this effect was not found in animals treated with minocycline **(panels I-L)**. Moreover, we observed a

significant increase in the end diastolic pressure (Ped) to volume relationship in vehicle treated animals, but not minocycline treated animals. **(panel L)**. n=5. * = $p < 0.05$, ** = $p < 0.01$, *** = $p < 0.001$.

7.4   Discussion

Here, we report the novel application of minocycline to improve autonomic function after acute SCI. We show that after severe T3 contusion minocycline reduces lesion area, increases the number of intact descending sympatho-excitatory axons, improves resting hemodynamics, reduces the severity of autonomic dysreflexia, and improves LV pressure-generating capacity. Notably, we found that minocycline maintained autonomic function despite no observable differences in motor behaviour. The superior sensitivity and specificity of autonomic function compared to motor function as a marker of treatment stratification exposes a new avenue to improve both preclinical and clinical trial design in the field of SCI. These findings also suggest that the lack of successful translation of novel therapies to treat SCI may be due to inherent shortcomings of focusing outcome assessments solely on motor function.

In accordance with previous work investigating the utility of minocycline to improve functional outcomes after SCI,[75,226,231-233] we found that animals treated with minocycline in the acute phase after injury had smaller lesion areas than vehicle controls. In addition, we found that the area of astrogliosis was extensive, characteristic of SCI, and a result of proliferating astrocytes as well as infiltrating ependymal cells through the central canal.[140,143] While the assessment of the lesion area in two sagittal sections is more variable than in serial cross sections, and limited in significance as an isolated outcome, we reasoned that if the lesion area shows a reduction, more descending sympatho-excitatory axons would thus be able to maintain

their connections to their caudal targets. To specifically examine this, we stained the spinal cord with TH, the rate-limiting step in the synthesis of catecholamines. Importantly, TH is maintained along the length of the axon in vesicles, allowing the visualization of the axon as it descends through the spinal cord. Using this approach, we identified that animals treated with minocycline showed increases preservation of TH positive axons, indicating a potentially more permissive environment for axon maintenance and establishment of novel connections. This finding is in line with our previous work, where we showed that minocycline can also preserve of descending corticospinal neurons and preserve motor function in a less severe midline contusion model.[226]

We further confirmed the possibility that minocycline preserves descending sympatho-excitatory axons by utilizing retrograde FluoroGold tracing in a subset of animals. This is a common approach that we have previously used to demonstrate that cardiovascular dysfunction after SCI is dependent on the disruption of sympatho-excitatory pathways extending from their cell bodies within the RVLM and traversing the spinal cord lesion. [24,174] Importantly, we found that animals treated with the vehicle control had zero (one animal had one identified FG neuron) FG labelled neurons traversing the injury site that projected from the RVLM. In contrast, animals treated with minocycline had on average 60 neurons identified using our analysis in the RVLM, approximately in line with the number we have found following a more moderate injury.[174] As such, we posit that minocycline aids in the preservation of descending sympatho-excitatory axons after severe T3 spinal cord contusion. This has important functional considerations, as we have shown that the number of descending sympatho-excitatory axons necessary for proper cardiovascular control after SCI is relatively small, owing potentially to the early evolutionary origin of autonomic systems. Therefore, any maintenance of these axons is likely to have important functional considerations for individuals with SCI.

148

Our functional data show that animals treated with minocycline had higher resting blood pressure, potentially indicating a preservation of input to the blood vessels from sympathetic preganglionic neurons. This notion is supported by our retrograde tracing finding. Furthermore, we examined the severity of autonomic dysreflexia as this outcome is one of the most significant cardiovascular complications observed after SCI.[21,88,240] In fact, we and others have shown that autonomic dysreflexia can lead to life-threatening elevations in blood pressure, resulting in myocardial infarction, retinal detachment, posterior reversible encephalopathy syndrome, and even death.[79,88,241] Furthermore, our recent work has shown that repetitive autonomic dysreflexia in the rodent exacerbates both cardiac dysfunction[170] and cerebrovascular dysfunction after experimental SCI.[242] Put together, these findings suggest that autonomic dysreflexia is one of the primary mechanisms by which individuals with SCI exhibit increased risk for both heart disease[11] and stroke.[11,15] We found that with the treatment of minocycline, the severity of autonomic dysreflexia was reduced by approximately 30%. Importantly, we found that minocycline did not alter the lumbosacral afferent plasticity that is observed after SCI, which has been critically linked to the severity of autonomic dysreflexia.[37,41,44] One previous experiment utilizing a neuroprotective strategy observed similar outcomes, showing no differences between treated groups in terms of the degree of afferent sprouting.[58] However, one study did find that the addition of a neuroprotective agent did in fact increase the degree of afferent sprouting, attributed to a more permissive environment for axonal growth.[56] As such, we felt it prudent to explore this mechanism to: 1) ensure any functional improvements we observed were not a result of reduced afferent plasticity, but could be attributed to decreased lesion size and increased preservation of descending sympatho-excitatory axons, and 2) to ensure minocycline did not exacerbate this pathophysiological mechanism associated with the development and severity of

149

autonomic dysreflexia. While not completely curative of the condition, a reduction in the severity of autonomic dysreflexia of this magnitude has critical implications on cardiovascular end-organ health,[11,242] and is in line with previous neuroprotective efforts aimed at reducing the severity of autonomic dysreflexia.[56,58,66-71]

One of our objectives was to investigate the utility of using cardiovascular outcomes as a potentially more sensitive method to detect both differences between groups of animals, and also to utilize this as a predictive measure of treatment stratification. Using linear discriminant analysis we found that the severity of autonomic dysreflexia was highly sensitive and specific when predicting treatment stratification. Given the limitation of outcome sensitivity in current human clinical trial development for SCI, we believe this is an important finding. It is important to note that we did not observe between group differences for BBB score which is most likely a result of our significant injury severity. Further, we do recognize the limitations of this analysis as BBB scores could have been complemented with other measures of motor function. However, in the clinic only one metric of motor/sensory improvement is primarily used. As such, we believe this is a rational comparison and worth further discussion. The ability to sensitively detect changes in individuals with SCI in response to treatment is important as it could significantly reduce the number of individuals needed in a clinical trial to demonstrate efficacy. The sole reliance on motor and sensory function as outcomes in SCI may in fact hinder the translation of new drugs into clinical use, as potential benefits on systems other than motor and sensory function may be missed.

Lastly, we aimed to determine if minocycline administration mitigated the decline in cardiac structure and function that we have previously described **(see Chapters 5 and 6)**.[127,198,243,244] We found that animals with severe T3 had significantly smaller LV cavity sizes

and volumetric indices, which were not improved in animals treated with minocycline. Based on our previous work demonstrating that passive hind-limb exercise does improve these indices,[210] this suggests that animals treated with minocycline do not gain improvements in LV pre-load compared to vehicle treated animals. However, we found that animals treated with minocycline had preserved pressure-generating capacity compared to vehicle-treated animals. This, in addition to our findings demonstrating preserved load-independent function following minocycline treatment, suggest that preservation of descending sympatho-excitatory pathways is critical to maintain these aspects of LV function.

7.5   Conclusion

Minocycline administered in the acute phase after T3 experimental SCI significantly reduces lesion area. We reasoned that this would increase the number of descending sympatho-excitatory axons traversing the injury site. We confirmed this notion using a histological examination of spared TH+ axons and retrograde FluoroGold tracing, where we found that in contrast to vehicle treated animals, where there was a near absence of descending sympatho-excitatory axons crossing the injury site, minocycline treated animals demonstrated numbers more consistent with a moderate injury type. We found that the preservation of these axons led to important functional improvements, characterized by increased resting blood pressure, reduced severity of autonomic dysreflexia, and improved LV pressure-generating capacity. Lastly, that the severity of autonomic dysreflexia was a more sensitive and specific predictor of treatment stratification strongly suggests future work consider the inclusion of more primitive autonomic system assessments in their outcome measures. Further work should consider deeper examination of lesion site characteristics, as well as extensive dose-response experiments.

151

The work contained within the preceding chapters has developed a framework to test neuroprotective therapies to improve autonomic dysfunction after severe SCI. Moreover, these data show that minocycline, which has already started phase III clinical trial,[215] leads to improved hemodynamic and cardiac function. While these results are extremely promising, clinical trials in the area of neuroprotection and SCI are fraught with difficulty. Excluding the significant limitations of trial funding, participant recruitment, and the limitations of current outcome measures, widespread integration of a neuroprotective drug into standard clinical care can expose potential complications not initially realised (as was the case for methylprednisolone[214]). As a prudent approach to continue our attempt to optimize the recovery of autonomic dysfunction, our findings have now been extrapolated into experiments further testing promising neuroprotective agents, which may have beneficial effects that exceed those of minocycline **(Wings for Life funded grant based on work contained within this thesis).**

In addition to the search for novel neuroprotective treatments through traditional means, there are two further important aspects to consider when working in the field of neuroprotective therapies in SCI: 1) biomarkers of injury severity, and 2) rationale drug repurposing. One main reason biomarkers are positioned to play such a critical role in SCI clinical trials is our inability to always acquire a valid baseline clinical assessment due to the severity and complexity of the initial trauma upon admission to the hospital, as well as the difficulty in predicting functional recovery from assessments in the early hours after injury. In the next chapter **(Chapter 8)** I will develop a framework grounded in systems genetics to guide the identification and validation of 1) biomarkers of SCI severity, and 2) drug repurposing tools. For these experiments, a field-standard T10 contusion was used to first align our framework with the existing corpus of data examining the transcriptomic and proteomic response to injury.

Chapter 8: Integrated systems analysis reveals conserved gene networks underlying response to spinal cord injury[6]

8.1   Introduction

Spinal cord injury (SCI) results in impairment of motor, sensory, and autonomic systems, causing profound dysregulation of almost every bodily function. The failure of large-scale clinical trials of drug therapies in acute SCI,[214-216] and the lack of success in translating preclinical therapies to humans,[97] leaves clinicians without effective treatment options for SCI. As such, hemodynamic management and surgical decompression remain the only options to influence neurological outcomes immediately following acute SCI, typically with only marginal improvements.[245-247] The absence of an effective treatment for SCI reflects the complexity of the pathophysiologic mechanisms activated by central nervous system (CNS) injury. The additive effects of the immune response,[248,249] multiple forms of cell death,[250,251] neuronal growth suppression,[252,253] and the formation of an inhibitory glial scar[254] pose a challenge to the development of new therapeutic strategies.

A major obstacle to the development of targeted therapies for SCI is the fragmentary state of our understanding of SCI pathophysiology. The response to trauma within the human spinal

---

[6] A version of chapter 8 has been submitted. **Squair, J.W.,** Kwon, B.K., Krassioukov, A.V., West, C.R., Foster, L.J., Skinnider, M.A. Integrated systems analysis reveals conserved gene networks underlying response to spinal cord injury.

cord is mediated by multiple coordinated molecular pathways, yet these processes are rarely studied in an integrated manner. An additional challenge in translation of novel therapies is the reliance of clinical trials on standardized neurological assessments for patient enrollment and stratification.[211] These measures are highly variable, operator-dependent, and may be impossible to perform in many SCI patients.[255] Systems biology approaches provide powerful means to elucidate the coordinated molecular processes underlying the pathophysiology of complex diseases.[256-259] In particular, gene coexpression network analysis can complement reductionist descriptions of isolated gene functions by identifying networks of genes responsible for driving disease processes.[260,261] Further, systems-level analyses may have the potential to suggest novel biomarkers capable of stratifying injury severity and predicting functional recovery, and consequently to facilitate the translation of new therapies for acute SCI.

In the present study, we describe an integrated systems biology approach to study the pathophysiology of SCI. We systematically survey decades of biomedical literature in order to establish the complete set of genes implicated in the response to SCI by small-scale experiments. We then integrate this literature-curated gene set with unbiased gene expression data from the human spinal cord. We use weighted gene coexpression network analysis (WGCNA) to establish the normal biological processes within the healthy human spinal cord, and conduct a meta-analysis of publically available gene expression data to define the gene regulatory network signature of the coordinated physiological response to SCI. We validate our findings at the transcriptomic and proteomic levels, and leverage the resulting systems-level understanding of SCI pathophysiology to define candidate biomarkers for stratification of injury severity and prediction of functional recovery.

8.2 Materials and methods

8.2.1 Systematic analysis of spinal cord injury literature

We searched PubMed for articles investigating the molecular pathophysiology of SCI published prior to February 2016, using combinations of "spinal cord injury" and one of "proteomics," "proteome," "proteomic," "biomarkers," "biomarker," "RNA-seq," and "microarray" as search terms. 556 papers were identified that met these criteria. These were subsequently filtered to exclude papers that did not include a valid control group, included exclusively in vitro data, did not include primary data, or examined a tissue other than spinal cord. As previous studies have suggested that small-scale and high-throughput experiments may be largely complementary, or lead to divergent biological conclusions, we considered only small-scale experiments in the literature curation process, defined here as experiments reporting differential regulation of fewer than 100 genes or proteins. Ultimately, data from 67 manuscripts was collected. The original accessions used to identify genes or proteins associated with SCI in each publication were retained. If only the gene name and no unambiguous identifier was noted, the UniProt accession of the gene in the relevant species was manually retrieved. We applied a strict, majority voting-based method to map rat, mouse, and rabbit genes to their human orthologs with maximum accuracy.[304] Specifically, we mapped orthologs from rat, mouse, and rabbit genes to human using seven different ortholog databases [EggNOG,[305] Ensembl,[306] NCBI Gene,[307] HomoloGene,[308] InParanoid,[309] and OrthoDB[310]], and considered human genes as "consensus orthologs" only if they were detected in at least half of those databases containing an entry for the target model organism protein. All genes were mapped to Ensembl identifiers in Bioconductor.[311]

8.2.2 Validation of literature-curated spinal cord injury genes

We established the functional coherence and biological relevance of our literature-curated SCI gene set using four lines of evidence: protein-protein interactions (PPIs), interactome largest connected components (LCCs), shared Gene Ontology (GO) terms, and recovery with DIAMOnD,[263] a disease gene prediction algorithm. To investigate the tendency of our literature-curated gene set to participate in PPIs, we initially analyzed a recently described high-quality human interactome.[312] We subsequently reproduced our results in two additional human interactome databases restricted to binary and co-complex interactions, obtained from HINT (version 4),[313] in order to establish that the enrichment for protein-protein interactions was not a function of the experimental technique used to detect the interaction. Self-interactions were removed and original accessions were mapped to Ensembl gene identifiers. To evaluate the impact of the experimental method used to detect PPIs, we analyzed high-quality binary and co-complex interactomes from HINT separately. Network operations, including creation of induced subgraphs and calculation of largest connected components, were performed in the R package igraph.[314] Randomized networks were generated using a degree-preserving algorithm[315] to control for network topology, with 1,000 randomized networks generated to calculate empirical P values. We additionally evaluated the tendency for literature-curated proteins to participate in the same protein complexes by retrieving random sets of proteins of equivalent size from hu.MAP[316] and calculating the number of co- complex interactions, a process that was repeated 1000 times.

GO terms were retrieved from the UniProt-GOA database.[317] To control for the effect of

annotation, only genes annotated with at least three GO terms were considered.[318] We compared

the number of shared GO terms within each ontological category at four breadth cutoffs between

all pairs of literature-curated genes to the number of shared GO terms between random sets of

genes annotated with at least three GO terms.

To evaluate the ability of a recently described algorithm for disease gene prioritization,

DIAMOnD, we randomly withheld 20% of literature-curated genes and evaluated the fraction

recovered within the first 1,000 iterations of DIAMOnD. This was compared to the ability of

DIAMOnD to recover an equivalent number of randomly selected genes, using randomly

selected seed genes from the human genome. This process was bootstrapped 1,000 times and

results were reproduced using the InWeb InBioMap interactome (version 2016 09 12).[304]

8.2.3   Gene co-expression network analysis of human spinal cord

Raw gene read count and RPKM data was downloaded from the GTEx portal, version V6p.[269]

Only genes with expression estimates > 0.1 RPKM in $\geq$ 10 individuals were considered. The

distribution of RPKMs in each sample was quantile transformed using the average empirical

distribution observed across all samples, and inverse quantile normalization to the standard

normal distribution was performed for each gene. Gene coexpression analysis was performed

using the WGCNA package.[270] Briefly, a signed pairwise gene correlation matrix was

constructed using biweight midcorrelation[319] and considering a maximum of 5% of samples as

outliers on either side of the median. The correlation matrix was raised to the power $\beta = 5$, the

minimum value satisfying the scale-free topology criterion $R^2 > 0.8$, to create an adjacency

matrix. The adjacency matrix was used to calculate the topological overlap matrix (TOM), which

was subsequently clustered based on the dissimilarity of gene connectivity. Coexpressed gene modules were defined from the resulting tree using the dynamic tree cut method,[270] with a minimum module size of 20 and a cut height of 0.2.

8.2.4 Module preservation in human, rat, and mouse microarray data

We queried ArrayExpress[320] with the search term "spinal cord" to identify samples from Affymetrix GeneChip Rat Genome 230 2.0, Human Genome U133 Plus 2.0, and Mouse Genome 430 2.0 microarrays. Experiments with fewer than five samples were excluded. Additionally, experiments or samples analyzing individual cell populations (e.g., neurons) within the spinal cord rather than homogenized tissue, fetal spinal cord, or spinal cord neoplasms were excluded. Raw expression profiles were normalized with the MAS5 algorithm[321] within the R package affy.[322] Only probesets that were called as present in at least 80% of samples were retained. ComBat was used to adjust for batch effects, where each experiment corresponded to a single batch.[271] Affymetrix probeset identifiers were mapped to Ensembl gene accessions using Bioconductor. Genes with multiple probes were represented by the median expression value. Mouse and rat accessions were further mapped to consensus human orthologs using the majority-voting procedure described above. Module preservation was assessed using the $Z_{summary}$ statistic, calculated using the modulePreservation function in the WGCNA R package with 100 permutations.

8.2.5 Meta-analysis of co-expression network dysregulation following spinal cord injury

Data from five studies investigating the transcriptomic response to SCI (GSE464, GSE5296, GSE45006, GSE45376, and GSE69334) was obtained from ArrayExpress. Normalization and

mapping to human orthologs was performed as described above. For GSE464, MAS5 normalization was performed within the R package xps, as the Rat Genome U34 chip was not supported by the affy package. For GSE45376, quantile normalization of raw expression estimates was performed as described for GTEx data. Differential expression analyses of each processed dataset were performed with treatment-contrasts parametrization in the limma package,[323] using the geneSetTest function to perform a mean-rank gene-set enrichment test for both up and downregulation of each module, before applying Bonferroni correction. We additionally analyzed differential expression of each module at 1 day, 3 days, 7 days, and 28 days following SCI in order to evaluate module expression at acute, subacute, and chronic time points.

8.2.6   Functional characterization of spinal cord modules

To construct enrichment maps for consensus modules implicated in the response to SCI by meta-analysis, we identified overrepresented gene sets from GO[317] and the CGP (chemical and genetic perturbagens) and TFT (transcription factor targets) subsets of MSigDB.[275] Genes were mapped to Ensembl accessions prior to enrichment analysis with the HTSanalyzeR package,[324] using 1,000 permutations and a minimum gene set size of 5. Significantly enriched gene sets were visualized as an enrichment map,[276] in which nodes represent gene sets and edges connect related gene sets. Clusters of gene sets within the resulting enrichment maps were manually identified and annotated. Cell type specificity was assessed using microarray,[279] RNA-seq,[277] and proteomic[278] data from cell populations within the mouse CNS, using the R package pSI to test for enrichment of cell type-specific genes.[325] We analyzed a wide range of cell types, including neurons, astrocytes, and microglia,[277-279] as well as oligodendrocytes at various points in

maturation (i.e., "oligodendrocyte precursor cell," "myelinating oligodendrocyte," "oligodendrocyte;"[277,279]). We included additional comparisons in microglia from both newborn and adult mice (i.e., "adult microglia," "young microglia;"[278]), developing in vitro neurons and oligodendrocytes through the first two weeks of maturation (DIV: day in vitro[278]), as well as isolated and cultured astrocytes.[279]

8.2.7   Severity-dependent expression of spinal cord modules

Raw microarray data was obtained from ArrayExpress (GSE464)[265,281,320] and processed as described above. Injuries annotated as "moderate" and "severe" were grouped together on the basis of identical histological and functional outcomes in the experimental model.[281] To identify modules enriched for genes whose expression was correlated with injury severity, we calculated a previously described gene-level score[265] by multiplying the Spearman correlation coefficient between gene expression and height of weight drop by the negative logarithm of the P value, then performed mean-rank gene-set enrichment tests and applied Bonferroni correction. Only samples from the lesion site were considered. Initial analysis of differentially expressed genes revealed that all but a single probeset on the U34A chip were consistently downregulated following injury, likely due to the biased composition of this chip. Therefore, samples collected using this chip were omitted when calculating correlation between injury severity and module eigengenes to reduce bias. Module eigengenes were calculated using the moduleEigengenes function from the WGCNA package.

8.2.8   Ethical approval

Ethical approval was obtained by the University of British Columbia Behavioural Research

Ethics Board (A14-0152) and all procedures strictly adhere to the guidelines issues by the Canadian Council for Animal Care.

8.2.9 Spinal cord surgery and animal care

Ethical approval was obtained by the University of British Columbia Behavioural Research Ethics Board (A14-0152) and all procedures strictly adhere to the guidelines issues by the Canadian Council for Ani- mal Care. Animals were started on prophylactic enrofloxin (Baytril; 10 mg kg^{-1}, s.c., Associated Veterinary Purchasing (AVP), Langley, Canada) three days prior to surgery. On the day of spinal cord contusion animals were anesthetized using isoflurane (initial induction 5% and maintained on a Bain's system at 2%). After achieving surgical depth of anesthesia, pre- operative buprenorphine (Temgesic; 0.02 mg kg^{-1}, s.c., McGill University), enrofloxin (Baytril; 10 mg kg^{-1}, s.c., Associated Veterinary Purchasing (AVP), Langley, Canada), and Ringers solution were administered subcutaneously. The skin was prepared by shaving the surgical site, followed by three successive chlorohexidine and 70% ethanol washes. A dorsal midline incision was made from T5 to L2. The T9 spinous process was identified and a laminectomy was performed to expose the T10 spinal segment. Following this the animal was transferred to the Infinite-Horizons (IH) impactor stage, where the T8 and T10 spinous processes were securely clamped using modified Allis forceps. The animal was stabilized on the platform and the impactor tip (2.0 mm) was properly aligned using a 3-dimensional coordinate system moving platform. The position of the impactor was confirmed as midline by two separate experimenters. The IH system was set to deliver an impact of 100 or 200 kdyn of pre-defined force. Following hemostasis, the deep and superficial paraspinal muscles were sutured using 5-0 Monocryl sutures (Ethicon, USA), followed by 5-0 Prolene (Ethicon, USA) sutures in the skin.

Animals were then given 5 mL of Ringers solution subcutaneously and allowed to recover in a temperature controlled environment (Animal Intensive Care Unit, Los Angeles, CA, USA). Post-operatively, animals were given buprenorphine (10 mg kg-1, s.c.) and enrofloxin (0.02 mg kg-1, s.c.) once daily for three days, after which buprenorphine was given on an as needed basis. Bladders were manually expressed for the duration of the experiment (7 days post-injury).

8.2.10 Tissue processing

Animals were overdosed with a lethal dose of 10% chlorohydrate (i.p.), after which a thoracotomy was performed. Animals were transcardially cleared with 300 mL of PBS. Next, the spinal cord lesion site was dissected 2 mm caudal and rostral to the visual epicentre. This sample was homogenized and split into two parts for transcriptomic and proteomic processing.

8.2.11 RNA isolation and sequencing

10 mg of spinal cord parenchyma surrounding the injury site was stored in RLT buffer containing beta-mercaptoethanol until RNA isolation. Total RNA was purified using the Qiagen RNeasy Mini Kit according to the manufacturer's instructions, eluting in 30 μL of water. 500 ng RNA was used for library preparation with Illumina's TruSeq Stranded mRNA kit (Illumina, San Diego, CA). Libraries were pooled and sequenced on the Illumina NextSeq in high output mode, generating paired-end 75-base pair reads. Library preparation and sequencing were performed by the Sequencing and Bioinformatics Consortium at the University of British Columbia.

8.2.12 Transcriptome analysis

Quality control checks using FastQC and principal components analysis revealed a single sample as an outlier, which was discarded prior to further analysis. Sequences were pseudoaligned to the Ensembl 89 version of the Rattus norvegicus transcriptome, including coding and non-coding

162

transcripts, with Salmon (version 0.8.2),[326] using 100 bootstraps to compute abundance estimates. Rat genes were mapped to human orthologs using the majority- voting procedure described above. Salmon output was converted into a format compatible with sleuth[87] for differential expression analysis using wasabi (https://github.com/COMBINE-lab/wasabi). Differential expression was assessed using sleuth (version 0.29.0), representing severity as a continuous covariate (0, 100, or 200 kdyn of force). Genes were ranked by the fold change estimates computed by sleuth to perform mean-rank gene-set enrichment tests for module up- and downregulation. Hub genes were identified by ranking genes by their correlation to the module eigengene in the human spinal cord samples,[328] and identifying the 10% most connected genes in the module. To evaluate the ability of hub gene expression to stratify SCI severity, we constructed linear discriminant analysis models using the R package MASS.[255] The accuracy of each model in classifying moderately and severely injured rats was assessed using leave-one- out cross-validation.

8.2.13 Mass spectrometric analysis

Parenchyma tissue samples were lysed by 2.8 mm ceramic bead (Qiagen) prior to homogenization with a single 20 sec 5000 rpm on Precellys 24 (Bertin Tech- nologies) in 4% (w/v) SDS in 100 mM Tris pH 8.8 and 20 mM DTT. The lysate was heated at 99°C for 10 minutes, and cell debris was spun out and protein concentration estimated by BCA assay (Thermo). An equivalent protein amount for each sample was loaded onto 10% SDS PAGE gel and visualized by colloidal Coomassie.[329] Each lane was fractionated into 5 pieces and trypsin digested out of the gel.[330] Peptide samples were purified by solid phase extraction on C-18 STop And Go Extraction (STAGE) Tips,[331] and analyzed by a quadrupole–time of flight mass spec-

trometer (Impact II; Bruker Daltonics) coupled to an Easy nano LC 1000 HPLC (ThermoFisher Scientific) using an analytical column that was 40–50 cm long, with a 75 μm inner diameter fused silica with an integrated spray tip pulled with P-2000 laser puller (Sutter Instruments), packed with 1.9 μm diameter ReprosilPur C-18-AQ beads (Maisch, www.Dr-Maisch.com), and operated at 50°C with in-house built column heater. Buffer A consisted of 0.1% aqueous formic acid, and buffer B consisted of 0.1% formic acid in acetonitrile. A standard 60 min peptide separation was done per injection, and the column was washed with 100% buffer B before re-equilibration with buffer A. The Impact II was set to acquire in a data-dependent auto- MS/MS mode with inactive focus fragmenting the 20 most abundant ions (one at the time at a 18 Hz rate) after each full-range scan from m/z 200 to m/z 2,000 at 5 Hz rate. The isolation window for MS/MS was 2–3 depending on the parent ion mass to charge ratio, and the collision energy ranged from 23 to 65 eV depending on ion mass and charge. Parent ions were then excluded from MS/MS for the next 0.4 min and reconsidered if their intensity increased more than five times. Singly charged ions were excluded from fragmentation.

Analysis of mass spectrometry data was performed using MaxQuant[332] version 1.5.3.30. The search was performed against a database comprised of the protein sequences from Uniprot Rattus norvegicus entries plus common contaminants with variable modifications of methionine oxidation, and N-acetylation of the proteins, and enabling LFQ and match between run options. Only those peptides exceeding the individually calculated 99% confidence limit (as opposed to the average limit for the whole experiment) were considered as accurately identified.

8.2.14 Proteomic analysis

Module preservation at the proteomic level was quantified using the modulePreservation

function, using Spearman correlation to calculate coexpression similarity. A mean-rank gene set enrichment test was used to test for module up- and downregulation, prior to Bonferroni correction. Linear discriminant analysis of annexin A1 was performed as described above.

8.2.15 Availability of data

The RNA-seq dataset has been deposited to the NCBI Gene Expression Omnibus with the accession number GSE115067.

8.3 Results

8.3.1 Systematic literature analysis identifies genes associated with response to spinal cord injury

Despite decades of study, an integrated understanding of the pathophysiological response to SCI remains elusive. This gap represents a central challenge to the development of targeted therapies for SCI. We hypothesized that such an integrated understanding could be achieved by integrating the vast corpus of SCI literature, collected by small-scale experimentation over several decades, within an unbiased, genome-wide frame- work. An overview of our experimental design is shown in **Figure 8.1**.
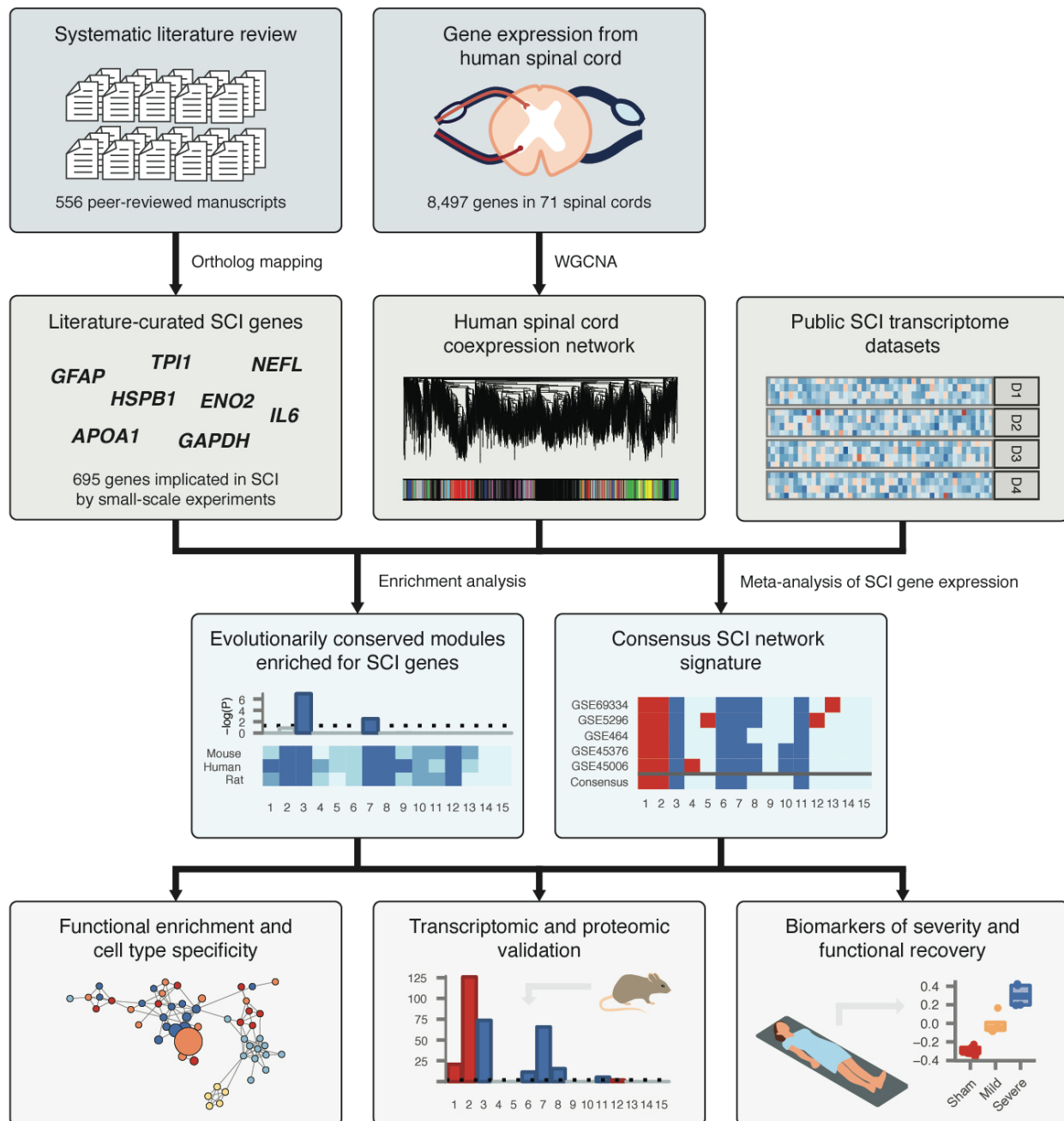
Figure 8.1: Schematic overview of our systems biology approach to SCI pathophysiology integrating small-scale experiments with high-throughput data.

Systematic analysis of over 500 manuscripts revealed the complete set of genes implicated in

SCI pathophysiology by small-scale experiments. SCI genes were integrated with unbiased, genome-wide gene expression data from healthy human spinal cord to identify coexpressed gene subnetworks enriched for known SCI genes. Meta-analysis of SCI gene expression data revealed consensus patterns of subnetwork differential expression after SCI. The resulting consensus network signature of the response to SCI in human spinal cord was subjected to functional enrichment and cell type analyses, validated at the transcriptomic and proteomic levels, and leveraged to nominate quantitative biomarkers of SCI severity.

As a first step, we sought to systematically establish the complete set of genes implicated in the physiological response to SCI. We conducted a systematic analysis of the SCI literature, reviewing over 500 papers, in order to reveal a set of 695 unique human genes associated with the response to SCI by small-scale experiments. Of these genes, 559 were upregulated following SCI, 213 were downregulated, and the protein products of 9 were differentially phosphorylated. Among all genes, 151 were associated with the response to SCI by more than one study **(Figure 8.2A)**. The complete set includes genes that have been associated with SCI in a wide range of experimental models of SCI, in addition to human injuries **(Figure 8.3A)**; in multiple species, including human as well as rat, mouse, and rabbit **(Figure 8.3B)**; using a range of experimental techniques **(Figure 8.2B)**; and at a variety of timepoints, from 1 hour to 6 months post-injury **(Figure 8.3C)**.
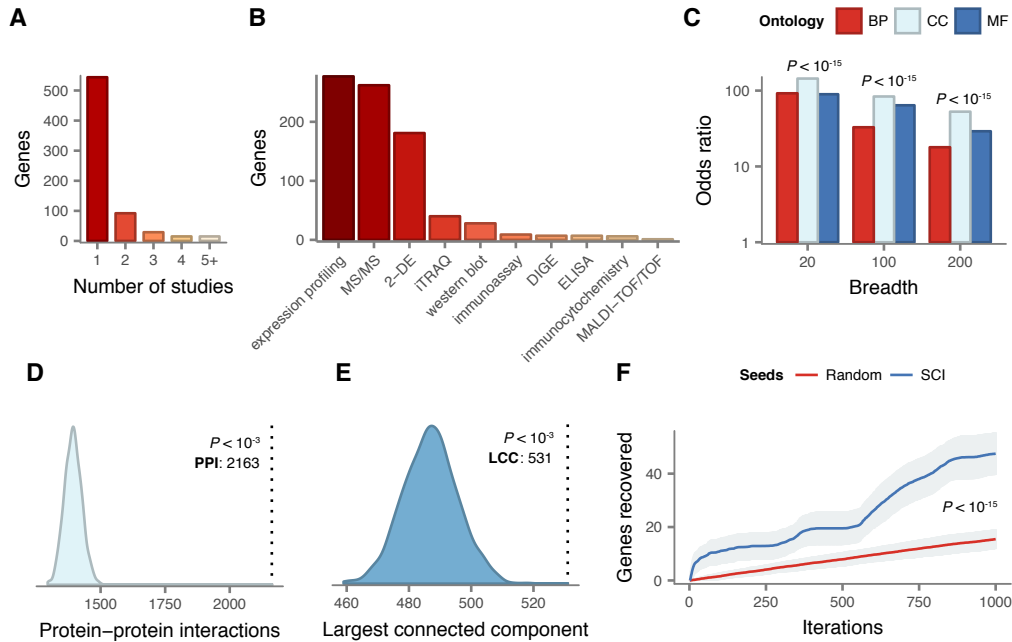
Figure 8.2: Literature curation and validation of genes implicated in the physiological response to SCI by small-scale experiments.

(A) Number of small-scale studies implicating each gene in SCI pathophysiology in the literature-curated (LC) gene set. **(B)** Experimental techniques used to associate LC genes with response to SCI in the LC gene set. **(C)** Enrichment for shared Gene Ontology terms among LC genes (all $P < 10^{-15}$). **(D)** Number of protein-protein interactions (PPIs) between LC genes observed in the high-confidence human interactome[312] (dotted line) and 1,000 randomized interactome networks (density), revealing significant enrichment for PPIs between LC genes relative to random expectation ($P < 10^{-3}$). **(E)** Size of the largest connected component (LCC) between LC genes in the high-confidence human interactome (dotted line) and 1,000 randomized interactome networks (density), revealing LC genes occupy a distinct region of the human interactome ($P < 10^{-3}$). **(F)** LC genes are prioritized by a disease gene prediction algorithm[263] ($P < 10^{-15}$, Kolmogorov– Smirnov test).
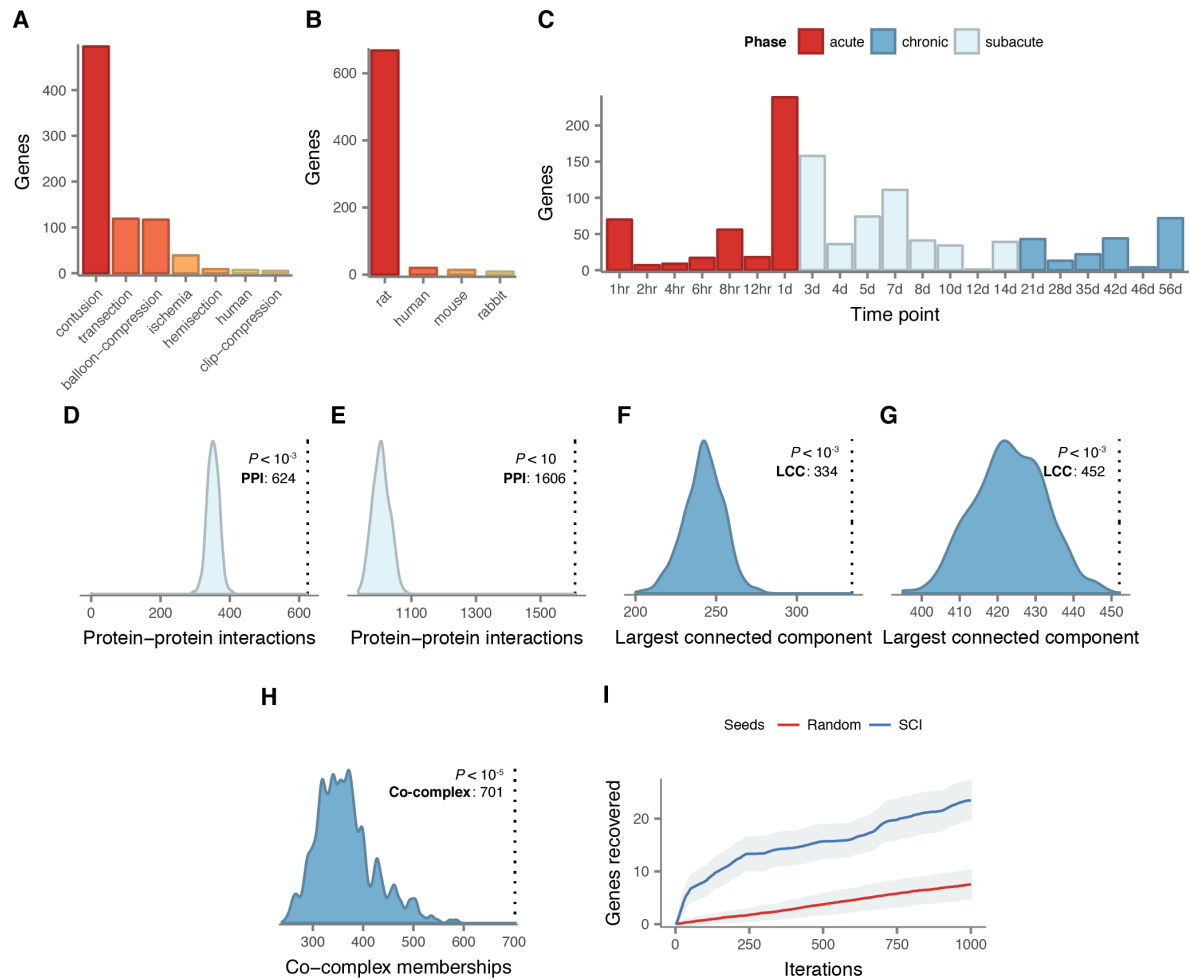
Figure 8.3: Validation of the complete set of genes implicated in the physiological response to SCI.

(A) Experimental models of SCI employed to associate literature-curated (LC) genes with response to SCI in the LC gene set. **(B)** Species in which LC genes were associated with response to SCI in the LC gene set. **(C)** Time points at which LC genes were associated with response to SCI in the LC gene set. **(D–E)** Number of binary **(D)** or co-complex **(E)** protein-protein interactions (PPIs) between LC genes observed in a second high-quality human interactome[304] (dotted line) and 1,000 randomized interactome networks (density), confirming

169

significant enrichment for PPIs between LC genes relative to random expectation ($P < 10^{-3}$) regardless of experimental method. **(F–G)** Size of the largest connected component (LCC) between LC genes in binary **(F)** or co-complex **(G)** high-quality human interactomes (dotted line) and 1,000 randomized interactome networks (density), revealing LC genes occupy a distinct region of the human interactome ($P < 10^{-3}$) regardless of experimental method. **(H)** Number of intra-complex co-memberships between LC genes (dotted line) and 1,000 randomized gene sets (density) observed in a global map of human protein complexes[316], revealing significant tendency for LC genes to participate in the same protein complex ($P < 10^{-3}$). **(I)** LC genes are prioritized by a disease gene prediction algorithm[263] in an interactome including orthologous interactions detected in model organisms.[304]

8.3.2 Validation of literature-curated spinal cord injury genes

We validated the biological relevance of our literature-curated (LC) SCI gene set using multiple lines of evidence. First, we established that LC genes were more likely to share common biological functions than random sets of genes, using annotations from the Gene Ontology.[262] Because functional annotations may be specific or broad, we confirmed that the enrichment held regardless of the number of genes to which each term was annotated **(Figure 8.2C)**. Next, we investigated the tendency for the protein products of LC genes to physically interact. Significant enrichment for protein- protein interactions (PPIs) between LC genes was observed relative to random expectation (**Figure 8.2D**, empirical $P < 10^{-3}$), and we additionally established that this enrichment was not a function of the experimental technique employed for interaction detection (all $P < 10^{-3}$, **Figure 8.3D–E**). Genes implicated in a variety of complex diseases by genome-

wide association studies (GWAS) have been found to form distinct modules of densely

interacting proteins within the human interactome.[263] We therefore evaluated whether this same

principle held for SCI by calculating the size of the largest connected component (LCC) between

LC genes, and found that LC genes collectively formed a significantly larger subnetwork than

random expectation (**Figure 8.2E**, empirical $P < 10^{-5}$), a finding that was again reproduced in

independent interaction datasets ($P < 10^{-5}$, **Figure 8.3F–G**). Literature-curated genes also

displayed a significant tendency to participate in the same protein complexes **(Figure 8.3H)**.

Finally, LC genes were preferentially recovered by a disease gene prediction algorithm when a

subset of them were randomly withheld, and the remainder used to prioritize additional disease

genes (**Figure 8.2F** and **Figure 8.3I**). Thus, LC genes represent a biologically relevant and

functionally coherent set of genes, which converge on a common protein interaction module

within the human interactome.

8.3.3   Gene coexpression network analysis of human spinal cord

Multiple lines of evidence support the functional coherence of the set of genes implicated in SCI

by small- scale experiments. However, these studies nonetheless have appreciable false positive

and false negative rates, and are limited by sociological and experimental biases. We therefore

sought to integrate knowledge from the SCI corpus within an unbiased, genome-wide

framework. We hypothesized that unsupervised gene coexpression network analysis of human

spinal cord would provide a powerful method to integrate these literature-curated genes in a

systems-level context, as this method has recently been powerfully applied to develop insights

into the etiologies of a number of neurological[258,264,265,266] or psychiatric diseases.[256,267,268]

We constructed gene coexpression networks in human spinal cord using RNA-seq data from 71 post-mortem human spinal cords from the Genotype-Tissue Expression project (GTEx).[269] We applied WGCNA[270] to group the human spinal cord transcriptome into 15 distinct modules of coexpressed genes. These modules represent networks of genes that share highly related patterns of expression in the human spinal cord. In order to establish the reproducibility of these spinal cord gene expression modules in an independent dataset, we constructed a second human spinal cord gene coexpression network from public microarray data, using established techniques to control for batch effects.[271,272] Module conservation was quantified using the $Z_{summary}$ statistic.[273] Despite the small sample size of our microarray-based human spinal cord coexpression network (n = 34), seven of 15 modules showed strong evidence of reproducibility ($Z_{summary} > 10$), with an additional two modules showing moderate evidence of reproducibility ($Z_{summary} > 5$) **(Figure 8.4A)**. Only two of 15 modules showed no evidence of reproducibility ($Z_{summary} < 2$).

Next, we investigated the evolutionary conservation of human spinal cord coexpression modules in mouse and rat, two of the most commonly used model organ- isms for studies of SCI pathophysiology. We compiled hundreds of microarray samples from mouse (n = 415) and rat (n = 268) spinal cords from the Gene Expression Omnibus, and constructed gene coexpression net- works for the mouse and rat spinal cords, again using established batch effect correction methods. Five modules showed strong evidence of evolutionary conservation ($Z_{summary} > 10$) in both species, while another four modules showed moderate evidence of conservation ($Z_{summary} > 5$) in at least one species, and only two modules showed no evidence of conservation in either species ($Z_{summary} < 2$) **(Figure 8.4A)**. Notably, the same five modules that showed the strongest evidence of reproducibility (M2, M3, M7, M8, and M12) also showed the strongest evidence of

172

conservation in rat and mouse. Thus, at least at the systems level, the architecture of the spinal cord transcriptome is substantially conserved between human and model organisms, supporting our approach of integrating data from small-scale studies of mammalian model organisms.

In order to integrate the LC gene set with the spinal cord coexpression network, we next tested for enrichment of LC genes within each module **(Figure 8.4B)**. Two modules, M3 and M7, were significantly enriched for LC genes (Fisher's exact test, Bonferroni-corrected $P = 3.8 \times 10^{-8}$ and 2.0×10^{-3}, respectively). These modules consist of 746 and 330 genes, respectively, and both are among the most reproducible and conserved in the spinal cord **(Figure 8.4A)**. We confirmed the robustness of the observed enrichment by randomly removing seed genes from the LC set, and by randomly adding false positive genes to the LC set. Both M3 and M7 remained significantly enriched for literature-curated genes despite the removal of a large number of seed genes, or the addition of a large number of random genes **(Figure 8.4C)**: M3 remained significantly enriched for literature-curated genes even after the removal of approximately 70% of genes from the seed set, compared to approximately 50% for M7. Moreover, M3 remained significantly enriched for seed genes even after the size of the literature-curated set was doubled by addition of random false positives.

Finally, to assess the relationships between modules, we constructed a module meta-network based on the eigengene of each module, defined as the first principal component of module expression **(Figure 8.4D)**.[274] In the resulting network, M3 and M7 clustered together, as would be expected given the strong correlation between their eigengenes (Spearman's $\rho = 0.54$, $P = 1.6 \times 10^{-6}$). These results suggest that the expression of these two modules in the spinal cord is highly correlated.

173

In summary, gene coexpression network analysis identified five highly conserved and reproducible modules, two of which are significantly and robustly enriched for literature-curated genes, and whose expression is highly correlated.
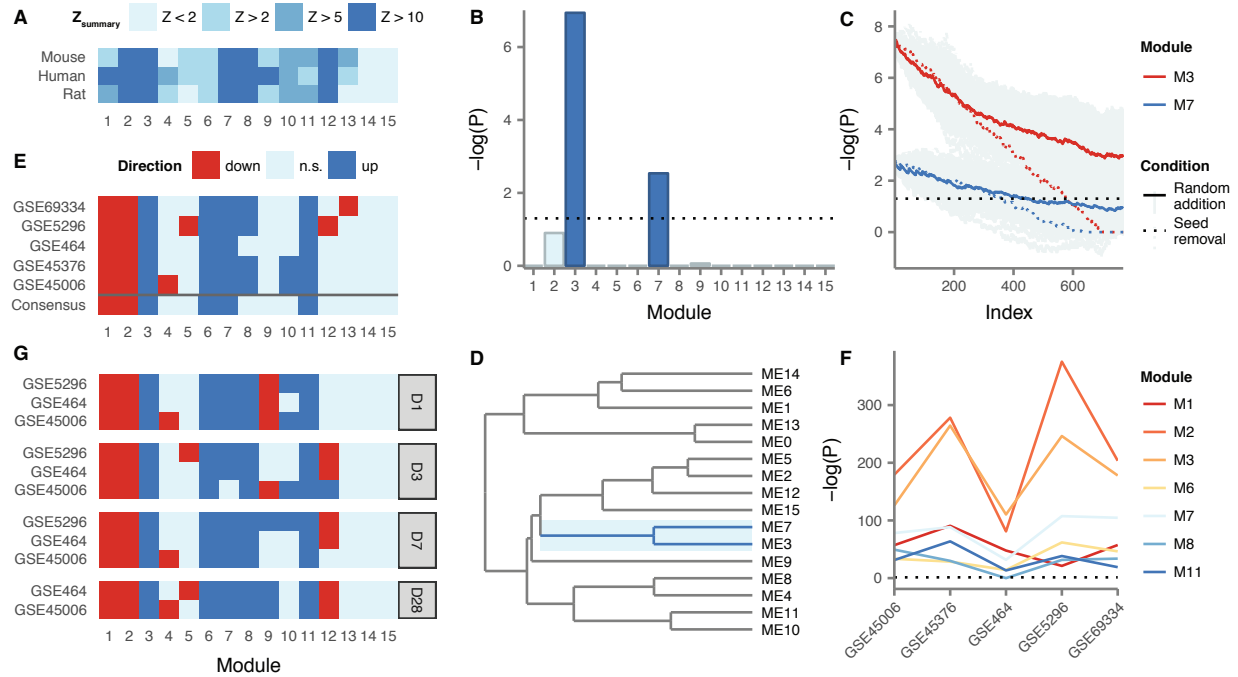
Figure 8.4: Gene coexpression modules in the human spinal cord and their differential expression in SCI.

(A) Reproducibility of human spinal cord modules in a microarray dataset and conservation in mouse and rat. **(B)** Enrichment of M3 and M7 for literature-curated SCI genes. **(C)** Robustness of M3 and M7 enrichment for literature-curated SCI genes. **(D)** Eigengene network for human spinal cord modules. **(E)** Differential expression of spinal cord modules following SCI in five datasets, and consensus. **(F)** Evidence for differential expression of six consensus modules and one majority module (M8). **(G)** Time-dependent expression of spinal cord modules at acute, subacute, and chronic time points following SCI.

174

8.3.4   Meta-analysis of coexpression network dysregulation in spinal cord injury

We next characterized the role of M3 and M7, as well as other highly conserved coexpression modules, in the pathophysiological response to SCI. We performed a meta-analysis of five mouse and rat transcriptomic studies of SCI within the context of our spinal cord coexpression network, in order to identify consensus changes in the spinal cord transcriptome at the module level in response to SCI **(Figure 8.4E).** This analysis identified M3, M6, M7, and M11 as consensus upregulated, and M1 and M2 as consensus downregulated, following SCI. One other module, M8, was upregulated following SCI in four of five datasets, while the remaining eight modules did not show robust evidence of differential expression. Among all seven modules, M2, M3, and M7 consistently showed the strongest evidence of differential expression (Fig. 3F, $P \leq 1.2 \times 10^{-78}$, 2.0×10^{-55}, and 1.7×10^{-14}, respectively). Notably, among these modules, M2, M3, M7 were strongly conserved and reproducible in mouse, rat, and human networks ($Z_{summary} > 10$), whereas M1, M6, and M11 displayed only moderate evidence of conservation ($2 < Z_{summary} < 10$), suggesting these modules may capture human- specific aspects of spinal cord transcriptome organization that are relevant in the response to SCI.

Because the pathophysiological processes underlying primary and secondary injury in SCI are incompletely understood, we additionally investigated the expression of spinal cord modules at acute, subacute, and chronic timepoints. Consensus module expression was remarkably consistent at all timepoints studied **(Figure 8.4G)**. However, analysis of the temporal regulation of spinal cord modules revealed consensus downregulation of M9 at the most acute time point after SCI, but consensus upregulation at a chronic time point. These results suggest

M9 may be specifically involved in the transition between acute and chronic physiological responses following SCI. Thus, by integrating gene coexpression network analysis with a meta-analysis of the SCI transcriptome, we reveal a consensus network signature associated with the response to SCI, and a network module specifically implicated in the transition from acute to chronic injury processes.

8.3.5   Functional characterization of consensus signature modules

We sought to characterize the biological significance of the modules implicated in the physiological response to SCI by integrating functional annotations from the Gene Ontology[262] and molecular signatures from MSigDB.[275] To visualize statistically overrepresented gene sets, we constructed enrichment maps for each consensus signature module[276] (**Figure 8.5A–B** and **Figures 8.6-8.9**). To appreciate the cell type- specificity of each module, we additionally conducted a meta-analysis of transcriptomic and proteomic profiles from the major cell types of the CNS **(Figure 8.5C)**.[277-279] M1 was an oligodendrocyte module, associated with axon ensheathment and myelination, whereas M2 was a neuronal module implicated in synaptic transmission. M3 was enriched for markers of microglia and vascular endothelial cells, and biological processes such as inflammatory response and response to wounding, while M7 was a microglial module enriched for annotations related to the immune response. M9 was enriched for astrocyte markers and terms such as oxidation-reduction process, as well as the term central nervous system development, which may be related to its upregulation at chronic time points following SCI. M6 and M11 were not significantly associated with any specific cell type, and were enriched for terms including cellular protein modification process and mitochondrial translation, respectively.

Figure 8.5: Biological characterization of spinal cord modules
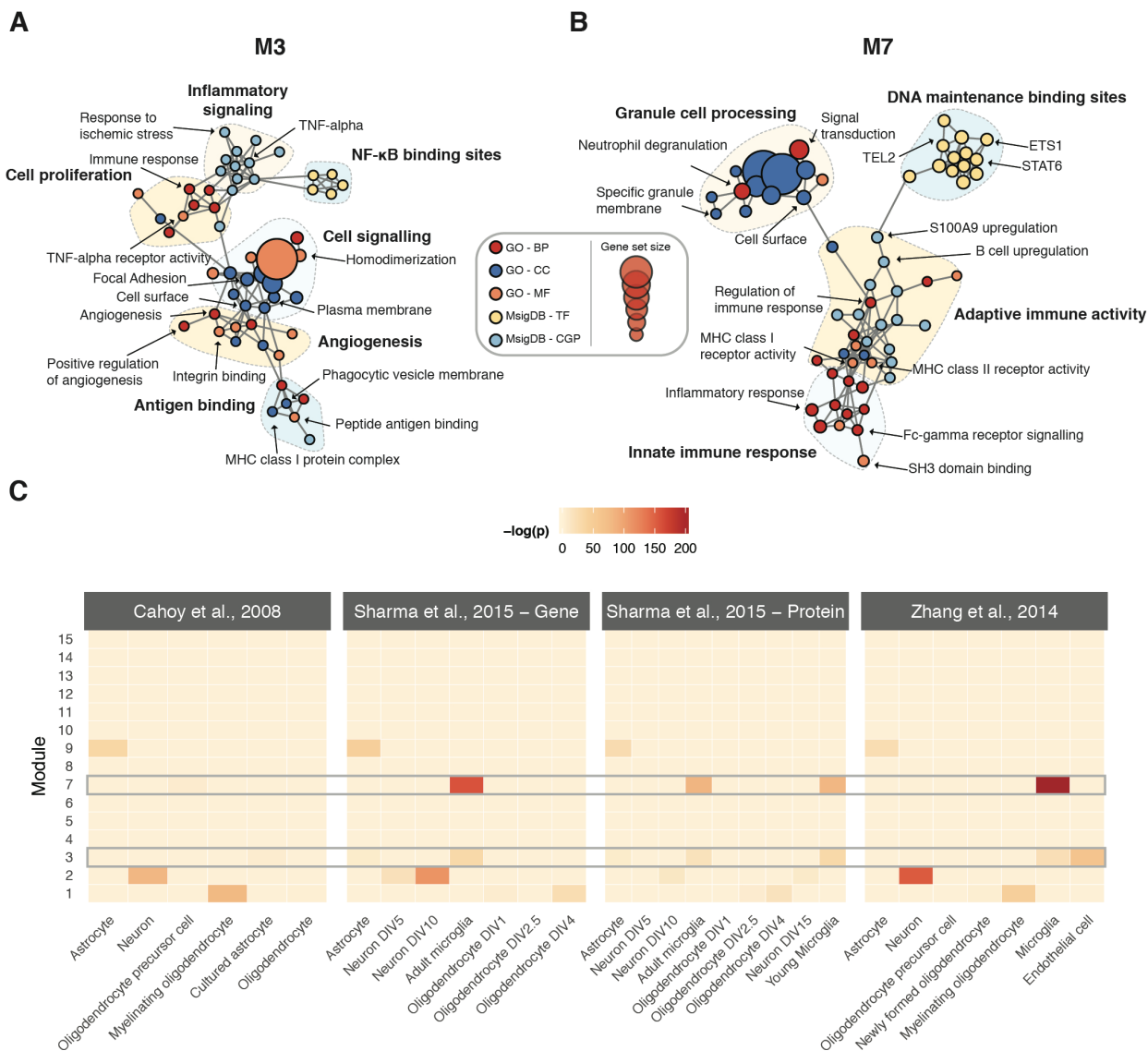
(A–B) Enrichment maps[276] for modules M3 and M7. **(C)** Meta-analysis of cell type-specific marker gene enrichment in human spinal cord modules at the transcriptomic and proteomic levels.
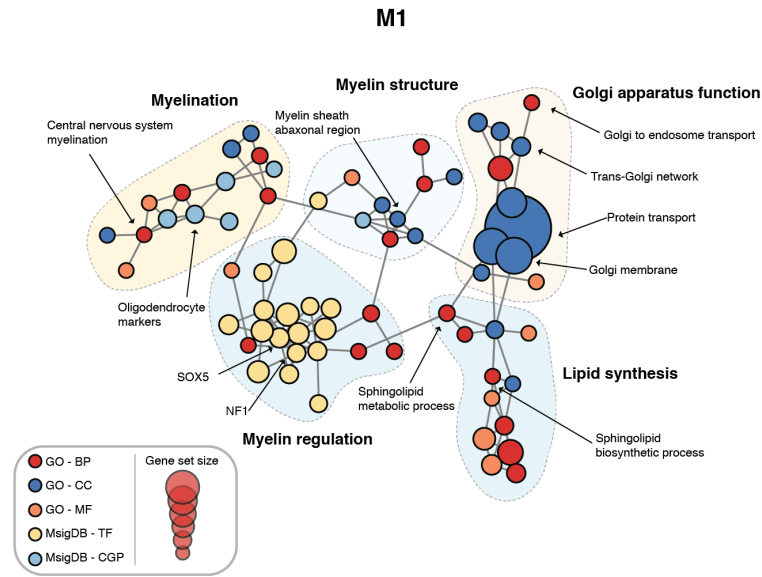
Figure 8.6: Enrichment map for human spinal cord module M1.
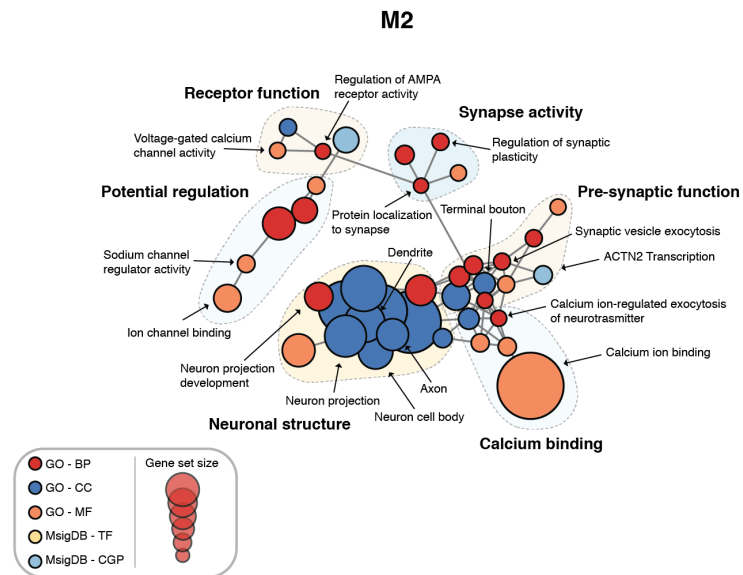
Figure 8.7: Enrichment map for human spinal cord module M2.
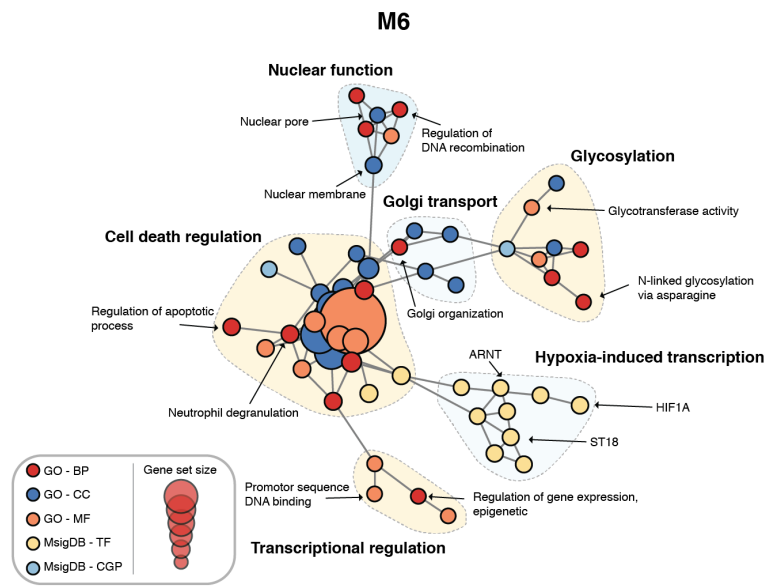
Figure 8.8: Enrichment map for human spinal cord module M6.
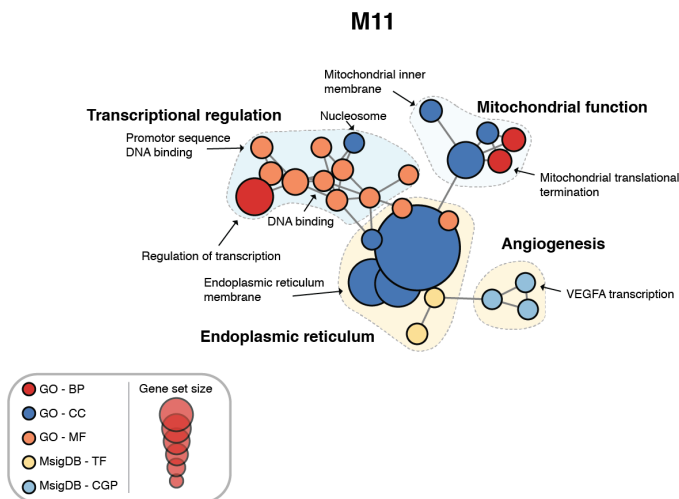
Figure 8.9: Enrichment map for human spinal cord module M11.

8.3.6   Network analysis of spinal cord injury severity and recovery

The finding that M3 is a highly conserved and reproducible gene coexpression module, with the most significant enrichment for literature-curated genes and strong evidence of upregulation following SCI, suggested that this module plays a key pathophysiological role in SCI. We focused on the role of M3 in SCI by investigating the relationship between M3 expression and two key clinical parameters in SCI: injury severity and recovery of sensory and motor function.

We first re-analyzed gene expression data from a mouse model of severity-dependent injury to identify relationships between consensus module expression and injury severity.[280,281] Strikingly, M3 was the sole module enriched for genes positively correlated to injury severity, whereas M1, M2, and M9 were enriched for genes anti-correlated to injury severity **(Figure 8.10A)**. We investigated this effect further by considering the correlations between module eigengenes, which provide a summary of the expression profile of each module, and injury severity. This analysis revealed that the M3 eigengene was the most strongly correlated with injury severity (Spearman's $\rho = 0.65$, $P = 1.6 \times 10^{-19}$), with a clear separation in M3 expression between the mild, severe, and sham injury groups at 7 days post-injury **(Figure 8.10E)**.

In order to validate the severity-dependent upregulation of M3 following SCI, we conducted a prospective experimental SCI study, using the field standard contusion injury model at the T10 segment, and performed RNA sequencing of the spinal cord parenchyma in rats subjected to moderate, severe, or sham injuries ($n = 5$ per group). Our RNA-seq data reproduced the consensus network signature derived from our meta-analysis of microarray datasets, emphasizing the robustness of this systems-level characterization of SCI pathophysiology **(Figure 8.10F)**. In addition, we confirmed the significant association between injury severity and

180

the M3 eigengene **(Figure 8.10E**; Spearman's $\rho = 0.94$, $P = 4.2 \times 10^{-7}$). Thus, insights into the network-level organization of the transcriptome in SCI derived from a meta-analysis of publicly available data replicate in an independently collected dataset.

Together, these results emphasized the severity- dependent upregulation of M3 following SCI, and suggested that the expression of a gene or combination of genes that accurately summarize the transcriptional status of M3 has the potential to serve as an objective biomarker of SCI severity. To evaluate the potential of such an indicator as a biomarker of injury severity, we focused on the hub genes of M3. These genes are the most central and interconnected within the module, based on their correlation to the module eigengene, and are highly enriched for functionally relevant genes such as drivers of disease pathophysiology[256] or therapeutic targets.[282] Consistent with these findings, the hubness of M3 genes (that is, their correlation to the M3 eigengene in human spinal cord) was significantly associated with their predictive power as a biomarker of injury severity (**Figure 8.10D**; Spearman's $\rho = 0.23$, $P = 3.9 \times 10^{-7}$). Among M3 hubs, six genes stratified rats by SCI severity with an accuracy greater than 90%, including ANXA1, COLGALT1, IFNGR2, SHC1, SOD2, and TBC1D2B **(Figure 8.10G)**. Remarkably, expression levels of ANXA1 (annexin A1) stratified moderately and severely injured rats with perfect accuracy **(Figure 8.10I)**. Annexin A1 has previously been associated with SCI by three small-scale studies, each employing divergent model organisms, spinal cord levels, and injury models, emphasizing the robustness of the association between SCI and annexin upregulation.[283-285]

While our integrative analyses of public and newly acquired transcriptomic data established a strong relationship between M3 expression and SCI severity, post-transcriptional

regulation can result in marked differences between gene and protein expression levels, particularly in complex tissues such as those of the CNS.[278,286] To further explore the potential of M3 hubs as biomarkers of SCI severity, we therefore performed quantitative proteomic profiling of the same rat spinal cords. We first sought to establish that the overall structure of the spinal cord coexpression network was conserved between the transcriptomic and proteomic levels. Despite having limited power to detect module preservation due to the small size of our proteomic sample (n = 15), both M3 and M7 displayed highly significant evidence of reproducibility between the RNA and protein levels (**Figure 8.10C**; $Z_{summary}$ = 6.8 and 7.3, respectively). Furthermore, we identified substantial overall agreement between proteomic data and the consensus network signature derived from transcriptomic meta-analysis, further validating the robustness of our systems-level portrait of SCI pathophysiology **(Figure 8.10F)**. Finally, we confirmed the severity-dependent upregulation of both the M3 eigengene and annexin A1 in particular (**Figure 8.10H** and **Figure 8.10J**), finding that AnxA1 protein levels stratified both moderate and severe in- juries with an accuracy of 93%. Thus, systems-level insights into SCI pathophysiology derived from integrative transcriptomic analyses extend to the proteomic level and nominate quantitative biomarkers of SCI severity.

Given the strong relationship between injury severity and M3 expression, we hypothesized that targeting the transcriptional profile of this module could represent a viable strategy for development of novel therapies for SCI. To explore this hypothesis, we analyzed gene expression data from a recent trial of a neurotrophic factor, neurotrophin-3 (NT-3), which promoted sensory and motor recovery after SCI.[287,288] Remarkably, all six consensus modules derived from our meta-analysis, including M3, were differentially expressed at the lesion site in

the opposite direction **(Figure 8.10F)** in rats treated with NT-3. Intriguingly, the sole other

differentially expressed module was M9, which we previously observed to exhibit a strongly

time-dependent expression profile, and which was enriched for genes associated with

neurogenesis. In rats treated with NT-3, known for its role in neuronal differentiation, axonal

growth, and chemotropic guidance,[289,290] M9 was strongly upregulated at the lesion site relative

to the experimental control ($P = 7.4 \times 10^{-6}$). Moreover, the M3 eigengene was significantly

downregulated in NT- 3-treated rats relative to controls (**Figure 8.10K**; one-tailed Wilcoxon

rank-sum test, $P = 2.0 \times 10^{-3}$). These results indicate that reversal of the transcriptome changes

observed in response to SCI is associated with functional recovery in a rat model, and highlight

M3 expression as a predictor of functional recovery.
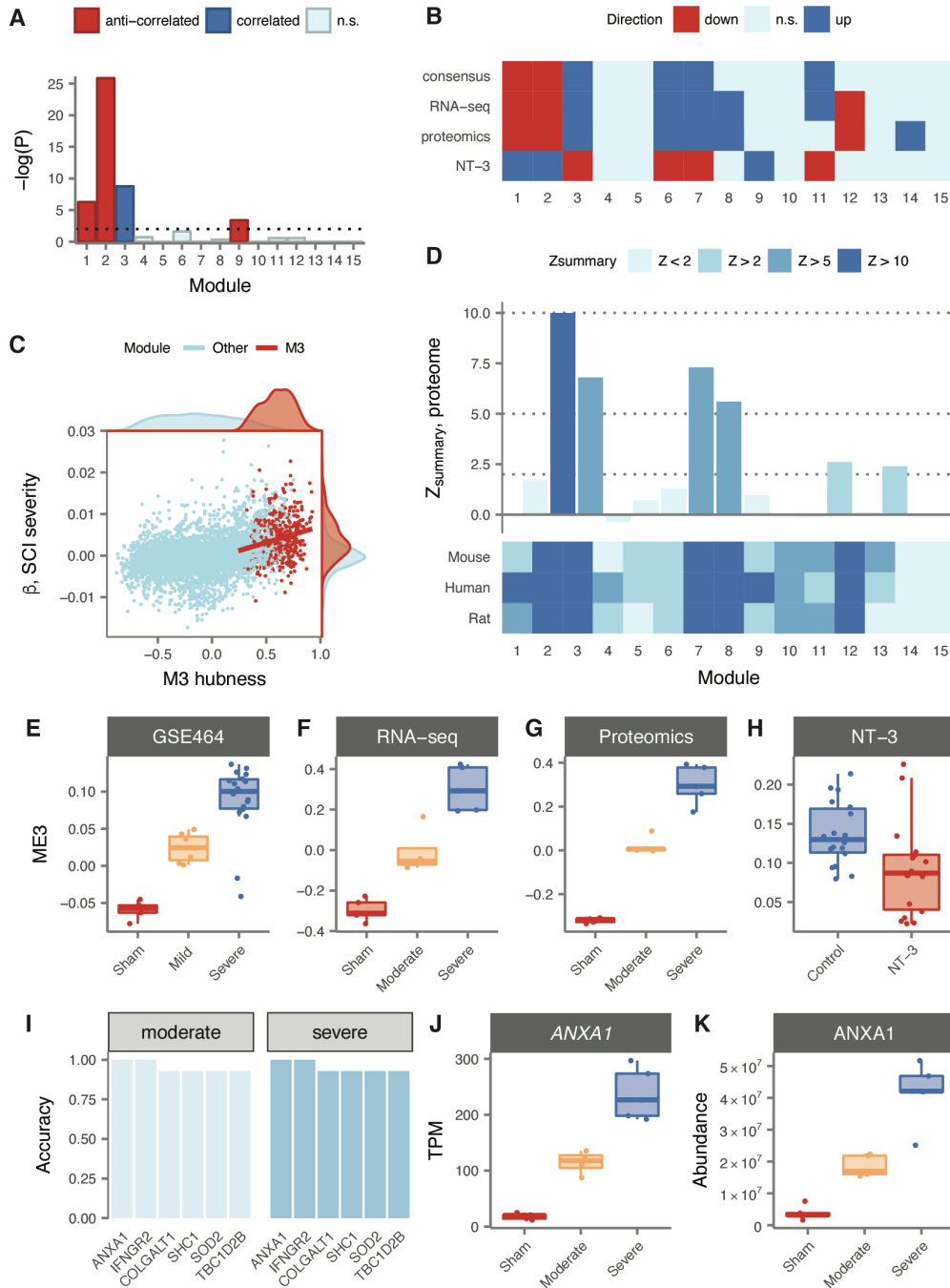
Figure 8.10: Relationship of spinal cord modules to injury severity and functional recovery.

(A) Enrichment of spinal cord modules for genes correlated or anticorrelated to injury severity in a mouse model. **(B)** Consensus network signature of SCI pathophysiology, validation in independent transcriptomic and proteomic datasets, and reversal in functional recovery. **(C)**

Gene expression correlation to M3 eigengene predicts association to SCI severity. **(D)**
Reproducibility and evolutionary conservation of spinal cord modules and their preservation at
the proteomic level. **(E–F)** Relationship between M3 eigengene and injury severity at 7 days
post-injury in a mouse model **(E)**, and in our own RNA-seq **(F)** and proteomics **(G)** datasets.
(H) Downregulation of the M3 eigengene following treatment with NT-3, a neurotrophic agent
that promotes functional recovery in acute SCI. **(I)** Six genes classify moderate and severe
injuries in transcriptomic data with 90% or greater accuracy. **(J–K)** Gene expression and protein
abundance of annexin A1 in sham, moderate, and severe SCI.

8.4 Discussion

The fragmentary understanding of the coordinated pathophysiological processes activated in the
human spinal cord by SCI represents a central obstacle to the development of therapies capable
of influencing neurological outcomes. In this study, we developed an integrated, systems-level
approach to understand the molecular mechanisms underlying SCI pathophysiology. We
leveraged large-scale RNA-seq data from healthy subjects to reveal gene regulatory relationships
in the human spinal cord. By integrating multiple gene expression datasets from experimental
models of SCI, we identified gene subnetworks implicated by consensus in the
pathophysiological response to SCI, and reproduced these signatures at both the transcriptomic
and proteomic levels in an animal trial. The observation that seven different gene modules were
robustly associated with the response to SCI, either by consensus differential regulation (M1,
M2, M3, M7, M11) or by a strongly time-dependent course of expression (M9), is consistent
with the notion that the pathophysiology of SCI is highly complex.[97] Our results provide a
framework to understand the diverse, coordinated processes in the spinal cord following SCI.

185

In order to prioritize gene subnetworks, we conducted a systematic analysis of the SCI literature, and integrated genes implicated in the SCI response by small-scale experiments into our network analysis. This approach is conceptually similar to the integration of GWAS or *de novo* mutation data into gene regulatory networks, as has previously been described for a number of diseases [e.g., [265,266,291-293]]. The relatively high false-positive rates of small-scale experiments, as well as their appreciable false-negative rates, are mitigated by unbiased integration of data from small-scale experiments into a genome-wide framework. More generally, our experimental design provides an approach to extend gene coexpression network analysis to acquired and traumatic conditions, using samples from healthy tissues.

A major challenge to the translation of preclinical therapies for acute SCI is the use of standardized neurological assessments to enroll and stratify patients in large clinical trials.[211] In this context, objective biomarkers capable of accurately stratifying injury severity have the potential to facilitate translation by accelerating the pace of patient enrolment.[255,294] We found that M3 was the sole module enriched for genes whose expression correlated with injury severity in a mouse model, and that its eigengene was likewise most strongly associated with severity. We subsequently reproduced this correlation in our own transcriptomic and proteomic datasets. The severity-dependent upregulation of M3 following SCI, and its preservation at the proteomic level, suggests that its expression has the potential to stratify injury severity in a clinical context. Furthermore, this expression pattern was reversed with administration of NT-3, a treatment that promotes motor and sensory recovery.[288] These findings have several implications for the discovery and translation of new SCI therapies. The identification of drugs that reverse transcriptional changes associated with SCI has the potential to provide a new strategy for

preclinical lead discovery. Moreover, analyzing the effect of a desired treatment on M3 expression, or our consensus network signature more generally, may rep- resent an effective technique to validate the efficacy of preclinical therapies.

Among M3 hub genes, which reflect the expression of the entire module, we found that both the RNA and protein levels of ANXA1 (annexin A1) demonstrated a strong ability to discriminate between injuries of different severities. Annexin A1 is a member of the annexin superfamily of calcium dependent phospholipid-binding proteins, and plays a role in mediating anti-inflammatory effects through inhibition of phospholipase A2 activity,[295,296] decreasing leukocyte activation[297,298] and reducing expression of pro-inflammatory cytokines.[299,300] ANXA1 is primarily expressed in microglia, where it regulates the selective removal of apoptotic neurons.[300] Correspondingly, ANXA1 knockout mice are characterized by exaggerated inflammatory responses, as well as a blunted response to the anti-inflammatory effects of glucocorticoids.[301] ANXA1 is upregulated in multiple diseases characterized by aberrant neuroinflammation.[295,300,302] Importantly, multiple studies have previously reported upregulation of ANXA1 in SCI,[283-285] with peak expression at 7 days post injury,[303] and upregulation of ANXA1 is associated with functional recovery after SCI.[296] Notably, ANXA1 was previously identified as a biomarker of SCI severity in a study that included both rat and human samples.[284] Our independent finding here that ANXA1 is a strong candidate for a severity-dependent biomarker of SCI suggests that our systems-level approach can drive rational selection of novel potential biomarkers. However, although we observed substantial conservation of M3 between human and rat at the systems level, this finding does not preclude the possibility that individual genes diverge in their expression following acute SCI between human and rodents. Further

studies in humans are therefore needed to conclusively establish the validity of ANXA1 as a biomarker of SCI severity.

8.5   Conclusions

In summary, our systems biology approach identifies evolutionarily conserved and reproducible gene subnetworks with robust evidence for differential regulation following SCI, and provides a genome-wide view of the pathophysiological processes triggered by SCI. Our findings provide new, data-driven strategies to identify and translate novel therapies for SCI.

8.6   Transition to clinical practice

The work described thus far in this thesis provides a framework to test potential neuroprotective therapies aimed at reducing autonomic dysfunction. I have established a model that replicates chronic autonomic consequences of SCI, and show that this model is amenable to neuroprotection. Our systems biology approach provides additional and necessary mechanistic insight to identify and validate novel biomarkers of injury severity, as well as to repurpose known and clinically approved drugs. However, the road to clinical translation is long. Therefore, while we improve our methods for rationale drug repurposing and examine these potential therapies in pre-clinical models, I next aimed to examine an immediately implementable neuroprotective strategy in humans with acute SCI. The final chapter of this thesis **(Chapter 9)** will examine how combatting neurogenic shock by optimizing hemodynamic management can improve neurologic recovery in more than 90 individuals with acute traumatic SCI.

Chapter 9: Spinal cord perfusion pressure predicts neurological recovery in acute spinal cord injury[7]

9.1 Introduction

The current clinical practice guidelines for hemodynamic management of acute spinal cord injury (SCI) recommend that the mean arterial pressure be maintained between 85-90 mmHg for the first seven days post-injury, with the use of vasopressors if necessary.[332–335] A potentially important limitation with the present approach is the exclusive focus on mean arterial pressure (MAP), and not the spinal cord perfusion pressure (SCPP). In traumatic brain injury, hemodynamic management includes monitoring of intracranial pressure to calculate and act upon cerebral perfusion pressure.[336–338]

Recent groundbreaking work by Papadopoulos and colleagues has shown that pressure catheters placed subdurally at the site of injury predict neurologic outcome at 9-12 months post-injury.[339] We too have also been monitoring spinal cord perfusion pressure but with standard lumbar intrathecal catheters. We have reported on the use of lumbar intrathecal catheters to drain

---

cerebrospinal fluid in acute spinal cord injury patients,[340] but the utility of monitoring cerebrospinal fluid pressure in the lumbar spine (distal to injury) as it relates to neurological recovery has not yet been evaluated.

The aim of the present study was to determine the independent relationship of SCPP (measured with a lumbar intrathecal catheter) to neurological outcome, and to determine a clinically useful nadir below which patients are at risk for poor neurological recovery. We hypothesized that those individuals exposed to low SCPP during the first five-days post injury would be more likely to have poor neurological recovery. Additionally, we aimed to answer the critical question: *what is the ideal hemodynamic management strategy to promote neurological improvement?*

9.2   Methods

9.2.1   Clinical trial enrollment

Patient recruitment began at our single institution in March 2006 and was expanded into a multi-center prospective observational study in September 2012 with sites in Halifax, London, Ontario, and Montreal. Individuals sustaining an acute SCI were enrolled if they met the following inclusion criteria: 1) American Spinal Injury Association Impairment Scale (AIS) grade A, B, (motor-complete) or C (motor-incomplete) spinal cord injury upon presentation; 2) spinal bony injury between C1 and L1 inclusive; 3) the ability to have a lumbar catheter inserted within 48 h of injury; and 4) the ability to be assessed clinically for a valid, reliable neurologic examination. Exclusion criteria included: concomitant head injuries, concomitant major trauma to the chest, pelvis, or extremities that required invasive intervention (e.g., internal or external fixation), or were too sedated or intoxicated to provide a valid neurologic examination.

9.2.2 Standard protocol approvals, registrations, and patient consents

The clinical trial protocol for conducting this prospective observational study at this single institution was approved by our local institutional review board (#H10-01091); a subsequent multi-center extension of this study is registered with ClinicalTrials.gov (NCT01279811). Patient consent was obtained according to the declaration of Helsinki. All methodology and results are presented according to the STROBE statement.[341]

9.2.3 Hemodynamic monitoring

For cerebrospinal fluid (CSF) pressure monitoring, an intrathecal catheter (PERIFIX[BL[1]® FX 19 gauge [25/CS], 100 cm, SPRINGWND, radiopaque open tip epidural catheter [Braun Mnf #333514], or an EDM, barium impregnated, 80 cm, 1.5 mm O.D./0.7 mm I.D., closed tip lumbar catheter [Medtronic REF 46914] was inserted in the lumbar spine at L2/3 or L3/4. The catheter was advanced 15–20 cm from the entry point on the skin surface, secured with a sterile dressing, and then brought out over the shoulder and secured with Mepore® tape along its exposed length. The intrathecal catheter was then connected to a Duet® External Drainage and Monitoring System (Medtronic REF #46914). MAP was monitored via a standard arterial catheter placed during initial management. Both the CSFP and MAP pressure transducers were connected to a General Electric Carescape® patient monitor (B850) for monitoring of CSFP and arterial waveforms and pressures. These monitors are tested and calibrated annually to confirm accuracy to within +/- 2 mmHg. Both the CSFP and arterial pressure transducers were zeroed to atmosphere and leveled at the phlebostatic axis. The CSF catheters were kept in place for up to 120 h.[340] Digital data from patient monitors were sampled continuously and also manually

recorded hourly. SCPP was calculated as the difference between MAP and CSFP, and was therefore not provided to clinicians in real time. MAP was targeted at 80 to 85 mmHg during the first 120 hours after enrollment. Initial support of the MAP was by volume augmentation (i.e. crystalloid, colloid, or whole blood as required) followed by the initiation of vasopressor support with norepinephrine, phenylephrine, dopamine or, in a few instances, a combination of two of these vasopressors. The decision of how to support the target MAP was at the discretion of the attending Anesthesiologist or Intensivist. CSFP was not manipulated.

9.2.4   Neurological outcome assessment

Upon presentation, all patients underwent formal neurological testing according to the International Standards for Neurological Classification of SCI (ISNCSCI) and were assigned a baseline AIS grade.[20] All baseline neurological examinations and subsequent neurological monitoring were conducted by clinical staff specifically trained to conduct the ISNCSCI examination. The ISNCSCI examination was repeated at six-months post-injury, at which point the majority of neurologic recovery has occurred.[211] AIS conversion was defined as a change in one AIS grade.

9.2.5   Statistical analysis

We used the statistical computing software R (R Core Team, 2012) to examine differences in hemodynamic patterns between individuals with AIS A/B versus AIS C using independent samples t-tests. Next, a case-control design was implemented, where participants were stratified according to their AIS conversion status. For logistic regression models, conversion status was used as the outcome variable, with MAP, CSFP, or SCPP inserted as independent fixed factors.

Multiple observations for each participant were corrected through clustering. To provide clinically relevant management guidelines, we systematically examined the relative risk of conversion by determining exposure to different hemodynamic cut-offs. To visualize the combined contributions of MAP and CSFP to conversion risk we used additive relative risk modeling (RR_1+RR_2-1). We performed univariate regression of the number of times an individual deviated outside the set cut-off. We examined differences in the number of times individuals deviated outside of each cut-off between those that AIS converted versus those that did not using independent samples t-tests. Univariate Kaplan-Meier models and Cox proportional hazard models were used to assess risk for conversion, and also to assess risk for total motor score improvement ≥ 6.

To determine the ideal hemodynamic management strategy to promote neurological improvement we used relative risk iterations to determine the MAP, CSFP, and SCPP where the relative risk of motor score improvement was 1 (i.e., a "transition point" where the likelihood of neurologic improvement and deterioration were equal), and examined the linear relationship with motor score improvement. The relative contributions of MAP and CSFP were visualized using additive relative risk modelling ($RR1+RR2-1$). We then tested the hypothesis that the percent of time an individual spends within the 'ideal' hemodynamic target is linearly related to motor improvement. For each hemodynamic parameter we tested five management targets. The percentage of time spent within each of these targets was determined by the number of data-points at or above the target, with a 5% error to adjust for minor drops or elevations. The linear relationship between time spent within the target range and motor score recovery was then determined. Lastly, using American Spinal Injury Association Impairment Scale (AIS) conversion (defined as improvement by one grade) as a binary outcome, we determined whether

individuals who stayed within the target range displayed significantly greater neurological improvement versus those that did not stay in the target range. We tested this using Fisher's exact test. Data are presented as -log10(p) of the Fisher's exact test p-value. For all comparisons, an alpha of 0.05 was defined.

9.3   Results

9.3.1   Participants

102 individuals were monitored following acute spinal cord injury. Two individuals died in hospital. Eight individuals were lost to follow-up. There were 72 males and 20 females. Cervical injuries were most common (n= 55) followed by thoracic (n= 28), and lumbar (n=9). Average time to decompression was 20±11 hours from the time of injury. Further demographics are reported in **Table 9.1**. No infectious or other complications resulted from the lumbar catheter placement.

Table 9.1: Patient descriptive data stratified by initial AIS grade

Item	Total Sample (n=92)	AIS A/B (n=75)	AIS C(n=17)
Age	43 ± 16	40 ± 15	53 ± 15
Level of Injury			
Cervical	54	43	12
Thoracic	28	24	4
Lumbar	9	8	1
UEMS	31 ± 18	32 ± 19	26 ± 17
LEMS	3.1 ± 7.5	0.73 ± 2.5	14 ± 12.2**
TMS	34 ± 20	32 ± 19	39 ± 20
TTD	20 ± 11	20 ± 11	22 ± 10
Hemodynamics			
MAP	85 ± 6	84 ± 6	89 ± 6 *
CSFP	16 ± 5	16 ± 5	14 ± 3*
SCPP	69 ± 9	68 ± 8	75 ± 8*

9.3.2 Hemodynamics during the first five-days post-injury differs by initial injury severity

During the first five-days post-injury we found MAP ($\beta=0.038$ mmHg) and SCPP ($\beta= 0.067$ mmHg) increased and CSFP ($\beta=-0.029$ mmHg) decreased with time (hour) post-injury ($p< 0.001$ for all; **Figure 9.1**). Individuals with AIS C on initial designation had significantly higher MAP ($\beta = 4.0$mmHg, $p=0.028$) and SCPP ($\beta=6.4$mmHg, $p = 0.008$) than individuals with AIS A and B, while CSFP was significantly lower in AIS C ($p = 0.031$).
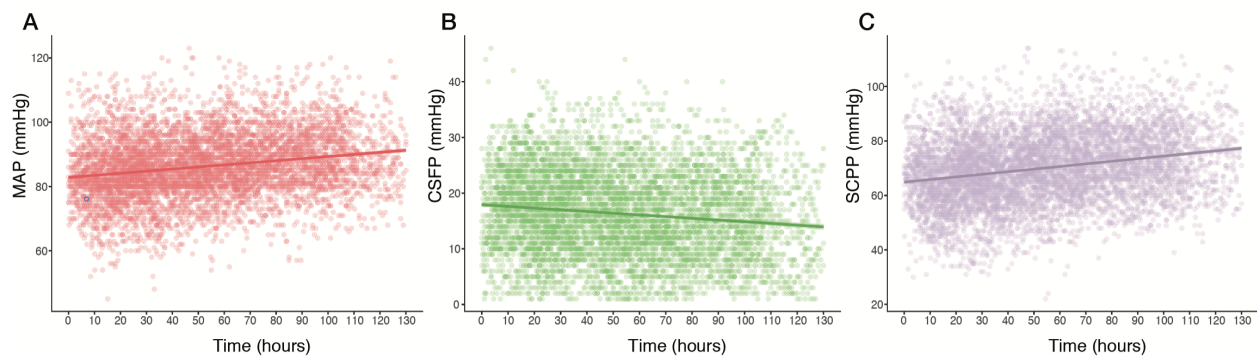
Figure 9.1: Raw hemodynamic data

Data were collected on an hourly basis for each participant and plotted over time post-injury (dots). Fitted linear regression lines represent the association between measurement and time for

all individuals. *Abbreviations*: MAP: mean arterial pressure, CSFP: cerebrospinal fluid pressure, SCPP: spinal cord perfusion pressure.

9.3.3 Six-month follow-up neurologic recovery data

From baseline to follow-up there was a significant improvement in upper extremity motor score (30.68 ± 18.17 vs. 36.68 ± 15.25), lower extremity motor score (3.09 ± 7.51 vs. 13.46 ± 18.54), and total motor score (33.79 ± 19.57 vs. 49.61 ± 26.70) across all participants (all $p<1.25e-09$). Conversion between AIS grades from baseline to follow-up is reported in **Table 9.2.** At the 6-month follow-up, 43 individuals converted AIS grade in a positive direction, and none converted AIS grade in a negative direction **(Table 9.2)**. We found no significant association between time to decompression and AIS conversion at 6 months ($p=0.16$).

Table 9.2: Patient AIS grades at baseline and follow-up

	Follow-up AIS			
Baseline AIS	AIS A	AIS B	AIS C	AIS D
AIS A	41	8	6	2
AIS B	0	7	4	7
AIS C	0	0	1	16

Abbreviations: AIS: American Spinal Injuries Association
Impairment Scale

9.3.4 Spinal cord perfusion pressure is positively associated with increased odds of conversion

We found that both MAP (OR=1.037, CI=1.011-1.063, p=0.004) and CSFP (OR=0.958, CI=0.923-0.995, p=0.027) during the first five-days post-injury were independently predictive of a positive conversion at 6 months. In an independent logistic regression, we found SCPP was

predictive of positive conversion at 6 months, whereby for every 5 mmHg higher spinal cord perfusion pressure the odds of converting were increased by 19.5% (OR=1.039, CI=1.011-1.063, p=0.004) Further, we found similar results when examining motor score improvement, instead of conversion status (MAP: OR=1.038, CI=1.013-1.064, p=0.003; CSFP: OR=0.956, CI=0.921-0.992, p=0.002; SCPP: OR=1.039, CI=1.016-1.063, p=0.001).

9.3.5 Systematic relative risk permutations reveal optimal hemodynamic management parameters

By systematically altering hemodynamic cut-offs we show that relative risk for not improving an AIS grade (i.e., having poor neurological recovery) continually increases as individuals are exposed to lower MAP, higher CSFP, and lower SCPP **(Figure 9.2).** Next, using additive relative risk calculations we visualized the risk of exposure to both low MAP and high CSFP **(Figure 9.3).** Using this, we suggest that SCPP should be maintained above 50 mmHg through a combination of MAP and CSFP manipulations **(Figure 9.3)**. To validate our suggested monitoring strategy, we performed univariate linear regression and demonstrate that the number of times SCPP drops below 50 mmHg is a predictor of conversion status (OR: 0.9, CI: 0.81-0.98, p=0.031; **Table 9.1**), while a MAP or CSFP cut-off did not predict any clinical outcome (all p > 0.32). Moreover, the number of times individuals drop below SCPP 50 mmHg was higher in those that did not convert (p = 0.023; **Figure 9.4)**, while this effect was not found for a MAP cut-off of 70 mmHg (all p > 0.34).
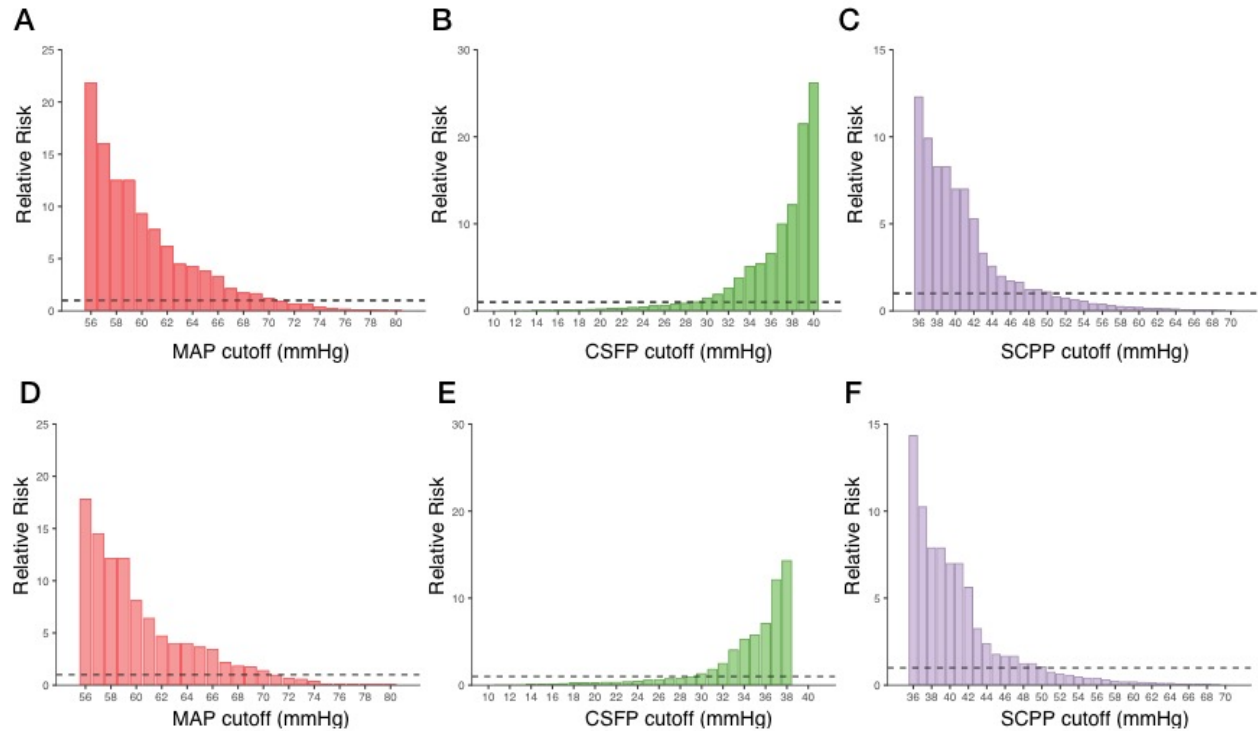
Figure 9.2: Relative risk of not positively converting AIS grade

Relative risk of not positively converting AIS grade from baseline to 6 months increases with poor hemodynamic management during the first 5 days post-injury. Using systematic iterative relative risk calculations we demonstrate that an individual exposed to low mean arterial pressure (**panel A**, MAP), high cerebrospinal fluid pressure (**panel B**, CSFP), or low spinal cord perfusion pressure (**panel C**, SCPP) increases their risk of poor neurological outcome, and that this risk increases with more dramatic changes in hemodynamics. Dotted line represents a relative risk of 1. Thresholds for crossing a relative risk of 1 for MAP, CSFP, and SCPP were: 70 mmHg, 29 mmHg, and 50 mmHg, respectively. This finding was consistent in a sub-analysis where only individuals with a baseline AIS score of "A" were considered (n = 57; **panels D-F**).

One factor to consider is whether this relationship is dependent upon baseline injury severity. We found that the relationships between SCPP and outcome were identical when considering only the AIS A patients (**Figure 9.4D-F**). Lastly, by setting an exposure cut-off at 50 mmHg for SCPP we observed a significant likelihood ratio test for both conversion and improvement in total motor score under a Cox hazard ratio model in both our complete sample and our AIS A individuals **(Figure 9.5)**. Conversely, for an exposure cut-off of 70 mmHg for MAP, the hazard ratio models were not significant for conversion status or motor score improvement, in both our full sample and in a sub-analysis of AIS A only individuals (all p > 0.22).
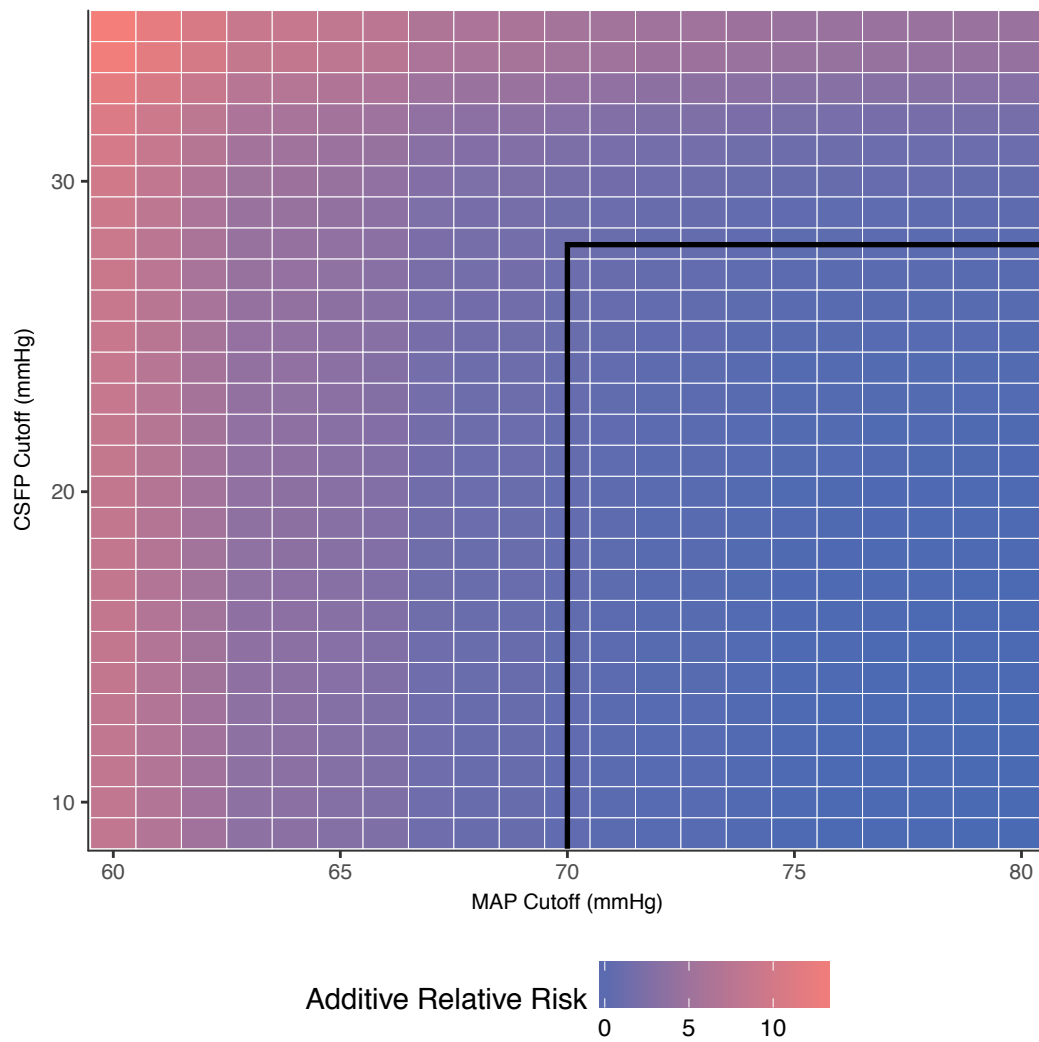
Figure 9.3: Additive relative risk matrix reveals optimal hemodynamic management range. By combining our relative risk data from mean arterial pressure (MAP) and cerebrospinal fluid pressure (CSFP) we determine that MAP should be maintained above 70 mmHg and CSFP below 29 mmHg (where blue is a low relative risk of poor conversion). The black line represents the ideal clinical management scenario.

All participants (n=92)

AIS A participants (n=57)
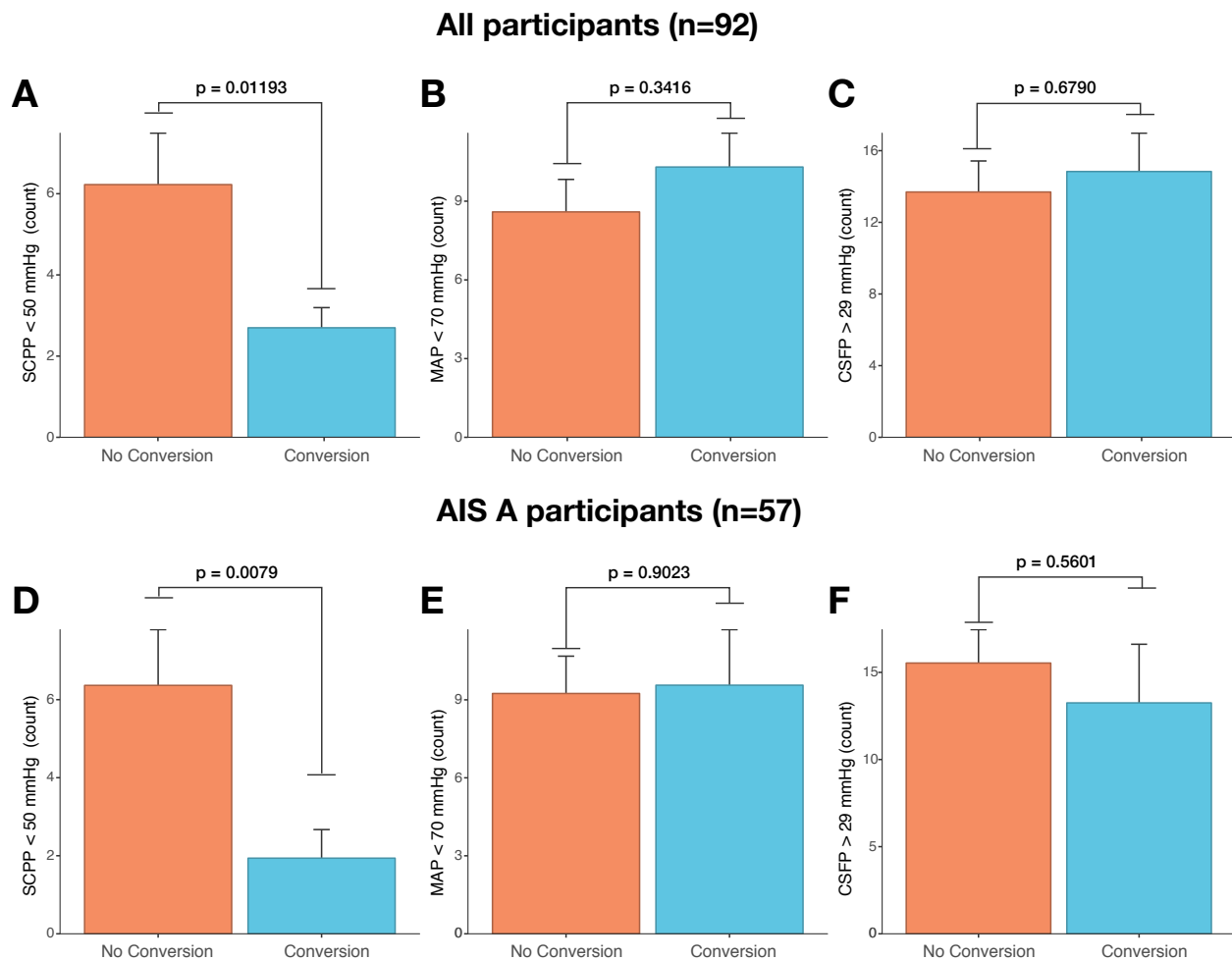
Figure 9.4: Frequency of deviations outside cut-offs between conversion status.

The number of times (count) individuals drop below set cut-offs is significantly different between those that do not convert (orange) and those that convert (blue). This effect was observed only for spinal cord perfusion pressure (**panel A**, SCPP), but not for either mean arterial pressure (**panel B**, MAP) or cerebrospinal fluid pressure cut-offs (**panel C**, CSFP). This finding was consistent in a sub-analysis where only individuals with a baseline AIS score of "A" were considered (n = 57; **panels D-F**). Bar plots represent the mean and error bars the standard error. Note: CSFP cut-offs represent the number of times an individual exceeds the pressure value. Cut-offs were established based on relative risk thresholds obtained from **Figure 3.2**.

201
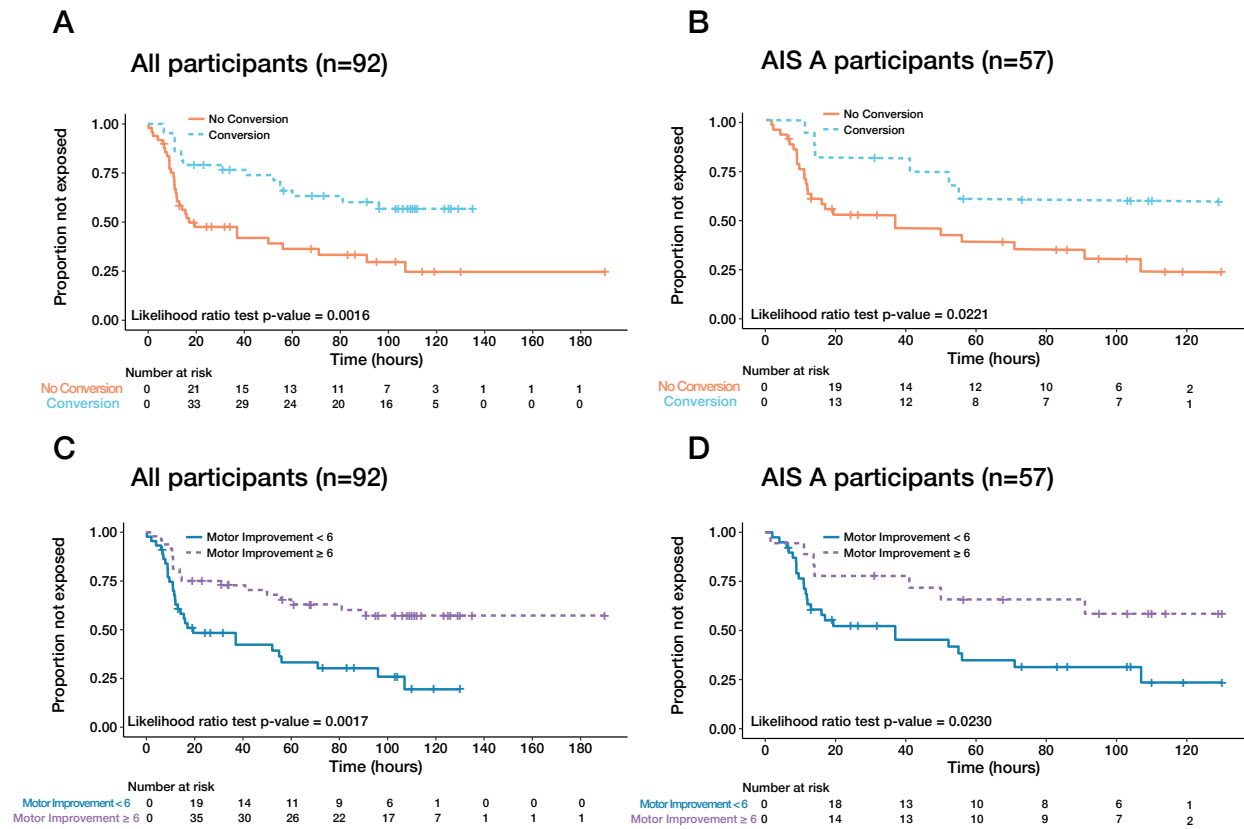
Figure 9.5: Low perfusion pressure exposures occur primarily within the first day post-injury.

Kaplan-Meier plot of exposure status to spinal cord perfusion pressure below 50 mmHg, split by

conversion (**panels A, B**) or by total motor score improvement (**panels C, D**). Cox proportional

hazard models revealed a statistically significant likelihood ratio test between those who

neurologically improved (i.e. conversion (p=0.0018) and total motor score improvement

(p=0.0017) versus those that did not improve. This finding was consistent in a sub-analysis

where only individuals with a baseline AIS score of "A" were considered (n = 57; **panels B, D;**

p=0.0221, p=0.0230).

9.3.6 Relative risk transition points reveal key relationship between hemodynamic management and motor improvement

Our results suggest there is a clear nadir below which patients should not fall below. However, an additional important question remains: *what is the ideal hemodynamic management strategy to promote neurological improvement?* To address this question, we examined the relative risk of AIS conversion across the physiological range of CSFP, MAP, and SCPP. We found that a clear transition point could be identified **(Figure 9.6A)**, suggesting a first potential target for hemodynamic management. We also iterated this same analysis across the entire range of total motor score (TMS) improvements **(see Figure 9.6B for examples of transition points at TMS improvements of 15 or 30 points)**. We observed a significant positive (negative for CSFP) linear relationship between motor recovery and MAP and SCPP relative risk transition points **(Figure 9.6C; Table 9.3)**. Importantly, the direct down- (but not right-) ward shift for TMS **(Figure 9.6D)** shows that the transition point for MAP remains constant at around 75 mm Hg despite the fact that TMS recovery is increasing from 20 to 50, while the 'transition-point' for SCPP is continually increasing as TMS recovery increases.

Table 9.3: Linear model results for relative risk transition points

Outcome	Measure	R2	p
CSFP	TMS	0.91	3.37E-27
MAP	TMS	0.66	3.37E-13
SCPP	TMS	0.84	3.91E-21

Abbreviations: CSFP: cerebrospinal fluid pressure; MAP: mean arterial pressure; SCPP: spinal cord perfusion pressure; TMS: total motor score.

9.3.7 Time spent within key hemodynamic targets is associated with neurological recovery

It is important to recognize that even when a hemodynamic target is established (e.g. "maintain MAP above 85 mm Hg for 7d"), patients often inadvertently fall below this target, even when managed in an intensive care setting.[245,348] Thus, we analyzed how "adherence" to key hemodynamic target ranges for each parameter influenced motor score recovery. We found that adherence to hemodynamic cutoffs was positively associated with TMS recovery **(Figure 9.7A)** and that conservative management targets tended to result in a stronger relationship between motor recovery and time spent within the target range (**Figure 9.7**, **Table 9.4**).

Next, we show that it is primarily adherence to SCPP targets, and not MAP targets, that is related to significant neurological improvement **(Figure 9.8A)**. We found that this trend holds in subsamples of individuals with cervical injuries **(Figure 9.8B)** and individuals presenting with AIS A injuries **(Figure 9.8C).** We show that in general, SCPP targets of 60 and 65 mmHg lead to the most stable observation of significant neurological improvement, and also allow for lower clinical adherence rates (~60-80%). Lastly, we show that low hemodynamic management targets require perfect clinical adherence to significantly improve neurological outcomes (**Figure 9.8A**). This finding validates our previous results, where we show that these criteria represent not a target, but a 'nadir' which patients should not fall below. Put together, these results provide key ranges to guide hemodynamic management targets, but also suggest that specific targets should be set in concordance with expected clinical adherence rates, which we have shown to be particularly troublesome in acute SCI management.[245,348]
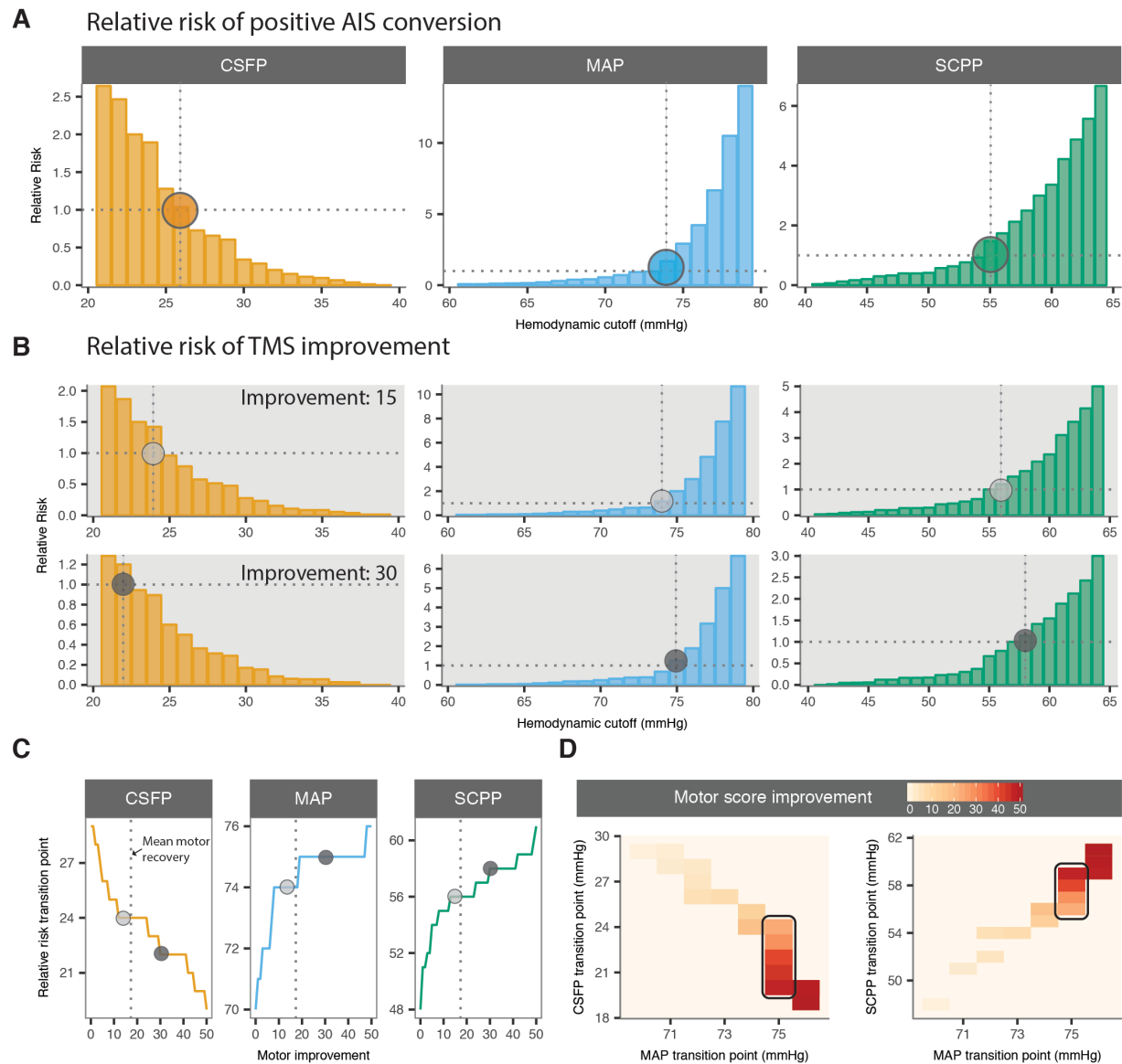
Figure 9.6: Relative risk transition-point analysis.

[A] The relative risk of positive conversion of American Spinal Injury Association Impairment

Scale (AIS) of at least one grade was examined across a range of hemodynamic parameters. We

identified a "transition point", where the relative risk crosses 1 (colored circles), representing the

point at which statistical improvement above average is achieved. [B] Next, we iterated this same

analysis across the entire range of motor score improvements. We looked at the range of motor

score improvements across all subjects – as some individuals improved considerably, while

others did not. We then looked at the hemodynamic parameters of these individuals (MAP,

CSFP, SCPP) and determined at what point for each of these parameters was the "relative risk"

of achieving that particular motor recovery 1. So for example, for a TMS recovery of 15 points,

the relative risk of achieving this degree of recovery was 1 with a MAP of 74 mm Hg, a CSFP of

24 mm Hg, and a SCPP of 56 mm Hg (light grey circles), whereas for a TMS recovery of 30

points, the relative risk of achieving this degree of recovery was 1 with a MAP of 75 mm Hg, a

CSFP of 21mm Hg, and a SCPP of 58 mm Hg (dark grey circles) [C] By projecting the concept

of panel B across the entire range of total motor score improvements (see light and dark grey

circles for reference to panel B) we observed a significant linear relationship (all $R^2 > 0.65$, p <

$3.37e^{-13}$), whereby higher motor score improvements were associated with higher 'transition-

points', and that this trend continued beyond the average motor score improvement (grey dotted

line). Additionally, we found that these relationships persisted in a subsample of the most

severely injured individuals deemed AIS A at baseline (n=57; data not shown). [D] Importantly,

with increasing motor score recovery we found that the mean arterial pressure transition point

remained relatively constant (black rectangle regions), while the cerebrospinal fluid pressure and

spinal cord perfusion pressure transition points continued to change. This can be visualized in

panel D where the MAP transition point is maintained at 75, despite increasing motor score

improvements (i.e., darker tiles). Abbreviations: TMS=total motor score, CSFP=cerebrospinal

fluid pressure, MAP=mean arterial pressure, SCPP=spinal cord perfusion pressure.

A Hemodynamic target comparisons and identification
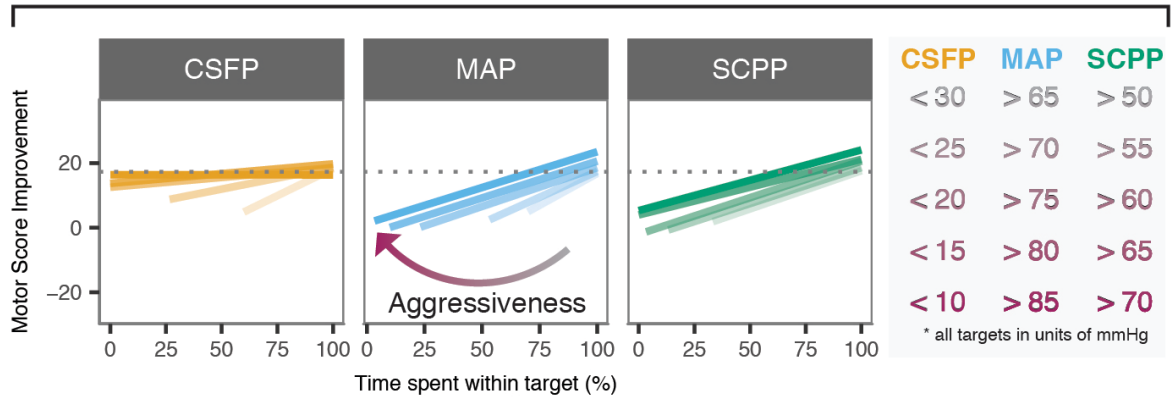
B Individual hemodynamic target regressions

207
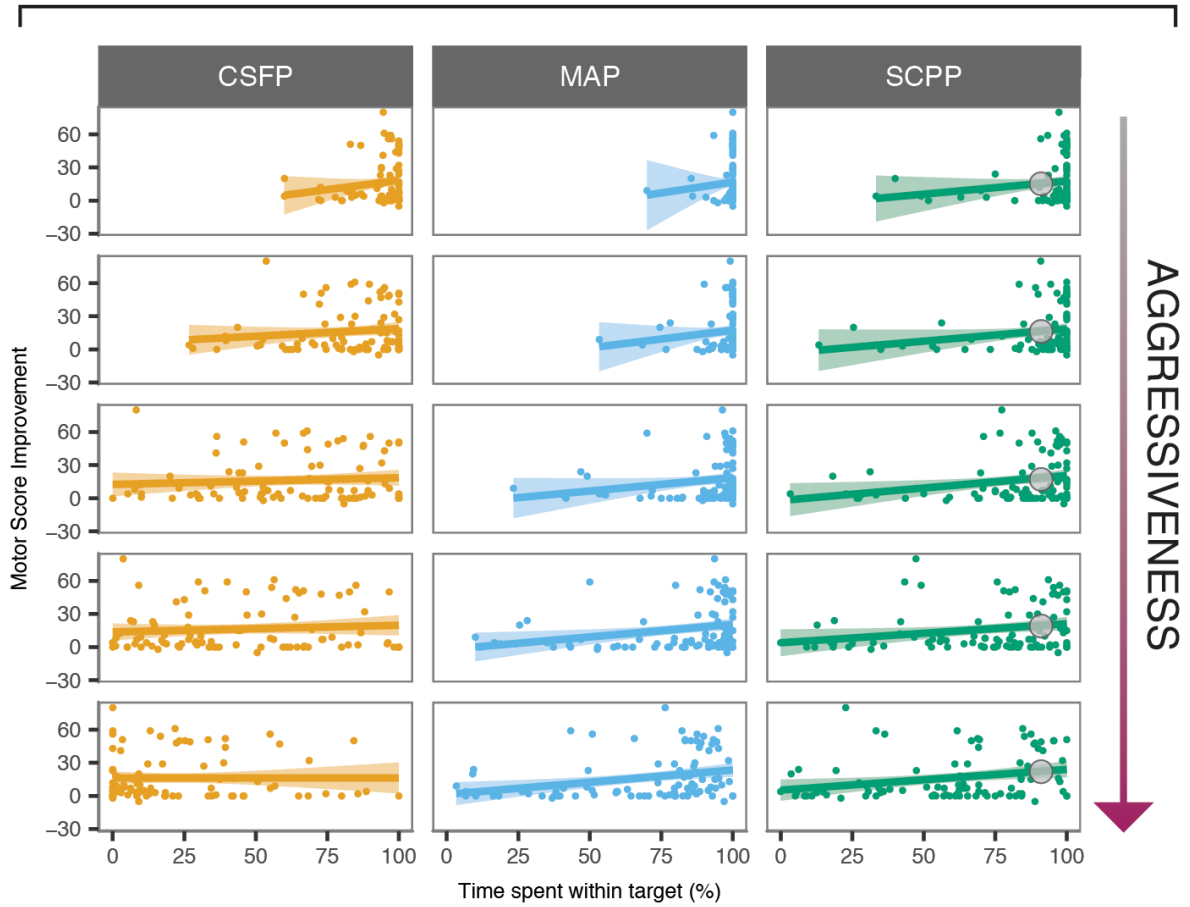
Figure 9.7: Clinical adherence regressions reveal relationship with neurological recovery. Linear relationships between motor score improvement and time spent within the target range are displayed. [A] Five different hemodynamic targets were tested, where an increase in motor recovery for a given time spent within the target was observed. To clearly observe the underlying data, the raw data points and linear projection are presented for each hemodynamic target in [B]. Importantly, these data show that for a given adherence rate the predicted motor score improvement increases with more aggressive (i.e., higher MAP, higher SCPP, lower CSFP) management strategies. For example, at a 90% adherence rate to SCPP targets (grey circles), the predicted motor score improvement increases from 17 to 22 as the target becomes more aggressive. Moreover, for non-aggressive targets, even with 100% adherence the predicted motor score improvement does not exceed the population average. Statistical information for these figures can be found in Table e-4. Abbreviations: TMS=total motor score, CSFP=cerebrospinal fluid pressure, MAP=mean arterial pressure, SCPP=spinal cord perfusion pressure. Dotted line in panel A represents mean motor score improvement across our entire sample.

A Management targets

CSFP	MAP	SCPP
< 30	> 65	> 50
< 25	> 70	> 55
< 20	> 75	> 60
< 15	> 80	> 65
< 10	> 85	> 70

* all targets in units of mmHg

B AIS Conversion - Entire Sample
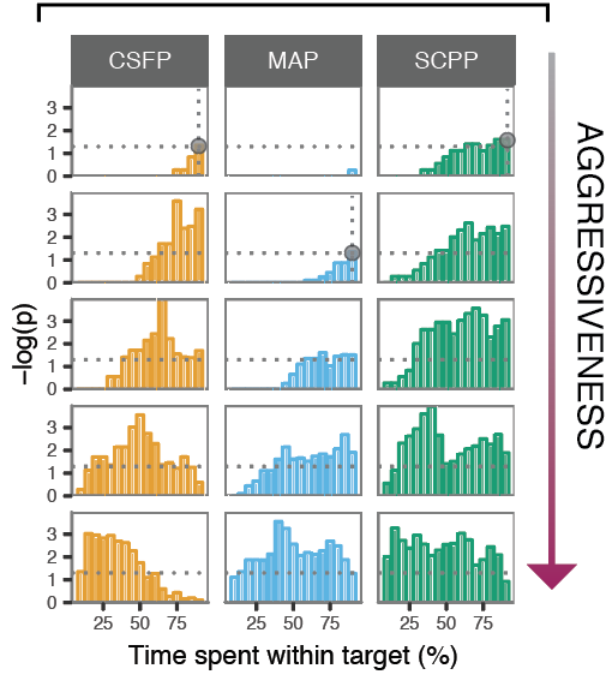
C AIS Conversion - Cervical Injuries
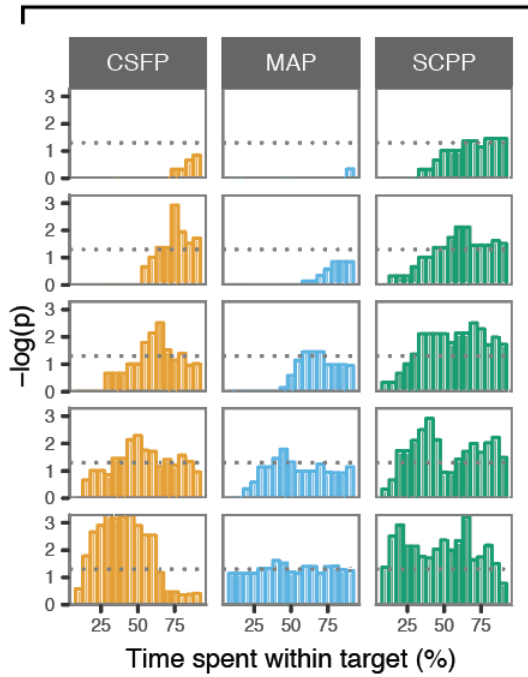
D AIS Conversion - AIS A Baseline
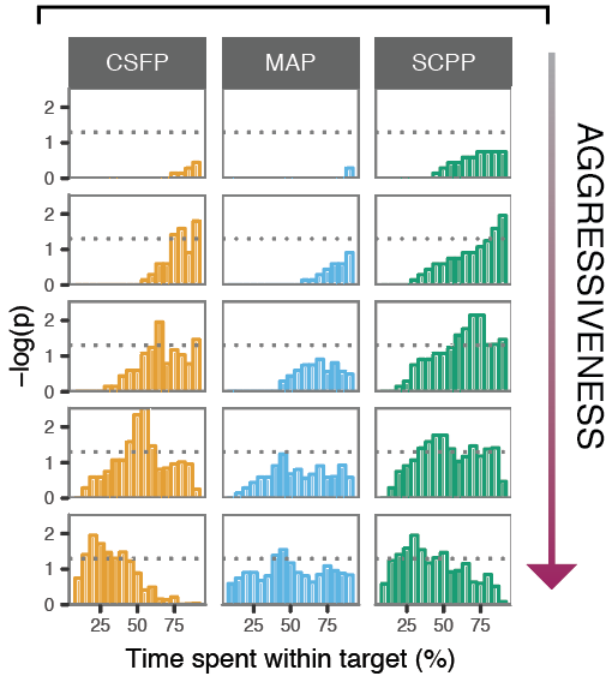
Figure 9.8: Adherence to hemodynamic management targets leads to improved neurological recovery.

Fisher's exact test results for 5% bins of time spent within the target range. Five different hemodynamic targets were tested **(Panel A). Panel B** represents the results from American Spinal Injury Association Impairment Scale (AIS) Conversion from our complete sample**,** while **panel C** represents the results from only individuals with cervical level injuries, and **panel D** only individuals presenting with an individual score of "A" on the AIS. Each subpanel, from left to right, indicates the hemodynamic target being tested, and the y-axis the -log10(p) of the Fisher's exact test. Bars exceeding the horizontal grey dotted line (i.e., $p < 0.05$) are cases where those individuals who are maintained within the target range at a given % are observed to have greater motor recovery than random expectation. Grey circles represent the clinical nadirs above which individuals should be maintained, as we have previously reported.[6] Aggressiveness describes the management criteria utilized (see **panel A, Figure 2** [i.e., higher MAP, higher SCPP, lower CSFP]). Abbreviations: TMS=total motor score, CSFP=cerebrospinal fluid pressure, MAP=mean arterial pressure, SCPP=spinal cord perfusion pressure. Dotted line represents a significance level of 0.05.

Table 9.4: Linear regression results for time spent within hemodynamic targets and motor score improvement.

Outcome	Measure	Target	Beta	R2	p
MAP	TMS	85	0.2213	0.0803	**0.0036**
MAP	TMS	80	0.2278	0.0615	**0.0098**
MAP	TMS	75	0.2399	0.0246	0.0728
MAP	TMS	70	0.3203	0.0066	0.2082
MAP	TMS	65	0.3934	-0.0053	0.4727
CSFP	TMS	10	-0.0002	-0.0111	0.9984
CSFP	TMS	15	0.0602	-0.0035	0.4099
CSFP	TMS	20	0.0604	-0.0045	0.4423
CSFP	TMS	25	0.1359	0.0043	0.2403
CSFP	TMS	30	0.3351	0.0093	0.1771
SCPP	TMS	70	0.1877	0.0572	**0.0124**
SCPP	TMS	65	0.1718	0.0390	**0.0329**
SCPP	TMS	60	0.2264	0.0525	**0.0159**
SCPP	TMS	55	0.2226	0.0261	**0.0671**
SCPP	TMS	50	0.2361	0.0109	0.1609

Abbreviations: CSFP: cerebrospinal fluid pressure; MAP: mean arterial pressure; SCPP: spinal cord perfusion pressure; TMS: total motor score. Bold values indicate significant regressions.

9.4   Discussion

We provide evidence from our multi-centre trial that SCPP as measured by lumbar intrathecal catheterization is a predictor of neurological outcome following traumatic SCI. Moreover, using systematic observations of relative risk we show that exposure to low SCPP increases the risk of poor neurological recovery. We substantiate this finding by demonstrating that the number of times individuals deviate outside specific SCPP cut-offs is related to poor neurological recovery. We found this relationship held in a sub-analysis of individuals with neurologically complete injuries (AIS A). We found that low SCPP was primarily occurring in the first few days after injury. Conversely, the number of times individuals deviated outside a mean arterial pressure or CSFP cut-off was not predictive of neurological outcome. Lastly, we demonstrate how clinical adherence rates influence the relationship between hemodynamic management and neurological outcomes and highlight that adherence to SCPP targets, not MAP targets, was the best indicator of improved neurological recovery, supporting our concept of a hemodynamic nadir. Given this

clear relationship, we provide a road-map for clinical centers to guide the development of hemodynamic targets that are in line with their expected adherence rates.

The influence of current hemodynamic management practices of augmenting MAP on neurological outcome in acute SCI is still unclear.[244,342] Arguably the most compelling supportive evidence is a recent study that reported improved neurological outcomes when MAP was consistently above 70-75 mmHg during the first week, which is 10-15 mmHg below the current clinical guidelines.[244] Although our relative risk analysis indicates that risk for poor neurological improvement occurs when mean arterial pressure falls below 70 mmHg, we show that using such a MAP cut-off is not a good indicator of whether neurological improvement will occur. Conversely, using three different statistical approaches, we found that using a SCPP cut-off of 50mmHg is a robust marker of whether neurological outcomes will improve.

Our findings are conceptually in agreement with Papadopolous and colleagues, who demonstrated that intraspinal pressure measured at the site of injury can predict neurological outcome in SCI.[339] A distinct difference, however, is that Papadopolous and colleagues measured intraspinal pressure at the injury site whereas we measured CSFP caudal to the injury site within the lumbar cistern. They revealed that the pressure was greatest at the site of occlusion, directly at the injury level, and that this was equivalent to the pressure recorded from inside the injured spinal cord.[16] We too have suggested that occlusion of the cerebrospinal fluid space due to swelling might establish differential pressures across the injury site.[340,344] It is recognized, however, that spinal cord swelling post-injury is variable amongst patients, and the degree of swelling also changes with time. Measurement of CSFP in the lumbar cistern would therefore not necessarily be an invalid reflection of what is occurring at the injury site. However, an assessment of how such pressures could be used and – importantly – whether they reflected

neurologic outcome, was warranted. Obviously, the advantage of measuring cerebrospinal fluid pressure with lumbar catheterization is related to the ease of application, technical familiarity of the procedure, and lack of risk of mechanically damaging the already injured spinal cord with the pressure catheter.

It is notable (and perhaps not surprising) that our proposed management strategy is strikingly similar to that which is currently applied in the setting of traumatic brain injury, where intracranial cerebral perfusion pressure monitoring is the mainstay of acute management.[337,338,345,346] While the most recent neurosurgical guidelines provide Level IIB evidence to maintain cerebral perfusion pressure between 60-70 mmHg,[346] the authors acknowledge that the lower limit of this monitoring is currently unknown. Here, we suggest a cut-off of at least 50 mmHg in traumatic spinal cord injury. It is of note that our derived perfusion pressure cut-off of 50 mmHg is supported by canine work, where spinal cord microvessel flow was preserved only when SCPP was maintained above 50 mmHg.[347] Such a SCPP could potentially be achieved by either raising mean arterial pressure with vasopressors or lowering cerebrospinal fluid pressure with drainage of CSF (or some combination of both). Lowering the cerebrospinal fluid pressure by draining CSF may allow one to achieve the desired SCPP with a lower MAP, thereby reducing the need for extensive vasopressor support, which comes with its own complications.[332,342] Therefore, although we found that stricter targets may be more forgiving to lower clinical adherence, we suggest the optimal approach may be to set more modest hemodynamic targets that 1) maintain patients above the critical nadir, and 2) will be achieved with a high level clinical adherence. Specifically, our data suggest that a target SCPP of 60 or 65 mmHg may be optimal, as our experience suggests this can be achieved with

good patient tolerance and our current data indicate this target leads to improved neurological outcomes while allowing for non-perfect clinical adherence.

It is important to note the potential influence of decompression within our data. We believe that early surgical decompression is beneficial for neurologic recovery, and the average time to decompression was less than 24 hours post-injury (considered to be "early" surgery). The exact effect of surgical decompression on SCPP is unclear without a method of directly measuring it at the injury site, but we have previously reported a surprising increase in CSFP post-decompression.[340] Such increases coupled with a low MAP may result in periods of low SCPP in the post-injury period.

Together, our findings suggest that optimizing SCPP during the acute post-SCI period provides a novel target to improve neurological outcome. By utilizing diverse statistical methodology we provide multiple lines of evidence that maintaining SCPP above 50 mmHg through both MAP and CSFP monitoring is associated with better neurological outcome. The combination of hemodynamic targets that can be maintained with high clinical adherence, along with the avoidance of our defined 'nadir' thus represents a first and important step towards this ultimate goal of empirical management strategies.

Chapter 10: Conclusion

10.1 General summary

In this thesis I examined the clinical reality of autonomic dysfunction after SCI, developed a clinically relevant rodent model, investigated the impact of neuroprotective pharmacology on autonomic function, and deployed a framework built around systems genetics to better understand how to target conserved molecular responses. Additionally, I used data from a multi-centre clinical trial to show that optimization of cardiovascular parameters can be used as an immediately implementable 'neuroprotective' strategy to improve neurologic outcomes.

The implementation of a severe thoracic contusion model builds on foundational work using spinal cord transection and clip compression as models to examine autonomic dysfunction in the rodent **(see Chapter 1).** Importantly, the current model uses the Infinite-Horizons impactor, which is a mainstay of pre-clinical SCI research and a common device in many laboratories **(see Chapter 4)**. Therefore, this is an important extension and allows this model to be easily implemented in numerous laboratories. I show that this model develops classical measures of autonomic dysfunction (i.e., low resting blood pressure, autonomic dysreflexia); however, I also implemented a testing platform for the assessment of load-dependent and load-independent cardiac function **(see Chapters 5 and 6).** This thesis significantly extends previous work investigating cardiac dysfunction in SCI by dissecting the relative impairments of pressure and volume generating capacity of the left-ventricle using gold-standard pressure-volume catheterization. Using beta-agonists, the current data additionally show that pressure generating capacity is heavily dependent on sympathetic input, providing a rational hypothesis for the use of neuroprotection to restore pressure generating capacity of the left ventricle.

Next, I show that our model is amenable to neuroprotective therapies **(see Chapter 7)**. Minocycline has shown robust pre-clinical effects on motor function, and is now in phase III clinical trial. However, its effect on the cardiovascular system has been largely unexplored. The current data suggest that reducing the severity of the lesion and preserving sympatho-excitatory axons can lead to functional improvements in hemodynamic control (i.e., reduce the severity of autonomic dysreflexia) and improve pressure generating capacity of the left-ventricle. In the broader context of neuroprotection and autonomic function in SCI, the reductions in the severity of autonomic dysreflexia are largely in line with those previously reported using other agents **(see Chapter 1; Table 1.1)**. However, our use of minocycline represents the first examination of a clinically approved drug used for neuroprotection with the goal to improve autonomic function.

Next, I used an integrated systems genetic approach **(see Chapter 8)** to identify a conserved gene subnetwork enriched for genes associated with the response to SCI and thus provide a framework to test novel biomarkers and identify clinically approved drugs with neuroprotective potential. Importantly, this project collates information from the existing corpus of SCI literature examining genetic and proteomic responses to injury. These large datasets were leveraged to identify novel and potential biomarkers of injury severity. While this project was completed using a T10 contusion model to align with existing transcriptomic and proteomic experiments, further work will examine whether this response is consistent in the upper thoracic region, as well as to examine the transcriptomic response to SCI at a deeper resolution. Additionally, these results will be used for drug repurposing efforts with the goal to identify novel compounds that most significantly reverse the transcriptomic and proteomic response to injury.

Lastly, the hypothesis that individuals with optimized hemodynamic management experience significantly greater neurologic improvement was tested **(see Chapter 9)**. This project is the result of a decade of clinical data collection, and is already serving as a foundational piece in the development of guidelines for the management of acute SCI. However, future work will test whether maintaining individuals within our specified hemodynamic ranges leads to improved outcomes in prospective trials, which are ongoing. Additionally, novel biomarkers of injury severity are being integrated and may be informed by our systems biology framework.

In conclusion, the work presented in this thesis is informed by and built upon a comprehensive understanding of SCI literature, a broad understanding of the field, as well as the priorities of individuals with SCI. The models and outcome assessment platforms developed in our rodent studies have already been implemented in other centres to examine a host of potential methods to improve autonomic function after SCI. Our insight into the physiological changes in left-ventricular function as well as our data showing the necessity of sympathetic input to maintain pressure-generating capacity represent key mechanistic findings that have changed our understanding of cardiac dysfunction after SCI. Further work will leverage these platforms for large-scale experiments on promising neuroprotective drugs, to integrate clinical outcome measures with a deep understanding of the integrated transcriptome-wide response to injury, and to further develop and validate our guidelines for hemodynamic management of individuals with acute SCI.

References

1. Hughes, J.T. (1988). The Edwin Smith Surgical Papyrus: an analysis of the first case reports of spinal cord injuries. Spinal Cord 26, 71-82.

2. Adams, M. and Cavanagh, J. (2004). International Campaign for Cures of Spinal Cord Injury Paralysis (ICCP): another step forward for spinal cord injury research. Spinal Cord 42, 273-280.

3. Krassioukov, A., Biering-Sørensen, F., Donovan, W., Kennelly, M., Kirshblum, S., Krogh, K., Alexander, M.S., Vogel, L. and Wecht, J. (2012). International standards to document remaining autonomic function after spinal cord injury. The journal of spinal cord medicine 35, 201-210.

4. Krassioukov, A., Karlsson, A.K., Wecht, J.M., Wuermser, L.A., Mathias, C.J. and Marino, R.J. (2006). Assessment of autonomic dysfunction following spinal cord injury: rationale for additions to International Standards for Neurological Assessment. Journal of Rehabilitation Research and Development 44, 103-112.

5. Giannantoni, A., Di Stasi, S., Scivoletto, G., Mollo, A., Silecchia, A., Fuoco, U. and Vespasiani, G. (1998). Autonomic dysreflexia during urodynamics. Spinal Cord 36, 756-760.

6. Karlsson, A. (1999). Autonomic dysreflexia. Spinal Cord 37, 383-391.

7. Lee, B., Karmakar, M., Herz, B. and Sturgill, R. (1995). Autonomic dysreflexia revisited. The Journal of Spinal Cord Medicine 18, 75-87.

8. Mathias, C. and Frankel, H. (1992). Autonomic disturbances in spinal cord lesions. In: Autonomic failure. 3rd ed. Bannister, R., CJ, M. (eds). Oxford University Press: Oxford, pps. 839-881.

218

9. Illman, A., Stiller, K. and Williams, M. (2000). The prevalence of orthostatic hypotension during physiotherapy treatment in patients with an acute spinal cord injury. Spinal Cord 38, 741-747.

10. Stiens, S., Johnson, M. and Lyman, P. (1995). Cardiac rehabilitation in patients with spinal cord injuries. Physical Medicine and Rehabilitation Clinics of North America 6, 263-263.

11. Cragg, J.J., Noonan, V.K., Krassioukov, A. and Borisoff, J. (2013). Cardiovascular disease and spinal cord injury Results from a national population health survey. Neurology 81, 723-728.

12. Lieberman, J.A., Hammond, F.M., Barringer, T.A., Norton, H., Goff Jr, D.C., Bockenek, W.L. and Scelza, W.M. (2011). Comparison of coronary artery calcification scores and National Cholesterol Education program guidelines for coronary heart disease risk assessment and treatment paradigms in individuals with chronic traumatic spinal cord injury. The Journal of Spinal Cord Medicine 34, 233-240.

13. Myers, J., Lee, M. and Kiratli, J. (2007). Cardiovascular disease in spinal cord injury: an overview of prevalence, risk, evaluation, and management. American Journal of Physical Medicine & Rehabilitation 86, 142-152.

14. Wahman, K., Nash, M.S., Lewis, J.E., Seiger, Å. and Levi, R. (2011). Cardiovascular disease risk and the need for prevention after paraplegia determined by conventional multifactorial risk models: the Stockholm spinal cord injury study. Journal of Rehabilitation Medicine 43, 237-242.

15. Wu, J.C., Chen, Y.C., Liu, L., Chen, T.J., Huang, W.C., Cheng, H. and Tung-Ping, S. (2012). Increased risk of stroke after spinal cord injury A nationwide 4-year follow-up

cohort study. Neurology 78, 1051-1057.

16.   Hou, S., Tom, V.J., Graham, L., Lu, P. and Blesch, A. (2013). Partial restoration of cardiovascular function by embryonic neural stem cell grafts after complete spinal cord transection. The Journal of Neuroscience 33, 17138-17149.

17.   Inskip, J., Ramer, L., Ramer, M. and Krassioukov, A. (2008). Autonomic assessment of animals with spinal cord injury: tools, techniques and translation. Spinal Cord 47, 2-35.

18.   Krassioukov, A. and Weaver, L. (1996). Anatomy of the autonomic nervous system. Physical Medicine and Rehabilitation 10, 1-14.

19.   Curt, A., Nitsche, B., Rodic, B., Schurch, B. and Dietz, V. (1997). Assessment of autonomic dysreflexia in patients with spinal cord injury. Journal of Neurology, Neurosurgery & Psychiatry 62, 473-477.

20.   Kirshblum, S.C., Burns, S.P., Biering-Sorensen, F., Donovan, W., Graves, D.E., Jha, A., Johansen, M., Jones, L., Krassioukov, A. and Mulcahey, M. (2011). International standards for neurological classification of spinal cord injury (Revised 2011). The Journal of Spinal Cord Medicine 34, 535.

21.   Krassioukov, A. and Claydon, V.E. (2006). The clinical problems in cardiovascular control following spinal cord injury: an overview. Progress in Brain Research 152, 223-229.

22.   Bilello, J.F., Davis, J.W., Cunningham, M.A., Groom, T.F., Lemaster, D. and Sue, L.P. (2003). Cervical spinal cord injury and the need for cardiovascular intervention. Archives of Surgery 138, 1127-1129.

23.   Furlan, J.C., Fehlings, M.G., Shannon, P., Norenberg, M.D. and Krassioukov, A.V. (2003). Descending vasomotor pathways in humans: correlation between axonal

preservation and cardiovascular dysfunction after spinal cord injury. Journal of neurotrauma 20, 1351-1363.

24.   Krassioukov, A. and Fehlings, M. (1999). Effect of graded spinal cord compression on cardiovascular neurons in the rostro-ventro-lateral medulla. Neuroscience 88, 959-973.

25.   West, C.R., Bellantoni, A. and Krassioukov, A.V. (2013). Cardiovascular function in individuals with incomplete spinal cord injury: a systematic review. Topics in spinal cord injury rehabilitation 19, 267-278.

26.   Kirshblum, S.C., House, J.G. and O'connor, K.C. (2002). Silent autonomic dysreflexia during a routine bowel program in persons with traumatic spinal cord injury: a preliminary study. Archives of physical medicine and rehabilitation 83, 1774-1776.

27.   Ekland, M.B., Krassioukov, A.V., McBride, K.E. and Elliott, S.L. (2008). Incidence of autonomic dysreflexia and silent autonomic dysreflexia in men with spinal cord injury undergoing sperm retrieval: implications for clinical practice. The journal of spinal cord medicine 31, 33.

28.   Eltorai, I., Kim, R., Vulpe, M., Kasravi, H. and Ho, W. (1992). Fatal cerebral hemorrhage due to autonomic dysreflexia in a tetraplegic patient: case report and review. Spinal Cord 30, 355-360.

29.   Pine, Z.M., Miller, S.D. and Alonso, J.A. (1991). Atrial fibrillation associated with autonomic dysreflexia. American Journal of Physical Medicine & Rehabilitation 70, 271-273.

30.   Yarkony, G.M., Katz, R.T. and Wu, Y.C. (1986). Seizures secondary to autonomic dysreflexia. Arch Phys Med Rehabil 67, 834-835.

31.   Alexander, M., Biering-Sorensen, F., Bodner, D., Brackett, N., Cardenas, D., Charlifue,

S., Creasey, G., Dietz, V., Ditunno, J. and Donovan, W. (2009). International standards to document remaining autonomic function after spinal cord injury. Spinal Cord 47, 36-43.

32.   Krassioukov, A., Furlan, J.C. and Fehlings, M.G. (2003). Autonomic dysreflexia in acute spinal cord injury: an under-recognized clinical entity. Journal of Neurotrauma 20, 707-716.

33.   Cormier, C.M., Mukhida, K., Walker, G. and Marsh, D.R. (2010). Development of autonomic dysreflexia after spinal cord injury is associated with a lack of serotonergic axons in the intermediolateral cell column. Journal of neurotrauma 27, 1805-1818.

34.   Hasséssian, H., Poulat, P., Hamel, E., Reader, T.A. and Couture, R. (1993). Spinal cord serotonin receptors in cardiovascular regulation and potentiation of the pressor response to intrathecal substance P after serotonin depletion. Canadian journal of physiology and pharmacology 71, 453-464.

35.   Sato, A. and Schmidt, R.F. (1973). Somatosympathetic reflexes: afferent fibers, central pathways, discharge characteristics. Physiol Rev 53, 916-947.

36.   Krassioukov, A., Johns, D.G. and Schramm, L.P. (2002). Sensitivity of sympathetically correlated spinal interneurons, renal sympathetic nerve activity, and arterial pressure to somatic and visceral stimuli after chronic spinal injury. Journal of neurotrauma 19, 1521-1529.

37.   Krenz, N. and Weaver, L. (1998). Sprouting of primary afferent fibers after spinal cord transection in the rat. Neuroscience 85, 443-458.

38.   Russell, F., King, R., Smillie, S.-J., Kodji, X. and Brain, S. (2014). Calcitonin Gene-Related Peptide: Physiology and Pathophysiology. Physiological reviews 94, 1099-1142.

39.   Weaver, L.C., Marsh, D.R., Gris, D., Brown, A. and Dekaban, G.A. (2006). Autonomic

dysreflexia after spinal cord injury: central mechanisms and strategies for prevention. Progress in Brain Research 152, 245-263.

40.   Llewellyn- Smith, I.J. and Weaver, L.C. (2001). Changes in synaptic inputs to sympathetic preganglionic neurons after spinal cord injury. Journal of Comparative Neurology 435, 226-240.

41.   Cameron, A.A., Smith, G.M., Randall, D.C., Brown, D.R. and Rabchevsky, A.G. (2006). Genetic manipulation of intraspinal plasticity after spinal cord injury alters the severity of autonomic dysreflexia. The Journal of Neuroscience 26, 2923-2932.

42.   Krassioukov, A. and Weaver, L.C. (1995). Episodic hypertension due to autonomic dysreflexia in acute and chronic spinal cord-injured rats. American Journal of Physiology-Heart and Circulatory Physiology 37, H2077.

43.   Maiorov, D., Krenz, N., Krassioukov, A. and Weaver, L. (1997). Role of spinal NMDA and AMPA receptors in episodic hypertension in conscious spinal rats. American Journal of Physiology-Heart and Circulatory Physiology 42, H1266.

44.   Krenz, N.R., Meakin, S.O., Krassioukov, A. and Weaver, L.C. (1999). Neutralizing intraspinal nerve growth factor blocks autonomic dysreflexia caused by spinal cord injury. The Journal of Neuroscience 19, 7405-7414.

45.   Ramer, L.M., van Stolk, A.P., Inskip, J.A., Ramer, M.S. and Krassioukov, A.V. (2012). Plasticity of TRPV1-expressing sensory neurons mediating autonomic dysreflexia following spinal cord injury. Frontiers in physiology 3.

46.   Yeoh, M., McLachlan, E.M. and Brock, J.A. (2004). Tail arteries from chronically spinalized rats have potentiated responses to nerve stimulation in vitro. The Journal of physiology 556, 545-555.

223

47.   Alan, N., Ramer, L.M., Inskip, J.A., Golbidi, S., Ramer, M.S., Laher, I. and Krassioukov, A.V. (2010). Recurrent autonomic dysreflexia exacerbates vascular dysfunction after spinal cord injury. The Spine Journal 10, 1108-1117.

48.   Arnold, J.M.O., Teasell, R.W., MacLeod, A.P., Brown, J.E. and Carruthers, S.G. (1993). Increased venous alpha-adrenoceptor responsiveness in patients with reflex sympathetic dystrophy. Annals of internal medicine 118, 619-621.

49.   Kaufmann, H. (1996). Consensus statement on the definition of orthostatic hypotension, pure autonomic failure and multiple system atrophy. Clinical autonomic research: official journal of the Clinical Autonomic Research Society 6, 125-126.

50.   Claydon, V.E. and Krassioukov, A. (2006). Orthostatic hypotension and autonomic pathways after spinal cord injury. Journal of Neurotrauma 23, 1713-1725.

51.   Amar, A.P. and Levy, M.L. (1999). Pathogenesis and pharmacological strategies for mitigating secondary damage in acute spinal cord injury. Neurosurgery 44, 1027-1039.

52.   Dusart, I. and Schwab, M. (1994). Secondary cell death and the inflammatory reaction after dorsal hemisection of the rat spinal cord. European Journal of Neuroscience 6, 712-724.

53.   Popovich, P.G., Wei, P. and Stokes, B.T. (1997). Cellular inflammatory response after spinal cord injury in sprague- dawley and lewis rats. Journal of Comparative Neurology 377, 443-464.

54.   Kwon, B.K., Fisher, C.G., Dvorak, M.F. and Tetzlaff, W. (2005). Strategies to promote neural repair and regeneration after spinal cord injury. Spine 30, S3-S13.

55.   Kwon, B.K., Okon, E., Hillyer, J., Mann, C., Baptiste, D., Weaver, L.C., Fehlings, M.G. and Tetzlaff, W. (2011). A systematic review of non-invasive pharmacologic

neuroprotective treatments for acute spinal cord injury. Journal of Neurotrauma 28, 1545-1588.

56. Gris, D., Marsh, D.R., Dekaban, G.A. and Weaver, L.C. (2005). Comparison of effects of methylprednisolone and anti-CD11d antibody treatments on autonomic dysreflexia after spinal cord injury. Experimental Neurology 194, 541-549.

57. Marsh, D.R., Wong, S.T., Meakin, S.O., MacDonald, J.I., Hamilton, E.F. and Weaver, L.C. (2002). Neutralizing intraspinal nerve growth factor with a trkA-IgG fusion protein blocks the development of autonomic dysreflexia in a clip-compression model of spinal cord injury. Journal of Neurotrauma 19, 1531-1541.

58. Webb, A.A., Chan, C.B., Brown, A. and Saleh, T.M. (2006). Estrogen reduces the severity of autonomic dysfunction in spinal cord-injured male mice. Behavioural Brain Research 171, 338-349.

59. Jacob, J., Pniak, A., Weaver, L. and Brown, A. (2001). Autonomic dysreflexia in a mouse model of spinal cord injury. Neuroscience 108, 687-693.

60. Bartholdi, D. and Schwab, M.E. (1997). Expression of pro- inflammatory cytokine and chemokine mRNA upon experimental spinal cord injury in mouse: An in situ hybridization study. European Journal of Neuroscience 9, 1422-1438.

61. Kerr, B.J. and Patterson, P.H. (2004). Potent pro-inflammatory actions of leukemia inhibitory factor in the spinal cord of the adult mouse. Experimental Neurology 188, 391-407.

62. Klusman, I. and Schwab, M.E. (1997). Effects of pro-inflammatory cytokines in experimental spinal cord injury. Brain Research 762, 173-184.

63. Cuzzocrea, S., Riley, D.P., Caputi, A.P. and Salvemini, D. (2001). Antioxidant therapy: a

new pharmacological approach in shock, inflammation, and ischemia/reperfusion injury. Pharmacological Reviews 53, 135-159.

64. Hall, E.D. (1994). Free radicals in central nervous system injury. New Comprehensive Biochemistry 28, 217-238.

65. Kakulas, B.A. (1999). A review of the neuropathology of human spinal cord injury with emphasis on special features. The Journal of Spinal Cord Medicine 22, 119.

66. Fleming, J.C., Bao, F., Chen, Y., Hamilton, E.F., Relton, J.K. and Weaver, L.C. (2008). α4β1 integrin blockade after spinal cord injury decreases damage and improves neurological function. Experimental Neurology 214, 147-159.

67. Gris, D., Marsh, D.R., Oatway, M.A., Chen, Y., Hamilton, E.F., Dekaban, G.A. and Weaver, L.C. (2004). Transient blockade of the CD11d/CD18 integrin reduces secondary damage after spinal cord injury, improving sensory, autonomic, and motor function. The Journal of Neuroscience 24, 4043-4051.

68. Marsh, D. and Flemming, J. (2010). Inhibition of CXCR1 and CXCR2 chemokine receptors attenuates acute inflammation, preserves gray matter and diminishes autonomic dysreflexia after spinal cord injury. Spinal Cord 49, 337-344.

69. Ditor, D.S., Bao, F., Chen, Y., Dekaban, G.A. and Weaver, L.C. (2006). A therapeutic time window for anti-CD11d monoclonal antibody treatment yielding reduced secondary tissue damage and enhanced behavioral recovery following severe spinal cord injury. Journal of Neurosurgery: Spine 5, 343-352.

70. Ditor, D.S., John, S.M., Roy, J., Marx, J.C., Kittmer, C. and Weaver, L.C. (2007). Effects of polyethylene glycol and magnesium sulfate administration on clinically relevant neurological outcomes after spinal cord injury in the rat. Journal of Neuroscience

Research 85, 1458-1467.

71. Rabchevsky, A.G., Patel, S.P., Lyttle, T.S., Eldahan, K.C., O'Dell, C.R., Zhang, Y., Popovich, P.G., Kitzman, P.H. and Donohue, K.D. (2012). Effects of gabapentin on muscle spasticity and both induced as well as spontaneous autonomic dysreflexia after complete spinal cord injury. Frontiers in Physiology 3.

72. Bevilacqua, M.P. (1993). Endothelial-leukocyte adhesion molecules. Annual Review of Immunology 11, 767-804.

73. Streit, W.J., Semple-Rowland, S.L., Hurley, S.D., Miller, R.C., Popovich, P.G. and Stokes, B.T. (1998). Cytokine mRNA profiles in contused spinal cord and axotomized facial nucleus suggest a beneficial role for inflammation and gliosis. Experimental Neurology 152, 74-87.

74. Casha, S., Yu, W. and Fehlings, M. (2001). Oligodendroglial apoptosis occurs along degenerating axons and is associated with FAS and p75 expression following spinal cord injury in the rat. Neuroscience 103, 203-218.

75. Tetzlaff, W., Okon, E.B., Karimi-Abdolrezaee, S., Hill, C.E., Sparling, J.S., Plemel, J.R., Plunet, W.T., Tsai, E.C., Baptiste, D. and Smithson, L.J. (2011). A systematic review of cellular transplantation therapies for spinal cord injury. Journal of Neurotrauma 28, 1611-1682.

76. Kalinčík, T., Choi, E.A., Féron, F., Bianco, J., Sutharsan, R., Hayward, I., Mackay-Sim, A., Carrive, P. and Waite, P.M. (2010). Olfactory ensheathing cells reduce duration of autonomic dysreflexia in rats with high spinal cord injury. Autonomic Neuroscience 154, 20-29.

77. Kalinčík, T., Jozefcikova, K., Sutharsan, R., Mackay-Sim, A., Carrive, P. and Waite, P.M.

(2010). Selected changes in spinal cord morphology after T4 transection and olfactory ensheathing cell transplantation. Autonomic Neuroscience 158, 31-38.

78. West, C.R., Inskip, J., ., Ramer, L., Cragg, J. and Krassioukov, A. (2012). Effect of hind-limb cycling on severity of orthostatic hypotension and autonomic dysreflexia in rats with SCI. Top Spinal Cord Inj Rehabil 19, 3.

79. Phillips, A.A., and Krassioukov, A. V. (2015). Contemporary cardiovascular concerns after spinal cord injury: Mechanisms, maladaptations, and management. J. Neurotrauma 32, 1927–1942.

80. Hinchey, J., Chaves, C., Appignani, B., Breen, J., Pao, L., Wang, A., Pessin, M.S., Lamy, C., Mas, J.-L., and Caplan, L.R. (1996). A reversible posterior leukoencephalopathy syndrome. N. Engl. J. Med. 334, 494–500.

81. Hefzy, H.M., Bartynski, W.S., Boardman, J.F., and Lacomis, D. (2009). Hemorrhage in posterior reversible encephalopathy syndrome: imaging and clinical features. Am. J. Neuroradiol. 30, 1371–1379.

82. Cord, S., Presenting, I., and Facilities, H. (2002). Acute management of autonomic dysreflexia: individuals with spinal cord injury presenting to health-care facilities. J. Spinal Cord Med. 25 Suppl 1, S67–S88.

83. Edvardsson, B., and Persson, S. (2010). Reversible cerebral vasoconstriction syndrome associated with autonomic dysreflexia. J. Headache Pain 11, 277–80.

84. Chaves, C.J., and Lee, G. (2008). Reversible posterior leukoencephalopathy in a patient with autonomic dysreflexia: a case report. Spinal Cord 46, 760–1.

85. Matias, A.C., Rocha, J., Cerqueira, M.E., and Pereira, J.M. (2013). Autonomic dysreflexia and posterior reversible encephalopathy syndrome. Am. J. Phys. Med. Rehabil. 92, 453–8.

86.   McKinney, A.M., Sarikaya, B., Gustafson, C., and Truwit, C.L. (2012). Detection of microhemorrhage in posterior reversible encephalopathy syndrome using susceptibility-weighted imaging. Am. J. Neuroradiol. 33, 896–903.

87.   Krassioukov, A. V, Gelb, A.W., and Weaver, L.C. (1993). Action of propofol on central sympathetic mechanisms controlling blood pressure. Can. J. Anaesth. 40, 761–769.

88.   Wan, D., and Krassioukov, A. V. (2014). Life-threatening outcomes associated with autonomic dysreflexia: A clinical review. J. Spinal Cord Med. 37, 2–10.

89.   West, C.R., Crawford, M.A., Laher, I., Ramer, M.S., and Krassioukov, A. V. (2015). Passive Hind-Limb Cycling Reduces the Severity of Autonomic Dysreflexia After Experimental Spinal Cord Injury. Neurorehabil. Neural Repair 30, 317–327.

90.   Phillips, A.A., Matin, N., Frias, B., Zheng, M.M.Z., Jia, M., West, C., Dorrance, A.M., Laher, I., and Krassioukov, A. V. (2016). Rigid and remodelled: cerebrovascular structure and function after experimental high-thoracic spinal cord transection. J. Physiol. 594, 1677–88.

91.   Krassioukov, A. V, and Weaver, L.C. (1996). Morphological changes in sympathetic preganglionic neurons after spinal cord injury in rats. Neuroscience 70, 211–225.

92.   Hou, S., Duale, H., Cameron, A.A., Abshire, S.M., Lyttle, T.S., and Rabchevsky, A.G. (2008). Plasticity of lumbosacral propriospinal neurons is associated with the development of autonomic dysreflexia after thoracic spinal cord transection. J. Comp. Neurol. 509, 382–99.

93.   Squair, J.W., West, C.R., and Krassioukov, A. V. (2015). Neuroprotection, Plasticity

Manipulation, and Regenerative Strategies to Improve Cardiovascular Function following Spinal Cord Injury. J. Neurotrauma 32, 609–21.

94.   Sekhon, L.H., and Fehlings, M.G. (2001). Epidemiology, demographics, and pathophysiology of acute spinal cord injury. Spine (Phila. Pa. 1976). 26, S2–12.

95.   Kwon, B.K., Oxland, T.R., and Tetzlaff, W. (2002). Animal models used in spinal cord regeneration research. Spine (Phila. Pa. 1976). 27, 1504–10.

96.   Young, W. (2002). Spinal cord contusion models. Prog. Brain Res. 137, 231–55.

97.   Ramer, L.M., Ramer, M.S., and Bradbury, E.J. (2014). Restoring function after spinal cord injury: towards clinical translation of experimental strategies. Lancet Neurol. 13, 1241–1256.

98.   Tator, C.H. (2006). Review of treatment trials in humanspinal cord injury: Issues, difficulties, and recommendations. Neurosurgery 59, 957–982.

99.   Nathan, P.W., and Smith, M.C. (1987). The location of descending fibres to sympathetic preganglionic vasomotor and sudomotor neurons in man. J. Neurol. Neurosurg. Psychiatry 50, 1253–62.

100.   Nathan, P.W., Smith, M.C., and Deacon, P. (1990). The Corticospinal Tracts in Man. Brain 113, 303–324.

101.   Anderson, K.D. (2004). Targeting recovery: priorities of the spinal cord-injured population. J. Neurotrauma 21, 1371–1383.

102.   Osborn, J.W., Taylor, R.F., and Schramm, L.P. (1990). Chronic cervical spinal cord injury and autonomic hyperreflexia in rats. Am. J. Physiol. 258, R169–74.

103. Weaver, L.C., Verghese, P., Bruce, J.C., Fehlings, M.G., Krenz, N.R., and Marsh, D.R. (2001). Autonomic dysreflexia and primary afferent sprouting after clip-compression injury of the rat spinal cord. J. Neurotrauma 18, 1107–19.

104. Joshi, M., and Fehlings, M.G. (2002). Development and characterization of a novel, graded model of clip compressive spinal cord injury in the mouse: Part 2. Quantitative neuroanatomical assessment and analysis of the relationships between axonal tracts, residual tissue, and locomotor recovery. J. Neurotrauma 19, 191–203.

105. Joshi, M., and Fehlings, M.G. (2002). Development and characterization of a novel, graded model of clip compressive spinal cord injury in the mouse: Part 1. Clip design, behavioral outcomes, and histopathology. J. Neurotrauma 19, 175–90.

106. Maiorov, D.N., Fehlings, M.G., and Krassioukov, A. V. (1998). Relationship Between Severity of Spinal Cord Injury and Abnormalities in Neurogenic Cardiovascular Control in Conscious Rats. J. Neurotrauma 15, 365–374.

107. Nout, Y.S., Beattie, M.S., and Bresnahan, J.C. (2012). Severity of locomotor and cardiovascular derangements after experimental high-thoracic spinal cord injury is anesthesia dependent in rats. J. Neurotrauma 29, 990–9.

108. Sandrow, H.R., Shumsky, J.S., Amin, A., and Houle, J.D. (2008). Aspiration of a cervical spinal contusion injury in preparation for delayed peripheral nerve grafting does not impair forelimb behavior or axon regeneration. Exp. Neurol. 210, 489–500.

109. Dunham, K.A., Siriphorn, A., Chompoopong, S., and Floyd, C.L. (2010). Characterization of a graded cervical hemicontusion spinal cord injury model in adult male rats. J. Neurotrauma 27, 2091–106.

110. Popovich, P.G., Lemeshow, S., Gensel, J.C., and Tovar, C.A. (2012). Independent evaluation of the effects of glibenclamide on reducing progressive hemorrhagic necrosis after cervical spinal cord injury. Exp. Neurol. 233, 615–22.

111. Lee, J.H.T., Streijger, F., Tigchelaar, S., Maloon, M., Liu, J., Tetzlaff, W., and Kwon, B.K. (2012). A contusive model of unilateral cervical spinal cord injury using the infinite horizon impactor. J. Vis. Exp. 65, 1–7.

112. Nicaise, C., Frank, D.M., Hala, T.J., Authelet, M., Pochet, R., Adriaens, D., Brion, J.-P., Wright, M.C., and Lepore, A.C. (2013). Early phrenic motor neuron loss and transient respiratory abnormalities after unilateral cervical spinal cord contusion. J. Neurotrauma 30, 1092–9.

113. Singh, A., Krisa, L., Frederick, K.L., Sandrow-Feinberg, H., Balasubramanian, S., Stackhouse, S.K., Murray, M., and Shumsky, J.S. (2014). Forelimb locomotor rating scale for behavioral assessment of recovery after unilateral cervical spinal cord injury in rats. J. Neurosci. Methods 226, 124–31.

114. James, N.D., Shea, J., Muir, E.M., Verhaagen, J., Schneider, B.L., and Bradbury, E.J. (2015). Chondroitinase gene therapy improves upper limb function following cervical contusion injury. Exp. Neurol. 271, 131–135.

115. Jin, Y., Bouyer, J., Haas, C., and Fischer, I. (2015). Evaluation of the anatomical and functional consequences of repetitive mild cervical contusion using a model of spinal concussion. Exp. Neurol. 271, 175–88.

116. Lane, M.A., Lee, K.-Z., Salazar, K., O'Steen, B.E., Bloom, D.C., Fuller, D.D., and Reier, P.J. (2012). Respiratory function following bilateral mid-cervical contusion injury in the

adult rat. Exp. Neurol. 235, 197–210.

117.   Anderson, K.D., Sharp, K.G., and Steward, O. (2009). Bilateral cervical contusion spinal cord injury in rats. Exp. Neurol. 220, 9–22.

118.   Onifer, S.M., Nunn, C.D., Decker, J.A., Payne, B.N., Wagoner, M.R., Puckett, A.H., Massey, J.M., Armstrong, J., Kaddumi, E.G., Fentress, K.G., Wells, M.J., West, R.M., Calloway, C.C., Schnell, J.T., Whitaker, C.M., Burke, D.A., and Hubscher, C.H. (2007). Loss and spontaneous recovery of forelimb evoked potentials in both the adult rat cuneate nucleus and somatosensory cortex following contusive cervical spinal cord injury. Exp. Neurol. 207, 238–47.

119.   Landrum, L.M., Thompson, G.M., and Blair, R.W. (1998). Does postsynaptic alpha 1-adrenergic receptor supersensitivity contribute to autonomic dysreflexia? Am. J. Physiol. 274, H1090–8.

120.   West, C.R., Popok, D., Crawford, M.A., and Krassioukov, A. V. (2015). Characterizing the temporal development of cardiovascular dysfunction in response to spinal cord injury. J. Neurotrauma 32, 922–30.

121.   Mayorov, D.N., Adams, M.A., and Krassioukov, A. V. (2001). Telemetric blood pressure monitoring in conscious rats before and after compression injury of spinal cord. J. Neurotrauma 18, 727–36.

122.   Ramsey, J.B.G., Ramer, L.M., Inskip, J.A., Alan, N., Ramer, M.S., and Krassioukov, A. V. (2010). Care of rats with complete high-thoracic spinal cord injury. J. Neurotrauma 27, 1709–22.

123.   Scheff, S.W., Rabchevsky, A.G., Fugaccia, I., Main, J.A., and Lumpp, J.E. (2003).

Experimental modeling of spinal cord injury: characterization of a force-defined injury device. J. Neurotrauma 20, 179–93.

124.   Basso, D.M., Beattie, M.S., and Bresnahan, J.C. (1995). A Sensitive and Reliable Locomotor Rating Scale for Open Field Testing in Rats. J. Neurotrauma 12, 1–21.

125.   Biernaskie, J., Sparling, J.S., Liu, J., Shannon, C.P., Plemel, J.R., Xie, Y., Miller, F.D., and Tetzlaff, W. (2007). Skin-derived precursors generate myelinating Schwann cells that promote remyelination and functional recovery after contusion spinal cord injury. J. Neurosci. 27, 9545–59.

126.   Bailey, J.M. (1997). Context-sensitive half-times and other decrement times of inhaled anesthetics. Anesth. Analg. 85, 681–6.

127.   West, C.R., Crawford, M.A., Poormasjedi-Meibod, M., Currie, K.D., Fallavollita, A., Yuen, V., McNeill, J.H., and Krassioukov, A. V. (2014). Passive hind-limb cycling improves cardiac function and reduces cardiovascular disease risk in experimental spinal cord injury. J. Physiol. 592, 1771–1783.

128.   Sparling, J.S., Bretzner, F., Biernaskie, J., Assinck, P., Jiang, Y., Arisato, H., Plunet, W.T., Borisoff, J., Liu, J., Miller, F.D., and Tetzlaff, W. (2015). Schwann Cells Generated from Neonatal Skin-Derived Precursors or Neonatal Peripheral Nerve Improve Functional Recovery after Acute Transplantation into the Partially Injured Cervical Spinal Cord of the Rat. J. Neurosci. 35, 6714–6730.

129.   Lein, E.S., et al. (2006). Genome-wide atlas of gene expression in the adult mouse brain. Nature 445, 168–176.

130.   Card, J.P., Sved, J.C., Craig, B., Raizada, M., Vazquez, J., and Sved, A.F. (2006). Efferent

projections of rat rostroventrolateral medulla C1 catecholamine neurons: Implications for the central control of cardiovascular regulation. J. Comp. Neurol. 499, 840–59.

131. Haselton, J.R., and Guyenet, P.G. (1989). Electrophysiological characterization of putative C1 adrenergic neurons in the rat. Neuroscience 30, 199–214.

132. Schreihofer, A.M., and Guyenet, P.G. (1997). Identification of C1 presympathetic neurons in rat rostral ventrolateral medulla by juxtacellular labeling in vivo. J. Comp. Neurol. 387, 524–36.

133. Kalia, M., Fuxe, K., and Goldstein, M. (1985). Rat medulla oblongata. III. Adrenergic (C1 and C2) neurons, nerve fibers and presumptive terminal processes. J. Comp. Neurol. 233, 333–49.

134. Maiorov, D.N., Weaver, L.C., and Krassioukov, A. V. (1997). Relationship between sympathetic activity and arterial pressure in conscious spinal rats. Am. J. Physiol. 272, H625–31.

135. Krassioukov, A. V. (2009). Autonomic function following cervical spinal cord injury. Respir. Physiol. Neurobiol. 169, 157–164.

136. West, C.R., Mills, P., and Krassioukov, A. V. (2012). Influence of the neurological level of spinal cord injury on cardiovascular outcomes in humans: a meta-analysis. Spinal Cord 50, 484–492.

137. Phillips, A.A., Krassioukov, A. V, Ainslie, P.N., and Warburton, D.E.R. (2014). Perturbed and spontaneous regional cerebral blood flow responses to changes in blood pressure after high-level spinal cord injury: the effect of midodrine. J. Appl. Physiol. 116, 645–653.

138. Phillips, A. a, Warburton, D.E., Ainslie, P.N., and Krassioukov, A. V. (2014). Regional neurovascular coupling and cognitive performance in those with low blood pressure secondary to high-level spinal cord injury: improved by alpha-1 agonist midodrine hydrochloride. J. Cereb. Blood Flow Metab. 34, 1–8.

139. Lujan, H.L., and DiCarlo, S.E. (2007). T5 spinal cord transection increases susceptibility to reperfusion-induced ventricular tachycardia by enhancing sympathetic activity in conscious rats. Am. J. Physiol. Heart Circ. Physiol. 293, H3333–9.

140. Silver, J., and Miller, J.H. (2004). Regeneration beyond the glial scar. Nat. Rev. Neurosci. 5, 146–56.

141. Horner, P.J., Power, A.E., Kempermann, G., Kuhn, H.G., Palmer, T.D., Winkler, J., Thal, L.J., and Gage, F.H. (2000). Proliferation and differentiation of progenitor cells throughout the intact adult rat spinal cord. J. Neurosci. 20, 2218–28.

142. Björklund, A., and Lindvall, O. (2000). Self-repair in the brain. Nature 405, 892–3, 895.

143. Johansson, C.B., Momma, S., Clarke, D.L., Risling, M., Lendahl, U., and Frisén, J. (1999). Identification of a neural stem cell in the adult mammalian central nervous system. Cell 96, 25–34.

144. Takahashi, M., Arai, Y., Kurosawa, H., Sueyoshi, N., and Shirai, S. (2003). Ependymal cell reactions in spinal cord segments after compression injury in adult rat. J. Neuropathol. Exp. Neurol. 62, 185–94.

145. David, S., and Lacroix, S. (2003). Molecular approaches to spinal cord repair. Annu. Rev. Neurosci. 26, 411–40.

146. Ruggiero, D.A., Cravo, S.L., Arango, V., and Reis, D.J. (1989). Central control of the circulation by the rostral ventrolateral reticular nucleus: anatomical substrates. Prog. Brain Res. 81, 49–79.

147. Li, Y.W., Bayliss, D.A., and Guyenet, P.G. (1995). C1 neurons of neonatal rats: intrinsic beating properties and alpha 2-adrenergic receptors. Am. J. Physiol. 269, R1356–69.

148. Krassioukov, A. V, and Weaver, L.C. (1993). Connections between the pontine reticular formation and rostral ventrolateral medulla. Am. J. Physiol. 265, H1386–92.

149. Lebedev, V.P., Krasyukov, A. V, and Nikitin, S.A. (1986). Electrophysiological study of sympathoexcitatory structures of the bulbar ventrolateral surface as related to vasomotor regulation. Neuroscience 17, 189–203.

150. Beluli, D.J., and Weaver, L.C. (1991). Areas of rostral medulla providing tonic control of renal and splenic nerves. Am. J. Physiol. 261, H1687–92.

151. Beluli, D.J., and Weaver, L.C. (1991). Differential control of renal and splenic nerves without medullary topography. Am. J. Physiol. 260, H1072–9.

152. Feldberg, W. (1976). The ventral surface of the brain stem: a scarcely explored region of pharmacological sensitivity. Neuroscience 1, 427–41.

153. Hayes, K., and Weaver, L.C. (1990). Selective control of sympathetic pathways to the kidney, spleen and intestine by the ventrolateral medulla in rats. J. Physiol. 428, 371–85.

154. Ruggiero, D.A., Ross, C.A., Anwar, M., Park, D.H., Joh, T.H., and Reis, D.J. (1985). Distribution of neurons containing phenylethanolamine N-methyltransferase in medulla and hypothalamus of rat. J. Comp. Neurol. 239, 127–54.

155. Ross, C.A., Ruggiero, D.A., Joh, T.H., Park, D.H., and Reis, D.J. (1984). Rostral ventrolateral medulla: selective projections to the thoracic autonomic cell column from the region containing C1 adrenaline neurons. J. Comp. Neurol. 228, 168–85.

156. Ruggiero, D.A., Cravo, S.L., Golanov, E., Gomez, R., Anwar, M., and Reis, D.J. (1994). Adrenergic and non-adrenergic spinal projections of a cardiovascular-active pressor area of medulla oblongata: quantitative topographic analysis. Brain Res. 663, 107–20.

157. Aguayo, A.J., Rasminsky, M., Bray, G.M., Carbonetto, S., McKerracher, L., Villegas-Pérez, M.P., Vidal-Sanz, M., and Carter, D.A. (1991). Degenerative and regenerative responses of injured neurons in the central nervous system of adult mammals. Philos. Trans. R. Soc. Lond. B. Biol. Sci. 331, 337–43.

158. Lieberman, A.R. (1971). The axon reaction: a review of the principal features of perikaryal responses to axon injury. Int. Rev. Neurobiol. 14, 49–124.

159. Tetzlaff, W., Kobayashi, N.R., Giehl, K.M., Tsui, B.J., Cassar, S.L., and Bedard, A.M. (1994). Response of rubrospinal and corticospinal neurons to injury and neurotrophins. Prog. Brain Res. 103, 271–86.

160. Yan, Q., Elliott, J., and Snider, W.D. (1992). Brain-derived neurotrophic factor rescues spinal motor neurons from axotomy-induced cell death. Nature 360, 753–5.

161. Ackery, A.D., Norenberg, M.D., and Krassioukov, A. (2007). Calcitonin gene-related peptide immunoreactivity in chronic human spinal cord injury. Spinal Cord 45, 678–86.

162. Basso, D.M., Beattie, M.S., and Bresnahan, J.C. (1996). Graded histological and locomotor outcomes after spinal cord contusion using the NYU weight-drop device versus transection. Exp. Neurol. 139, 244–56.

163. Kessler, K.M., Pina, I., Green, B., Burnett, B., Laighold, M., Bilsker, M., Palomo, A.R., and Myerburg, R.J. (1986). Cardiovascular findings in quadriplegic and paraplegic patients and in normal subjects. Am. J. Cardiol. 58, 525–530.

164. West, C.R., Campbell, I.G., Shave, R.E., and Romer, L.M. (2012). Resting cardiopulmonary function in Paralympic athletes with cervical spinal cord injury. Med. Sci. Sports Exerc. 44, 323–329.

165. Eysmann, S.B., Douglas, P.S., Katz, S.E., Sarkarati, M., and Wei, J.Y. (1995). Left ventricular mass and diastolic filling patterns in quadriplegia and implications for effects of normal aging on the heart. Am. J. Cardiol. 75, 201–3.

166. La Fountaine, M.F., Wecht, J.M., Rosado-Rivera, D., Cirnigliaro, C.M., Spungen, A.M., and Bauman, W.A. (2010). The QT variability index and cardiac autonomic modulation: perspectives from apparently healthy men with spinal cord injury. Cardiology 117, 253–9.

167. Lujan, H.L., Palani, G., and DiCarlo, S.E. (2010). Structural neuroplasticity following T5 spinal cord transection: increased cardiac sympathetic innervation density and SPN arborization. Am. J. Physiol. Regul. Integr. Comp. Physiol. 299, R985-95.

168. Lujan, H.L., Janbaih, H., and DiCarlo, S.E. (2012). Dynamic interaction between the heart and its sympathetic innervation following T5 spinal cord transection. J. Appl. Physiol. 113, 1332–41.

169. Houtman, S., Oeseburg, B., MTE, H., S., H., B., O., Houtman, S., Oeseburg, B., and Hopman, M.T. (2000). Blood volume and hemoglobin after spinal cord injury. Am. J. Phys. Med. Rehabil. 79, 260–265.

170. West, C.R., Squair, J.W., Currie, K.D., McCracken, L., Somvanshi, R., Yuen, V., Phillips, A.A., Kumar, U., McNeill, J., and Krassioukov, A. (2016). Cardiac consequences of autonomic dysreflexia in spinal cord injury. Hypertension. 68(5), 1281-1289.

171. Pacher, P., Nagayama, T., Mukhopadhyay, P., Bátkai, S., and Kass, D.A. (2008). Measurement of cardiac function using pressure-volume conductance catheter technique in mice and rats. Nat. Protoc. 3, 1422–34.

172. Bigford, G.E., Bracchi-Ricard, V.C., Keane, R.W., Nash, M.S., and Bethea, J.R. (2013). Neuroendocrine and cardiac metabolic dysfunction and NLRP3 inflammasome activation in adipose tissue and pancreas following chronic spinal cord injury in the mouse. ASN Neuro 5, 243–55.

173. Strack, A.M., Sawyer, W.B., Marubio, L.M., and Loewy, A.D. (1988). Spinal origin of sympathetic preganglionic neurons in the rat. Brain Res. 455, 187–91.

174. Squair, J.W., West, C.R., Popok, D., Assinck, P., Liu, J., Tetzlaff, W., and Krassioukov, A. V. (2016). High Thoracic Contusion Model for the Investigation of Cardiovascular Function after Spinal Cord Injury. J. Neurotrauma 34(3), 671-684.

175. Inskip, J.A., Ramer, L.M., Ramer, M.S., Krassioukov, A. V., and Claydon, V.E. (2012). Spectral Analyses of Cardiovascular Control in Rodents with Spinal Cord Injury. J. Neurotrauma 29, 1638–1649.

176. Schmittgen, T.D., and Livak, K.J. (2008). Analyzing real-time PCR data by the comparative CT method. Nat. Protoc. 3, 1101–1108.

177. Burkhoff, D., Mirsky, I., and Suga, H. (2005). Assessment of systolic and diastolic

ventricular properties via pressure-volume analysis: a guide for clinical, translational, and basic researchers. Am. J. Physiol. Heart Circ. Physiol. 289, H501-12.

178. de Groot, P.C., van Dijk, A., Dijk, E., and Hopman, M.T. (2006). Preserved cardiac function after chronic spinal cord injury. Arch. Phys. Med. Rehabil. 87, 1195–200.

179. Levine, B.D., Zuckerman, J.H., and Pawelczyk, J.A. (1997). Cardiac Atrophy After Bed-Rest Deconditioning : A Nonneural Mechanism for Orthostatic Intolerance. Circulation 96, 517–525.

180. Perhonen, M.A., Zuckerman, J.H., and Levine, B.D. (2001). Deterioration of Left Ventricular Chamber Performance After Bed Rest : "Cardiovascular Deconditioning" or Hypovolemia? Circulation 103, 1851–1857.

181. Claydon, V.E., and Krassioukov, A. V. (2008). Clinical correlates of frequency analyses of cardiovascular control after spinal cord injury. Am. J. Physiol. Heart Circ. Physiol. 294, H668-78.

182. Schmid, A., Huonker, M., Stahl, F., Barturen, J.M., König, D., Heim, M., Lehmann, M., and Keul, J. (1998). Free plasma catecholamines in spinal cord injured persons with different injury levels at rest and during exercise. J. Auton. Nerv. Syst. 68, 96–100.

183. Schmid, A., Huonker, M., Barturen, J.-M., Stahl, F., Schmidt-Trucksass, A., Konig, D., Grathwohl, D., Lehmann, M., and Keul, J. (1998). Catecholamines, heart rate, and oxygen uptake during exercise in persons with spinal cord injury. J Appl Physiol 85, 635–641.

184. Zaglia, T., Milan, G., Franzoso, M., Bertaggia, E., Pianca, N., Piasentini, E., Voltarelli, V.A., Chiavegato, D., Brum, P.C., Glass, D.J., Schiaffino, S., Sandri, M., and Mongillo,

M. (2013). Cardiac sympathetic neurons provide trophic signal to the heart via 2-adrenoceptor-dependent regulation of proteolysis. Cardiovasc. Res. 97, 240–250.

185. Hein, S., Scholz, D., Fujitani, N., Rennollet, H., Brand, T., Friedl, A., and Schaper, J. (1994). Altered expression of titin and contractile proteins in failing human myocardium. J. Mol. Cell. Cardiol. 26, 1291–306.

186. Knöll, R., Hoshijima, M., Hoffman, H.M., Person, V., Lorenzen-Schmidt, I., Bang, M.-L., Hayashi, T., Shiga, N., Yasukawa, H., Schaper, W., McKenna, W., Yokoyama, M., Schork, N.J., Omens, J.H., McCulloch, A.D., Kimura, A., Gregorio, C.C., Poller, W., Schaper, J., Schultheiss, H.P., and Chien, K.R. (2002). The cardiac mechanical stretch sensor machinery involves a Z disc complex that is defective in a subset of human dilated cardiomyopathy. Cell 111, 943–55.

187. Penicka, M., Bartunek, J., Trakalova, H., Hrabakova, H., Maruskova, M., Karasek, J., and Kocka, V. (2010). Heart Failure With Preserved Ejection Fraction in Outpatients With Unexplained Dyspnea: A Pressure-Volume Loop Analysis. J. Am. Coll. Cardiol. 55, 1701–1710.

188. DeVeau, K.M., Martin, E.K., King, N.T., Shum-Siu, A., Keller, B.B., West, C.R., and Magnuson, D.S.K. (2016). Challenging cardiac function post-spinal cord injury with dobutamine. Auton. Neurosci. .

189. Thompson, E.W., Marino, T.A., Uboh, C.E., Kent, R.L., and Cooper, G. (1984). Atrophy reversal and cardiocyte redifferentiation in reloaded cat myocardium. Circ. Res. 54, 367–77.

190. Hein, S., Kostin, S., Heling, A., Maeno, Y., and Schaper, J. (2000). The role of the cytoskeleton in heart failure. Cardiovasc. Res. 45, 273–8.

191. Belin, R.J., Sumandea, M.P., Allen, E.J., Schoenfelt, K., Wang, H., Solaro, R.J., and de Tombe, P.P. (2007). Augmented protein kinase C-alpha-induced myofilament protein phosphorylation contributes to myofilament dysfunction in experimental congestive heart failure. Circ. Res. 101, 195–204.

192. Kuo, P.-L., Lee, H., Bray, M.-A., Geisse, N.A., Huang, Y.-T., Adams, W.J., Sheehy, S.P., and Parker, K.K. (2012). Myocyte shape regulates lateral registry of sarcomeres and contractility. Am. J. Pathol. 181, 2030–7.

193. Hansson, J., Vasan, R.S., Ärnlöv, J., Ingelsson, E., Lind, L., Larsson, A., Michaëlsson, K., and Sundström, J. (2011). Biomarkers of extracellular matrix metabolism (MMP-9 and TIMP-1) and risk of stroke, myocardial infarction, and cause-specific mortality: cohort study. PLoS One 6, e16185.

194. Hansson, J., Lind, L., Hulthe, J., and Sundström, J. (2009). Relations of serum MMP-9 and TIMP-1 levels to left ventricular measures and cardiovascular risk factors: a population-based study. Eur. J. Cardiovasc. Prev. Rehabil. 16, 297–303.

195. Braunwald, E., Ross, J., Gault, J.H., Mason, D.T., Mills, C., Gabe, I.T., and Epstein, S.E. (1969). NIH clinical staff conference. Assessment of cardiac function. Ann. Intern. Med. 70, 369–99.

196. Braunwald, E., Ross, J., and Sonnenblick, E.H. (1967). Mechanisms of contraction of the normal and failing heart. N. Engl. J. Med. 277, 1012–22 concl.

197. Garshick, E., Kelley, A., Cohen, S.A., Garrison, A., Tun, C.G., Gagnon, D., and Brown, R. (2005). A prospective assessment of mortality in chronic spinal cord injury. Spinal Cord 43, 408–416.

198. Squair, J.W., DeVeau, K.M., Harman, K.A., Poormasjedi-Meibod, M.S., Hayes, B., Liu J., Magnusun, D.S.K., Krassioukov, A.V., West, C.R. (2018). Spinal cord injury induced sympathetic decentralization causes cardiac atrophy and systolic dysfunction. Journal of Neurotrauma. 35(3):424-434.

199. Lujan, H.L., and DiCarlo, S.E. (2017). Fundamental hemodynamic mechanisms mediating the response to myocardial ischemia in conscious paraplegic mice: cardiac output versus peripheral resistance. Physiol. Rep. 5, e13214.

200. Langeland, S., Wouters, P.F., Claus, P., Leather, H.A., Bijnens, B., Sutherland, G.R., Rademakers, F.E., and D'hooge, J. (2006). Experimental assessment of a new research tool for the estimation of two-dimensional myocardial strain. Ultrasound Med. Biol. 32, 1509–1513.

201. Amundsen, B.H., Helle-Valle, T., Edvardsen, T., Torp, H., Crosby, J., Lyseggen, E., Støylen, A., Ihlen, H., Lima, J.A.C., Smiseth, O.A., and Slørdahl, S.A. (2006). Noninvasive myocardial strain measurement by speckle tracking echocardiography: validation against sonomicrometry and tagged magnetic resonance imaging. J. Am. Coll. Cardiol. 47, 789–93.

202. Raymond, J., Davis, G.M., Bryant, G., and Clarke, J. (1999). Cardiovascular responses to an orthostatic challenge and electrical-stimulation-induced leg muscle contractions in individuals with paraplegia. Eur. J. Appl. Physiol. Occup. Physiol. 80, 205–12.

203. Faghri, P.D., and Yount, J. (2002). Electrically induced and voluntary activation of physiologic muscle pump: a comparison between spinal cord-injured and able-bodied individuals. Clin. Rehabil. 16, 878–85.

204. Wecht, J.M., de Meersman, R.E., Weir, J.P., Bauman, W.A., and Grimm, D.R. (2000). Effects of autonomic disruption and inactivity on venous vascular function. Am J Physiol Hear. Circ Physiol 278, H515-520.

205. Miyatake, K., Yamagishi, M., Tanaka, N., Uematsu, M., Yamazaki, N., Mine, Y., Sano, A., and Hirama, M. (1995). New method for evaluating left ventricular wall motion by color-coded tissue doppler imaging: In vitro and in vivo studies. J. Am. Coll. Cardiol. 25, 717–724.

206. Nishimura, K., Okayama, H., Inoue, K., Saito, M., Yoshii, T., Hiasa, G., Sumimoto, T., Inaba, S., Ogimoto, A., Funada, J., and Higaki, J. (2012). Direct measurement of radial strain in the inner-half layer of the left ventricular wall in hypertensive patients. J. Cardiol. 59, 64–71.

207. Perhonen, M.A., Franco, F., Lane, L.D., Buckey, J.C., Blomqvist, C.G., Zerwekh, J.E., Peshock, R.M., Weatherall, P.T., and Levine, B.D. (2001). Cardiac atrophy after bed rest and spaceflight. J Appl Physiol 91, 645–653.

208. de Jonge, N., van Wichen, D.F., Schipper, M.E.I., Lahpor, J.R., Gmelig-Meyling, F.H.J., Robles de Medina, E.O., and de Weger, R.A. (2002). Left ventricular assist device in end-stage heart failure: persistence of structural myocyte damage after unloading. J. Am. Coll. Cardiol. 39, 963–969.

209. Teasell, R.W., Arnold, J.M.O., Krassioukov, A., and Delaney, G.A. (2000).

Cardiovascular consequences of loss of supraspinal control of the sympathetic nervous system after spinal cord injury. Arch. Phys. Med. Rehabil. 81, 506–516.

210. DeVeau, K.M., Harman, K.A., Squair, J.W., Krassioukov, A. V., Magnuson, D., and West, C.R. (2017). A comparison of passive hind-limb cycling and active upper-limb exercise provides new insights into systolic dysfunction following spinal cord injury. Am. J. Physiol. - Hear. Circ. Physiol.

211. Fawcett, J.W., Curt, A., Steeves, J.D., Coleman, W.P., Tuszynski, M.H., Lammertse, D., Bartlett, P.F., Blight, A.R., Dietz, V., Ditunno, J., Dobkin, B.H., Havton, L.A., Ellaway, P.H., Fehlings, M.G., Privat, A., Grossman, R., Guest, J.D., Kleitman, N., Nakamura, M., Gaviria, M., and Short, D. (2007). Guidelines for the conduct of clinical trials for spinal cord injury as developed by the ICCP panel: spontaneous recovery after spinal cord injury and statistical power needed for therapeutic clinical trials. Spinal Cord 45, 190–205.

212. Thibault-Halman, G., Rivers, C.S., Bailey, C.S., Tsai, E.C., Drew, B., Noonan, V.K., Fehlings, M.G., Dvorak, M.F., Kuerban, D., Kwon, B.K., and Christie, S.D. (2017). Predicting Recruitment Feasibility for Acute Spinal Cord Injury Clinical Trials in Canada Using National Registry Data. J. Neurotrauma 34, 599–606.

213. Tator, C.H., and Fehlings, M.G. (1999). Review of clinical trials of neuroprotection in acute spinal cord injury. Neurosurg. Focus 6, e8.

214. Bracken, M.B., Shepard, M.J., Collins, W.F., Holford, T.R., Young, W., Baskin, D.S., Eisenberg, H.M., Flamm, E., Leo-Summers, L., Maroon, J., Marshall, L.F., Perot, P.L., Piepmeier, J., Sonntag, V.K.H., Wagner, F.C., Wilberger, J.E., and Winn, H.R. (1990). A Randomized, Controlled Trial of Methylprednisolone or Naloxone in the Treatment of

Acute Spinal-Cord Injury. N. Engl. J. Med. 322, 1405–1411.

215. Casha, S., Zygun, D., McGowan, M.D., Bains, I., Yong, V.W., and Hurlbert, R.J. (2012). Results of a phase II placebo-controlled randomized trial of minocycline in acute spinal cord injury. Brain 135, 1224–1236.

216. Geisler, F.H., Coleman, W.P., Grieco, G., and Poonian, D. (2001). The Sygen multicenter acute spinal cord injury study. Spine (Phila Pa 1976) 26, S87-98.

217. Fehlings, M.G., Kopjar, B., and Grossman, R.G. (2016). 329   Efficacy and Safety of Riluzole in Acute Spinal Cord Injury. Neurosurgery 63, 196.

218. Teng, Y.D., Choi, H., Onario, R.C., Zhu, S., Desilets, F.C., Lan, S., Woodard, E.J., Snyder, E.Y., Eichler, M.E., and Friedlander, R.M. (2004). Minocycline inhibits contusion-triggered mitochondrial cytochrome c release and mitigates functional deficits after spinal cord injury. Proc. Natl. Acad. Sci. U. S. A. 101, 3071–6.

219. Wells, J.E.A., Hurlbert, R.J., Fehlings, M.G., and Yong, V.W. (2003). Neuroprotection by minocycline facilitates significant recovery from spinal cord injury in mice. Brain 126, 1628–37.

220. Yong, V.W., Wells, J., Giuliani, F., Casha, S., Power, C., and Metz, L.M. (2004). The promise of minocycline in neurology. Lancet Neurol. 3, 744–751.

221. Stirling, D.P. (2004). Minocycline Treatment Reduces Delayed Oligodendrocyte Death, Attenuates Axonal Dieback, and Improves Functional Outcome after Spinal Cord Injury. J. Neurosci. 24, 2182–2190.

222. Kobayashi, K., Imagama, S., and Ohgomori, T. (2013). Minocycline selectively inhibits M1 polarization of microglia. Cell death … .

223. Conover, W.J., and Iman, R.L. (1981). Rank Transformations as a Bridge between

Parametric and Nonparametric Statistics. Am. Stat. 35, 124–129.

224. Simard, J.M., Tsymbalyuk, O., Keledjian, K., Ivanov, A., Ivanova, S., and Gerzanich, V. (2012). Comparative effects of glibenclamide and riluzole in a rat model of severe cervical spinal cord injury. Exp. Neurol. 233, 566–574.

225. Soma, L.R. (1983). Anesthetic and analgesic considerations in the experimental animal. Ann. N. Y. Acad. Sci. 406, 32–47.

226. Stirling, D.P., Khodarahmi, K., Liu, J., McPhail, L.T., McBride, C.B., Steeves, J.D., Ramer, M.S., and Tetzlaff, W. (2004). Minocycline treatment reduces delayed oligodendrocyte death, attenuates axonal dieback, and improves functional outcome after spinal cord injury. J. Neurosci. 24, 2182–90.

227. Lee, S.M., Yune, T.Y., Kim, S.J., Park, D.W., Lee, Y.K., Kim, Y.C., Oh, Y.J., Markelonis, G.J., and Oh, T.H. (2003). Minocycline reduces cell death and improves functional recovery after traumatic spinal cord injury in the rat. J. Neurotrauma 20, 1017–1027.

228. Festoff, B.W., Ameenuddin, S., Arnold, P.M., Wong, A., Santacruz, K.S., and Citron, B.A. (2006). Minocycline neuroprotects, reduces microgliosis, and inhibits caspase protease expression early after spinal cord injury. J. Neurochem. 97, 1314–26.

229. Yune, T.Y., Lee, J.Y., Jung, G.Y., Kim, S.J., Jiang, M.H., Kim, Y.C., Oh, Y.J., Markelonis, G.J., and Oh, T.H. (2007). Minocycline alleviates death of oligodendrocytes by inhibiting pro-nerve growth factor production in microglia after spinal cord injury. J. Neurosci. 27, 7751–61.

230. Ha, K.-Y., Kim, Y.-H., Rhyu, K.-W., and Kwon, S.-E. (2008). Pregabalin as a neuroprotector after spinal cord injury in rats. Eur. Spine J. 17, 864–72.

231. Stivers, N.S., Pelisch, N., Orem, B.C., Williams, J., Nally, J.M., and Stirling, D.P. (2017). The toll-like receptor 2 agonist Pam3CSK4 is neuroprotective after spinal cord injury. Exp. Neurol. 294, 1–11.

232. Evans, T.A., Barkauskas, D.S., Myers, J.T., Hare, E.G., You, J.Q., Ransohoff, R.M., Huang, A.Y., and Silver, J. (2014). High-resolution intravital imaging reveals that blood-derived macrophages but not resident microglia facilitate secondary axonal dieback in traumatic spinal cord injury. Exp. Neurol. 254, 109–120.

233. Pallini, R., Fernandez, E., and Sbriccoli, A. (1988). Retrograde degeneration of corticospinal axons following transection of the spinal cord in rats. J. Neurosurg. 68, 124–128.

234. Sonmez, E., Kabatas, S., Ozen, O., Karabay, G., Turkoglu, S., Ogus, E., Yilmaz, C., Caner, H., and Altinors, N. (2013). Minocycline treatment inhibits lipid peroxidation, preserves spinal cord ultrastructure, and improves functional outcome after traumatic spinal cord injury in the rat. Spine (Phila. Pa. 1976). 38, 1253–9.

235. Chen, D., Zeng, W., Fu, Y., Gao, M., and Lv, G. (2015). Bone marrow mesenchymal stem cells combined with minocycline improve spinal cord injury in a rat model.8, 11957–11969.

236. Ahmad, M., Zakaria, A., and Almutairi, K.M. (2016). Effectiveness of minocycline and FK506 alone and in combination on enhanced behavioral and biochemical recovery from spinal cord injury in rats. Pharmacol. Biochem. Behav. 145, 45–54.

237. Wang, Z., Nong, J., Shultz, R.B., Zhang, Z., Kim, T., Tom, V.J., Ponnappan, R.K., and Zhong, Y. (2017). Local delivery of minocycline from metal ion-assisted self-assembled complexes promotes neuroprotection and functional recovery after spinal cord injury.

Biomaterials 112, 62–71.

238. Papa, S., Caron, I., Erba, E., Panini, N., De Paola, M., Mariani, A., Colombo, C., Ferrari, R., Pozzer, D., Zanier, E.R., Pischiutta, F., Lucchetti, J., Bassi, A., Valentini, G., Simonutti, G., Rossi, F., Moscatelli, D., Forloni, G., and Veglianese, P. (2016). Early modulation of pro-inflammatory microglia by minocycline loaded nanoparticles confers long lasting protection after spinal cord injury. Biomaterials 75, 13–24.

239. Cho, D.C., Cheong, J.H., Yang, M.S., Hwang, S.J., Kim, J.M., and Kim, C.H. (2011). The Effect of Minocycline on Motor Neuron Recovery and Neuropathic Pain in a Rat Model of Spinal Cord Injury. J. Korean Neurosurg. Soc. 49, 83.

240. Furlan, J.C., Fehlings, M.G., Halliday, W., and Krassioukov, A. V. (2003). Autonomic dysreflexia associated with intramedullary astrocytoma of the spinal cord. Lancet. Oncol. 4, 574–5.

241. Squair, J.W., Phillips, A.A., Harmon, M., and Krassioukov, A. V. (2016). Emergency management of autonomic dysreflexia with neurologic complications. CMAJ .

242. Phillips, A., Matin, N., West, C., Zheng, A., Galea, L., Dorrance, A., Laher, I., and Krassioukov, A. (2015). Autonomic Dysreflexia Impairs Cerebrovascular Health and Cognition in Experimental Spinal Cord Injury. FASEB J. 29, 800.10.

243. Squair, J.W., Liu, J., Tetzlaff, W., Krassioukov, A.V., West, C.R. (2017). Spinal cord injury induced cardiomyocyte atrophy and impaired cardiac function are severity dependent. Experimental Physiology. 103(2):179-189.

244. Poormasjedi-Meibod M.S., Mansouri, M., Fossey, M., Squair, J.W., Liu, J., McNeill, J.H., West, C.R. (2018). Experimental spinal cord injury causes left-ventricular atrophy and is associated with an upregulation of proteolytic pathways. Journal of Neurotrauma.

In press.

245. Hawryluk, G., Whetstone, W., Saigal, R., Ferguson, A., Talbott, J., Bresnahan, J., Dhall, S., Pan, J., Beattie, M., Manley, G.: Mean Arterial Blood Pressure Correlates with Neurological Recovery after Human Spinal Cord Injury: Analysis of High Frequency Physiologic Data. Journal of Neurotrauma 32(24), 1958–67 (2015).

246. Tee, J.W., Altaf, F., Belanger, L.M., Ailon, T., Street, J., Paquette, S.J., Boyd, M.C., Fisher, C.G., Dvorak, M.F., Kwon, B.K.: Mean arterial blood pressure management of acute spinal cord injured patients during the pre-hospital and early admission period. Journal of Neurotrauma 34(6), 1271–1277 (2016).

247. Fehlings, M.G., Vaccaro, A., Wilson, J.R., Singh, A., Cadotte, D.W., Harrop, J.S., Aarabi, B., Shaffrey, C., Dvorak, M., Fisher, C., Arnold, P., Massicotte, E.M., Lewis, S., Rampersaud, R.: Early versus delayed decompression for traumatic cervical spinal cord injury: Results of the surgical timing in acute spinal cord injury study (STASCIS). PLoS ONE 7(2), 32037 (2012).

248. Kigerl, K.A., Gensel, J.C., Ankeny, D.P., Alexander, J.K., Donnelly, D.J., Popovich, P.G.: Identification of Two Distinct Macrophage Subsets with Divergent Effects Causing either Neurotoxicity or Regeneration in the Injured Mouse Spinal Cord. Journal of Neuroscience 29(43), 13435–13444 (2009).

249. Demjen, D., Klussmann, S., Kleber, S., Zuliani, C., Stieltjes, B., Metzger, C., Hirt, U.a., Walczak, H., Falk, W., Essig, M., Edler, L., Krammer, P.H., Martin-Villalba, A.: Neutralization of CD95 ligand promotes regeneration and functional recovery after spinal cord injury. Nature Medicine 10(4), 389–95 (2004).

250. Springer, J.E., Azbill, R.D., Knapp, P.E.: Activation of the caspase-3 apoptotic cascade in

traumatic spinal cord injury. Nature Medicine 5(8), 943–946 (1999). doi:10.1038/11387

251. Crowe, M.J., Bresnahan, J.C., Shuman, S.L., Masters, J.N., Beattie, M.S.: Apoptosis and delayed degeneration after spinal cord injury in rats and monkeys. Nature Medicine 3(1), 73–76 (1997).

252. GrandPre, T., Nakamura, F., Vartanian, T., Strittmatter, S.M.: Identification of the Nogo inhibitor of axon regeneration as a Reticulon protein. Nature 403(6768), 439–44 (2000).

253. Schnell, L., Schwab, M.E.: Axonal regeneration in the rat spinal cord produced by an antibody against myelin-associated neurite growth inhibitors. Nature 343(6255), 269–272 (1990).

254. Bradbury, E.J., Moon, L.D.F., Popat, R.J., King, V.R., Bennett, G.S., Patel, P.N., Fawcett, J.W., McMahon, S.B.: Chondroitinase ABC promotes functional recovery after spinal cord injury. Nature 416(6881), 636–640 (2002).

255. Kwon, B.K., Streijger, F., Fallah, N., Noonan, V.K., B´elanger, L.M., Ritchie, L., Paquette, S.J., Ailon, T., Boyd, M.C., Street, J., Fisher, C.G., Dvorak, M.F.: Cerebrospinal Fluid Biomarkers To Stratify Injury Severity and Predict Outcome in Human Traumatic Spinal Cord Injury. Journal of Neurotrauma 34(3), 567–580 (2017).

256. Voineagu, I., Wang, X., Johnston, P., Lowe, J.K., Tian, Y., Horvath, S., Mill, J., Cantor, R.M., Blencowe, B.J., Geschwind, D.H.: Transcriptomic analysis of autistic brain reveals convergent molecular pathology. Nature 474(7351), 380–384 (2011).

257. Parikshak, N.N., Luo, R., Zhang, A., Won, H., Lowe, J.K., Chandran, V., Horvath, S., Geschwind, D.H.: Integrative functional genomic analyses implicate specific molecular pathways and circuits in autism. Cell 155(5), 1008–1021 (2013)

258. Zhang, B., Gaiteri, C., Bodea, L.-G., Wang, Z., McElwee, J., Podtelezhnikov, A.A.,

Zhang, C., Xie, T., Tran, L., Dobrin, R., Fluder, E., Clurman, B., Melquist, S., Narayanan, M., Suver, C., Shah, H., Mahajan, M., Gillis, T., Mysore, J., MacDonald, M.E., Lamb, J.R., Bennett, D.A., Molony, C., Stone, D.J., Gudnason, V., Myers, A.J., Schadt, E.E., Neumann, H., Zhu, J., Emilsson, V.: Integrated systems approach identifies genetic nodes and networks in late-onset Alzheimer's disease. Cell 153(3), 707–20 (2013).

259. Johnson, M.R., Shkura, K., Langley, S.R., Delahaye-Duriez, A., Srivastava, P., Hill, W.D., Rackham, O.J., Davies, G., Harris, S.E., Moreno-Moral, A., et al.: Systems genetics identifies a convergent gene network for cognition and neurodevelopmental disease. Nature Neuroscience 19(2), 223–232 (2016)

260. Zhang, B., Horvath, S.: A general framework for weighted gene co-expression network analysis. Statistical Applications in Genetics and Molecular Biology 4(1) (2005)

261. Parikshak, N.N., Gandal, M.J., Geschwind, D.H.: Systems biology and gene networks in neurodevelopmental and neurodegenerative disorders. Nature Reviews Genetics 16(8), 441–458 (2015)

262. Ashburner, M., Ball, C.A., Blake, J.A., Botstein, D., Butler, H., Cherry, J.M., Davis, A.P., Dolinski, K., Dwight, S.S., Eppig, J.T., Harris, M.A., Hill, D.P., Issel-Tarver, L., Kasarskis, A., Lewis, S., Matese, J.C., Richardson, J.E., Ringwald, M., Rubin, G.M., Sherlock, G.: Gene ontology: tool for the unification of biology. The Gene Ontology Consortium. Nature Genetics 25(1), 25–9 (2000).

263. Ghiassian, S.D., Menche, J., Barab́asi, A.-L.: A DIseAse MOdule Detection (DIAMOnD) Algorithm Derived from a Systematic Analysis of Connectivity Patterns of Disease Proteins in the Human Interactome. PLoS Computational Biology 11(4),

1004120 (2015).

264. Langfelder, P., Cantle, J.P., Chatzopoulou, D., Wang, N., Gao, F., Al-Ramahi, I., Lu, X.-H., Ramos, E.M., El-Zein, K., Zhao, Y., Deverasetty, S., Tebbe, A., Schaab, C., Lavery, D.J., Howland, D., Kwak, S., Botas, J., Aaronson, J.S., Rosinski, J., Coppola, G., Horvath, S., Yang, X.W.: Integrated genomics and proteomics define huntingtin CAG length-dependent networks in mice. Nature neuroscience 19(4), 623–33 (2016).

265. Delahaye-Duriez, A., Srivastava, P., Shkura, K., Langley, S.R., Laaniste, L., Moreno-Moral, A., Danis, B., Mazzuferi, M., Foerch, P., Gazina, E.V., Richards, K., Petrou, S., Kaminski, R.M., Petretto, E., Johnson, M.R.: Rare and common epilepsies converge on a shared gene regulatory network providing opportunities for novel antiepileptic drug discovery. Genome Biology 17(1), 245 (2016).

266. Johnson, M.R., Behmoaras, J., Bottolo, L., Krishnan, M.L., Pernhorst, K., Santoscoy, P.L.M., Rossetti, T., Speed, D., Srivastava, P.K., Chadeau-Hyam, M., Hajji, N., Dabrowska, A., Rotival, M., Razzaghi, B., Kovac, S., Wanisch, K., Grillo, F.W., Slaviero, A., Langley, S.R., Shkura, K., Roncon, P., De, T., Mattheisen, M., Niehusmann, P., O'Brien, T.J., Petrovski, S., von Lehe, M., Hoffmann, P., Eriksson, J., Coffey, A.J., Cichon, S., Walker, M., Simonato, M., Danis, B., Mazzuferi, M., Foerch, P., Schoch, S., De Paola, V., Kaminski, R.M., Cunliffe, V.T., Becker, A.J., Petretto, E.: Systems genetics identifies Sestrin 3 as a regulator of a proconvulsant gene network in human epileptic hippocampus. Nature Communications 6, 6031 (2015).

267. Chen, C., Cheng, L., Grennan, K., Pibiri, F., Zhang, C., Badner, J.A., Members of the Bipolar Disorder Genome Study (BiGS) Consortium, E.S., Gershon, E.S., Liu, C.: Two gene co-expression modules differentiate psychotics and controls. Molecular Psychiatry

18(12), 1308–14 (2013).

268. Fromer, M., Roussos, P., Sieberts, S.K., Johnson, J.S., Kavanagh, D.H., Perumal, T.M., Ruderfer, D.M., Oh, E.C., Topol, A., Shah, H.R., Klei, L.L., Kramer, R., Pinto, D., Guˉmuˉ̧s, Z.H., Cicek, A.E., Dang, K.K., Browne, A., Lu, C., Xie, L., Readhead, B., Stahl, E.A., Xiao, J., Parvizi, M., Hamamsy, T., Fullard, J.F., Wang, Y.-C., Mahajan, M.C., Derry, J.M.J., Dudley, J.T., Hemby, S.E., Logsdon, B.A., Talbot, K., Raj, T., Bennett, D.A., De Jager, P.L., Zhu, J., Zhang, B., Sullivan, P.F., Chess, A., Purcell, S.M., Shinobu, L.A., Mangravite, L.M., Toyoshiba, H., Gur, R.E., Hahn, C.-G., Lewis, D.A., Haroutunian, V., Peters, M.A., Lipska, B.K., Buxbaum, J.D., Schadt, E.E., Hirai, K., Roeder, K., Brennand, K.J., Katsanis, N., Domenici, E., Devlin, B., Sklar, P.: Gene expression elucidates functional impact of polygenic risk for schizophrenia. Nature Neuroscience 19(11), 1442–1453 (2016).

269. GTEx Consortium, T.G.: The Genotype-Tissue Expression (GTEx) project. Nature Genetics 45(6), 580–5 (2013).

270. Langfelder, P., Horvath, S.: WGCNA: an R package for weighted correlation network analysis. BMC Bioinformatics 9(1), 559 (2008).

271. Leek, J.T., Johnson, W.E., Parker, H.S., Jaffe, A.E., Storey, J.D.: The sva package for removing batch effects and other unwanted variation in high-throughput experiments. Bioinformatics (Oxford, England) 28(6), 882–3 (2012).

272. Vandenbon, A., Dinh, V.H., Mikami, N., Kitagawa, Y., Teraguchi, S., Ohkura, N., Sakaguchi, S.: Immuno-navigator, a batch-corrected coexpression database, reveals cell type-specific gene networks in the immune system. Proceedings of the National Academy of Sciences 113(17), 2393–2402 (2016)

273. Langfelder, P., Luo, R., Oldham, M.C., Horvath, S.: Is my network module preserved and reproducible? PLoS Computational Biology 7(1), 1001057 (2011).

274. Langfelder, P., Horvath, S.: Eigengene networks for studying the relationships between co-expression modules. BMC Systems Biology 1(1), 54 (2007).

275. Liberzon, A., Subramanian, A., Pinchback, R., Thorvaldsdóttir, H., Tamayo, P., Mesirov, J.P.: Molecular signatures database (msigdb) 3.0. Bioinformatics 27(12), 1739–1740 (2011)

276. Merico, D., Isserlin, R., Stueker, O., Emili, A., Bader, G.D.: Enrichment map: a network-based method for gene-set enrichment visualization and interpretation. PloS one 5(11), 13984 (2010)

277. Zhang, Y., Chen, K., Sloan, S.A., Bennett, M.L., Scholze, A.R., O'Keeffe, S., Phatnani, H.P., Guarnieri, P., Caneda, C., Ruderisch, N., Deng, S., Liddelow, S.A., Zhang, C., Daneman, R., Maniatis, T., Barres, B.A., Wu, J.Q.: An RNA-Sequencing Transcriptome and Splicing Database of Glia, Neurons, and Vascular Cells of the Cerebral Cortex. Journal of Neuroscience 34(36), 11929–11947 (2014).

278. Sharma, K., Schmitt, S., Bergner, C.G., Tyanova, S., Kannaiyan, N., Manrique-Hoyos, N., Kongi, K., Cantuti, L., Hanisch, U.-K., Philips, M.-A., et al.: Cell type–and brain region–resolved mouse brain proteome. Nature neuroscience 18(12), 1819 (2015)

279. Cahoy, J.D., Emery, B., Kaushal, A., Foo, L.C., Zamanian, J.L., Christopherson, K.S., Xing, Y., Lubischer, J.L., Krieg, P.A., Krupenko, S.A., et al.: A transcriptome database for astrocytes, neurons, and oligodendrocytes: a new resource for understanding brain development and function. Journal of Neuroscience 28(1), 264–278 (2008)

280. Di Giovanni, S., Knoblach, S.M., Brandoli, C., Aden, S.A., Hoffman, E.P., Faden, A.I.:

Gene profiling in spinal cord injury shows role of cell cycle in neuronal death. Annals of Neurology 53(4), 454–68 (2003).

281. De Biase, A., Knoblach, S.M., Di Giovanni, S., Fan, C., Molon, A., Hoffman, E.P., Faden, A.I.: Gene expression profiling of experimental traumatic spinal cord injury as a function of distance from impact site and injury severity. Physiological Genomics 22(3), 368–81 (2005).

282. Horvath, S., Zhang, B., Carlson, M., Lu, K., Zhu, S., Felciano, R., Laurance, M., Zhao, W., Qi, S., Chen, Z., et al.: Analysis of oncogenic signaling networks in glioblastoma identifies aspm as a molecular target. Proceedings of the National Academy of Sciences 103(46), 17402–17407 (2006)

283. Didangelos, A., Puglia, M., Iberl, M., Sanchez-Bellot, C., Roschitzki, B., Bradbury, E.J.: High-throughput proteomics reveal alarmins as amplifiers of tissue pathology and inflammation after spinal cord injury. Scientific reports 6, 21607 (2016)

284. Moghieb, A., Bramlett, H.M., Das, J.H., Yang, Z., Selig, T., Yost, R.A., Wang, M.S., Dietrich, W.D., Wang, K.K.: Differential neuroproteomic and systems biology analysis of spinal cord injury. Molecular & Cellular Proteomics 15(7), 2379–2395 (2016)

285. Gao, Q., Liang, Y., Yang, X., Liu, G., Li, X., Zhu, B., Liu, J., Yang, M., Xia, W., Dong, J., et al.: Differential protein expression in spinal cord tissue of a rabbit model of spinal cord ischemia/reperfusion injury. Neural regeneration research 7(20), 1534 (2012)

286. Fortelny, N., Overall, C.M., Pavlidis, P., Freue, G.V.C.: Can we predict protein from mrna levels? Nature 547(7664), 19 (2017)

287. Duan, H., Ge, W., Zhang, A., Xi, Y., Chen, Z., Luo, D., Cheng, Y., Fan, K.S., Horvath, S., Sofroniew, M.V., Cheng, L., Yang, Z., Sun, Y.E., Li, X.: Transcriptome analyses

reveal molecular mechanisms underlying functional recovery after spinal cord injury. Proceedings of the National Academy of Sciences of the United States of America 112(43), 13360–5 (2015).

288.   Yang, Z., Zhang, A., Duan, H., Zhang, S., Hao, P., Ye, K., Sun, Y.E., Li, X.: NT3-chitosan elicits robust endogenous neurogenesis to enable functional recovery after spinal cord injury. Proceedings of the National Academy of Sciences of the United States of America 112(43), 13354–9 (2015).

289.   Alto, L.T., Havton, L.A., Conner, J.M., Hollis II, E.R., Blesch, A., Tuszynski, M.H.: Chemotropic guidance facilitates axonal regeneration and synapse formation after spinal cord injury. Nature neuroscience 12(9), 1106 (2009)

290.   Anderson, M.A., Burda, J.E., Ren, Y., Ao, Y., O'Shea, T.M., Kawaguchi, R., Coppola, G., Khakh, B.S., Deming, T.J., Sofroniew, M.V.: Astrocyte scar formation aids central nervous system axon regeneration. Nature 532(7598), 195 (2016)

291.   Calabrese, G.M., Mesner, L.D., Stains, J.P., Tommasini, S.M., Horowitz, M.C., Rosen, C.J., Farber, C.R.: Integrating GWAS and Co-expression Network Data Identifies Bone Mineral Density Genes SPTBN1 and MARK3 and an Osteoblast Functional Module. Cell Systems 4(1), 1–14 (2016).

292.   Li, J., Shi, M., Ma, Z., Zhao, S., Euskirchen, G., Ziskin, J., Urban, A., Hallmayer, J., Snyder, M.: Integrated systems analysis reveals a molecular network underlying autism spectrum disorders. Molecular Systems Biology 10(12), 774–774 (2014).

293.   Huan, T., Meng, Q., Saleh, M.A., Norlander, A.E., Joehanes, R., Zhu, J., Chen, B.H., Zhang, B., Johnson, A.D., Ying, S., Courchesne, P., Raghavachari, N., Wang, R., Liu, P., O'Donnell, C.J., Vasan, R., Munson, P.J., Madhur, M.S., Harrison, D.G., Yang, X., Levy,

D.: Integrative network analysis reveals molecular mechanisms of blood pressure regulation. Molecular Systems Biology 11(4), 799–799 (2015).

294. Streijger, F., Skinnider, M.A., Rogalski, J.C., Balshaw, R., Shannon, C.P., Prudova, A., Belanger, L., Ritchie, L., Tsang, A., Christie, S., et al.: A targeted proteomics analysis of cerebrospinal fluid after acute human spinal cord injury. Journal of neurotrauma 34(12), 2054–2068 (2017)

295. Elderfield, A., Bolton, C., Flower, R.: Lipocortin 1 (annexin 1) immunoreactivity in the cervical spinal cord of lewis rats with acute experimental allergic encephalomyelitis. Journal of the neurological sciences 119(2), 146–153 (1993)

296. Liu, N.-K., Zhang, Y.P., Han, S., Pei, J., Xu, L.Y., Lu, P.-H., Shields, C.B., Xu, X.-M.: Annexin a1 reduces inflammatory reaction and tissue damage through inhibition of phospholipase a2 activation in adult rats following spinal cord injury. Journal of Neuropathology & Experimental Neurology 66(10), 932–943 (2007)

297. Perretti, M., Flower, R.J.: Modulation of il-1-induced neutrophil migration by dexamethasone and lipocortin 1. The Journal of Immunology 150(3), 992–999 (1993)

298. D'Acquisto, F., Paschalidis, N., Sampaio, A.L., Merghani, A., Flower, R.J., Perretti, M.: Impaired t cell activation and increased th2 lineage commitment in annexin-1-deficient t cells. European journal of immunology 37(11), 3131–3142 (2007)

299. Sudlow, A.W., Carey, F., Forder, R., Rothwell, N.J.: The role of lipocortin-1 in dexamethasone-induced suppression of pge2 and tnfα release from human peripheral blood mononuclear cells. British journal of pharmacology 117(7), 1449–1456 (1996)

300. McArthur, S., Cristante, E., Paterno, M., Christian, H., Roncaroli, F., Gillies, G.E., Solito, E.: Annexin a1: a central player in the anti-inflammatory and neuroprotective role of

microglia. The Journal of Immunology 185(10), 6317–6328 (2010)

301. 301. Hannon, R., Croxtall, J.D., Getting, S.J., Roviezzo, F., Yona, S., Paul-Clark, M.J., Gavins, F.N., Perretti, M., Morris, J.F., Buckingham, J.C., et al.: Aberrant inflammation and resistance to glucocorticoids in annexin 1-/- mouse. The FASEB Journal 17(2), 253–255 (2003)

302. Elderfield, A.-J., Newcombe, J., Bolton, C., Flower, R.: Lipocortins (annexins) 1, 2, 4 and 5 are increased in the central nervous system in multiple sclerosis. Journal of neuroimmunology 39(1), 91–100 (1992)

303. Liu, N., Han, S., Lu, P.-H., Xu, X.-M.: Upregulation of annexins i, ii, and v after traumatic spinal cord injury in adult rats. Journal of neuroscience research 77(3), 391–401 (2004)

304. Li, T., Wernersson, R., Hansen, R.B., Horn, H., Mercer, J., Slodkowicz, G., Workman, C.T., Rigina, O., Rapacki, K., Stærfeldt, H.H., Brunak, S., Jensen, T.S., Lage, K.: A scored human protein-protein interaction network to catalyze genomic interpretation. Nature Methods 14(1), 61–64 (2017).

305. Huerta-Cepas, J., Szklarczyk, D., Forslund, K., Cook, H., Heller, D., Walter, M.C., Rattei, T., Mende, D.R., Sunagawa, S., Kuhn, M., Jensen, L.J., von Mering, C., Bork, P.: eggNOG 4.5: a hierarchical orthology framework with improved functional annotations for eukaryotic, prokaryotic and viral sequences. Nucleic acids research 44(D1), 286–93 (2016).

306. Kinsella, R.J., Kahari, A., Haider, S., Zamora, J., Proctor, G., Spudich, G., Almeida-King, J., Staines, D., Derwent, P., Kerhornou, A., Kersey, P., Flicek, P.: Ensembl BioMarts: a hub for data retrieval across taxonomic space. Database 2011(0), 030–030

(2011).

307. Brown, G.R., Hem, V., Katz, K.S., Ovetsky, M., Wallin, C., Ermolaeva, O., Tolstoy, I., Tatusova, T., Pruitt, K.D., Maglott, D.R., Murphy, T.D.: Gene: a gene-centered information resource at NCBI. Nucleic Acids Research 43(D1), 36–42 (2015).

308. Agarwala, R., Barrett, T., Beck, J., Benson, D.A., Bollin, C., Bolton, E., Bourexis, D., Brister, J.R., Bryant, S.H., Canese, K., Cavanaugh, M., Charowhas, C., Clark, K., Dondoshansky, I., Feolo, M., Fitzpatrick, L., Funk, K., Geer, L.Y., Gorelenkov, V., Graeff, A., Hlavina, W., Holmes, B., Johnson, M., Kattman, B., Khotomlianski, V., Kimchi, A., Kimelman, M., Kimura, M., Kitts, P., Klimke, W., Kotliarov, A., Krasnov, S., Kuznetsov, A., Landrum, M.J., Landsman, D., Lathrop, S., Lee, J.M., Leubsdorf, C., Lu, Z., Madden, T.L., Marchler-Bauer, A., Malheiro, A., Meric, P., Karsch-Mizrachi, I., Mnev, A., Murphy, T., Orris, R., Ostell, J., O'Sullivan, C., Palanigobu, V., Panchenko, A.R., Phan, L., Pierov, B., Pruitt, K.D., Rodarmer, K., Sayers, E.W., Schneider, V., Schoch, C.L., Schuler, G.D., Sherry, S.T., Siyan, K., Soboleva, A., Soussov, V., Starchenko, G., Tatusova, T.A., Thibaud-Nissen, F., Todorov, K., Trawick, B.W., Vakatov, D., Ward, M., Yaschenko, E., Zasypkin, A., Zbicz, K.: Database resources of the National Center for Biotechnology Information. Nucleic Acids Res. 46(D1), 8–13 (2018)

309. Sonnhammer, E.L.L., Ostlund, G.: InParanoid 8: orthology analysis between 273 proteomes, mostly eukaryotic. Nucleic Acids Research. 43(D1), 234–239 (2015).

310. Zdobnov, E.M., Tegenfeldt, F., Kuznetsov, D., Waterhouse, R.M., Sim̃ao, F.A., Ioannidis, P., Seppey, M., Loetscher, A., Kriventseva,   E.V.: OrthoDB v9.1: cataloging evolutionary and functional annotations for animal, fungal, plant, archaeal, bacterial and

viral orthologs. Nucleic Acids Research 45(D1), 744–749 (2017).

311. Huber, W., Carey, V.J., Gentleman, R., Anders, S., Carlson, M., Carvalho, B.S., Bravo, H.C., Davis, S., Gatto, L., Girke, T., Gottardo, R., Hahne, F., Hansen, K.D., Irizarry, R.A., Lawrence, M., Love, M.I., MacDonald, J., Obenchain, V., Ole, A.K., Pages, H., Reyes, A., Shannon, P., Smyth, G.K., Tenenbaum, D., Waldron, L., Morgan, M.: Orchestrating high-throughput genomic analysis with Bioconductor. Nat. Methods 12(2), 115–121 (2015)

312. Menche, J., Sharma, A., Kitsak, M., Ghiassian, S.D., Vidal, M., Loscalzo, J., Barabasi, A.-L.: Uncovering disease-disease relationships through the incomplete interactome. Science 347(6224), 1257601–1257601 (2015).

313. Das, J., Yu, H.: HINT: High-quality protein interactomes and their applications in understanding human disease. BMC Systems Biology 6(1), 92 (2012).

314. Csardi, G., Nepusz, T.: The igraph software package for complex network research. InterJournal Complex Systems 1695, 1695 (2006)

315. Maslov, S., Sneppen, K.: Specificity and Stability in Topology of Protein Networks. Science 296(5569), 910–913 (2002).

316. Drew, K., Lee, C., Huizar, R.L., Tu, F., Borgeson, B., McWhite, C.D., Ma, Y., Wallingford, J.B., Marcotte, E.M.: Integration of over 9,000 mass spectrometry experiments builds a global map of human protein complexes. Molecular Systems Biology 13(6), 932 (2017)

317. Dimmer, E.C., Huntley, R.P., Alam-Faruque, Y., Sawford, T., O'Donovan, C., Martin, M.J., Bely, B., Browne, P., Mun Chan, W., Eberhardt, R., Gardner, M., Laiho, K., Legge, D., Magrane, M., Pichler, K., Poggioli, D., Sehra, H., Auchincloss, A., Axelsen, K.,

Blatter, M.-C., Boutet, E., Braconi-Quintaje, S., Breuza, L., Bridge, A., Coudert, E., Estreicher, A., Famiglietti, L., Ferro-Rojas, S., Feuermann, M., Gos, A., Gruaz-Gumowski, N., Hinz, U., Hulo, C., James, J., Jimenez, S., Jungo, F., Keller, G., Lemercier, P., Lieberherr, D., Masson, P., Moinat, M., Pedruzzi, I., Poux, S., Rivoire, C., Roechert, B., Schneider, M., Stutz, A., Sundaram, S., Tognolli, M., Bougueleret, L., Argoud-Puy, G., Cusin, I., Duek- Roggli, P., Xenarios, I., Apweiler, R.: The UniProt-GO Annotation database in 2011. Nucleic Acids Research 40(D1), 565–570 (2012).

318.   Hein, M.Y., Hubner, N.C., Poser, I., Cox, J., Nagaraj, N., Toyoda, Y., Gak, I.A., Weisswange, I., Mansfeld, J., Buchholz, F., Hyman, A.A., Mann, M.: A human interactome in three quantitative dimensions organized by stoichiometries and abundances. Cell 163(3), 712–23 (2015).

319.   Langfelder, P., Horvath, S.: Fast R Functions for Robust Correlations and Hierarchical Clustering. Journal of Statistical Software 46(11) (2012)

320.   Kolesnikov, N., Hastings, E., Keays, M., Melnichuk, O., Tang, Y.A., Williams, E., Dylag, M., Kurbatova, N., Brandizi, M., Burdett, T., Megy, K., Pilicheva, E., Rustici, G., Tikhonov, A., Parkinson, H., Petryszak, R., Sarkans, U., Brazma, A.: ArrayExpress update–simplifying data submissions. Nucleic Acids Research 43(D1), 1113–1116 (2015).

321.   Hubbell, E., Liu, W.-M., Mei, R.: Robust estimators for expression analysis. Bioinformatics (Oxford, England) 18(12), 1585–92 (2002)

322.   Gautier, L., Cope, L., Bolstad, B.M., Irizarry, R.A.: Affy - Analysis of Affymetrix GeneChip data at the probe level. Bioinformatics 20(3), 307–315 (2004).

323.   Ritchie, M.E., Phipson, B., Wu, D., Hu, Y., Law, C.W., Shi, W., Smyth, G.K.: limma

powers differential expression analyses for RNA-sequencing and microarray studies. Nucleic acids research 43(7), 47 (2015).

324. Wang, X., Terfve, C., Rose, J.C., Markowetz, F.: HTSanalyzeR: an R/Bioconductor package for integrated network analysis of high-throughput screens. Bioinformatics 27(6), 879–880 (2011)

325. Dougherty, J.D., Schmidt, E.F., Nakajima, M., Heintz, N.: Analytical approaches to RNA profiling data for the identification of genes enriched in specific cells. Nucleic Acids Research 38(13), 4218–4230 (2010).

326. Patro, R., Duggal, G., Love, M.I., Irizarry, R.A., Kingsford, C.: Salmon provides fast and bias-aware quantification of transcript expression. Nat. Methods 14(4), 417–419 (2017)

327. Pimentel, H., Bray, N.L., Puente, S., Melsted, P., Pachter, L.: Differential analysis of RNA-seq incorporating quantification uncertainty. Nat. Methods 14(7), 687–690 (2017)

328. Horvath, S., Dong, J.: Geometric interpretation of gene coexpression network analysis. PLoS Comput. Biol. 4(8), 1000117 (2008)

329. Candiano, G., Bruschi, M., Musante, L., Santucci, L., Ghiggeri, G.M., Carnemolla, B., Orecchia, P., Zardi, L., Righetti, P.G.: Blue silver: a very sensitive colloidal Coomassie G-250 staining for proteome analysis. Electrophoresis 25(9), 1327–1333 (2004)

330. Shevchenko, A., Wilm, M., Vorm, O., Mann, M.: Mass spectrometric sequencing of proteins silver-stained polyacrylamide gels. Anal. Chem. 68(5), 850–858 (1996)

331. Ishihama, Y., Rappsilber, J., Andersen, J.S., Mann, M.: Microcolumns with Self-assembled Particle Frits for Proteomics

332. Cox, J., Mann, M.: MaxQuant enables high peptide identification rates, individualized p.p.b.-range mass accuracies and proteome-wide protein quantification. Nat. Biotechnol.

26(12), 1367–1372 (2008)

333. Inoue T, Manley GT, Patel N, Whetstone WD. Medical and surgical management after spinal cord injury: vasopressor usage, early surgerys, and complications. J Neurotrauma. Mary Ann Liebert, Inc. 140 Huguenot Street, 3rd Floor New Rochelle, NY 10801 USA; 2014;31:284–291.

334. Vale FL, Burns J, Jackson AB, Hadley MN. Combined medical and surgical treatment after acute spinal cord injury: results of a prospective pilot study to assess the merits of aggressive medical resuscitation and blood pressure management. J Neurosurg. Journal of Neurosurgery Publishing Group; 1997;87:239–246.

335. Ploumis A, Yadlapalli N, Fehlings MG, Kwon BK, Vaccaro AR. A systematic review of the evidence supporting a role for vasopressor support in acute SCI. Spinal Cord. Nature Publishing Group; 2010;48:356–362.

336. Ryken TC, Hurlbert RJ, Hadley MN, et al. The Acute Cardiopulmonary Management of Patients With Cervical Spinal Cord Injuries. Neurosurgery [online serial]. 2013;72:84–92.

337. Walters BC, Hadley MN, Hurlbert RJ, et al. Guidelines for the management of acute cervical spine and spinal cord injuries: 2013 update. Neurosurgery. LWW; 2013;60:82–91.

338. Melhem S, Shutter L, Kaynar AM. A trial of intracranial pressure monitoring in traumatic brain injury. Crit Care. Epub 2014.:1–3.

339. Robertson CS, Contant CF, Narayan RK, Grossman RG. Cerebral blood flow, AVDO2, and neurologic outcome in head-injured patients. J Neurotrauma [online serial]. 1992;9 Suppl 1:S349-58.

340. Maas A, Stocchetti N, Bullock R. Moderate and severe traumatic brain injury in adults. Lancet Neurol. Epub 2008.

341. Saadoun S, Chen S, Papadopoulos MC. Intraspinal pressure and spinal cord perfusion pressure predict neurological outcome after traumatic spinal cord injury. J Neurol Neurosurg Psychiatry. Epub 2016 Nov 18.:jnnp-2016-314600.

342. Kwon BK, Curt A, Belanger LM, et al. Intrathecal pressure monitoring and cerebrospinal fluid drainage in acute spinal cord injury: a prospective randomized trial. J Neurosurg Spine. 2009;10:181–193.

343. Elm E Von, Altman D, Egger M, Pocock S. The Strengthening the Reporting of Observational Studies in Epidemiology [STROBE] statement: guidelines for reporting observational studies. Gaceta. Epub 2008.

344. Readdy WJ, Saigal R, Whetstone WD, et al. Failure of Mean Arterial Pressure Goals to Improve Outcomes Following Penetrating Spinal Cord Injury. Neurosurgery. Epub 2016 May.

345. Phang I, Papadopoulos MC. Intraspinal Pressure Monitoring in a Patient with Spinal Cord Injury Reveals Different Intradural Compartments: Injured Spinal Cord Pressure Evaluation (ISCoPE) Study. Neurocrit Care. 2015;23:414–418.

346. Jones CF, Newell RS, Lee JHT, Cripton PA, Kwon BK. The pressure distribution of cerebrospinal fluid responds to residual compression and decompression in an animal model of acute spinal cord injury. Spine (Phila Pa 1976). 2012;37:E1422-31.

347. Ghajar J. Traumatic brain injury. Lancet. 2000;356:923–929.

348. Carney N, Totten AM, O'Reilly C, et al. Guidelines for the Management of Severe Traumatic Brain Injury, Fourth Edition. Neurosurgery. Epub 2016 Sep 20.:1.

349. Griffiths IR, Pitts LH, Crawford RA, Trench JG. Spinal cord compression and blood flow. I. The effect of raised cerebrospinal fluid pressure on spinal cord blood flow. Neurology. 1978;28:1145–1151.

350. Kong CY, Hosseini AM, Belanger LM, et al. A prospective evaluation of hemodynamic management in acute spinal cord injury patients. Spinal Cord. 2013;51:466–471.